

DOT/FAA/AR-95/29, I

Office of Aviation Research  
Washington, D.C. 20591

# Fiber Composite Analysis and Design: Composite Materials and Laminates, Volume I

October 1997

Final Report

This document is available to the U.S. public  
through the National Technical Information  
Service, Springfield, Virginia 22161.

**DTIC QUALITY INSPECTED 3**



U.S. Department of Transportation  
Federal Aviation Administration

19980406 035

## **NOTICE**

This document is disseminated under the sponsorship of the U.S. Department of Transportation in the interest of information exchange. The United States Government assumes no liability for the contents or use thereof. The United States Government does not endorse products or manufacturers. Trade or manufacturer's names appear herein solely because they are considered essential to the objective of this report.



1. Report No. DOT/FAA/AR-95/29, I		2. Government Accession No.		3. Recipient's Catalog No.	
4. Title and Subtitle  FIBER COMPOSITE ANALYSIS AND DESIGN: COMPOSITE MATERIALS AND LAMINATES, VOLUME I				5. Report Date October 1997	
				6. Performing Organization Code	
7. Author(s) Z. Hashin, B.W. Rosen, E. A. Humphreys, C. Newton, and S. Chatterjee				8. Performing Organization Report No.	
9. Performing Organization Name and Address  Materials Sciences Corporation Suite 250, 500 Office Center Drive Fort Washington, PA 19034				10. Work Unit No. (TRAIS)	
				11. Contract or Grant No. DTFA03-92-P-01952	
12. Sponsoring Agency Name and Address  U.S. Department of Transportation Federal Aviation Administration Office of Aviation Research Washington, DC 20591				13. Type of Report and Period Covered  Final Report	
				14. Sponsoring Agency Code AAR-430	
15. Supplementary Notes  Federal Aviation Administration William J. Hughes Technical Center COTR: Donald W. Oplinger					
16. Abstract  This document, originally published as Federal Aviation Administration (FAA) technical report DOT/FAA/CT-85/6, provides an extensive background on the characteristics and mechanics of fiber reinforced composites which permits engineers experienced in the evaluation of structures involving conventional materials—especially metals—to extend their competence to the assessment of fibrous composite structures. The emphasis is on the definition of the nature and magnitude of the differences associated with the use of composites rather than conventional materials and especially toward the elucidation of the reasons for the differences and their implications for design evaluation. Accordingly, a broad spectrum of technologies is involved, ranging from detailed methods of analysis to the more qualitative discussions on methods of analysis and design. The material is divided into two major categories: (1) composite materials and laminates, treated in this volume and (2) structures, presented as volume II in a separate FAA technical report (DOT/FAA/CT-88/18) which is currently undergoing similar revision and should be available early in 1998. The present volume has been revised to include significant advancements in the state of the art in the design of composite structures as well as in the mechanics analysis of composites.					
17. Key Words  Fibrous composite materials, Structural behavior, Design and analysis, Applied mechanics, Static behavior, Fatigue, Environmental effects			18. Distribution Statement  This document is available to the public through the National Technical Information Service, Springfield, Virginia 22161		
19. Security Classif. (of this report)  Unclassified		20. Security Classif. (of this page)  Unclassified		21. No. of Pages 339	
				22. Price	

## FOREWORD

This book results from the continuing efforts by Materials Sciences Corporation (MSC) staff members, over the past decade, to provide training materials in composites for use by engineers of the Federal Aviation Administration (FAA). This version was prepared by MSC staff with contract support from the FAA William J. Hughes Technical Center, Atlantic City International Airport, New Jersey, most recently under Contract No. DTFA03-92-P-01952.

Major contributions to this book have been provided during various periods of time by Sailendra N. Chatterjee, Zvi Hashin, Crystal Newton, and B. Walter Rosen with the assistance of Norris F. Dow and Edward A. Humphreys. The authors express appreciation to Mary Jane Schnabel, Beverly Lazurus, and Donna Brennan for production assistance and to various MSC staff members for helpful discussions and assistance. The authors acknowledge the assistance of Donald W. Oplinger, Lawrence Neri, and David Nesterok, the FAA Technical Monitors, for this project and express their sincere appreciation to Joseph Soderquist of the FAA for providing continued and much needed motivation, help, and encouragement.

*More important than any one new material or any one new application is the new "materials" concept itself. It marks a shift from concern with substances to concern with structures, a shift from artisan to scientist as man's artificer, a shift from chemistry to physics as the basic discipline, and a shift, above all, from the concrete experience of the workshop to abstract mathematics, a shift from starting with what nature provides to what man wants to accomplish.*

Peter F. Drucker  
The Age of Discontinuity

## FAA PREFACE

The transition of composite materials from a laboratory experiment to practical use in civil and military production aircraft is a reality. During the process, many potential problems were uncovered, addressed, and resolved. For example, in the 1970's, the concerns with moisture absorption and the potential release of carbon fibers in aircraft accidents involving fire were resolved. Progress has proceeded from military aircraft to commercial transport aircraft, and now, to the high level of interest shown by the general aviation community. This progress reflects a growth of confidence in the use of composites and a recognition of the cost and performance advantages associated with such materials.

Composite materials can be tailored to meet the needs of specific strength and stiffness requirements; and as such, these materials are ideally suited to aircraft designs in which high performance and low weight are necessary. At the same time, these materials experience directionality of properties. Such anisotropy requires a redirection in the analytical thought processes of aircraft structural engineers.

The FAA has therefore supported the development of this text in order to assist certification and design engineers in assessing the response of composite materials, laminates, and structures to mechanical loading and environmental conditions. The treatment of material in this text fosters first an understanding of the mechanics of composite materials at the constituent level followed by an evaluation of the response of laminates. The material in Volume I serves as the basis for the treatment of structures to be provided in Volume II. Recommended methods can be utilized in relatively simple programs for programmable calculators or microcomputers; however, the use of these programs must be based on a sound understanding of the underlying physical concepts which are provided herein.

Although this text was initially developed for FAA use, the nature of the material covered makes it suitable for study by designers and graduate students in the field of engineering mechanics. The scope of the text may be regarded as appropriate for a one semester, graduate level course. Students will find that the fundamental issues are supplemented by a treatment of real world issues, a desirable feature for practicing engineers.

*Hic liber magni ponderis* is a fundamental treatise on the design and analysis of composite material structures. It is anticipated that revisions will be made to this text periodically to reflect specialized topics and technology advances, as this is an evolving technology with advances being made continuously.

Joseph R. Soderquist  
National Resource Specialist;  
Advanced Nonmetallic Materials  
Federal Aviation Administration

## PREFACE

Fiber composites have been developed to take advantage of unique properties found in materials in fibrous form. Many materials in the form of fine filaments exhibit strength and stiffness characteristics far greater than those of the same material in bulk form. The combination of such filaments with a suitable matrix can yield a composite with properties superior to the same material in bulk.

The concept is not new, but the emphasis has changed. Perhaps the earliest composites were the mud bricks reinforced with straw used in Biblical times. Here the mud (the matrix material) was the important element, and the straw was added to make the mud serve adequately as a material of construction. For today's composites, the matrix serves rather to make the fiber properties accessible. Hence, the title of this book, *Fiber Composite Analysis and Design*. The fiber comes first, and the technology with which this book is concerned is primarily directed toward the utilization of the potential provided by advanced fibers.

During the last 30 years, a wide range of new fibers has been introduced into the marketplace, creating both new design opportunities and new problems for the designer. The technology of using such fibers is not a simple one, but progress has been made toward its mastery. Such progress is ongoing, particularly in the area of failure of composites. This book focuses on the principles which underlie the behavior of composites and forms the foundation for ongoing developments.

The object of this book is to provide an adequate background of knowledge of the characteristics and mechanics of fiber composites so that an engineer experienced in the assessment of the performance of conventional materials can extend his competence to the assessment of composites. A broad spectrum of technologies is involved, ranging from detailed methods of analysis to more qualitative considerations of methods of design and evaluation. Throughout, the emphasis is directed toward the definition of the nature and magnitude of the differences associated with the use of composites rather than conventional materials and especially toward the elucidation of the reasons for the differences and their implications for design evaluation.

This book was originally published as a FAA report DOT/FAA/CT-85/6, *Fiber Composite Analysis and Design, Vol. I, Composite Materials and Laminates*. Since then the state of the art as well as the mechanics of composite materials have made significant advancements. This is a revision of the original report with significant changes in the sections which deal with fatigue. In addition, since many new fibers and matrix materials have been developed, a new chapter has been added in order to attempt a broader coverage of the constituents. Various other sections have been revised for clarity and other reasons.

## TABLE OF CONTENTS

	Page
EXECUTIVE SUMMARY	xxiii
CHAPTER 1. INTRODUCTION AND OVERVIEW	1-1
1.1 Composite Materials	1-1
1.2 Constituent Characteristics	1-2
1.2.1 Fiber Materials	1-2
1.2.2 Matrix Materials	1-4
1.3 Fiber Composite Materials	1-6
1.3.1 Terminology	1-7
1.3.2 Basic Elastic Properties	1-9
1.3.3 Typical Fiber Composite Material Properties	1-11
1.3.4 Reinforcement Forms Other Than Continuous Filaments	1-14
1.3.5 Fabrication Processes	1-14
1.4 The Design Cycle for Composite Structures	1-15
1.5 Service Characteristics	1-17
1.5.1 Durability	1-17
1.5.2 Fatigue	1-17
1.5.3 Environmental Effects	1-18
1.5.4 Damage Tolerance	1-18
1.5.5 Test, Inspection, and Repair	1-18
1.6 Overview	1-19
1.6.1 Unidirectional Composites	1-19
1.6.2 Laminate Properties	1-20
1.6.3 Test Methods	1-21
1.6.4 Structural Analysis	1-23
1.6.5 Structural Design	1-25
1.7 Concluding Remarks	1-25
CHAPTER 2. CONSTITUENT PROPERTIES	2-1
2.1 Fibers	2-1
2.1.1 Carbon	2-2

2.1.1.1	Methods of Manufacture	2-2
2.1.1.2	Available Forms	2-2
2.1.1.3	Outstanding Characteristics	2-2
2.1.2	Glass	2-5
2.1.2.1	Method of Manufacture	2-6
2.1.2.2	Available Forms	2-7
2.1.2.3	Surface Treatment	2-7
2.1.2.4	Outstanding Characteristics	2-7
2.1.3	Quartz	2-8
2.1.4	Alumina	2-8
2.1.5	Silicon Carbide	2-9
2.1.6	Kevlar	2-9
2.1.6.1	Available Forms	2-9
2.1.6.2	Surface Treatment	2-9
2.1.6.3	Outstanding Characteristics	2-9
2.1.7	Boron	2-12
2.1.8	Polyethylene	2-13
2.2	Matrix Materials	2-14
2.2.1	Polyesters	2-14
2.2.2	Epoxies	2-14
2.2.2.1	Curing	2-16
2.2.2.2	Additives	2-16
2.2.2.3	Environmental Factors	2-16
2.2.2.4	Outstanding Characteristics	2-16
2.2.3	Phenolics	2-16
2.2.4	Polyimides	2-17
2.2.5	Thermoplastics	2-17
REFERENCES		2-20
CHAPTER 3. UNIDIRECTIONAL FIBER COMPOSITES		3-1
3.1	Fiber Composites: Physical Properties	3-1
3.1.1	Elastic Properties	3-3

3.1.1.1	Composite Properties	3-3
3.1.1.2	Relations Between Composite and Constituent Properties	3-13
3.1.2	Thermal Expansion and Moisture Swelling	3-26
3.1.3	Viscoelastic Properties	3-38
3.1.4	Conduction and Moisture Diffusion	3-49
3.2	Fiber Composites: Strength and Failure	3-53
3.2.1	Axial Tensile Strength	3-54
3.2.1.1	Fiber Strength	3-57
3.2.1.2	Weakest-Link Failure	3-60
3.2.1.3	Cumulative-Weakening Failure	3-61
3.2.1.4	Internal Stresses	3-63
3.2.1.5	Fiber Break Propagation Failure	3-65
3.2.1.6	Cumulative Group Mode Failure	3-66
3.2.1.7	Fracture Mechanics	3-67
3.2.1.8	Concluding Remarks	3-68
3.2.2	Axial Compressive Strength	3-69
3.2.3	Matrix Mode Strength	3-77
3.2.4	Remarks on Strength Analysis	3-79
3.2.5	Strength Under Combined Stress	3-80
3.2.6	Fatigue Failure	3-90
3.2.6.1	Uniaxial Loading—Axial Tension-Tension Fatigue	3-91
3.2.6.1.1	Damage Growth	3-97
3.2.6.1.2	Effects of Constituents	3-99
3.2.6.1.3	Phenomenological Models	3-101
3.2.6.2	Combined Cyclic Stress	3-102
3.2.6.3	Cumulative Damage	3-106
3.2.6.4	Concluding Remarks	3-108
	REFERENCES	3-109
	APPENDIX TO CHAPTER 3—GENERAL BOUNDS FOR EFFECTIVE ELASTIC MODULI	3-117
	CHAPTER 4. LAMINATES	4-1
4.1	Terminology	4-2
4.2	Lamina Stress-Strain Relations	4-2
4.3	Lamination Theory	4-12

4.4	Laminate Properties	4-19
4.4.1	Symmetric Laminates	4-20
4.4.2	Unsymmetric Laminates	4-34
4.4.3	Thermal Expansion	4-37
4.4.4	Moisture Expansion	4-48
4.4.5	Conductivity	4-49
4.5	Thermal and Hygroscopic Analysis	4-50
4.6	Laminate Stress Analysis	4-54
4.6.1	Stresses due to Mechanical Loads	4-55
4.6.2	Stresses due to Temperature and Moisture	4-60
4.6.3	Netting Analysis	4-65
4.6.4	Interlaminar Stresses	4-68
4.6.5	Nonlinear Stress Analysis	4-73
4.7	Subcritical Damages, Strength, and Failure	4-77
4.7.1	Initial Failure and Subcritical Damages	4-77
4.7.2	Subsequent Failures	4-79
4.7.3	Strength	4-86
4.7.4	Fracture Near Holes, Notches, or Cutouts	4-88
4.8	Fatigue	4-95
4.8.1	Continuous Laminates	4-96
4.8.1.1	Failure Models Based Upon Lamina Properties	4-98
4.8.1.1.1	Initial Failure	4-98
4.8.1.1.2	Residual Properties	4-100
4.8.1.1.3	Subsequent Failures	4-103
4.8.1.1.4	Concluding Remarks	4-108
4.8.1.2	Failure Models Based Upon Dispersed Defects	4-109
4.8.1.2.1	A Wearout Model	4-109
4.8.1.2.2	Application to Composites	4-112
4.8.1.2.3	Concluding Remarks	4-115
4.8.1.3	Macromechanical (Curve Fitting) Models for Fatigue Lifetime	4-115
4.8.1.3.1	Representative Models	4-116
4.8.1.3.2	Concluding Remarks	4-118



4.8.1.4	Properties for Design	4-118
4.8.1.4.1	Allowable Stresses	4-118
4.8.1.4.2	Cumulative Damage	4-122
4.8.1.4.3	Statistical Characterization	4-124
4.8.2	Laminates with Discontinuities	4-126
4.8.2.1	Damage Initiation and Growth at Unloaded Holes, Notches, or Cutouts	4-127
4.8.2.2	Growth of Interlaminar Disbonds	4-134
4.8.3	Impact and Damage Tolerance	4-135
4.8.4	Fatigue Design Philosophy	4-140
REFERENCES		4-141
APPENDIX TO CHAPTER 4—Laminate Level Failure Analysis		4-149

## LIST OF FIGURES

Figure	Page
1.1 Stress-Strain Diagrams for Various Fibers	1-4
1.2 Characteristic Stress-Strain Diagrams for Three Classes of Matrix Materials	1-5
1.3 Basic Fiber Composite Elements and Axis Systems	1-6
1.4 Idealized Lamina Cross Section Perpendicular to the Fibers	1-6
1.5 Typical Nonuniform Dispersion of Fibers in a Lamina Cross Section	1-7
1.6 Scanning Electron Microscope Views of a Composite at Various Magnifications	1-8
1.7 Schematic Representation of the Averaging of Nonuniform Stresses in Heterogeneous Materials for Equivalence to Uniform Stress in a Homogeneous Material	1-9
1.8 The Directional Nature of Composites, Indicated by the Radial Distance From the Origin at any Angle	1-9
1.9 Loading Conditions for the Evaluation of Basic Elastic Properties	1-11
1.10 Approximate Ranges of Values of Strength/Weight and Stiffness/Weight Ratios for Structural Metals and for Composites of Various Reinforcement Configurations	1-13
1.11 The Design Cycle for Composite Structures Introduces the Requirement for Designing Material as Well as Structure	1-16
1.12 Characteristic Relationships Between Fiber and Composite Stiffness	1-17
1.13 The Objective of Laminate Analysis: To Determine the Overall Properties of the Laminate in Terms of the Properties of the Individual Plies and Their Orientation	1-20
1.14 Characteristic Variations in Laminate Properties With Ply Orientation Are Suggested by a Simple $0^\circ/\pm\theta^\circ$ Configuration as $\theta$ Is Varied From $0^\circ$ to $90^\circ$	1-22
1.15 The Directional Properties of Composites May Lead to Problems in Testing	1-23
1.16 Reinforcement Configuration Has a Marked Influence on the Buckling Strength of Composite Plates in Compression as Shown by This Comparison of $0^\circ/90^\circ$ and $\pm\theta^\circ$ Laminate	1-24

2.1	The Long "Floats" Between Crossovers in Both Warp and Fill Directions, as in the Eight-Harness Satin Weave Shown, Provide Near Straight Yarns in a Biaxial Reinforcing Pattern, Approximating in One Ply the Properties of a Crossply Laminate	2-8
3.1	Microstructure of Unidirectional Composites	3-2
3.2	Unidirectionally Reinforced Lamina	3-2
3.3	Structure of Carbon and Graphite Fibers	3-7
3.4	Variation of Stress and Strain in Fiber Direction—Axial Loading	3-8
3.5	Variation of Stress and Strain Transverse to Fibers—Transverse Loading	3-9
3.6	Basic Loading to Define Effective Elastic Properties	3-12
3.7	Models for Numerical Computation of Properties	3-15
3.8	Composite Cylinder Assemblage—Construction	3-15
3.9	Composite Cylinder Assemblage	3-15
3.10	Longitudinal Shear Modulus, $G_L^*$ , Hexagonal Array of Circular Fibers and Composite Cylinder Assemblage	3-20
3.11	Transverse Section Through Unidirectional Fiber Composite	3-20
3.12	Transverse Young's Modulus, $E_T^*$ , of Boron-Reinforced Epoxy, Comparison of Theory and Experiment	3-21
3.13	Transverse Young's Modulus, $E_T^*$ , of Glass-Reinforced Epoxy, Comparison of Theory and Experiment	3-21
3.14	Thermal Expansion	3-29
3.15	Effective Thermal Expansion Coefficients—CCA Model	3-33
3.16	Effect of Fiber Fraction on Thermal Expansion for Representative Carbon/Epoxy Composite	3-33
3.17	Viscoelasticity	3-39
3.18	Creep Compliance for 5208 Resin as a Function of Temperature	3-40

3.19	Viscoelasticity of Fiber Composites	3-41
3.20	Viscoelasticity in Shear	3-42
3.21	Calculated Amplitude of Angle of Twist in Torsional Vibrations of a Unidirectionally Reinforced Glass/Epoxy Cylinder	3-49
3.22	One-Dimensional Heat Conduction Through a Slab	3-51
3.23	Single Filament Tensile Strength	3-55
3.24	Perturbation of Stresses in the Vicinity of a Broken Fiber End	3-56
3.25	Variation of Mean and Range of Individual Fiber Strength Values	3-58
3.26	Strength Length Variation of Fiber Strengths Following Weibull Statistical Distribution Functions	3-60
3.27	Geometry of Composite for Statistical Tensile Failure Model	3-62
3.28	Variation of Fiber Bundle Strength With Fiber Coefficient of Variation	3-63
3.29	Distribution of Damage in a Fiber Composite Material Resulting From an Applied Tensile Load	3-64
3.30	Photoelastic Stress Pattern for an Individual E-Glass Fiber Embedded in an Epoxy Material	3-70
3.31	Analytical Model for Compressive Strength of Fibrous Composites	3-70
3.32	Compressive Strength of Glass-Reinforced Epoxy Composites	3-72
3.33a	An Inclined Group of Fibers Under Compression and Shear Stress and Strain	3-74
3.33b	Increases in Shear Stress and Point of Instability for Small Imperfection	3-74
3.33c	Shear Failure for Large Imperfections	3-75
3.34	Local Fiber Failure Mechanisms Resulting From Compression of Kevlar/Epoxy	3-76
3.35a	Shear Failure Under Transverse Compression	3-78
3.35b	Shear Failure Under Longitudinal Shear	3-79
3.36	Failure Surfaces in Stress Space for HS Graphite/Epoxy, 60% Fibers	3-80

3.37	Typical Failure of [0] Boron/Epoxy Laminates Subjected to Longitudinal Tension-Tension Fatigue Loading	3-83
3.38	Typical Failure of Unidirectional Boron/Epoxy Laminates Subjected to Transverse Tension-Tension Fatigue Loading	3-84
3.39	Tensile Fiber Failure Mode	3-85
3.40	Tensile Matrix Failure Mode	3-85
3.41	Off-Axis Specimen	3-87
3.42	Failure Modes—Off-Axis Specimens	3-88
3.43	Static Off-Axis Strength Versus Angle	3-89
3.44	Uniform Sinusoidal Cyclic Stress for Fatigue Testing	3-91
3.45	Classification of Fatigue Cycles	3-92
3.46	S-N Curve for Cyclic Stress of Graphite/Epoxy Composite in the Fiber Direction	3-93
3.47	Typical S-N Curves Showing the Effect of Different Loadings on Carbon/Epoxy Composites	3-94
3.48	Schematic Illustration of Metal Fatigue	3-95
3.49	Characteristics of the Goodman Diagram	3-96
3.50	Goodman Diagram for Representative Unidirectional Composites	3-97
3.51	Strain-Life Diagrams Showing Various Regions of Different Tensile Fatigue Damage Mechanisms	3-98
3.52	Effects of Fiber Type on Stress Versus Log-Life Curves of Unidirectional Composites	3-99
3.53	Strain Log-Life Curves for Unidirectional Composites	3-100
3.54	Slopes of Normalized Stress Log-Life Curves Versus Fiber Modulus	3-101
3.55	Fatigue Failure Surface Family	3-104
3.56	Combined Cyclic Stress Problem	3-105
3.57	Cumulative Damage Problem	3-106

3.58	Palmgren-Miner Rule	3-107
4.1	Coordinate Systems	4-6
4.2	Extensional-Shear Coupling	4-9
4.3	Variation of $E_x$ with Angle and $G_{12}$ for Typical Graphite/Epoxy Materials	4-12
4.4	Laminate Construction	4-13
4.5	Plate Deformations and Strains	4-15
4.6	Stress and Moment Resultants	4-16
4.7	Stresses and Stress and Moment Resultants	4-16
4.8	Laminate Elastic Constants for HM-Graphite/Epoxy	4-21
4.9	Extensional-Shear Coupling and Poisson's Ratio	4-23
4.10	Laminate Example	4-25
4.11	Thermally Induced Loads	4-38
4.12	Thermal Expansion Coefficients for HM-Graphite/Epoxy	4-47
4.13	Shear Thermal Expansion Effects	4-47
4.14	Effects of Moisture and Temperature on Lamina Stiffness	4-50
4.15	Effects of Moisture and Temperature on Lamina Longitudinal Strength	4-51
4.16	Effects of Moisture and Temperature on Lamina Matrix Dominated Strengths	4-51
4.17	Moisture as a Function of Exposure Time for SP-313 Crossply Laminate	4-54
4.18	Laminate Construction, Interlaminar Stress Example	4-68
4.19	Equilibrium and Boundary Conditions	4-69
4.20	Interlaminar Normal Stresses and Moment Equilibrium	4-69
4.21	X Equilibrium and Boundary Conditions	4-70
4.22	Interlaminar Stress Normalized With Respect to the Applied Strain	4-71

4.23	Interlaminar Normal Stresses and Stacking Sequence Normalized With Respect to the Applied Strain	4-72
4.24	Interlaminar Shear Stresses and Stacking Sequence Normalized With Respect to the Applied Strain	4-73
4.25	Nondimensional Ramberg-Osgood Stress-Strain Curves	4-74
4.26	Stress-Strain Response, Tensile $N_{xx}$ Loading	4-81
4.27	Stress-Strain Response, Tensile $N_{yy}$ Loading	4-81
4.28	Stress-Strain Response, Tensile $N_{xy}$ Loading	4-82
4.29	Laminate Failure Surface for Combined In-Plane Extensional Stress States	4-83
4.30	Laminate Failure Surface for Combined In-Plane Extensional and Shear Stress States	4-84
4.31	Tensile Strength of $(0_l/\pm 45_j/90_k)_s$ Family of HM-Graphite/Epoxy Laminates	4-87
4.32	Laminate Theory Calculations for Stresses Around a Hole	4-89
4.33	Interlaminar Shear Stress at a Hole	4-89
4.34	Interlaminar Normal Stress at a Hole	4-90
4.35	Distribution of Stress $\sigma_{yy}(x, 0)$ Near a Circular Hole in a Homogeneous Orthotropic Infinite Plate	4-91
4.36	Stress Distribution Around a Hole in a Finite Width Plate	4-92
4.37	Idealized Limit Cases for Failure	4-93
4.38	Representation of Characteristic Dimensions for Semiempirical Fracture Theories	4-94
4.39	Approximate Failure Theories	4-95
4.40	Fatigue-Life Diagram for a Crossply Graphite/Epoxy Composite	4-97
4.41	Initial Fatigue Failure $(0^\circ/90^\circ/\pm 45^\circ/90^\circ/0^\circ)_s$	4-100
4.42	Residual Strength and Fatigue Life	4-101

4.43	Residual Strength-Life Curves for (a) Glass, (b) Carbon, and (c) Kevlar Fiber-Reinforced Crossply Laminates	4-102
4.44	Stiffness Loss in Some Glass-Reinforced Composites	4-103
4.45	Typical Failures of $[\pm 45]_s$ Boron/Epoxy Laminates Subjected to Longitudinal Tension-Tension Fatigue Loading	4-104
4.46	Typical Failures of $[0_2/\pm 45]_s$ Boron/Epoxy Laminates Subjected to Longitudinal Tension Loading	4-105
4.47	Slope of Curves of Stress (Normalized by Static Strength) Versus Log Life as a Function of Fiber Modulus in Unidirectional and Crossply Laminates	4-107
4.48	Typical S-N Curves	4-108
4.49	Metal Wearout	4-111
4.50	Time-Dependent Strength	4-111
4.51	Damage Growth	4-112
4.52	Observed Static and Fatigue Failure Modes in Tension	4-113
4.53	Changes in Flaw Distribution Function	4-114
4.54	Translation from Static Strength to Lifetime	4-114
4.55	Comparison of Two Different Expressions Used to Fit Experimental S-N Data	4-117
4.56	Statistical Material Properties	4-119
4.57	P-S-N Curves	4-120
4.58	Statistical Residual Strength Data	4-120
4.59	Probability of Static Failure	4-121
4.60	Methodology for Failure Analysis With Consideration of Load Cycling Effects	4-131
4.61	C-Scans of Specimen of $[0_2/\pm 45]_{ss}$ Carbon/Epoxy Laminate at Different Load Cycle Levels	4-132
4.62	Axial Section of Specimen of $[0_2/\pm 45]_{ss}$ Carbon/Epoxy Laminate	4-133
4.63	Transverse Section of Specimen of $[0_2/\pm 45]_{ss}$ Carbon/Epoxy Laminate	4-133



4.64	Impact of Compression Loaded $[(\pm 45/0)_2/\pm 45/0/90]_{2s}$ Graphite/Epoxy Laminate	4-137
4.65	Residual Compressive Strength of Impact/Compression Loaded $[(\pm 45/0)_2/\pm 45/0/90]_{2s}$ Graphite/Epoxy Laminate	4-137

## LIST OF TABLES

Table		Page
1.1	Properties of Fiber Materials	1-3
1.2	Properties of Typical Fiber/Epoxy Composites and Structural Metals	1-12
1.3	Conceptual Outline of Laminate Analysis	1-21
1.4	Conceptual Outline of Composite Test Methods	1-22
1.5	Conceptual Outline of Composites Structural Analysis	1-24
1.6	Conceptual Outline for Composites Design	1-25
2.1	Properties of Carbon Fibers	2-3
2.2	Properties of Glass and Ceramic Fibers	2-5
2.3	Properties of Aramid Fibers	2-10
2.4	Properties of Boron and Polyethylene Fibers	2-12
2.5	Properties of Thermoset Matrix Materials	2-15
2.6	Properties of Thermoplastic Matrix Materials	2-18
3.1	Comparison of Effective Elastic Properties Predicted by CCA Analysis and Hexagonal Array Numerical Analysis	3-19
3.2	Elastic Properties of Graphite/Aluminum Composite	3-23
3.3	Elastic Properties of Carbon and Graphite Fibers Computed From Ultrasonic Measurement of Effective Fiber Composite Moduli	3-24
3.4	Calculated Thermoelastic Properties for Typical Unidirectional Fiber Composites	3-34

3.5	Effective Swelling Coefficients	3-37
3.6	Analogous Quantities	3-50
4.1	Properties of a High-Modulus Graphite/Epoxy Lamina	4-22
4.2	Elastic Properties of Laminates	4-24
4.3	Extensional and Bending Stiffnesses	4-30
4.4	Bending-Twisting Coupling	4-31
4.5	Bending Extensional Coupling Effects on Stiffness of a $(0/\pm 45/90)$ Graphite/Epoxy Laminate	4-37
4.6	Laminate Elastic Constants	4-67
4.7	Ply Stresses (ksi) at First Ply Failure, $(0/\pm 45)_s$ Laminate	4-83
4.8	Failure Loads and Modes $[0/\pm 45]_s$ Laminate	4-85
4.9	Failure Criteria	4-130

## GLOSSARY OF TERMS AND ACRONYMS

- Angle-Ply Laminate - A laminate containing plies of  $\pm \theta$  orientations only.
- Anisotropic - Not isotropic.
- Balanced Laminate - A laminate in which all plies oriented at angles,  $\theta$ , other than  $0^\circ$  and  $90^\circ$  occur in  $\pm \theta$  pairs (not necessarily adjacent).
- Bending-Twisting Coupling - A property of certain classes of laminates which exhibit twisting curvatures when subjected to bending moments.
- Crossply Laminate - A laminate which has plies oriented at  $0^\circ$  and  $90^\circ$  only.
- Extensional-Bending Coupling - A property of certain classes of laminates which exhibit bending curvatures when subjected to extensional loads.
- Extensional-Shear Coupling - A property of certain classes of laminates which exhibit shear strains when subjected to extensional loading.
- Fiber Volume Fraction,  $v_f$  - The ratio of volume of fiber material to total volume of the composite, usually expressed as a percent.
- Homogeneous - A material description indicating no material variation with spatial coordinates.
- Interlaminar - Relating to effects between plies.
- Intralaminar - Relating to effects within a ply.
- Isotropic - A material description which indicates identical material properties in all directions.
- Lamina (plural - laminae) - A layer or ply of material.
- Lamina Coordinates - Coordinate system having axes in the principal material directions of a lamina.
- Laminate - A number of laminae bonded together.
- Laminate Coordinates - A reference coordinate system (used to describe the properties of a laminate), generally in the direction of principal axes, when they exist.
- Orthotropic - A material description indicating three mutually orthogonal axes of elastic symmetry.

Quasi-Isotropic	- A laminate in which the elastic properties within the laminate plane are isotropic. Laminate strengths are typically not isotropic.
RVE	- A representative volume element containing several elements of the phases (fiber and matrix in a unidirectional material) in a composite.
Stacking Sequence	- A description of a laminate which details the ply orientations and their sequence in the laminate.
Symmetric Laminate	- A laminate in which the construction above the midsurface is a mirror image of the construction below the midsurface.
Translaminar	- Relating to events or effects crossing boundaries between laminae.
Yarns, Roving	- Long multiple (thousands or more) filament bundles, a form in which fibers are usually supplied.
Woven Fabrics	- Fabric reinforcements or prepregs in various weave configurations.

## EXECUTIVE SUMMARY

This document, originally published as FAA technical report DOT/FAA/CT-85/6, Fiber Composite Analysis and Design, Vol. I, Composite Materials and Laminates, provides an extensive background on the characteristics and mechanics of fiber reinforced composites which permits engineers experienced in the evaluation of structures involving conventional materials—especially metals—to extend their competence to the assessment of fibrous composite structures. The emphasis is on the definition of the nature and magnitude of the differences associated with the use of composites rather than conventional materials and especially toward the elucidation of the reasons for the differences and their implications for design evaluation. Accordingly, a broad spectrum of technologies is involved, ranging from detailed methods of analysis to more qualitative discussions on methods of analysis and design. The material is divided into two major categories: (1) composite materials and laminates, treated in this volume and (2) structures, presented as volume II in a separate FAA technical report (DOT/FAA/CT-88/18, Fiber Composite Analysis Design Vol. II, Structures), which is currently undergoing similar revision and should be available early in 1998. The present volume has been revised to include significant advancements in the state of the art as well as the mechanics of composites.

The present volume is a revision of the original 1988 report, with significant changes in sections 3.2.6 and 4.8 dealing with fatigue. In addition, since many new fibers and matrix materials have been developed since the release of the original report while others are no longer in production, section 2.1 of the previous release has been expanded here to a full chapter (chapter 2) to provide a broader coverage of the constituents. Accordingly, chapter 3 of the present volume includes material previously identified as sections 2.2 and 2.3, while the present chapter 4 on laminates is the material previously identified as chapter 3. Various other sections have been revised for clarity and improvements in accuracy.

Chapter 1 of this volume gives an overview of the subject dealing with the characteristics of composite materials, their potential for structural applications, the reasons for their use, and general principles for their utilization. A detailed technical review of available constituent materials and their properties is given in chapter 2. The subject of unidirectional composites, which consists of aligned continuous fibers embedded in a matrix material, is addressed in chapter 3. The principles of micromechanics, which provides a basis for relating the stiffnesses, strengths, and other properties of the composite to those of its constituents are discussed in some detail. The reasons for the highly anisotropic character of fiber composites are explained. Differences between the fatigue failure processes in fiber composites and those in metals are also described in this chapter. Chapter 4 deals with laminate theory based on the inclusion of layers or plies of different orientations in the laminate as needed to provide a good balance of effective properties in various directions. Modulus, strength, and thermoelastic properties of various laminates are treated. Fatigue, impact, and other damage tolerance characteristics of multidirectionally reinforced laminates are also discussed.

## CHAPTER 1. INTRODUCTION AND OVERVIEW

*There is no straw given to thy servants yet  
they say to us - make bricks.*

Exodus, Chapter 5

*Union gives strength.*

Aesop's Fables

The use of combinations of materials to compensate for the shortcomings of one, as in the mud bricks of Biblical times, or to capitalize on the advantages of another, as in today's composites, has a long history. The Roman engineers used the concept to utilize the properties of stone as the aggregate in concrete to build structures that survived the Roman empire. Unfortunately, the concept died with the Romans and was not rediscovered until the advent of Portland cement. The Japanese combined hard but brittle materials with ductile ones to make laminated swords with properties respectable by today's standards. Today both classes of composites continue to be developed: the mud brick has evolved into the filled plastic with ever growing applications in fields where cost is the prime concern. Where performance is the criterion, as in aerospace structures, fiber composites predominate. The bases for this predominance are sound and many faceted.

In this chapter, we shall discuss, in general fashion, the characteristics of composite materials, their potentials for performance, the reasons for their use, and the general principles involved in their utilization.

### 1.1 COMPOSITE MATERIALS.

A composite material is usually defined as a combination of two or more materials with significantly different macro-level properties. Such materials are made for improving structural, thermal, or other characteristics of a single material. A typical composite contains one or more discontinuous phases (called reinforcements, since they are usually stronger or stiffer than the other) in a continuous phase (the matrix). Some examples of modern day composites are concrete, filled plastics, and unidirectional continuous or chopped fiber reinforced composites. Multidirectionally reinforced composites, such as laminates and fabric or three-dimensionally reinforced materials, are also used widely. Mechanical, physical, or other properties of a composite depend on those of the constituents and their distribution. Some of the properties, e.g., orientation of fibers, shape, size, size distribution, etc., are strong functions of the arrangement of the constituents. Concentration is usually measured in terms of volume or weight fraction of the constituents, and its distribution is a measure of the homogeneity of the composite.

Laminated composites used in aerospace structures are made by stacking unidirectional fiber composite layers (laminae) of different orientations. Designing a laminate for a particular application is a difficult task because of the variety of choices available for fiber and matrix materials and the arrangement of the laminae (stacking sequence). Use of fabric-reinforced layers

(with fibers in two or more directions) has become common, providing another alternative for material design. Fortunately, the mechanics of unidirectional or fabric-reinforced layers as well as laminates have advanced to a stage such that reliable methods are now available for prediction of the properties of candidate materials from their constituents, and they are widely used in industry. By these methods, which are based on the principles of physics and mechanics, properties of a unidirectionally reinforced material can be obtained from those of its constituents as described in chapter 3. Chapter 4 deals with the relations between the properties of a laminate and those of the laminae. In many cases the fabric reinforced plates can be approximated as a laminate with laminae oriented in appropriate directions. However, methods are also available for predicting the properties of fabric reinforced materials with due consideration to the micro and ministructural details. The rest of this chapter is devoted to the various types of constituents (fibers and matrix), some basic concepts and definitions, reinforcements of various forms, fabrication processes, the art of designing composite structures, service characteristics of composites, and an overview of the subject. Various fibers and matrix materials and their properties are discussed in chapter 2, and as mentioned earlier, mechanics of the unidirectional fiber composite and laminates are addressed in chapters 3 and 4, respectively.

## 1.2 CONSTITUENT CHARACTERISTICS.

### 1.2.1 Fiber Materials.

Fiber reinforcement materials are available in a wide variety of forms:

1. Natural fibers, such as jute and sisal, were formerly used for economy but now are generally supplanted by synthetics with both better properties and lower costs.
2. Synthetic organic fibers, both thermoplastic such as nylon, polyester, polypropylene, etc., and thermosetting like the aramids (Kevlar™). The synthetics offer low densities and high strengths but (with the exception of Kevlar) low stiffnesses. Their range of application is limited because of their low stiffnesses.
3. Synthetic inorganic fibers, including glass, boron, carbon, aluminum oxide, and silicon carbide. The use of glass far outstrips the use of any other reinforcing fibers, primarily because its cost is far less than that of its competitors.

The wide range of properties available for reinforcements is indicated by the values in table 1.1. The densities range from 0.049 pounds per cubic inch (pci) ( $1.36 \text{ g/cm}^3$ ) for the polyester to 0.143 pci ( $3.96 \text{ g/cm}^3$ ) for the aluminum oxide. The strength variation is from 160,000 pounds per square inch (psi) ( $1.10 \text{ GN/m}^2$ ) for the polyester to 600,000 psi ( $4.13 \text{ GN/m}^2$ ) for the S-glass. The stiffnesses cover the range from 2,000,000 psi ( $13.8 \text{ GN/m}^2$ ) for the polyester to over 50,000,000 psi ( $345 \text{ GN/m}^2$ ) for the pitch-based carbon fibers, boron, silicon carbide, and aluminum oxide. One or more types of fibers may be combined with any of a number of matrix materials. Thus, the composite designer has available to him a far wider selection of mechanical properties than are available in conventional structural materials.

TABLE 1.1. PROPERTIES OF FIBER MATERIALS

• English Units

Material	Density pci	Longitudinal Young's Modulus, Msi	Tensile Strength ksi
Polyester	0.049	2.0	160
E-Glass	0.095	11.8	500
S-Glass	0.090	12.9	665
Kevlar 49*	0.052	18.5	560
T-300*	0.064	34.0	530
Boron	0.093	58.0	520
SiC (SCS-6*)	0.115	58.0	600
AS-4*	0.065	36.0	590
IM-6*	0.063	40.0	740
IM-7*	0.064	44.0	770
T-800*	0.065	42.7	796

• Standard International (SI) Units

Material	Density g/cm <sup>3</sup>	Longitudinal Young's Modulus, GN/m <sup>2</sup>	Tensile Strength GN/m <sup>2</sup>
Polyester	1.36	13.8	1.10
E-Glass	2.60	81.4	3.45
S-Glass	2.50	88.9	4.59
Kevlar 49*	1.44	128	3.86
T-300*	1.77	230	3.70
Boron	2.58	400	3.59
SiC (SCS-6*)	3.19	400	4.14
AS-4*	1.80	250	4.10
IM-6*	1.76	276	5.10
IM-7*	1.78	300	5.30
T-800*	1.81	294	5.49

\* Trade names



Almost all of these reinforcement materials (an exception is the polyester) are characterized by a linear stress-strain relationship over their entire tensile load range, as shown in figure 1.1. As can be seen, the very high modulus fibers are limited to one percent or less strain. Kevlar and the glasses can accommodate strains of 3 to 4 percent. In composites, however, the same linear range of response as in the fibers alone may not be achieved because of nonlinear responses of the matrix material.

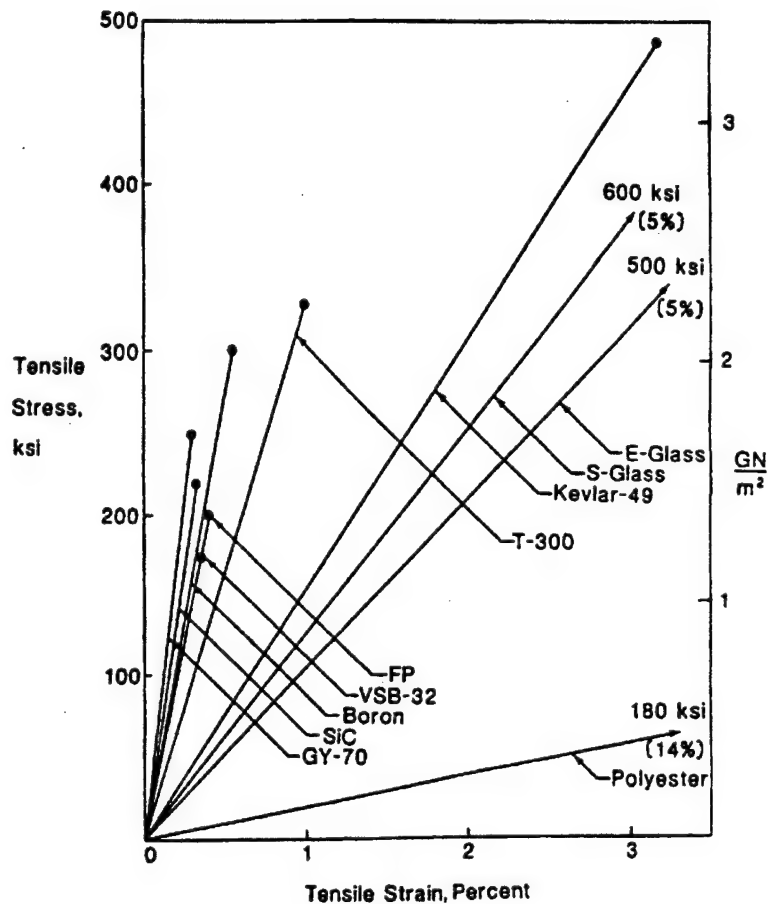


FIGURE 1.1. STRESS-STRAIN DIAGRAMS FOR VARIOUS FIBERS. Generally the stiffer the fiber, the smaller the strain at failure. Only the polyester stress-strain curve deviates appreciably from a straight line below the failure stress.

### 1.2.2 Matrix Materials.

Matrix materials cover the range from polymers to metals to ceramics. The polymers are characterized by low densities, relatively low strengths, a nonlinear stress-strain relationship (see figure 1.2), but relatively high strains to failure. Importantly, polymeric matrix composites can be more readily manufactured and can incorporate higher volume fractions of the reinforcing fibers than composites with metal or ceramic matrices. Hence, polymers are the most generally used matrix materials. Accordingly, the emphasis throughout this text will be upon the technology of polymeric matrix composites and upon methods of design, analysis, and evaluation to explain and minimize their shortcomings and maximize their advantages.

Polymeric matrix materials may be either thermoplastic or thermosetting. The thermoplastics (materials that can be heated and formed repetitively) are usually used for injection molding or possibly for thermoformable graphite laminates. The resins employed in injection molding, usually with chopped fiber reinforcements, include the acrylics, nylon, the vinyls (polyvinyl chloride, vinyl acetate, vinylidene chloride), polyethylenes, polypropylene, and ABS (acrylonitrile-butadiene-styrene); the resins used for laminates also include the acrylics and polysulfone or polyether sulfone. In general, these thermoplastic resins are more damage resistant and considered reworkable. For structural composites, the thermosetting resins are more generally the choice. These include the polyesters for low cost and high resistance to chemical degradation, the vinyl esters for strength combined with ease of processing, and the epoxies for highest strength. Other thermosetting resins may be employed for special properties as required: butadiene for improved electrical properties and the polyimides and silicones for use at elevated temperatures. Mention should also be made of some recent ultralightweight resins, such as phenolic triazine and benzocyclobutane (BCB). Because of its superior structural properties, epoxy may well be considered the baseline material for fiber composites, and it will be so treated herein.

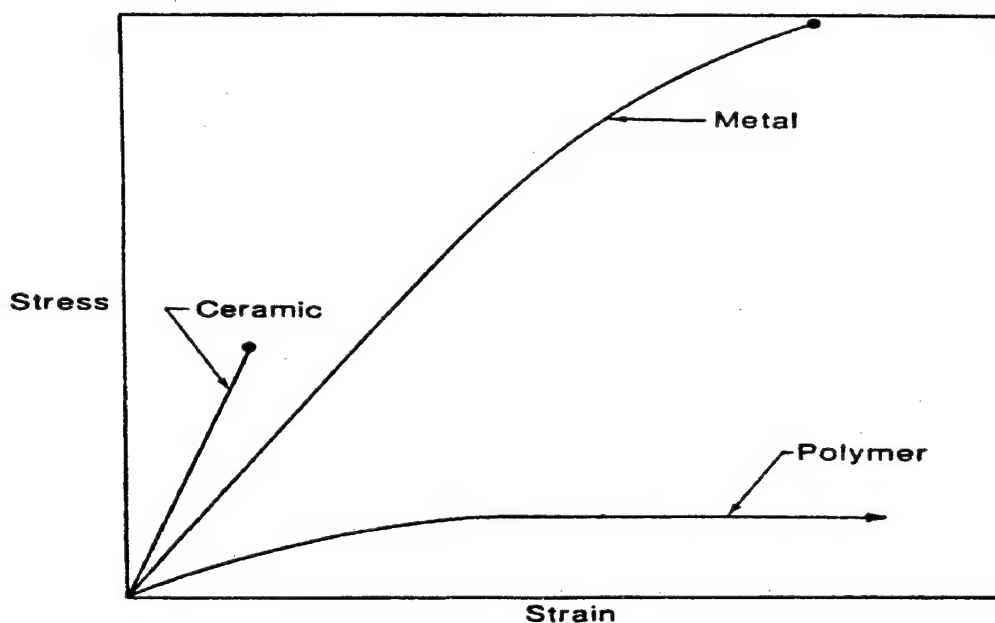


FIGURE 1.2. CHARACTERISTIC STRESS-STRAIN DIAGRAMS FOR THREE CLASSES OF MATRIX MATERIALS. The ceramics have linear stress-strain curves to failure and low failure strains. Curves for metals have an appreciable linear portion, yield before failure, and have many times the failing strains of ceramics. Polymers yield at low stresses and elongate even more than metals at failure.

### 1.3 FIBER COMPOSITE MATERIALS.

The fundamental building block upon which fiber composites are based is an element cut from a unidirectional array of fibers in a surrounding matrix, as illustrated in figure 1.3. In the element or lamina, the basic fiber unit is generally a multifilament yarn containing hundreds of individual filaments. These filament bundles may retain their individual identity as shown in figure 1.4 or, more commonly, they may disperse and intermingle to form a more or less uniform but random distribution of filaments throughout the cross section (figure 1.5).

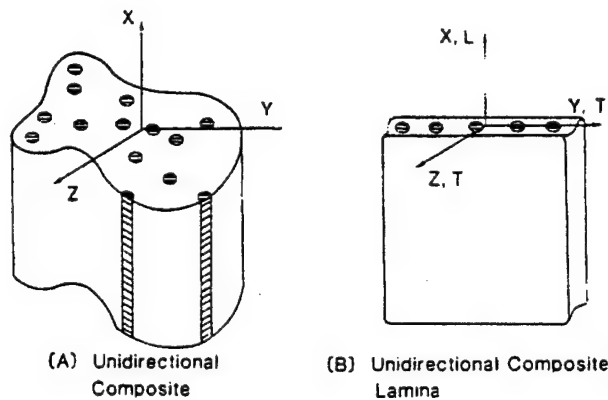


FIGURE 1.3. BASIC FIBER COMPOSITE ELEMENTS AND AXIS SYSTEMS. For a lamina the L and T are used as subscripts to identify the longitudinal and transverse directions.

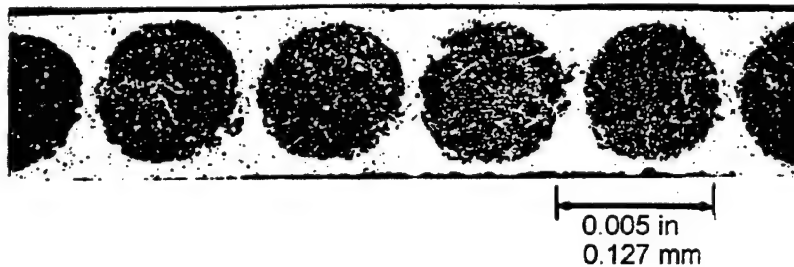


FIGURE 1.4. IDEALIZED LAMINA CROSS SECTION PERPENDICULAR TO THE FIBERS. This shows discrete yarns which are made up of a multiplicity of filaments.

Figure 1.5 shows the typical disarray encountered in a composite: irregular gaps and some contiguity. The particular cross section shown is that of glass filaments; carbon fibers would be similarly random in distribution and additionally would have some irregularity in fiber cross section. Similar shape irregularities are also evident in the crystal structure of metals at the appropriate level of magnification. In both metals and composites, a kind of orderly disorder which varies with the magnification can be seen.

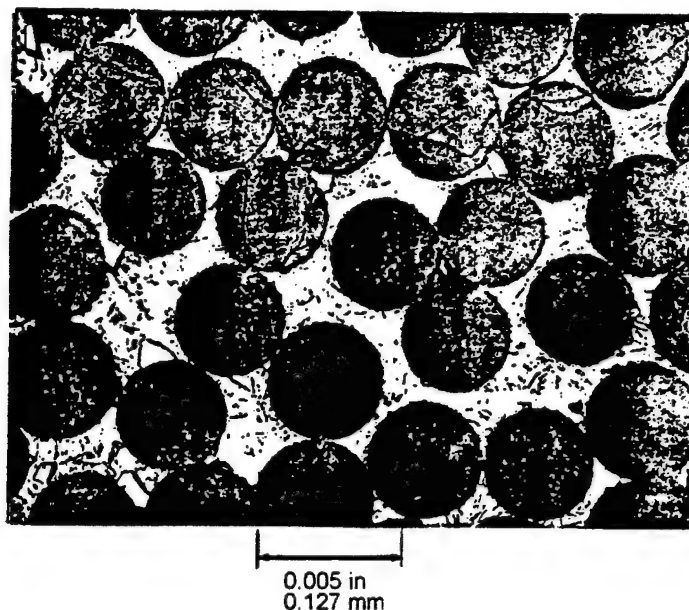


FIGURE 1.5. TYPICAL NONUNIFORM DISPERSION OF FIBERS IN A LAMINA CROSS SECTION

The implications of such a change with magnification levels are important for understanding the development of the analysis of the mechanics of composites. Consider, for example, the silicon carbide fibers embedded in a pyrolytic graphite matrix shown in figure 1.6. In the upper photograph, at the highest level of magnification, the individual constituents are identifiable. At this level, it appears appropriate to consider the properties of the local constituents. Thus, the fibers, for example, would be treated as brittle materials having a statistical strength distribution and some definable geometry. This constituent information defines a characteristic unit cell at the micro level. At the next lower level of magnification (at the center of the figure) a large number of these unit cells are seen. Together these may be considered to define a typical region, which may be called a representative volume element (RVE). The properties of this element may be considered to define the characteristics of the material. It is at the level of the RVE, corresponding to fiber bundles and their associated matrix, that the effective point properties of a composite material can be defined. These are the desired material properties which relate the average values of the state variables. From the RVE, the properties can be translated from the micro to the macro level. The properties of the assemblage of elements are point properties which vary from point to point, with the variation defining the statistical variability on the macro scale (the next level of magnification, as in the lower photo on the figure). These assemblages are still of very small dimensions compared to the overall material and, importantly, small compared to the characteristic dimension over which any of the average stress or strain variables would change significantly.

### 1.3.1 Terminology.

Before continuing with the discussion of micro and macro properties, let us define precisely the terminology to be used. Physical properties, such as stiffness, expansion coefficient, etc., are quantities relating state variables such as stress, strain, temperature, etc., in a material. If the



FIGURE 1.6. SCANNING ELECTRON MICROSCOPE VIEWS OF A COMPOSITE AT VARIOUS MAGNIFICATIONS SHOWING THE BLENDING OF THE NONUNIFORM CONSTITUENTS EVIDENT AT THE HIGHEST MAGNIFICATION INTO THE UNIFORMLY DISTRIBUTED ASSEMBLAGE OF THE COMPOSITE AS A WHOLE

properties vary from point to point, as for example at the RVE level in the composite, the material is identified as heterogeneous. If, as is often the case in composites, the average values of the state variables within an RVE are of concern, the term "effective properties" will be used. This effective properties concept is illustrated in figure 1.7, in which a heterogeneous material subjected to a uniform stress  $\sigma_0$  in the y-direction has an internal stress distribution that varies from point to point in the x-direction about an average value  $\sigma_0$  which is equivalent to the uniform stress  $\sigma_0$  in a homogeneous material.

If the properties vary with direction, the material is identified as anisotropic. There are many types of anisotropic materials. Those which exhibit particular symmetries have special names, such as orthotropic, cubic, etc. This is illustrated in the polar plot of figure 1.8, in which the distance from the origin in any direction is a measure of the material effective stiffness. Here both a unidirectional carbon fiber composite and a biaxial fiberglass fabric are shown to be anisotropic but in very different ways, while the aluminum is shown to be isotropic. The fiber composite shows a maximum stiffness in the fiber direction  $0^\circ$  and a minimum at  $90^\circ$ . The fabric shows the characteristic minimum stiffness in the bias ( $45^\circ$ ) direction of woven biaxial fabrics. The aluminum is uniformly stiff in all directions.

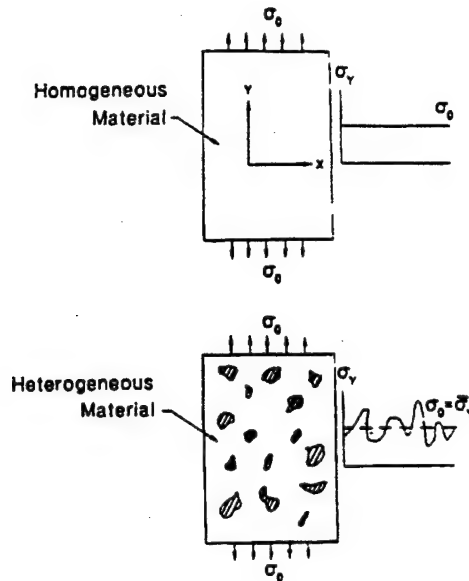


FIGURE 1.7. SCHEMATIC REPRESENTATION OF THE AVERAGING OF NONUNIFORM STRESSES IN HETEROGENEOUS MATERIALS FOR EQUIVALENCE TO UNIFORM STRESS IN A HOMOGENEOUS MATERIAL

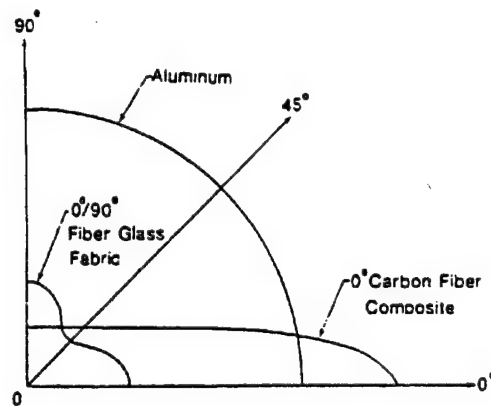


FIGURE 1.8. THE DIRECTIONAL NATURE OF COMPOSITES, INDICATED BY THE RADIAL DISTANCE FROM THE ORIGIN AT ANY ANGLE. Thus the isotropic properties of aluminum plot as a circular arc,  $0^\circ/90^\circ$  fabric has a minimum at  $45^\circ$ , and a unidirectional composite a maximum in the fiber direction.

### 1.3.2 Basic Elastic Properties.

A unidirectional fiber composite behaves like a homogeneous, anisotropic material. In general, the distribution of fibers over a given cross section is adequately random so that transversely they provide no preferential direction of reinforcement. Thus, the unidirectional composite is effectively transversely isotropic. It can be shown that the effective elastic properties of a transversely isotropic material can be fully characterized by five elastic constants, as illustrated in figure 1.9, and defined as follows. (Note that the transverse, or TT, plane is isotropic.)

1. A longitudinal Young's modulus  $E_L$  defined by the ratio of  $\sigma_L$ , the unidirectional stress in the fiber direction to the longitudinal strain  $\epsilon_L$ :

$$E_L = \frac{\sigma_L}{\epsilon_L} . \quad (1.1)$$

2. The associated Poisson's ratio  $\nu_L$  defined by the negative of the ratio of the associated transverse strain  $\epsilon_T$  to the longitudinal strain:

$$\nu_{LT} = \nu_L = - \frac{\epsilon_T}{\epsilon_L} . \quad (1.2)$$

3. A longitudinal shear modulus  $G_{LT}$ , defined by the inverse ratio of shear strain  $\gamma_{LT}$  to pure shear stress in the longitudinal plane  $\tau_{LT}$ :

$$G_{LT} = G_L = \frac{\tau_{LT}}{\gamma_{LT}} . \quad (1.3)$$

4. A transverse shear modulus  $G_{TT}$ , similar to  $G_{LT}$  but for pure shear stress and strain in the transverse plane:

$$G_{TT} = G_T = \frac{\tau_{TT}}{\gamma_{TT}} . \quad (1.4)$$

5. A transverse bulk modulus  $k$  defined for the case of equal transverse stresses  $\sigma_T$  which produce equal transverse strains  $\epsilon_T$  (in the absence of longitudinal strains). Then

$$k_{TT} = k = \frac{\sigma_T}{2\epsilon_T} . \quad (1.5)$$

With these five basic elastic constants evaluated, any other desired constant may be calculated. For example, the transverse Young's modulus  $E_T$ , which is the same in all directions in the TT plane, is given by

$$E_T = \frac{4kG_T}{k + \left[ 1 + \frac{4k\nu_L^2}{E_L} \right] G_T} . \quad (1.6)$$

Such properties and various relations among them will be discussed in detail in section 3.1.

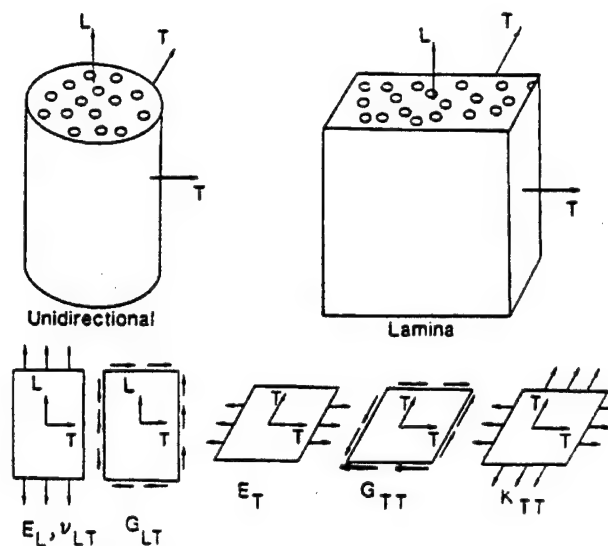


FIGURE 1.9. LOADING CONDITIONS FOR THE EVALUATION OF BASIC ELASTIC PROPERTIES

With basic elastic constants defined in terms of loading conditions, the way is clear for the measurement of the elastic properties needed for design and analysis. For metals, this empirical approach is both necessary and sufficient, as it is for the constituent properties in composites. Because composites have the additional complexity that their constituents may be combined in various ways, however, the experimental determination of the properties of the many combinations becomes a practical impossibility. Accordingly, analytical methods have been developed permitting the derivation of composite properties from the properties of their constituents. These methods will be discussed in subsequent chapters.

### 1.3.3 Typical Fiber Composite Material Properties.

Before proceeding to the detailed discussion of the technology involved in utilizing the potentials for performance offered by fiber properties such as those displayed in figure 1.1, it is perhaps wise to establish a proper perspective from the viewpoint of what has been done. To that end, table 1.2 and figure 1.10 have been prepared summarizing typical properties attained in the current state of the art.

Table 1.2 presents data on the mechanical properties of typical fiber composites, all employing epoxy as the matrix material and reinforcements (E-Glass, Kevlar, T-300, T-50, and GY-70) covering the range of stiffnesses  $77 \times 10^6$  to  $100 \times 10^6$  psi (72.3 to 530 GN/m<sup>2</sup>, see table 1.1) that are currently available. Also included for comparison in table 1.2 are properties for the aluminum alloys 2024-T3 and 7075-T6 and the chrome-molybdenum steel 4130. Evident from the table and characteristics of all the composites are the effectiveness of the fiber properties as reinforcement in the fiber direction and the ineffectiveness of reinforcement transverse to the fibers. These are a fact of life of unidirectional composites, and much of the material in the remainder of this book is concerned with the implications and treatment of these large disparities in properties.



TABLE 1.2. PROPERTIES OF TYPICAL FIBER/EPOXY COMPOSITES AND STRUCTURAL METALS

• English Units

Property	Unidirectional Composites, ( $v_f = 0.6$ )						Metals		
	E-Glass	Kevlar 49	T-300	VSB-32	Boron	GY-70	2024-T3	7075-T6	4130
Density, pci	0.070	0.047	0.053	0.059	0.067	0.058	0.100	0.101	0.283
$E_L$ , Msi	6.5	11.0	19.2	33.2	39.8	46.4	10.5	10.3	30.0
$E_T$ , Msi	1.7	0.8	1.5	1.0	2.2	0.8	10.5	10.3	30.0
$G_{LT}$ , Msi	0.64	0.3	0.95	0.8	7.5	0.6	4.0	4.0	12.0
$v_{LT}$	0.25	0.34	0.25	0.25	0.25	0.25	0.31	0.31	0.25
$\sigma_L^u$ , ksi	150	200	180	170	190	100	67	79	95
$\sigma_T^u$ , ksi	5	4	6.5	6	5	6	66	77	95
$\sigma_L^{cu}$ , ksi	80	40	120	100	360	90	50	69	160
$\sigma_T^{cu}$ , ksi	20	20	20	20	45	20	50	69	160
$\tau_{LT}^{su}$ , ksi	6	8	9	11	15	14	40	47	55

• Standard International (SI) Units

Property	Unidirectional Composites, ( $v_f = 0.6$ )						Metals		
	E-Glass	Kevlar 49	T-300	VSB-32	Boron	GY-70	2024-T3	7075-T6	4130
Density, g/cm <sup>3</sup>	1.94	1.30	1.47	1.63	1.86	1.61	2.77	2.80	7.84
$E_L$ , GN/m <sup>2</sup>	45	76	132	229	274	320	72.3	71.0	207
$E_T$ , GN/m <sup>2</sup>	12	5.5	10.3	6.9	15	5.5	72.3	71.0	207
$G_{LT}$ , GN/m <sup>2</sup>	4.4	2.1	6.5	5.5	52	4.1	27.6	27.6	82.7
$v_{LT}$	0.25	0.34	0.25	0.25	0.25	0.25	0.31	0.31	0.25
$\sigma_L^u$ , MN/m <sup>2</sup>	1000	1380	1240	1170	1310	690	462	544	655
$\sigma_T^u$ , MN/m <sup>2</sup>	34	28	45	41	34	41	455	530	655
$\sigma_L^{cu}$ , MN/m <sup>2</sup>	550	280	830	690	2480	620	345	475	1100
$\sigma_T^{cu}$ , MN/m <sup>2</sup>	140	140	140	140	310	140	345	475	1100
$\tau_{LT}^{su}$ , MN/m <sup>2</sup>	40	55	62	680	100	96	276	324	380

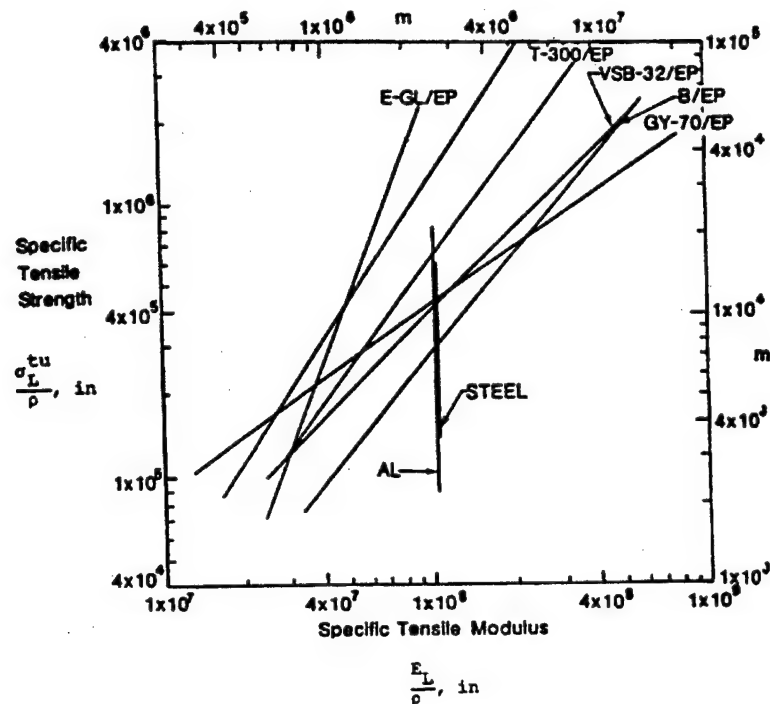


FIGURE 1.10. APPROXIMATE RANGES OF VALUES OF STRENGTH/WEIGHT AND STIFFNESS/WEIGHT RATIOS FOR STRUCTURAL METALS AND FOR COMPOSITES OF VARIOUS REINFORCEMENT CONFIGURATIONS

That the disparities can be successfully accommodated is obvious from the ever widening range of application of fiber composites. A proper perspective for this success can be attributed to Galileo, who defined an important measure of a material as the longest length of a uniform bar that could be hung vertically from a height without breaking. This measure of structural efficiency is simply the strength/density ratio of the material in the units of table 1.2 equal to  $\sigma_L^{tu}/\rho$ , in thousands of inches (meters). A similar measure of structural efficiency when deflection is of concern as well as strength is the modulus/density ratio. Thus,  $E_L/\rho$ , from table 1.2, is another measure of structural efficiency. These and other more detailed efficiency measures will be employed in later chapters for the evaluation of various applications of composites. For general comparisons of materials, the simple measures  $\sigma_L^{tu}/\rho$  and  $E_L/\rho$  are adequate to display graphically the potentials for weight saving in structural composites.

A comparison of this kind is presented in figure 1.10, on which are plotted the values of specific tensile strength  $\sigma_L^{tu}/\rho$  and specific modulus  $E_L/\rho$  for a wide range of types of composites and structural metals. For the metals, the ranges of strengths available through changes in heat treatment, alloy content, etc., are represented by the range of values of  $\sigma_L^{tu}/\rho$  covered by the vertical bars, i.e., the moduli are not affected by such changes. For the composites, however, both strength and stiffness may be substantially altered by changes in the reinforcement

configuration and volume fraction reinforcement. Hence, the bars representing the composites cover a range of values of both  $\sigma_L^m/\rho$  and  $E_L/\rho$ .

The maximum values of  $\sigma_L^m/\rho$  and  $E_L/\rho$  corresponding to the tops of the bars represent the substantial potentials for weight saving provided by fiber composites, factors of 2 to 3 in most cases, for either specific strength or modulus or both. Unfortunately, the practical attainment of these potentials is complicated by many less favorable factors, primarily low transverse properties. To provide improved transverse properties, composites are commonly made up into laminates with individual layers at different angles, like plywood. Thus, the laminate has enhanced transverse properties at the expense of some of the potential apparent in the unidirectional material. This loss of potential is evidenced by the lower portions of the bars on figure 1.10.

#### 1.3.4 Reinforcement Forms Other Than Continuous Filaments.

In addition to the continuous filaments with which this text is primarily concerned, and which, generally speaking, offer the greatest potential for performance, a variety of other forms of reinforcement are used in fiber composites. These include:

Chopped fibers—usually used in molding compounds, for ease of forming to complex shapes.

Continuous strand rovings—multiple filament bundles, for economy of manufacture of thick sections.

Mats—random or semioriented arrays of fibers of varying lengths, to provide economical reinforcement in bulk together with ease of forming to complex shapes for which performance requirements are less important than economy.

Woven fabrics—in various weave configurations, providing a compromise between the maximum performance attainable with unidirectional fibers and the ease of handling and formability of chopped fibers and mats.

For many manufacturing processes the reinforcements, whatever their form, are preimpregnated with resin to form a partially cured composite called a prepreg. This form can be converted to the desired final shape during the final curing step of the fabrication process.

#### 1.3.5 Fabrication Processes.

Fabrication processes for fiber composites in general involve some kind of die or mandrel to establish the desired shape, some means of fitting the fibers and resin to this shape, and means of applying proper curing conditions (temperature, pressure, and time along with provision for removal of excess resin and volatiles). Following are various ways by which these processes are carried out.

Contact molding—the reinforcements are placed in an open mold and cured. A flexible bag may be used to cover the composite and pressure or vacuum and heat applied to speed the cure and improve the quality of the part, in which case the process is called bag molding. Further increases in pressure can be achieved by the use of an autoclave. Contact molding is generally used when the quantities to be produced are not great enough to justify the cost of closed dies.

Compression and Injection Molding—matched dies (male and female) are used and the composite is either placed into the mold before it is closed (compression molding) or injected into the closed mold (injection molding). With the addition of heat and pressure, parts of uniform quality can be produced.

Filament winding—involves wrapping the filaments around the part. Filament winding machines of a high degree of sophistication have been developed for winding complex shapes with precisely oriented reinforcements.

Pultrusion—extrusion-like process, produces in a continuous process accurate, finished shapes of constant cross section efficiently and cost effectively.

This variety of fabrication processes makes available to the designer freedom to tailor the characteristics of fiber composites to meet the design requirements by precisely placing as many fibers as are wanted where they are wanted and in the directions in which they are wanted. For composites, accordingly, the design process becomes a complete cycle, from selection of constituents to final configuration, as discussed in the following section.

#### 1.4 THE DESIGN CYCLE FOR COMPOSITE STRUCTURES.

In any structural design problem, the first requirement is the determination of the governing design requirements, including not only functional requirements, i.e., mechanical, thermal, electrical, and chemical property requirements but also economic and performance objectives. To meet these requirements, the designer must select a material, a configuration, and a process for manufacture. This design process is essentially the same for composites and for conventional materials. With composites, however, there is an additional requirement that the material be designed along with the structure. Thus, there are more steps required in the design cycle than heretofore with metallic structures, as illustrated in figure 1.11.

The first of these steps (I in figure 1.11) is the selection of composite constituents and their volume fractions. These selections define the unidirectional composite (step II in figure 1.11) which is the basic element of the composite structural material. In general, however, multidirectional properties are required, and to provide these, a suitable multidirectional layup of the unidirectional basic element must be designed (step III in figure 1.11). It is only at this stage that the composite design cycle first reaches the starting point for design with isotropic metals. From this stage, the designer proceeds to the determination of the configuration of each of the structural elements (step IV in figure 1.11) and to the overall structural design configuration (step V in figure 1.11).

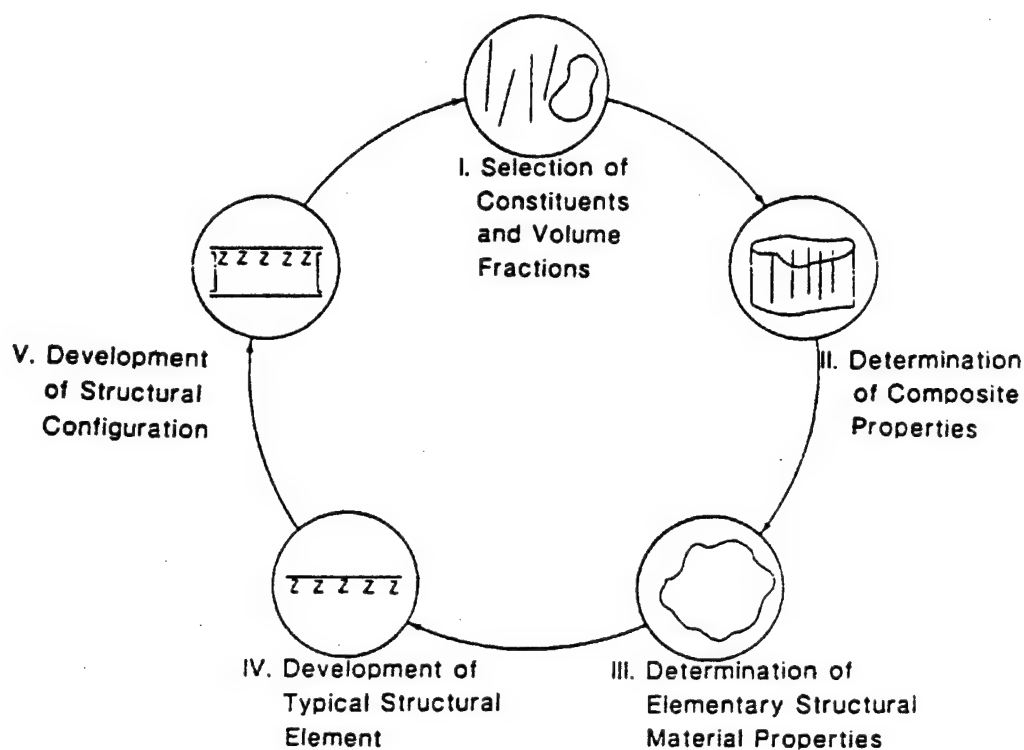


FIGURE 1.11. THE DESIGN CYCLE FOR COMPOSITE STRUCTURES INTRODUCES THE REQUIREMENT FOR DESIGNING MATERIAL AS WELL AS STRUCTURE

With composites, the possibilities of improvement in the design by reiteration of the design cycle are increased by the added steps in the design cycle. Thus, by the performance of a structural efficiency analysis of the structural design of V, guidelines may be generated for changes in constituent properties and laminate configurations, leading to improvements in performance of the composite structure.

For commercial applications, although high stiffness and strength must be achieved to attain low structural weight, long life and low manufacturing costs must be realized. Here the design process must place emphasis on the minimization of fabrication costs, as by integration of structural elements for reduction in part count. Here again the designer has the new flexibility provided by the ability to design the material as well as the structure, as suggested in figure 1.12. All of the usual constraints and requirements of the design process are amendable to treatment by design of both structure and material. The technology of structural design is long established; that of material design is new, but today it is sufficiently advanced that if it is understood in adequate depth it may be applied with confidence. The following chapters are directed toward the development of that understanding.

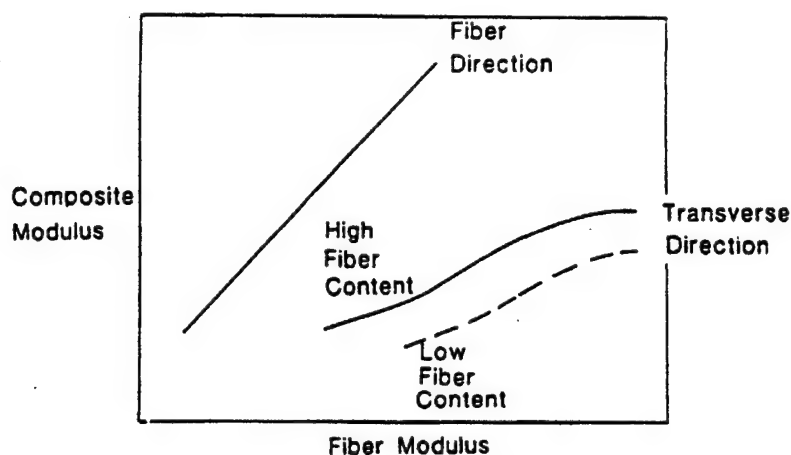


FIGURE 1.12. CHARACTERISTIC RELATIONSHIPS BETWEEN FIBER AND COMPOSITE STIFFNESS—DIRECTLY PROPORTIONAL IN THE FIBER DIRECTION BUT MUCH LESS THAN PROPORTIONAL TRANSVERSELY

## 1.5 SERVICE CHARACTERISTICS.

In addition to NASA and DoD programs, the greatest database of experience with composites in service has been established by marine applications. While the performance of composites in this area has been exemplary in almost all respects—structural integrity, ease of maintenance, and long service life—much of this durability derives from what would be considered overdesign in aircraft. Service characteristics for aircraft applications must be more thoroughly evaluated.

### 1.5.1 Durability.

Durability of fiber composites in aircraft is influenced by factors addressed quantitatively in design, such as fatigue loadings and environments to be encountered, and by service factors such as damage tolerance and inspection and repair in the field.

### 1.5.2 Fatigue.

Fatigue (to be treated in detail in succeeding chapters) characteristics of composites are different in many respects from those of metals. For simple tension of unidirectionally reinforced composites, fatigue limits are generally at higher percentages of tensile ultimate strengths. Thus, the composite durability in this regard might be expected to be superior to that of metals. For more complex loadings or reinforcement configurations, however, the superiority diminishes. In particular, compressive or fully reversed tension-compression load cycles tend to develop relatively more damage in composites than in metals. Intralaminar cracks and interlaminar defects grow from points of stress concentration more often than not at some interior layer where they are not evident to visual inspection. While methods of analysis are, indeed, complex, they can only be supplemented by tests, as the number of tests required to define fatigue properties adequately is prohibitive. Progress has been made in analytical methods, however, as will be described.

### 1.5.3 Environmental Effects.

Environmental effects upon the durability of composites further complicate the analysis of fatigue lifetimes. Temperature cycles between sunny tropical landing fields and subzero conditions at high altitudes induce thermal stresses due to differential expansions of fibers and matrix in the composite and due to differential expansions of adjoining structural components. Absorbed moisture in the composite induces expansions similar to those accompanying temperature increases. Both temperature and moisture increases in the material reduce its properties. Allowances for all these interacting effects must be made in the design and analysis of the composite.

### 1.5.4 Damage Tolerance.

As a general rule, the greater the ductility of a material, the greater its impact tolerance, and fibrous composites lack ductility. Of greatest concern in this area is the random, inadvertent type of damage inevitable in the long run in service. The stone bouncing up from the runway, the wrench dropped on the wing, the bird or hailstone that does not yield right of way to the airplane—any of which can cause a type of damage to which the composite is susceptible, that of lateral impact. Lateral impact on a fiber composite can induce a crazing, cracking type of damage which is usually most severe on the inner surface, often without detectable damage on the outer surface. Accompanying the inner surface damage may be internal disbonds and local separation of plies (i.e., delamination). While much research has been directed toward the alleviation of this problem, as by the addition of toughening agents to matrix materials, progress has not been significant. Fortunately, most lateral impact damage is not catastrophic and can be accommodated by adequate inspection and repair.

### 1.5.5 Test, Inspection, and Repair.

Determination of the adequacy of a composite at any stage of its service life is more complex than for metals. In the beginning, the fact that the composite material itself is designed and manufactured requires that it be inspected and qualified. In service, additional complexity arises because damage may develop internally as well as on the surface. Often internal damage such as disbonds may develop with no telltale surface evidence.

For quality control of the manufactured material, both destructive and nondestructive testing may be employed. Destructive testing involves cutting specimens from the material and identifying them as representative of that material for that structure and is employed, e.g., for (usually simple) tests of strength such as flexure or short beam shear or for tests of quality such as volume fraction reinforcement or void content. Nondestructive testing or evaluation (NDT or NDE) methods employ the transmission of nondestructive signals through the material. The signals may be thermal, electrical, ultrasonic, or x-ray. Automated scanning equipment is used to map the area in question and identify cracks, voids, disbonds, and the like. Details of equipment and methodology for NDE are given in the appropriate chapter in the text.

Repair techniques have been developed for the various types of damage encountered in service. The usual approach is the replacement of the damaged material together with the bonding or bolting of metal or composite reinforcing plates to adjacent surfaces to bridge the damaged area.

## 1.6 OVERVIEW.

In order to properly utilize the advantages of composite materials, it is necessary to develop an understanding of the analytical tools and methodologies that are employed in the design process. This section gives a brief overview of these design concepts and was written to delineate

1. the differences encountered in the characteristics of structures, because of the fact that they are made from composite materials instead of metals; and
2. the methods of evaluation, both analytical and experimental, that are available to be brought to bear upon the evaluation of those differences.

Thus, a basis is provided by the avoidance of problems with the use of composites and, hence, the successful utilization of their potentials.

To achieve the foregoing objectives, it is necessary to address many topics, ranging from fundamental mechanics to practical methods of manufacture. Moreover, in each category, the material must be sufficiently detailed to define not only possible problem areas but also the reasons for their existence and, hence, the appropriateness of the methods for their evaluation. Specifically, the material to be understood can be organized into the following categories:

- Unidirectional composites
- Laminates
- Test methods
- Structural analysis
- Structural design

The remainder of this section is devoted to an overview of each of these categories. However, this volume deals only with the first two topics. The last three are to be addressed in an accompanying volume.

### 1.6.1 Unidirectional Composites.

Various properties of unidirectional composites must be considered in detail in the characterization of this fundamental building block upon which the technology of fiber composites is based. These are all effective properties, i.e., relationships between statistical averages of state variables over representative volume elements sufficiently large to characterize the composite, as illustrated in figure 1.3 for tensile stress. Properties to be understood include:

- Elastic properties
- Thermal expansion coefficients
- Moisture swelling coefficients
- Viscoelastic properties
- Thermal and electrical conductivities
- Tensile, compressive, and shear strengths
- Strength under combined stresses
- Fatigue failure characteristics



Properties can be evaluated for various volume fraction reinforcement and for anisotropic as well as isotropic constituents. Both linear and nonlinear relationships exist between constituent properties and composite properties. For example, with a given matrix material, the composite Young's modulus is a linear function of the fiber modulus in the fiber direction but a highly nonlinear function of the fiber modulus transversely, as illustrated in figure 1.12. In all cases, formulae can be derived relating composite properties to the properties of the constituents.

### 1.6.2 Laminate Properties.

The objective of laminate analysis is to develop methods for calculating overall laminate properties given the unidirectional composite ply properties, as illustrated in figure 1.13. The outline of the concepts directed toward the achievement of this objective (table 1.3) reveals some of the complications encountered due to the many possible ways in which the individual laminae may be combined. Thus, while the stress-strain relations for each lamina can be found from the equations for the unidirectional composite, the combined behavior as a laminate must make assumptions about modes of deformation, account for symmetries of stacking, and develop models for overall failure, including interlaminar effects.

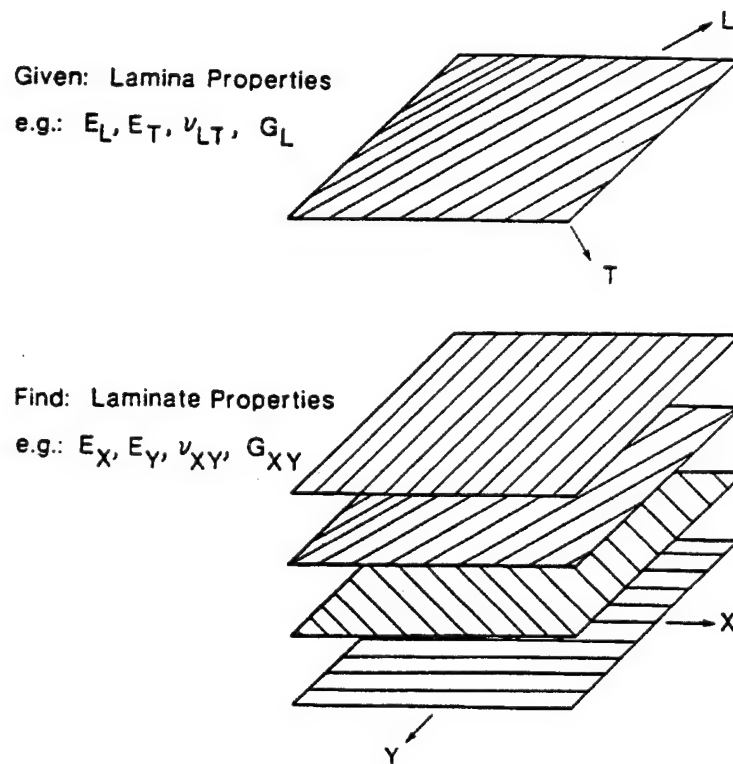


FIGURE 1.13. THE OBJECTIVE OF LAMINATE ANALYSIS: TO DETERMINE THE OVERALL PROPERTIES OF THE LAMINATE IN TERMS OF THE PROPERTIES OF THE INDIVIDUAL PLIES AND THEIR ORIENTATION

TABLE 1.3. CONCEPTUAL OUTLINE OF LAMINATE ANALYSIS

1.	Terminology
2.	Lamina Stress-Strain Relations
3.	Lamination Theory
4.	Laminate Behavior
	(a) Symmetric and Unsymmetric
	(b) Bending and Membrane
	(c) Thermo and Moisture Effects
5.	Netting Analysis
6.	Strength and Failure
7.	Inelastic Behavior
8.	Hygroscopic Analysis
9.	Interlaminar Stresses
10.	Fracture
11.	Fatigue
12.	Impact and Damage Tolerance

The lamination process does provide the designer with a powerful tool for adjusting properties to meet his requirements, as long as he is mindful of the interactions of those properties. For example, as shown in figure 1.14, the low oriented plies can be raised an order of magnitude by changes in ply orientations, with only a 50 percent decrease in longitudinal stiffness and no change in shear stiffness.

#### 1.6.3 Test Methods.

Although this topic is not discussed in this volume, a conceptual outline of composite test methods is given in table 1.4. Testing of composites, like their analysis and design, involves additional, separate procedures for constituents as well as for the composites themselves. Further, the sensitivity of composites to temperature and humidity demands tests in appropriate environments. For quality control, nondestructive evaluations are needed both on the production line and in the field, and adequate methods of repair must be applied for any damage found. In all of these areas, the techniques involved have enough differences from those associated with metals to deserve due consideration, with emphasis on aspects not encountered in the testing of conventional materials. The main thrust of the treatment of these various aspects of test methods for composites is toward the delineation of possible misleading results arising due to the unique response characteristics, not only those associated with unusual configurations, but especially those intrinsic to composites in general such as transverse and shear weaknesses.

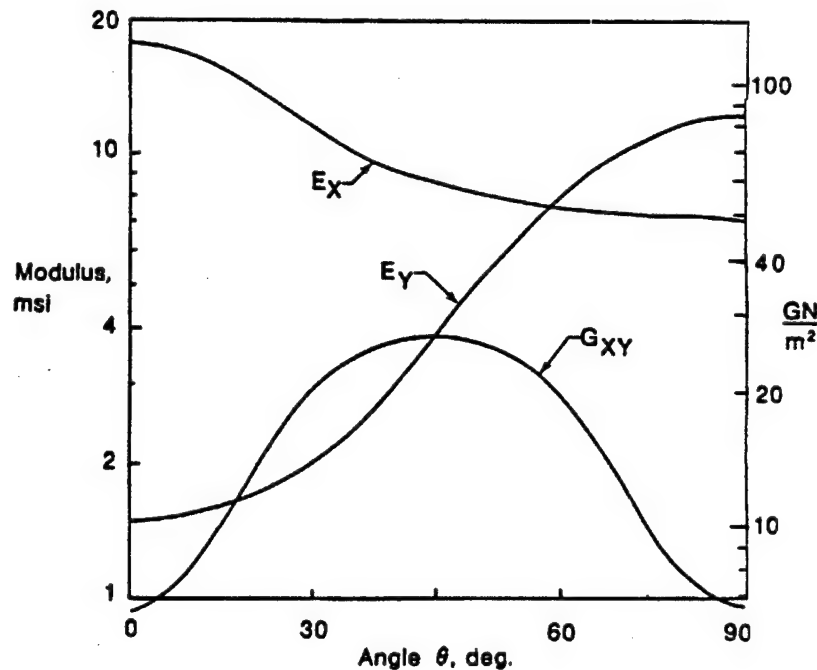


FIGURE 1.14. CHARACTERISTIC VARIATIONS IN LAMINATE PROPERTIES WITH PLY ORIENTATION ARE SUGGESTED BY A SIMPLE  $0^\circ/\pm\theta^\circ$  CONFIGURATION AS  $\theta$  IS VARIED FROM  $0^\circ$  TO  $90^\circ$ . The axial stiffness decreases from its maximum with all reinforcements at  $0^\circ$  to a minimum. The shear stiffness passes through a maximum at  $\theta=\pm 45^\circ$ .

TABLE 1.4. CONCEPTUAL OUTLINE OF COMPOSITE TEST METHODS

1. Constituent Test Methods
2. Physical Property Test Methods
3. Composite Test Methods
4. Environmental Test Methods
5. Structural Test Methods
6. Nondestructive Evaluation (NDE)
7. Repair Techniques
8. Evaluation of Design Allowables

The fundamentals of these problems are introduced schematically in figure 1.15. At the top of the figure, possible shearing distortions associated with simple tensile loadings are illustrated. These may arise, e.g., simply due to the stacking sequences of the plies in a laminate. The lower illustration suggests how such distortions may interact to yield complex modes of distortions under combined stresses. Among the implications is the important one that methods of load application (e.g., end fixtures) can be crucial to the outcome of even simple tests and may even be grossly misleading under complex conditions.

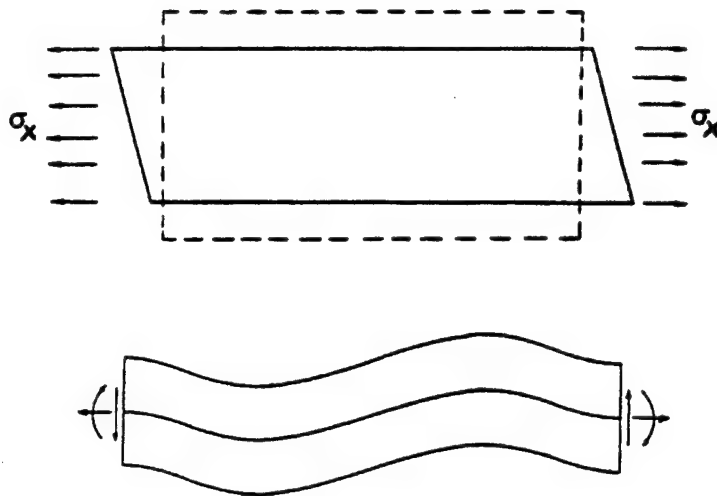


FIGURE 1.15. THE DIRECTIONAL PROPERTIES OF COMPOSITES MAY LEAD TO PROBLEMS IN TESTING, SUCH AS SHEAR DISTORTIONS DUE TO ASYMMETRIES WHEN AXIAL LOAD IS APPLIED AS SUGGESTED IN THE UPPER FIGURE OR LATERAL DISTORTIONS DUE TO LOW TRANSVERSE STIFFNESS AS IN THE LOWER FIGURE

Translation of test results to the establishment of design allowables is an area of composites technology which is still in a state of development. The definition of just what constitutes failure in a composite—a far more complex definition than in metals, and even for metals, still a controversial one in many cases—will require more guidance from field experience than has yet accumulated.

#### 1.6.4 Structural Analysis.

The analysis of composite structures is more complex than that of metal structures. Although it is often possible to utilize the effective properties of composites in conventional analysis procedures, it is sometimes necessary to distinguish between the macro and micro response and carry the analysis into the detail provided at the minor level. To employ the methodologies of structural analysis, including the topics listed in table 1.5, one must be able to define when one or the other of these levels of analysis is appropriate. One must also comprehend the differences encountered in structural response at the macro level from those for metals.

The differences can be substantial. For example, consider the buckling of a long, simply supported flat plate in compression. As illustrated in figure 1.16, the buckling stress can be increased appreciably by simply rotating a balanced (fifty percent  $0^\circ$ , fifty percent  $90^\circ$ )  $0^\circ/90^\circ$  laminate through an angle of  $45^\circ$  (giving equivalently a  $\pm 45^\circ$  reinforcement configuration), or intermediate values may be obtained at angles less than  $\pm 45^\circ$ . For metals, of course, there is no directional characteristic at all.

Because such differences can be encountered, one must understand the additional factors that need to be considered in composite analysis and utilize appropriate methods for their treatment.

TABLE 1.5. CONCEPTUAL OUTLINE OF COMPOSITES STRUCTURAL ANALYSIS

1.	Stress Analysis of Structural Elements
(a)	Beams
(b)	Plates
(c)	Shells
2.	Stability of Structural Elements
3.	Vibrations of Structural Elements
4.	Design and Analysis of Structural Joints
5.	Application of Numerical Analysis Techniques to Composite Structures

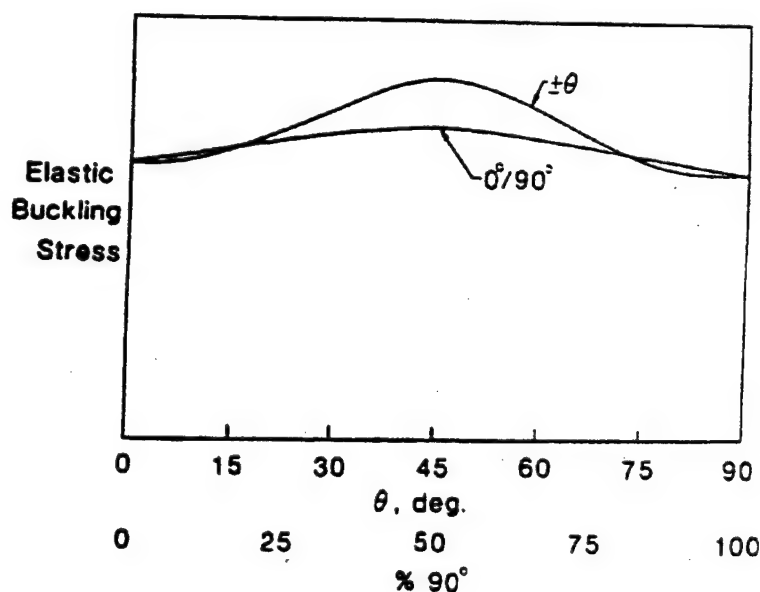


FIGURE 1.16. REINFORCEMENT CONFIGURATION HAS A MARKED INFLUENCE ON THE BUCKLING STRENGTH OF COMPOSITE PLATES IN COMPRESSION AS SHOWN BY THIS COMPARISON OF  $0^\circ/90^\circ$  AND  $\pm\theta$  LAMINATE. A  $\pm 45^\circ$  laminate has a substantially higher buckling stress than the same composite at  $0^\circ$  and  $90^\circ$ .

### 1.6.5 Structural Design.

The ultimate goal of this text is to provide an understanding of the employment of fiber composites in structural design. As the outline indicates (table 1.6), many aspects of the design process must be considered in light of the differences in characteristics between composites and metals beginning with the differences in design criteria and proceeding through detailed development of methodologies for design and evaluation to specific components of their application.

TABLE 1.6. CONCEPTUAL OUTLINE FOR COMPOSITES DESIGN

- |   |
|---|
| <ol style="list-style-type: none"><li>1. Review of Characteristic Differences in Design and Evaluation: Composite/Metal<ol style="list-style-type: none"><li>(a) Effects of Material Properties</li><li>(b) Typical Structural Elements</li></ol></li><li>2. Design Criteria</li><li>3. Development of Design and Evaluation Methodology<ol style="list-style-type: none"><li>(a) Minimum-Weight Design</li><li>(b) Cost Effectiveness</li><li>(c) Trade-Off Studies</li></ol></li><li>4. Review of Fabrication Techniques</li><li>5. Design and Evaluation of Aircraft Structural Components</li></ol> |
|---|

One of the methodologies that is especially important in composites because of its pertinence to both the design process and the process of evaluation is that of minimum-weight design. The principles of minimum-weight design are especially useful, not only for guidance in selections of both constituent materials and their configurations, but also to provide a yardstick for comparison among various approaches, including assessments of cost effectiveness.

### 1.7 CONCLUDING REMARKS.

The overview presented in this section describes the material to be presented in the two-volume text, of which this is the first. The material has been divided into two major categories; composite materials and laminates, treated herein, and structures, treated in volume II. This separation is a matter of convenience. An appreciation of the interrelationships among the various major topics is imperative to the successful application of composites.

## CHAPTER 2. CONSTITUENT PROPERTIES

*It is a capital mistake to theorize before one has data. Insensibly one begins to twist facts to suit theories, instead of theories to suit facts.*

Sir Arthur Conan Doyle,  
Adventures of Sherlock Holmes

Characteristics of composites inevitably stem from the properties of their constituents. Constituent properties were considered in a general way in chapter 1. As a basis for engineering, however, a more detailed, technical review of available constituent materials is needed. The constituents are the building blocks—the sophisticated building blocks—that have been developed which, properly used, can make truly advanced structures. Despite the sophistication, however, deficiencies still exist, and proper use demands that distinctions be made between merits and demerits. Accordingly, in the following review, emphasis is directed toward adequate definition of fundamental strengths and weaknesses, and representative values are given for properties rather than detailed values applicable to specific formulations.

### 2.1 FIBERS.

The most common classes of materials which have qualified as successful reinforcements are carbon and glass. Aramids have had qualified successes. Boron, alumina ( $\text{Al}_2\text{O}_3$ ), silicon carbide, and quartz are considered of interest for special applications. The following discussion will treat the carbon fibers and glass fibers in greatest depth and for the other fibers will be limited to consideration of their most significant properties.

The test methods used to obtain fiber properties should be considered briefly. Longitudinal mechanical properties are obtained from single fibers or bundles of fibers which may be dry or may be coated with various thicknesses of matrix material. The results will vary depending on the test method. In particular, the difficulty of obtaining transverse fiber properties from direct experimental measurements should be obvious. In a very limited number of cases, measurements have been made using an ultrasonic method [2.1]. Far more prevalent is the practice of measuring laminate properties and back-calculating transverse fiber properties using the analytical methods described in chapter 3. The two approaches have been compared for carbon fibers [2.2]. The transverse modulus calculated from lamina test results were significantly higher than those measured with the ultrasonic tests. Consequently, the use of laminate tests for determining the transverse properties should be considered. In the following chapters, emphasis is placed on transverse modulus values inferred from measurements made on composite specimens rather than directly from measurements on the fibers per se.

Properties for each material are presented in tables throughout this section. These data are provided to show the general trends in the material behavior. In many cases, complete data sets are not generally available, but existing information is shown. Where experimentally determined property values are not available for parameters required for calculations in the following

chapters, reasonable estimates are provided in parentheses. All of the data should be treated as generic information and not recommended for use in design.

### 2.1.1 Carbon.

Carbon fibers, often called graphite fibers although full graphitization is not achieved in their manufacture, are achieving wide acceptance for aircraft applications because of their advanced properties. Two categories of carbon fibers have predominated, distinguished primarily by their elastic moduli: high-strength carbon fibers with a typical modulus range 30-35 Msi (207-241 GPa) and high-modulus carbon fibers with a typical modulus range of 50-55 Msi (345-380 GPa). Properties of these fibers are given in table 2.1. Other higher-modulus carbon fibers, more loosely categorized as very high-modulus carbon fibers and ultrahigh-modulus carbon fibers, with moduli up to 120 Msi (830 GPa) are also available.

Both properties and costs of carbon fibers are in a state of flux relating to the methods of manufacture as described below.

#### 2.1.1.1 Methods of Manufacture.

Carbon fibers are manufactured by carbonization and graphitization from organic fiber precursors, primarily rayon, polyacrylonitrile (PAN), and pitch. For both rayon and PAN, in addition to carbonization and graphitization at temperatures of 2400 – 2700°F and 5400°F (1300 – 1500°C and 3000°C, respectively), stretching of the fibers is required to orient the molecular structure for maximum stiffness in the fiber direction. The pitch fibers do not require the stretching process, and the times at temperature required for them are less than for the rayon and PAN precursors. Pitch base fibers, accordingly, are potentially the cheapest.

All carbon fibers require surface treatment for adhesion to the matrix, most commonly a wet oxidation process together with the application of an organic coating.

#### 2.1.1.2 Available Forms.

Carbon fibers are available in a variety of forms—yarns (bundles of filaments), plied yarns (yarns twisted together), roving (large bundles of filaments, usually untwisted), and chopped strands (usually less than 2 inches (5 cm) long). The individual fiber diameters are approximately 0.0004 inch (0 .01 mm). Carbon fibers are also available in a variety of fabric forms.

#### 2.1.1.3 Outstanding Characteristics.

Carbon fibers are distinguished not only for their high stiffness and for their extremely high stiffness/density ratios but also for their near zero thermal expansion coefficients along the fiber direction. Their deficiencies are in the direction transverse to the fiber, where the higher the longitudinal modulus, the lower the transverse modulus.



TABLE 2.1. PROPERTIES OF CARBON FIBERS\*

• English Units

Property	Range	Examples			
		AS4*	IM7*	P120**	T300**
Longitudinal Tensile Modulus, $E_L$ , Msi	23 - 120	36	44	120	34
Transverse Tensile Modulus, $E_T$ , Msi	1.1 - 3.2				
Longitudinal Shear Modulus, $G_L$ , Msi	2.2 - 3.2				
Transverse Shear Modulus, $G_T$ , Msi	0.12 - 1.2			(0.38)†	(3.1)†
Longitudinal Poisson's Ratio, $\nu_L$	0.3 - 0.41				
Transverse Poisson's Ratio, $\nu_T$	0.35 - 0.45				
Tensile Strength, $\sigma_L^u$ , ksi	200 - 820	590	770	350	530
Strain at Tensile Ultimate, $\epsilon_L^u$ , %	0.3 - 1.81	1.65	1.81	0.29	1.4
Coefficient of Longitudinal Thermal Expansion, $\alpha_L$ , $10^{-6}/^{\circ}\text{F}$	-0.28 - -0.89			-0.8	-0.3
Coefficient of Transverse Thermal Expansion, $\alpha_T$ , $10^{-6}/^{\circ}\text{F}$	3.9 - 5.4				
Longitudinal Thermal Conductivity, $\mu_L$ , $\frac{\text{Btu} \cdot \text{in}}{\text{hr} \cdot \text{ft}^2 \cdot ^{\circ}\text{F}}$	60 - 4400			4400	60
Transverse Thermal Conductivity, $\mu_T$ , $\frac{\text{Btu} \cdot \text{in}}{\text{hr} \cdot \text{ft}^2 \cdot ^{\circ}\text{F}}$	10 - 12				
Density, $\rho$ , lb/in <sup>3</sup>	0.061 - 0.079	0.065	0.064	0.079	0.064

\*References 2.2 thru 2.8

†Back calculated in reference 2.2

\*\* Trade Names

TABLE 2.1. PROPERTIES OF CARBON FIBERS (continued)\*

• Standard International (SI) Units

Property	Range	Examples			
		AS4**	IM7**	P120**	T300**
Longitudinal Tensile Modulus, $E_L$ , GPa	160 - 830	250	300	830	230
Transverse Tensile Modulus, $E_T$ , GPa	7.6 - 22				
Longitudinal Shear Modulus, $G_L$ , GPa	15 - 22				
Transverse Shear Modulus, $G_T$ , GPa	2.8 - 8.3			(2.6)†	(8.3)†
Longitudinal Poisson's Ratio, $\nu_L$	0.3 - 0.41				
Transverse Poisson's Ratio, $\nu_T$	0.35 - 0.45				
Tensile Strength, $\sigma_L^u$ , MPa	1400 - 5600	4100	5300	2400	3700
Strain at Tensile Ultimate, $\epsilon_L^u$ , %	0.3 - 1.81	1.65	1.81	0.29	1.4
Coefficient of Longitudinal Thermal Expansion, $\alpha_L$ , $10^{-6}/K$	-0.5 - -1.6			-1.4	-0.5
Coefficient of Transverse Thermal Expansion, $\alpha_T$ , $10^{-6}/K$	7.0 - 9.7				
Longitudinal Thermal Conductivity, $\mu_L$ , $\frac{W}{m \cdot K}$	8.5 - 640			640	8.5
Transverse Thermal Conductivity, $\mu_T$ , $\frac{W}{m \cdot K}$	1.4 - 1.7				
Density, $\rho$ , gm/cm <sup>3</sup>	1.69 - 2.18	1.80	1.78	2.18	1.77

\*References 2.2 thru 2.8

†Back calculated in reference 2.2

\*\* Trade Names

### 2.1.2 Glass.

Two compositions of glass are predominately used in the aircraft industry - E-glass ( $\text{SiO}_2 \approx 62\%$ ,  $\text{Al}_2\text{O}_3 \approx 14.7\%$ ,  $\text{CaO} \approx 23.3\%$ ) and S-2 glass ( $\text{SiO}_2 \approx 65\%$ ,  $\text{Al}_2\text{O}_3 \approx 25\%$ ,  $\text{MgO} \approx 10\%$ ). Properties of these fibers are listed in table 2.2 with other related fibers. Significantly, despite the better mechanical properties in all categories shown for S-2 glass, the bottom line economy of E-glass has made it overwhelmingly the material of choice.

TABLE 2.2. PROPERTIES OF GLASS AND CERAMIC FIBERS\*

• English Units

Property	E-glass	S-2 glass	Astro-quartz II	Alumina	Silicon carbide
Longitudinal Tensile Modulus, $E_L$ , Msi	11.8	12.9	10	28-55	26-65
Transverse Tensile Modulus, $E_T$ , Msi	(12)†	(12)†	(10)†		(60)†
Longitudinal Shear Modulus, $G_L$ , Msi	(4)†	(6)†	(4)†		(25)†
Transverse Shear Modulus, $G_T$ , Msi	(4)†	(6)†	(4)†		(25)†
Longitudinal Poisson's Ratio, $\nu_L$	0.22	(0.2)†	(0.16)†		(0.15)†
Transverse Poisson's Ratio, $\nu_T$	(0.2)†	(0.2)†	(0.16)†		(0.15)†
Tensile Strength, $\sigma_L^u$ , ksi	500	665	870	200-266	290-570
Strain at Tensile Ultimate, $\epsilon_L^u$ , %	4.9	5.7	8.7	8.8	1.7-2.7
Coefficient of Longitudinal Thermal Expansion, $\alpha_L$ , $10^{-6}/^\circ\text{F}$	3.0	0.9	0.3		
Coefficient of Transverse Thermal Expansion, $\alpha_T$ , $10^{-6}/^\circ\text{F}$					
Longitudinal Thermal Conductivity, $\mu_L$ , $\frac{\text{Btu} \cdot \text{in}}{\text{hr} \cdot \text{ft}^2 \cdot ^\circ\text{F}}$	8.9		9.5		
Transverse Thermal Conductivity, $\mu_T$ , $\frac{\text{Btu} \cdot \text{in}}{\text{hr} \cdot \text{ft}^2 \cdot ^\circ\text{F}}$					
Density, $\rho$ , lb/in <sup>3</sup>	0.095	0.090	0.080	0.12-0.14	0.092-0.125

\*References 2.9 thru 2.14

†Rough estimate to start micromechanics analysis

TABLE 2.2. PROPERTIES OF GLASS AND CERAMIC FIBERS (continued)\*

• Standard International (SI) Units

Property	E-glass	S-2 glass	Astro-quartz II	Alumina	Silicon carbide
Longitudinal Tensile Modulus, $E_L$ , GPa	81.4	88.9	69	190-380	180-450
Transverse Tensile Modulus, $E_T$ , GPa	(81)†	(83)†	(70)†		(60)†
Longitudinal Shear Modulus, $G_L$ , GPa	(30)†	(40)†	(30)†		(25)†
Transverse Shear Modulus, $G_T$ , GPa	(30)†	(40)†	(30)†		(25)†
Longitudinal Poisson's Ratio, $\nu_L$	0.22	(0.2)†	(0.16)†		(0.15)†
Transverse Poisson's Ratio, $\nu_T$	(0.2)†	(0.2)†	(0.16)†		(0.15)†
Tensile Strength, $\sigma_L^m$ , MPa	3450	4590	6000	1380-1830	2000-3930
Strain at Tensile Ultimate, $\epsilon_L^m$ , %	4.9	5.7	8.7	8.8	1.7-2.7
Coefficient of Longitudinal Thermal Expansion, $\alpha_L$ , $10^{-6}/^{\circ}\text{C}$	5.4	1.6	0.5		
Coefficient of Transverse Thermal Expansion, $\alpha_T$ , $10^{-6}/^{\circ}\text{C}$					
Longitudinal Thermal Conductivity, $\mu_L$ , $\frac{\text{W}}{\text{m} \cdot \text{K}}$	1.3	1.4			
Transverse Thermal Conductivity, $\mu_T$ , $\frac{\text{W}}{\text{m} \cdot \text{K}}$					
Density, $\rho$ , $\text{gm/cm}^3$	2.6	2.5	2.2	3.3-3.9	2.5-3.5

\*References 2.9 thru 2.14

†Rough estimate to start micromechanics analysis

### 2.1.2.1 Method of Manufacture.

Glass fibers are made by pulling the molten state through relatively large multiple orifices at high velocities, the final diameters being controlled by the stretching external to the orifice. Individual filaments are coated with a sizing such as starch to avoid damage as the strands are given a slight twist to bring them together to form a yarn. A common number of individual filaments for yarn is 204.

#### 2.1.2.2 Available Forms.

Glass fibers are available in a variety of forms: yarns (bundles of filaments), plied yarns (yarns twisted together), roving (large bundles of filaments, usually untwisted), mat (continuous strands matted together), and chopped strands (usually less than 2 inches (5 cm) long). Fiber diameters vary from 0.00015 to 0.00052 inch (0.0038 to 0.0132 mm). A standard nomenclature has been developed to identify glass yarns e.g., ECG 150 4/2

where

E	E-glass
C	continuous filament
G	0.00036 in (0.091 mm) filament diameter
150	yarn weight in hundreds of yards per pound
4	4 basic yarn strands
2	2 plies of the 4-yarn strands

and where the third letter diameter key is as follows:

B	0.00015 in. (0.0038 mm)
C	0.00018 in. (0.0046 mm)
D	0.00021 in. (0.0053 mm)
E	0.00029 in. (0.0074 mm)
G	0.00036 in. (0.0091 mm)
H	0.00042 in. (0.0107 mm)
K	0.00051 in. (0.0130 mm)

Glass fibers are also available in a variety of woven fabric forms. For aircraft applications the most commonly encountered is an eight-harness satin weave, designated 181 style, designed to provide long "floats" of the yarns (one up, seven down, as illustrated in figure 2.1) for minimum out-of-straightness along the filaments.

#### 2.1.2.3 Surface Treatment.

For use as reinforcements, glass fibers generally require surface treatment for better adherence to the matrix. Most commonly used for this purpose are silane resins having molecules compatible with both the inorganic molecules of the glass and the organic molecules of the resin.

#### 2.1.2.4 Outstanding Characteristics.

The outstanding merits of the glass fibers are high strengths combined with a relatively high strain (~5%) to failure and low cost. They exhibit no outstanding unfavorable properties.

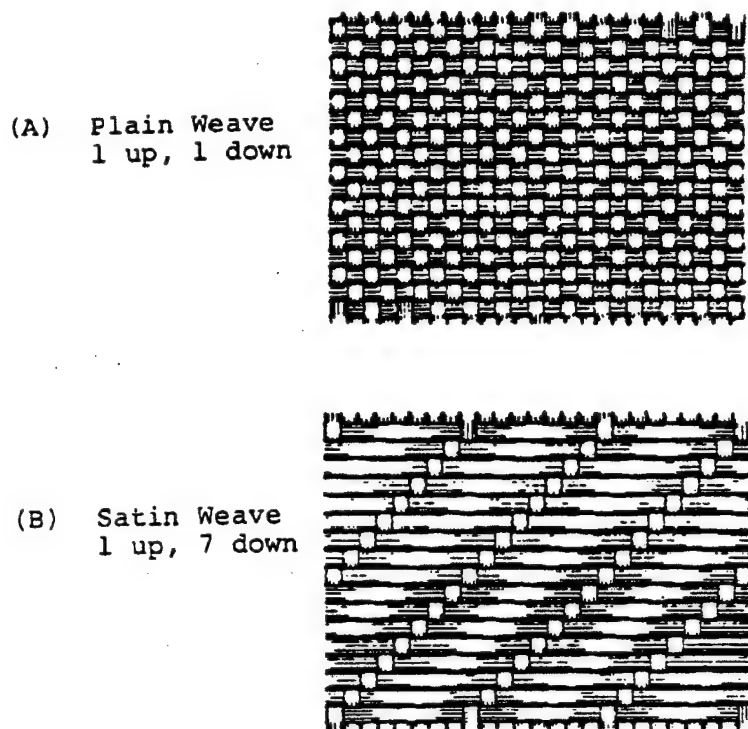


FIGURE 2.1. THE LONG "FLOATS" BETWEEN CROSSOVERS IN BOTH WARP AND FILL DIRECTIONS, AS IN THE EIGHT-HARNESS SATIN WEAVE SHOWN, PROVIDE NEAR STRAIGHT YARNS IN A BIAXIAL REINFORCING PATTERN, APPROXIMATING IN ONE PLY THE PROPERTIES OF A CROSSPLY LAMINATE

#### 2.1.3 Quartz.

Quartz fiber is silica glass of very high purity. It has the highest strength-to-weight ratio of any of the high-temperature materials. Quartz can be used for service temperatures up to 1920°F (1050°C). Available forms include plied yarns, rovings, and several forms of woven fabric. The same designation system, as is used for glass fibers, is used for quartz fibers with a "Q" prefix.

#### 2.1.4 Alumina.

Alumina or aluminum oxide filaments, e.g., FP produced by DuPont, have elastic properties similar to boron and silicon carbide but exhibiting very high compressive and relatively low tensile strengths. Like the SiC whisker/particle mixture, FP is used with metal matrices (magnesium and aluminum). The density of FP is the greatest of any of the filamentary reinforcements (0.143 pci or 3.96 g/cm<sup>3</sup>). This high density, together with its low tensile strength (table 2.2), limits its applicability to special problem areas.

### 2.1.5 Silicon Carbide.

Silicon carbide filaments have been made by three different processes including vapor deposition. Their most prominent properties cover the area of thermal resistance at temperatures in excess of 2640°F (1450°C) (see table 2.2), although the density of silicon carbide is substantially higher (0.115 pci or 3.19 g/cm<sup>3</sup>). Silicon carbide filaments are used primarily in metal matrix composites with matrix materials of aluminum, titanium, and molybdenum. Silicon carbide is also under development in a more economical form of a mixture of whiskers and particles produced by carbonization of rice hulls.

### 2.1.6 Kevlar.

Aramid fibers are now available in several forms distinguished primarily by their modulus. Properties of aramid fibers are given in table 2.3. The most common source for aramid is DuPont which produces three types of Kevlar.

#### 2.1.6.1 Available Forms.

Aramid fibers are available as untwisted yarns, roving, and woven fabric in various constructions. Each filament is nominally 0.00047 inch (0.0119 mm) in diameter.

#### 2.1.6.2 Surface Treatment.

Nominally, aramid fibers are available with no sizing or finish and require none for compatibility with resin matrix materials.

#### 2.1.6.3 Outstanding Characteristics.

The outstanding favorable characteristics of aramid are its low density (0.052 or 1.44 g/cm<sup>3</sup>) and high tensile strength, a maximum of 525 ksi (3.6 GN/m<sup>2</sup>) for optimum conditions of yarn impregnation and twist. Its unfavorable properties are low transverse stiffness and low compressive strength. Aramid/polymer composites exhibit high resistance to impact damage.

TABLE 2.3. PROPERTIES OF ARAMID FIBERS\*

• English Units

Property	Range	Examples			
		Kevlar 29	Kevlar 49	Kevlar 149	HM-50
Longitudinal Tensile Modulus, $E_L$ , Msi	12 - 25	12	18-19	25-27	12
Transverse Tensile Modulus, $E_T$ , Msi		(8)†	(11)†	(16)†	(8)†
Longitudinal Shear Modulus, $G_L$ , Msi		(0.3)†	(0.4)†	(0.6)†	(0.3)†
Transverse Shear Modulus, $G_T$ , Msi		(0.3)†	(0.4)†	(0.6)†	(0.3)†
Longitudinal Poisson's Ratio, $\nu_L$		(0.35)†	(0.35)†	(0.35)†	(0.35)†
Transverse Poisson's Ratio, $\nu_T$		(0.35)†	(0.35)†	(0.35)†	(0.35)†
Tensile Strength, $\sigma_L^u$ , ksi	450 - 600	525	525-600	500	450
Strain at Tensile Ultimate, $\epsilon_L^u$ , %	2.0 - 4.4	4-4.4	2.8-2.9	2.0	4.4
Coefficient of Longitudinal Thermal Expansion, $\alpha_L$ , $10^{-6}/^{\circ}\text{F}$	-3.0	-2.0	-3.5		
Coefficient of Transverse Thermal Expansion, $\alpha_T$ , $10^{-6}/^{\circ}\text{F}$	33				
Longitudinal Thermal Conductivity, $\mu_L$ , $\frac{\text{Btu} \cdot \text{in}}{\text{hr} \cdot \text{ft}^2 \cdot ^{\circ}\text{F}}$					
Transverse Thermal Conductivity, $\mu_T$ , $\frac{\text{Btu} \cdot \text{in}}{\text{hr} \cdot \text{ft}^2 \cdot ^{\circ}\text{F}}$					
Density, $\rho$ , lb/in <sup>3</sup>	0.050 - 0.052	0.052	0.052	0.052	0.050

\*References 2.15 thru 2.17

Rough estimate to start micromechanics analysis



TABLE 2.3. PROPERTIES OF ARAMID FIBERS (continued)\*

• Standard International (SI) Units

Property	Range	Examples			
		Kevlar 29	Kevlar 49	Kevlar 149	HM-50
Longitudinal Tensile Modulus, $E_L$ , GPa	83 - 190	93	120-130	170-190	83
Transverse Tensile Modulus, $E_T$ , GPa		(50)†	(80)†	(110)†	(50)†
Longitudinal Shear Modulus, $G_L$ , GPa		(2)†	(3)†	(4)†	(2)†
Transverse Shear Modulus, $G_T$ , GPa		(2)†	(3)†	(4)†	(2)†
Longitudinal Poisson's Ratio, $\nu_L$		(0.35)†	(0.35)†	(0.35)†	(0.35)†
Transverse Poisson's Ratio, $\nu_T$		(0.35)†	(0.35)†	(0.35)†	(0.35)†
Tensile Strength, $\sigma_L^m$ , MPa	3100 - 4100	3600	3600-4100	3400	3100
Strain at Tensile Ultimate, $\epsilon_L^m$ , %	2.0 - 4.4	4-4.4	2.8-2.9	2	4.4
Coefficient of Longitudinal Thermal Expansion, $\alpha_L$ , $10^{-6}/^{\circ}\text{C}$	-3.6 - -6.3	-3.6	-6.3		
Coefficient of Transverse Thermal Expansion, $\alpha_T$ , $10^{-6}/^{\circ}\text{C}$	59				
Longitudinal Thermal Conductivity, $\mu_L$ , $\frac{\text{W}}{\text{m} \cdot \text{K}}$					
Transverse Thermal Conductivity, $\mu_T$ , $\frac{\text{W}}{\text{m} \cdot \text{K}}$					
Density, $\rho$ , $\text{gm/cm}^3$	1.38 - 1.44	1.44	1.44	1.44	1.38

\*References 2.15 thru 2.17

†Rough estimate to start micromechanics analysis

### 2.1.7 Boron.

Boron filaments, fabricated by vapor deposition on fine tungsten or graphite filaments, have much greater diameters (0.004 inch or 0.1 mm) than other fibers. The large diameter makes them individually stiff and difficult to form to any but gentle radii. The manufacturing process holds little potential for cost reduction.

Properties of boron fibers are given in table 2.4. Most favorable is the combination of high strengths, both in tension and compression, and modulus of elasticity, not only along the fibers but also transversely. Not indicated in the table but also favorable is the fact that boron composites exhibit compressive strengths generally higher than those of carbon.

TABLE 2.4. PROPERTIES OF BORON AND POLYETHYLENE FIBERS\*

- English Units

Property	Boron	Polyethylene
Longitudinal Tensile Modulus, $E_L$ , Msi	40 - 55	17 - 25
Transverse Tensile Modulus, $E_T$ , Msi		
Longitudinal Shear Modulus, $G_L$ , Msi		
Transverse Shear Modulus, $G_T$ , Msi		
Longitudinal Poisson's Ratio, $\nu_L$		
Transverse Poisson's Ratio, $\nu_T$		
Tensile Strength, $\sigma_L^u$ , ksi	300 - 820	375 - 480
Strain at Tensile Ultimate, $\epsilon_L^u$ , %		0.7 - 3.5
Coefficient of Longitudinal Thermal Expansion, $\alpha_L$ , $10^{-6}/^{\circ}\text{F}$	2.5 - 3.0	
Coefficient of Transverse Thermal Expansion, $\alpha_T$ , $10^{-6}/^{\circ}\text{F}$		
Longitudinal Thermal Conductivity, $\mu_L$ , $\frac{\text{Btu} \cdot \text{in}}{\text{hr} \cdot \text{ft}^2 \cdot ^{\circ}\text{F}}$		
Transverse Thermal Conductivity, $\mu_T$ , $\frac{\text{Btu} \cdot \text{in}}{\text{hr} \cdot \text{ft}^2 \cdot ^{\circ}\text{F}}$		
Density, $\rho$ , lb/in <sup>3</sup>	0.090 - 0.093	0.035

\*References 2.18 thru 2.23

TABLE 2.4. PROPERTIES OF BORON AND POLYETHYLENE FIBERS (continued)\*

• Standard International (SI) Units

Property	Boron	Polyethylene
Longitudinal Tensile Modulus, $E_L$ , GPa	280 - 380	120 - 170
Transverse Tensile Modulus, $E_T$ , GPa		
Longitudinal Shear Modulus, $G_L$ , GPa		
Transverse Shear Modulus, $G_T$ , GPa		
Longitudinal Poisson's Ratio, $\nu_L$		
Transverse Poisson's Ratio, $\nu_T$		
Tensile Strength, $\sigma_L^u$ , MPa	2100 - 5700	2600 - 3300
Strain at Tensile Ultimate, $\epsilon_L^u$ , %		0.7 - 3.5
Coefficient of Longitudinal Thermal Expansion, $\alpha_L$ , $10^{-6}/^{\circ}\text{C}$	4.5 - 5.4	
Coefficient of Transverse Thermal Expansion, $\alpha_T$ , $10^{-6}/^{\circ}\text{C}$		
Longitudinal Thermal Conductivity, $\mu_L$ , $\frac{\text{W}}{\text{m} \cdot \text{K}}$		
Transverse Thermal Conductivity, $\mu_T$ , $\frac{\text{W}}{\text{m} \cdot \text{K}}$		
Density, $\rho$ , $\text{gm}/\text{cm}^3$	2.5 - 2.6	0.97

\*References 2.18 thru 2.23

### 2.1.8 Polyethylene.

Polyethylene fibers are based on ultrahigh molecular weight polyethylene. Advantages are low density and high strength and impact energy absorption. Properties for polyethylene fibers are shown in table 2.4.

## 2.2 MATRIX MATERIALS.

While reinforced plastics in general use, for which structural performance is subsidiary to cost and ease of manufacture, employ a variety of resins (predominately polyester and vinyl ester), epoxies are the resins most often used for the more demanding requirements in aircraft. Because of the widespread use of polyesters in general, however, a brief description of their characteristics is presented here as background material. The epoxies are discussed in some detail. The range of candidate matrix materials has expanded to include a variety of thermoset and thermoplastic polymers. A thermoset is a polymer that is substantially infusible and insoluble after being cured. A thermoplastic is a polymer that can be repeatedly softened by heating and hardened by cooling. In addition to epoxies and polyesters, thermosets to be considered include phenolics and polyimides. Thermoplastic materials to be considered are polyimides, polyether-ether-ketone (PEEK), polyamide, polyethylene, polypropylene, polysulfone, and poly(amide-imide). The material properties of matrix materials are generally isotropic.

### 2.2.1 Polyesters.

The polyesters are derived from unsaturated dibasic acids condensed with glycol. They are generally supplied as solutions in reactive monomers such as styrene, methyl methacrylate, or vinyl toluene. With the addition of heat or an initiator and catalyst, the polyester and monomer polymerize. The polymerization process is exothermic and the resin shrinkage is substantial: 7 to 9 percent. Typical resulting resin properties are shown in table 2.5.

### 2.2.2 Epoxies.

Although there are only two main types of epoxy resins, (1) condensation products of epichlorhydrin and bisphenol-A and (2) the same with novolac resins instead of bisphenol-A, the variety of characteristics available through the use of additives, changes in cure cycle, etc., is virtually unlimited. Available modifying and curing agents provide great latitude in the formulation of epoxy materials with the result that most manufacturers have their own proprietary formulations and cure cycles and resulting individualized properties. Ranges of properties for epoxy resins are shown in table 2.5. Typical properties actually achieved in aircraft applications are likely to be of the following magnitudes:

Tensile strength	9.5-11.5 ksi (66-79 MPa)
Compressive strength	17-24 ksi (120-170 MPa)
Young's modulus	0.45-0.50 ksi (3.1-3.4 GPa)
Density	0.042-0.045 lb/in <sup>3</sup> (1.15-1.25 g/cm <sup>3</sup> )

But all concerned must be aware of the ease with which variations from such typical values can be achieved. Factors involved in such variations are considered below.

TABLE 2.5. PROPERTIES OF THERMOSET MATRIX MATERIALS\*

• English Units

Property	Polyester	Epoxy	Phenolic	Polyimide
Young's Modulus, E, Msi	0.15-0.65	0.001-0.5	0.4-0.7	0.47-0.75
Poisson's Ratio, $\nu$		(0.3)†		
Tensile Strength, $\sigma^u$ , ksi	4-10	2-13	5-9	4.3-23
Compressive Strength, $\sigma^c$ , ksi	12-37	1-24	12-15	27-40
Strain at Tensile Ultimate, $\epsilon^u$ , %	1.7-2.6	3-6	1.5-2.0	1-8
Coefficient of Thermal Expansion, $\alpha$ , $10^{-6}/^{\circ}\text{F}$	39-56	11-56	38	8-28
Thermal Conductivity, $\mu$ , $\frac{\text{Btu} \cdot \text{in}}{\text{hr} \cdot \text{ft}^2 \cdot ^{\circ}\text{F}}$	1.2-1.4	1.2-3.6		2.5-6.8
Density, $\rho$ , lb/in <sup>3</sup>	0.041-0.053	0.035-0.051	0.045-0.048	0.044-0.052

• Standard International (SI) Units

Property	Polyester	Epoxy	Phenolic	Polyimide
Young's Modulus, E, GPa	1.0-4.5	0.007-3.4	2.8-4.8	3.2-5.2
Poisson's Ratio, $\nu$				
Tensile Strength, $\sigma^u$ , MPa	28-70	14-90	34-62	30-570
Compressive Strength, $\sigma^c$ , MPa	83-260	7-170	83-100	190-280
Strain at Tensile Ultimate, $\epsilon^u$ , %	1.7-2.6	3-6	1.5-2.0	1-8
Coefficient of Thermal Expansion, $\alpha$ , $10^{-6}/^{\circ}\text{C}$	70-100	20-100	68	15-50
Thermal Conductivity, $\mu$ , $\frac{\text{W}}{\text{m} \cdot \text{K}}$				
Density, $\rho$ , gm/cm <sup>3</sup>	1.12-1.46	0.96-1.40	1.24-1.32	1.22-1.43

\*References 2.24 thru 2.26

†Rough estimate to start micromechanics analysis

#### 2.2.2.1 Curing.

Epoxies are normally cured by cross-linking reactions with a curing agent. In most cases, no volatile by-products are formed, and the reaction can be completed at low or contact pressure. Epoxies shrink much less on curing than polyesters (3% versus 7% to 9%) and the exotherm during polymerization can generally be accelerated by the application of heat. Indeed, epoxy polymerization reactions seldom proceed to a complete cure without an extended postcure cycle at elevated temperature. Accelerators such as benzyl dimethylamine (BDMA) can speed up the process. An added 1 percent of BDMA can decrease the cure time from several hours to one hour as well as lower the required cure temperature. There is strong evidence [2.27] that these systems have not yet had the benefits of process optimization.

#### 2.2.2.2 Additives.

The addition of modifiers, such as polyamide resins or thiokols, will produce semirigid epoxy formulations. The usual objective here is an increase in toughness for shock absorbing properties and high impact strength. The semirigidity is generally accompanied by a strength decrease, however, and here again an optimization is needed.

#### 2.2.2.3 Environmental Factors.

Epoxies absorb moisture, generally up to 4-5 percent by weight. The absorbed moisture causes a growth of the resin, similar to a thermal expansion, and also causes a degradation in mechanical properties. Because of its large thermal expansion coefficient, epoxy also changes volume at a rate approximately ten times that of glass fibers and many times that of carbon fibers. Methods for the evaluation of these environmental effects will be treated in later chapters.

#### 2.2.2.4 Outstanding Characteristics.

Epoxies have proven to be versatile resins possessing the best combination of properties yet found for a wide range of composite requirements. They can be used for casting, impregnating, potting, laminating, and surface coating, and they are outstanding for adhesion to the reinforcing filaments and between plies. While the epoxies have demonstrated superiority, they still have deficiencies in strength and impact resistance. Much of the emphasis in the following chapters is directed toward the determination of the influence of these deficiencies upon overall composite performance.

#### 2.2.3 Phenolics.

Phenolics are based on the reaction of phenol and formaldehyde, condensation cured. One of the advantages of phenolics is the ability to form shapes with complex curves. Additionally, dimensional stability, creep resistance, and use at higher temperatures than thermoplastics can be advantageous. Typical properties for phenolics are found in table 2.5.

#### 2.2.4 Polyimides.

Both thermosetting and thermoplastic polyimides are available. The thermoset polyimides, derived from an additional reaction between imide monomers or oligomers, include bismaleimides and Diels-Alder types such as PMR-15. The thermoset polyimides are useful for mechanical properties such as creep resistance and tensile strength. The thermoplastic polyimides provide higher toughness and service temperatures. The thermoplastic polyimides are derived from the reaction between cyclic anhydrides and their derivatives and diamines. Typical properties are found in table 2.5 for thermoset polyimides and table 2.6 for thermoplastic polyimides [2.25].

#### 2.2.5 Thermoplastics.

Thermoplastics provide an advantage over thermosets in terms of processing speed. The thermoplastic materials are generally divided into two types - semicrystalline and amorphous [2.28]. The semicrystalline thermoplastics have a molecular structure that is, at least partially, an ordered array in three dimensions. The amorphous materials contain molecules that are unable to pack into such an ordered array. Advantages of the semicrystalline thermoplastics, which include polyether-ether-ketone (PEEK), polyethylene, polypropylene, polysulfone, and polyamide are toughness, good mechanical properties, and low moisture absorption. Primary advantages of the amorphous thermoplastics include high temperature capabilities, good mechanical properties, and chemical stability. The amorphous materials included in table 2.6 are the polysulfones and the polyamide-imides.

TABLE 2.6. PROPERTIES OF THERMOPLASTIC MATRIX MATERIALS\*

• English Units

Property	Polyimide	PEEK	Polyamide
Young's Modulus, E, Msi	3.0-4.1	0.57	0.39-1.1
Poisson's Ratio, $\nu$			
Tensile Strength, $\sigma^u$ , ksi	69-110		5.0-14
Compressive Strength, $\sigma^c$ , ksi	30-40		2.4-15
Strain at Tensile Ultimate, $\epsilon^u$ , %	1-60		55-300
Coefficient of Thermal Expansion, $\alpha$ , $10^{-6}/^{\circ}\text{F}$	25-31		45-83
Thermal Conductivity, $\mu$ , $\frac{\text{Btu} \cdot \text{in}}{\text{hr} \cdot \text{ft}^2 \cdot ^{\circ}\text{F}}$			1.5-1.7
Density, $\rho$ , lb/in <sup>3</sup>	0.046-0.052		0.038-0.042

• Standard International (SI) Units

Property	Polyimide	PEEK	Polyamide
Young's Modulus, E, GPa	21-28	3.9	2.7-7.6
Poisson's Ratio, $\nu$			
Tensile Strength, $\sigma^u$ , MPa	480-760		34-97
Compressive Strength, $\sigma^c$ , MPa	210-280		17-100
Strain at Tensile Ultimate, $\epsilon^u$ , %	1-60		55-300
Coefficient of Thermal Expansion, $\alpha$ , $10^{-6}/^{\circ}\text{C}$	45-56		
Thermal Conductivity, $\mu$ , $\frac{\text{W}}{\text{m} \cdot \text{K}}$			
Density, $\rho$ , gm/cm <sup>3</sup>	1.27-1.43		1.06-1.15

\*References 2.24, 2.25, 2.26, 2.29



TABLE 2.6. PROPERTIES OF THERMOPLASTIC MATRIX MATERIALS (continued)\*

• English Units

Property	Polyethylene (HMW)	Poly- propylene	Poly- sulfone	Poly(amide- imide)
Young's Modulus, E, Msi	0.1	0.16-0.22	0.36	0.65-0.92
Poisson's Ratio, $\nu$				
Tensile Strength, $\sigma^u$ , ksi	5.4	4.8-5.5	10.2	20-22
Compressive Strength, $\sigma^c$ , ksi		5.5-7.0	14-40	30-32
Strain at Tensile Ultimate, $\epsilon^u$ , %	400	30-530	50-100	6-8
Coefficient of Thermal Expansion, $\alpha$ , $10^{-6}/^{\circ}\text{F}$	80-160	38-110	13-22	17-25
Thermal Conductivity, $\mu$ , $\frac{\text{Btu} \cdot \text{in}}{\text{hr} \cdot \text{ft}^2 \cdot ^{\circ}\text{F}}$	2.28	1.21-1.36	1.8	1.5
Density, $\rho$ , lb/in <sup>3</sup>	0.034	0.033- 0.034	0.045	0.052

• Standard International (SI) Units

Property	Polyethylene (HMW)	Poly- propylene	Poly- sulfone	Poly(amide- imide)
Young's Modulus, E, GPa	0.7	1.1-1.5	2.5	4.5-6.3
Poisson's Ratio, $\nu$				
Tensile Strength, $\sigma^u$ , MPa	37	33-38	70	140-150
Compressive Strength, $\sigma^c$ , MPa		38-48	97-280	210-220
Strain at Tensile Ultimate, $\epsilon^u$ , %	400	30-530	50-100	6-8
Coefficient of Thermal Expansion, $\alpha$ , $10^{-6}/^{\circ}\text{C}$	140-290	68-200	23-40	31-45
Thermal Conductivity, $\mu$ , $\frac{\text{W}}{\text{m} \cdot \text{K}}$	0.33	0.17-0.20	0.26	0.22
Density, $\rho$ , gm/cm <sup>3</sup>	0.94	0.90-0.94	1.24-1.25	1.45

\*References 2.24, 2.26, 2.29

## REFERENCES

- 2.1. Smith, R.E., "Ultrasonic Elastic Constants of Carbon Fibers and Their Composites," *Journal of Applied Physics*, **43** (1972) p. 2555.
- 2.2. Kowalski, M., "Determining the Transverse Modulus of Carbon Fibers," *SAMPE Journal*, July 1987, pp. 38-42.
- 2.3. *Engineers' Guide to Composite Materials*, Eds. J.W. Weeton, D.M. Peters, and K.L. Thomas, ASM, Metals Park, OH (1987) pp. 5-9: 5-11.
- 2.4. Diefendorf, R.J., "Carbon/Graphite Fibers," *Materials Handbook, Volume 1: Composites*, ASM International, Metals Park, OH (1987) p. 51.
- 2.5. "Hercules Carbon Fiber Type AS4," Product Data Sheet Number 847-5, Hercules Incorporated, Wilmington, DE.
- 2.6. "Hercules Carbon Fiber Type IM7," Product Data Sheet Number 868-1, Hercules Incorporated, Wilmington, DE.
- 2.7. "THORNEL Graphite Fibers P-120 2K and P-120S 2K," Product Data Sheet F-7149, Revision 1, Amoco Performance Products, Inc., March 1991.
- 2.8. "THORNEL Carbon Fibers T-300 1K, 3K, 6K, 12K," Product Data Sheet F-7147, Amoco Performance Products, Inc., March 1991.
- 2.9. Miller, D.M., "Glass Fibers," *Engineered Materials Handbook, Volume 1 - Composites*, ASM International, Metals Park, OH (1987) pp. 45-48.
- 2.10. *Engineers' Guide to Composite Materials*, American Society for Metals, Metals Park, OH (1987) pp. 5-5, 5-12, 5-19.
- 2.11. *MIL-HDBK-17-3D, Polymer Matrix Composites*, Volume 3 - Utilization of Data, Section 2.3.7 (1994).
- 2.12. *MIL-HDBK-17-3D, Polymer Matrix Composites*, Volume 3 - Utilization of Data, Section 2.3.5 (1994).
- 2.13. Schoenberg, T., "Boron and Silicon Carbide Fibers," *Engineered Materials Handbook, Volume 1 - Composites*, ASM International, Metals Park, OH (1987) pp. 58-59.
- 2.14. Johnson, D.D. and Sowman, H.G., "Ceramic Fibers," *Engineered Materials Handbook, Volume 1 - Composites*, ASM International, Metals Park, OH (1987) pp. 62-63.
- 2.15. *MIL-HDBK-17-3D, Polymer Matrix Composites*, Volume 3 - Utilization of Data, Section 2.3.2 (1993).

- 2.16. *Engineers' Guide to Composite Materials*, Eds. J.W. Weeton, D.M. Peters, and K.L. Thomas, American Society for Metals, Metals Park, OH (1987) pp. 5-26, 5-34.
- 2.17. Pigliacampi, J.J., "Organic Fibers," *Engineered Materials Handbook, Volume 1, Composites*, ASM International, Metals Park, OH (1987) pp. 54-57.
- 2.18. *Engineers' Guide to Composite Materials*, American Society for Metals, Metals Park, OH (1987) pp. 5-13.
- 2.19. *MIL-HDBK-17-3D, Polymer Matrix Composites*, Volume 3 - Utilization of Data, Section 2.3.4 (1994).
- 2.20. "AVCO Boron Characteristics for Strength and Stiffness at Minimum Weight," Product Data Sheet 0481-2-2M.
- 2.21. *Engineers' Guide to Composite Materials*, American Society for Metals, Metals Park, OH (1987) pp. 5-26.
- 2.22. Pigliacampi, J.J., "Organic Fibers," *Engineered Materials Handbook, Volume 1, Composites*, ASM International, Metals Park, OH (1987) p. 56.
- 2.23. Spectra High Performance Fibers for Reinforced Composites, Product Data Sheet, Allied Signal, Inc. (1990).
- 2.24. *Modern Plastics Encyclopedia '92*, Ed. R. Greene, Mc-Graw-Hill, Inc., New York, October 1991.
- 2.25. Scola, D.A., "Polyimide Resins," *Engineered Materials Handbook, Volume 1, Composites*, ASM International, Metals Park, OH (1987) pp. 78-89.
- 2.26. Shah, V., *Handbook of Plastics Testing Technology*, John Wiley & Sons, New York (1984).
- 2.27. Palmer, R.J., "Investigation of the Effect of Resin Material on Impact Damage to Graphite/Epoxy Composites," NASA-CR-165677, March 1981.
- 2.28. *MIL-HDBK-17-3D, Polymer Matrix Composites*, Volume 3 - Utilization of Data, Section 2.2.2 (1994).
- 2.29. Gosnell, R.E., "Thermal Plastic Resins," *Engineered Materials Handbook, Volume 1, Composites*, ASM International, Metals Park, OH (1987) pp. 97-104.

## CHAPTER 3. UNIDIRECTIONAL FIBER COMPOSITES

The concept of designing a material to yield a desired set of properties has received impetus from the growing acceptance of composite materials. This utilization of the diversity of contemporary high-strength and high-stiffness fibers in various structural applications has motivated a new interest in the study of relationships between the mechanical and physical properties of composites and those of their constituents. The aims of such studies are, first, to provide the ability to analyze the performance of structures utilizing these heterogeneous materials, and second, to provide guidelines for the development of improved materials.

Inclusion in the structural design process of the material design phase has had a significant impact upon the entire design process, particularly upon the preliminary design phase. In this preliminary design, the number of materials which may be considered for a design generally will include many for which experimental material properties data are not available. Thus, preliminary material selection may be based on analytically predicted properties. These analytical methods are the result of studies of the relationship between effective properties of composites and the properties of their constituents (studies which, although not truly conducted at a microscopic level, are frequently described by the term "micromechanics"). The understanding of the relationships between the overall or average response of a composite and the properties of its constituents permits the representation of the inhomogeneous composite by an effective homogeneous (and generally anisotropic) material. The properties of this homogeneous material are the effective properties of the composite; that is, they are the properties which relate the average values of the state variables in the composite. When the effective properties of a unidirectional composite have been determined, the material may be viewed as a homogeneous anisotropic material for many aspects of the design process. The evaluation of these effective properties is the major topic of this chapter.

### 3.1 FIBER COMPOSITES: PHYSICAL PROPERTIES.

*I frame no hypotheses; for whatever is not deduced from the phenomena is to be called an hypothesis; and hypotheses, whether meta-physical or physical, whether of occult qualities or mechanical, have no place in experimental philosophy.*

Philosophiae Naturalis  
Principia Mathematica

A unidirectional fiber composite (UDC) consists of aligned continuous fibers which are embedded in a second material designated as the matrix (figures 3.1, 3.2). Fibers commonly used are glass, carbon, graphite, and boron; matrices are polymeric, such as epoxy and light (primarily aluminum) alloys. The physical properties of a UDC as measured by means of laboratory specimens will be called effective properties. A typical specimen is a flat coupon containing many fibers. Evidently, the effective physical properties are functions of fiber and matrix physical properties, of their volume fractions, and perhaps also of statistical parameters associated with fiber distribution. The fibers have, in general, circular cross sections with some variability diameters. A UDC is clearly anisotropic, since properties in the fiber direction are very different from properties transverse to the fibers.

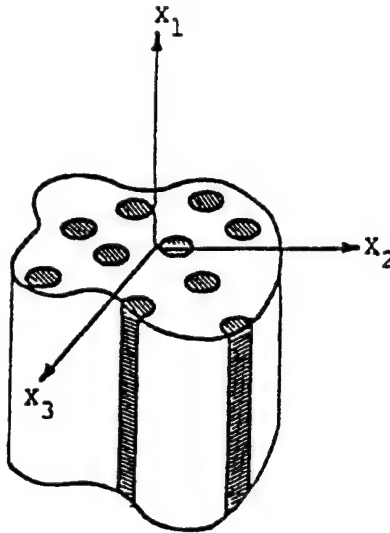


FIGURE 3.1. MICROSTRUCTURE OF UNIDIRECTIONAL COMPOSITES



FIGURE 3.2. UNIDIRECTIONALLY REINFORCED LAMINA

Effective properties of interest to the engineer are:

- Elastic Properties
- Thermal Expansion Coefficients
- Moisture Swelling Coefficients
- Viscoelastic Properties—Static and Dynamic
- Conductivity
- Moisture Diffusivity

Traditionally, material properties have been obtained experimentally and have been compiled in handbooks, but such an approach is not practical for fiber composites because of their large variety. There are many kinds of carbon and graphite fibers with different anisotropic properties and there are many kinds of matrix properties to be considered from the standpoint of both desired performance characteristics and the adverse influence of various environmental factors.

The experimental determination of all of the effective anisotropic properties of interest is clearly an impossible undertaking. It is necessary, therefore, to devise analytical procedures to determine the effective properties on the basis of fiber and matrix properties and volume fractions and perhaps some additional information about fiber distribution. The task of experiment is to check the validity of the analytical procedures. Thus, the properties are to be determined from the point of view of structural mechanics, not of materials science. Indeed, composite materials are complicated structures and not materials in the classical sense.

In the following, we shall discuss a variety of analytical results which may be used to determine the various properties of a UDC which are of engineering interest. Details of derivations are beyond the scope of the present work and may be found in references 3.1 and 3.2.

### 3.1.1 Elastic Properties.

The elastic properties of a material are a measure of its stiffness and are needed to determine the deformations which are produced by loads. In a UDC, the stiffness is provided by the fibers; the role of the matrix is to prevent lateral deflection as well as to provide for load sharing between fibers through the action of shear stresses. (See Section 3.2.1.3 on the role of the matrix in stress redistribution around broken fibers.) To illustrate this, let us compare a bundle of stiff fibers with a UDC containing the same amount of fibers embedded in a polymeric matrix. If the stiffness of the polymer is neglected by comparison with fiber stiffness, then the bundle and the UDC will have the same stiffness for a tensile load; in this case, the bundle fulfills the function of a rope. If, however, compressive load in the fiber direction is applied, the bundle will buckle at once, and thus, its stiffness for this load is zero. By contrast, the UDC has the same stiffness for compressive and tensile load since the matrix will prevent fiber buckling until quite elevated values of load. This will be discussed later under compressive strength. Similarly, the bundle has no transverse tensile stiffness since the fibers will separate at once. This again will be prevented in the UDC by the matrix.

In this section, we shall be concerned with the subject of analytical determination of the elastic properties of a UDC. Obviously, such properties are functions of those of the fibers and the matrix and of their relative volumes in the composite material. Clearly, the stiffness in the fiber direction is much larger than the stiffness transverse to the fibers. If a load is applied in the fiber direction, this is carried primarily by the fibers, which deform very little and also constrain the matrix to very small deformation. On the other hand, in the direction normal to the fibers, the matrix is a continuous load carrying structure and the fibers move with the deforming matrix, thus not significantly impeding the deformation. Therefore, the stiffness in the direction transverse to the fibers is much smaller than the stiffness in the fiber direction so that the unidirectional composite tends to be extremely anisotropic.

#### 3.1.1.1 Composite Properties.

For engineering purposes, it is necessary to determine such properties as Young's modulus in the fiber direction, Young's modulus transverse to the fibers, longitudinal shear modulus (i.e., for fibers sliding parallel to each other), and transverse shear modulus (i.e., for fibers sliding in the transverse direction), as well as various Poisson's ratios. This can be done in terms of simple analytical expressions, as will be explained in this section.

Elastic properties of homogeneous materials are defined by relations between homogeneous (constant) stress and strain. In the general anisotropic case, such relations are written

$$\sigma_{ij} = C_{ijkl} \epsilon_{kl} \quad (3.1a)$$

$$\epsilon_{ij} = S_{ijkl} \sigma_{kl} \quad (3.1b)$$

where all the subscripts range over 1, 2, and 3; repeated subscripts denote summation;  $C_{ijkl}$  is the fourth rank elastic moduli tensor; and  $S_{ijkl}$  is the fourth rank elastic compliance tensor. The notation for these fourth rank tensors is frequently simplified by an engineering representation utilizing two subscripts for each constant. This is accomplished by replacing each pair of subscripts in the stiffness and compliance tensor components with a single subscript according to the following plan:

$$\begin{array}{lll} 11 \rightarrow 1 & 22 \rightarrow 2 & 33 \rightarrow 3 \\ 23 \text{ \& } 32 \rightarrow 4 & 13 \text{ \& } 31 \rightarrow 5 & 12 \text{ \& } 21 \rightarrow 6 \end{array}$$

Although in isotropic materials we may take the "1" to "3" directions to be arbitrary, in a composite lamina we can consider "1" to be the direction parallel to the fiber axes, "2" to be the transverse in-plane direction, and "3" to be the transverse out-of-plane direction.

As a result of these substitutions, the engineering constants replace tensor components as shown by the following examples:

$$C_{1111} = C_{11}$$

$$S_{1112} = S_{12}$$

For the constants relating shear stress and strain, it is convenient to take advantage of the symmetry of the stress and strain components (e.g.,  $\epsilon_{ij} = \epsilon_{ji}$ ). Thus, for example, the expression

$$\begin{aligned} \sigma_{11} = & C_{1111} \epsilon_{11} + C_{1122} \epsilon_{22} + C_{1133} \epsilon_{33} + \\ & C_{1123} \epsilon_{23} + C_{1132} \epsilon_{32} + C_{1131} \epsilon_{31} + \\ & C_{1113} \epsilon_{13} + C_{1112} \epsilon_{12} + C_{1121} \epsilon_{21} \end{aligned}$$

may be written as

$$\begin{aligned} \sigma_{11} = & C_{11} \epsilon_{11} + C_{12} \epsilon_{22} + C_{13} \epsilon_{33} + \\ & 2C_{14} \epsilon_{23} + 2C_{15} \epsilon_{13} + 2C_{16} \epsilon_{12} \end{aligned}$$

Because of the various symmetries, there are in the most general case 21 independent elastic moduli or compliances.

When the material is isotropic, the stress-strain relations are

$$\begin{aligned}\sigma_{11} &= (\lambda + 2G) \epsilon_{11} + \lambda \epsilon_{22} + \lambda \epsilon_{33} \\ \sigma_{22} &= \lambda \epsilon_{11} + (\lambda + 2G) \epsilon_{22} + \lambda \epsilon_{33} \\ \sigma_{33} &= \lambda \epsilon_{11} + \lambda \epsilon_{22} + (\lambda + 2G) \epsilon_{33}\end{aligned}\tag{3.2a}$$

$$\begin{aligned}\sigma_{12} &= 2G\epsilon_{12} \\ \sigma_{23} &= 2G\epsilon_{23} \\ \sigma_{13} &= 2G\epsilon_{13}\end{aligned}\tag{3.2b}$$

$$\begin{aligned}\epsilon_{11} &= \frac{\sigma_{11}}{E} - \frac{\nu}{E} (\sigma_{22} + \sigma_{33}) \\ \epsilon_{22} &= \frac{\sigma_{22}}{E} - \frac{\nu}{E} (\sigma_{11} + \sigma_{33}) \\ \epsilon_{33} &= \frac{\sigma_{33}}{E} - \frac{\nu}{E} (\sigma_{11} + \sigma_{22})\end{aligned}\tag{3.2c}$$

where  $E$ ,  $\nu$ , and  $G$  are Young's modulus, Poisson's ratio, and shear modulus, respectively, and  $\lambda$  is called the Lamé modulus, given by  $\nu E / (1 + \nu)$  ( $1 - 2\nu$ ). Another important modulus is the bulk modulus  $K$  defined by

$$\begin{aligned}\sigma_{11} + \sigma_{22} + \sigma_{33} &= 3K(\epsilon_{11} + \epsilon_{22} + \epsilon_{33}) \\ K &= E / 3(1 - 2\nu)\end{aligned}\tag{3.3}$$

In the event that  $\epsilon_{11} = 0$ , it follows from (3.2a)

$$\begin{aligned}\sigma_{22} + \sigma_{33} &= 2k(\epsilon_{22} + \epsilon_{33}) \\ k &= \lambda + G = G / (1 - 2\nu)\end{aligned}\tag{3.4}$$

The modulus  $k$  is called the plane strain bulk modulus. The isotropic elastic material has two independent elastic moduli. There are thus various interrelations among the moduli entering into (3.1-3.4).



The above stress-strain relations are suitable for polymeric and metal matrices and for glass fibers. Carbon and graphite fibers, on the other hand, are highly anisotropic. Their microstructures (figure 3.3) reveal that the fibers are transversely isotropic with respect to the fiber axis  $x_1$ . The stress-strain relations of such a material have the form

$$\begin{aligned}\sigma_{11} &= n\epsilon_{11} + \ell\epsilon_{22} + \ell\epsilon_{33} \\ \sigma_{22} &= \ell\epsilon_{11} + (k+G_T)\epsilon_{22} + (k-G_T)\epsilon_{33} \\ \sigma_{33} &= \ell\epsilon_{11} + (k+G_T)\epsilon_{22} + (k-G_T)\epsilon_{33}\end{aligned}\tag{3.5a}$$

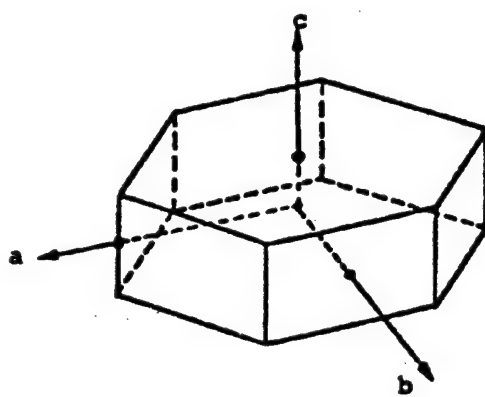
$$\begin{aligned}\sigma_{12} &= 2G_L \epsilon_{12} \\ \sigma_{23} &= 2G_T \epsilon_{23} \\ \sigma_{13} &= 2G_L \epsilon_{13}\end{aligned}\tag{3.5b}$$

$$\begin{aligned}\epsilon_{11} &= \frac{\sigma_{11}}{E_L} - \frac{\nu_L}{E_L} \sigma_{22} - \frac{\nu_L}{E_L} \sigma_{33} \\ \epsilon_{22} &= -\frac{\nu_L}{E_L} \sigma_{11} + \frac{\sigma_{22}}{E_T} - \frac{\nu_T}{E_T} \sigma_{33} \\ \epsilon_{33} &= -\frac{\nu_L}{E_L} \sigma_{11} - \frac{\nu_T}{E_T} \sigma_{22} + \frac{\sigma_{33}}{E_T}\end{aligned}\tag{3.5c}$$

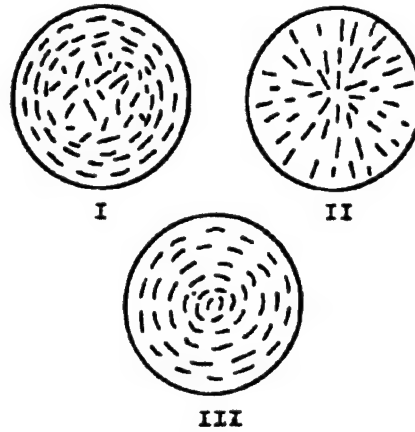
where

- $E_L$  - Young's modulus in fiber direction
- $E_T$  - Young's modulus in transverse direction
- $\nu_L$  - longitudinal Poisson's ratio
- $\nu_T$  - transverse Poisson's ratio
- $G_L$  - longitudinal shear modulus
- $G_T$  - transverse shear modulus
- $k$  - transverse bulk modulus
- $n$  - elastic modulus, also  $C_{11}$
- $\ell$  - elastic modulus, also  $C_{12}$

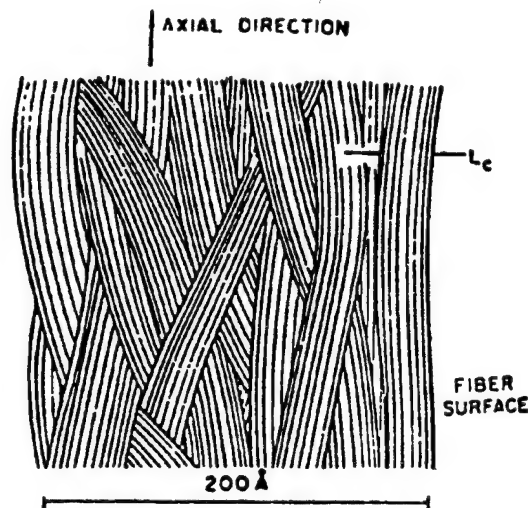
The material has five independent elastic moduli. There are, thus, various interrelations among the above moduli, some of which will be given below. The physical interpretation of elastic properties of a transversely isotropic material will be discussed further below in the context of a UDC and may be applied to the properties appearing in (3.5).



STRUCTURE OF GRAPHITE CRYSTAL



TYPES OF FIBER MICROSTRUCTURE



RIBBON TYPE STRUCTURE OF CARBON FIBERS

FIGURE 3.3. STRUCTURE OF CARBON AND GRAPHITE FIBERS

The fundamental property of a fiber composite or any other composite material is statistical homogeneity. This implies that the properties of a large enough sample element containing many fibers are the same as those of the entire specimen. Since the fibers are, in general, randomly placed, there is no preferred direction in the transverse  $x_2x_3$  plane (figure 3.1), which implies that the UDC is statistically transversely isotropic.

Experimental determination of the properties of homogeneous materials is based on induction of homogeneous states of stress and strain in suitable specimens. The mathematical interpretation is the application of suitable boundary conditions in terms of tractions or displacements which produce homogeneous states of stress and strain, or so-called homogeneous boundary conditions. Examples are simple tension, pure shear, and hydrostatic loading. An experimenter would naturally apply the same homogeneous boundary conditions to composite specimens. In this case, however, the states of stress and strain in the specimen are no longer homogeneous but highly complex. The variations of stress and strain on any plane through the composite material are random: there is nothing specific which distinguishes the variation on one plane from that on another. Such stress and strain fields are called statistically homogeneous. They consist essentially of constant averages with superposed random noise and are produced in geometrically statistically homogeneous specimens which are subjected to homogeneous boundary conditions. See figures 3.4 and 3.5 for examples. Consequently, effective elastic properties are defined by relations between average stress and average strain.

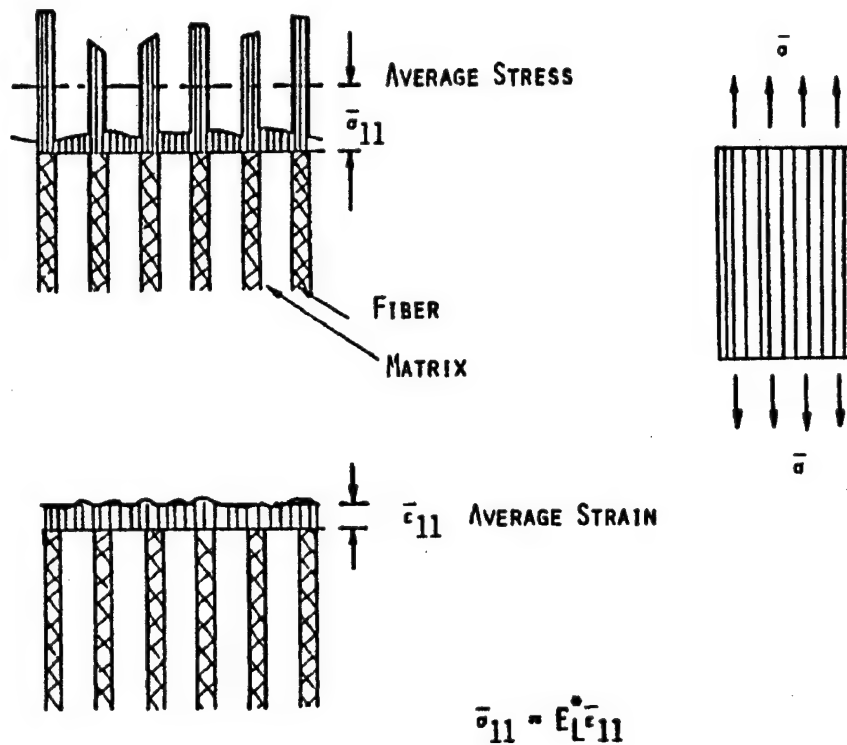
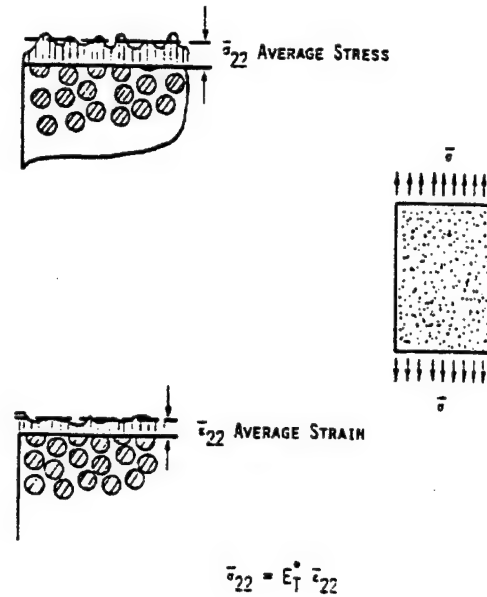


FIGURE 3.4. VARIATION OF STRESS AND STRAIN IN FIBER DIRECTION—AXIAL LOADING



$$\bar{\sigma}_{22} = E_T^* \bar{\epsilon}_{22}$$

FIGURE 3.5. VARIATION OF STRESS AND STRAIN TRANSVERSE TO FIBERS—TRANSVERSE LOADING

A typical transverse section of a unidirectional fiber composite was shown in figure 1.5. Because of the random nature of fiber placement, the material is statistically transversely isotropic. Its effective elastic stress-strain relations have the form

$$\begin{aligned} \bar{\sigma}_{11} &= n^* \bar{\epsilon}_{11} + \ell^* \bar{\epsilon}_{22} + \ell^* \bar{\epsilon}_{33} \\ \bar{\sigma}_{22} &= \ell^* \bar{\epsilon}_{11} + (k^* + G_T^*) \bar{\epsilon}_{22} + (k^* - G_T^*) \bar{\epsilon}_{33} \\ \bar{\sigma}_{33} &= \ell^* \bar{\epsilon}_{11} + (k^* + G_T^*) \bar{\epsilon}_{22} + (k^* - G_T^*) \bar{\epsilon}_{33} \end{aligned} \quad (3.6a)$$

$$\begin{aligned} \bar{\sigma}_{12} &= 2G_L^* \bar{\epsilon}_{12} \\ \bar{\sigma}_{23} &= 2G_T^* \bar{\epsilon}_{23} \\ \bar{\sigma}_{13} &= 2G_L^* \bar{\epsilon}_{13} \end{aligned} \quad (3.6b)$$

With inverse

$$\begin{aligned}
 \bar{\epsilon}_{11} &= \frac{\bar{\sigma}_{11}}{E_L^*} - \frac{\nu_L^*}{E_L^*} \bar{\sigma}_{22} - \frac{\nu_L^*}{E_L^*} \bar{\sigma}_{33} \\
 \bar{\epsilon}_{22} &= -\frac{\nu_L^*}{E_L^*} \bar{\sigma}_{11} + \frac{\bar{\sigma}_{22}}{E_T^*} - \frac{\nu_T^*}{E_T^*} \bar{\sigma}_{33} \\
 \bar{\epsilon}_{33} &= -\frac{\nu_L^*}{E_L^*} \bar{\sigma}_{11} - \frac{\nu_T^*}{E_T^*} \bar{\sigma}_{22} + \frac{\bar{\sigma}_{33}}{E_T^*}
 \end{aligned} \tag{3.6c}$$

It is seen that (3.6) is the precise analogue of (3.5) with average stresses and strains (indicated by overbars) replacing pointwise specified stresses and strains and effective moduli (indicated by asterisks) representing moduli of an equivalent homogeneous material.

The effective properties appearing above are to be interpreted as:

- $E_L^*$  - longitudinal Young's modulus, in fiber direction
- $\nu_L^*$  - associated longitudinal Poisson's ratio
- $E_T^*$  - transverse Young's modulus, normal to fibers
- $\nu_T^*$  - associated transverse Poisson's ratio (in transverse plane)
- $G_T^*$  - transverse shear modulus
- $G_L^*$  - longitudinal shear modulus
- $k^*$  - transverse bulk modulus
- $n^*, \ell^*$  - effective elastic moduli (see eq. 3.7)

It should be emphasized that the unidirectional fiber composite material is regarded as an effectively transversely isotropic material. Thus, there are five independent elastic constants. However, there are numerous ways to write the stress-strain relations utilizing various elastic constants. Any set of five independent constants may be chosen for convenience.

Interrelationships exist among many of the constants discussed herein, since only five are independent.

Figure 3.6 illustrates the loadings which are associated with these properties. The Poisson's ratio  $\nu_L^*$  is an abbreviated notation for  $\nu_{LT}^*$ , which defines the lateral strain in the transverse direction due to a stress in the fiber direction. Similarly, the Poisson's ratio  $\nu_T^*$  is an abbreviated notation for  $\nu_{TT}^*$ , which defines strain in transverse direction 3 due to stress in transverse direction 2 or vice versa. There is also a Poisson's ratio  $\nu_{TL}^*$  which defines strain in the longitudinal direction due to stress in the transverse direction. This is seldom used and does not enter into the stress-strain relations as presented here. Its value is given by  $\nu_{TL}^* = \nu_{LT}^* E_T^* / E_L^*$ .

All of these Poisson's ratios are illustrated in figure 3.6.

The longitudinal shear modulus  $G_L^*$  is an abbreviation for  $G_{LT}^* = G_{TL}^*$ , which is associated with shear acting on perpendicular longitudinal and transverse planes. Similarly, the transverse shear modulus  $G_T^*$  is an abbreviation of  $G_{TT}^*$  associated with shear on transverse perpendicular planes.

The effective modulus  $k^*$  is obtained by subjecting a specimen to the average state of strain with  $\bar{\epsilon}_{22} = \bar{\epsilon}_{33}$ , all other average strain components being zero, in which case it follows from (3.4) that

$$(\bar{\sigma}_{22} + \bar{\sigma}_{33}) = 2k^*(\bar{\epsilon}_{22} + \bar{\epsilon}_{33})$$

Unlike the other properties listed above,  $k^*$  is of little engineering significance but is of considerable analytical importance.

A comparison of the alternate forms of writing the stress-strain relations shows that the effective properties are interrelated as follows:

$$n^* = E_L^* + 4 k^* \nu_L^{*2} \quad (3.7a)$$

$$\ell^* = 2k^* \nu_L^* \quad (3.7b)$$

$$4/E_T^* = 1/G_T^* + 1/k^* + 4\nu_L^{*2}/E_L^* \quad (3.7c)$$

$$2/(1 - \nu_T^*) = 1 + k^*/(1 + 4k^*\nu_L^{*2}/E_L^*)G_T^* \quad (3.7d)$$

$$G_T^* = E_T^*/2(1 + \nu_T^*) \quad (3.7e)$$

The same interrelations are valid for the constituent properties of (3.5).

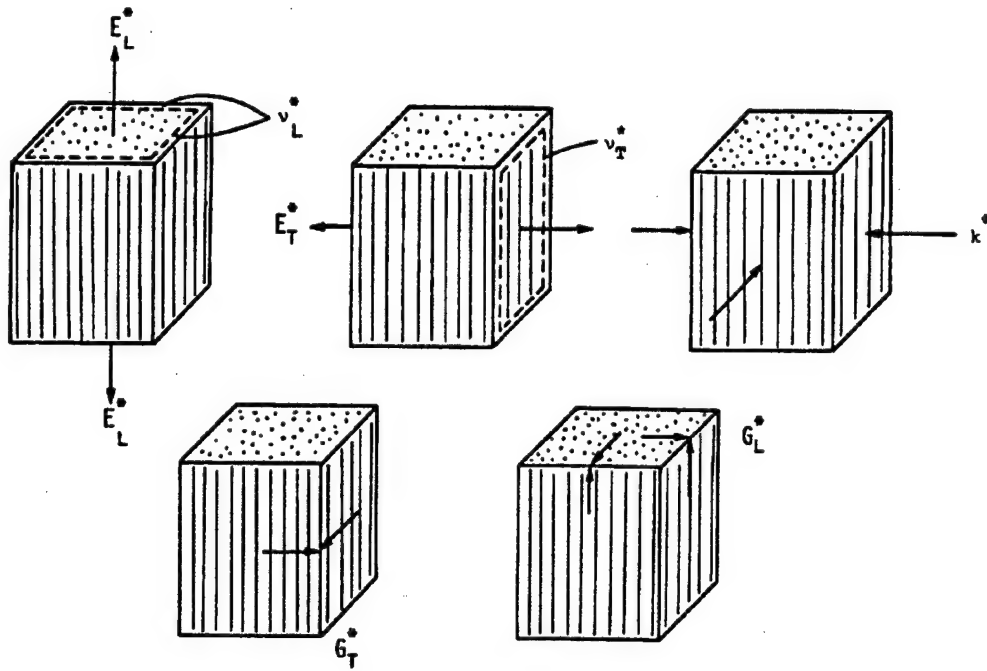


FIGURE 3.6. BASIC LOADING TO DEFINE EFFECTIVE ELASTIC PROPERTIES

Ordinarily, a transversely isotropic material has five independent elastic properties; however, it has been shown by Hill [3.3] that for the particular case of the effective moduli of a UDC, the following additional relations exist:

$$\begin{aligned} E_L^* &= \overline{E}_L + \left[ \frac{2(\nu_{Lf} - \nu_m)}{1/k_f - 1/k_m} \right]^2 \left( \frac{1}{k} - \frac{1}{k^*} \right) \\ \nu_L^* &= \overline{\nu} - \left[ \frac{(\nu_{Lf} - \nu_m)}{1/k_f - 1/k_m} \right] \left( \frac{1}{k} - \frac{1}{k^*} \right) \end{aligned} \quad (3.8)$$

Here

$$\begin{aligned}\bar{E} &= E_m v_m + E_{Lf} v_f \\ \bar{v} &= v_m v_m + v_{Lf} v_f \\ \frac{1}{k} &= \frac{v_m}{k_m} + \frac{v_f}{k_f}\end{aligned}\tag{3.9}$$

m - denotes matrix  
f - denotes fiber  
v - volume fraction

and the case under consideration involves isotropic matrix and transversely isotropic fibers. Relations (3.8) are general and are valid for any fiber shapes and distribution. They apply solely for a two-phase unidirectional fiber composite. In view of these relations the number of independent effective elastic moduli reduces to three. This means that if one of the three effective moduli in (3.8) can be found as a function of constituent properties, the other two will be defined by (3.8).

### 3.1.1.2 Relations Between Composite and Constituent Properties.

Computation of effective elastic moduli is a very difficult problem in elasticity theory. It is first necessary to assume a suitable arrangement of fibers, thus, a geometrical model of the UDC. Suitable homogeneous boundary conditions are then applied to fiber reinforced specimens. For example, to compute  $k^*$  it is convenient to apply the displacement boundary conditions

$$\begin{aligned}u_1(S) &= 0 \\ u_2(S) &= \epsilon^o x_2 \\ u_3(S) &= \epsilon^o x_3\end{aligned}\tag{3.10}$$

on the surface of a cylindrical specimen (figure 3.1). This implies that there is no external longitudinal deformation and that the plane is isotropic, preserving the shape of the cross section. It follows from the average strain theorem [3.1] that

$$\bar{\epsilon}_{22} = \bar{\epsilon}_{33} = \epsilon^o\tag{3.11}$$

and all other average strains vanish. Hence, from (3.6a)

$$\bar{\sigma}_{22} = \bar{\sigma}_{33} = 2k^* \epsilon^o\tag{3.12}$$

To find this average stress, however, it is necessary to determine in detail the elastic displacement fields in matrix and fibers. These displacements must satisfy the differential equation of elasticity theory in matrix and fibers, the displacement and traction continuity conditions at fiber-matrix interfaces, and the external boundary conditions (3.10). Once these displacements are known, the strain fields are computed by differentiation, the stress fields from the local



Hooke's laws, and then the stress average (3.12) which is necessarily proportional to  $\epsilon^0$ . Then  $2k^*$  is the coefficient of proportionality.

To compute  $E_T^*$ , consider the specimen shown in figure 3.2. Apply the uniform stress  $\epsilon^0$  to the two parallel faces, with normal in the  $x_3$  direction. All other traction components on the specimen surface vanish. It then follows from the average stress theorem [3.1] that the only surviving average stress is

$$\bar{\sigma}_{33} = \sigma^0$$

Then from (3.6)

$$E_T^* = \frac{\sigma^0}{\bar{\epsilon}_{33}}$$

$$\nu_T^* = -\frac{\bar{\epsilon}_{22}}{\bar{\epsilon}_{33}}$$

It is seen that the two effective properties  $E_T^*$  and  $\nu_T^*$  are determined by computation of  $\bar{\epsilon}_{22}$  and  $\bar{\epsilon}_{33}$ . This again requires solution of the appropriate elasticity boundary value problem for the fiber composite specimen.

In view of the difficulty of the problem, only a very limited number of simple models permit exact analysis. One kind of model is periodic arrays of identical circular fibers, e.g., square periodic arrays and hexagonal periodic arrays (figure 3.7). These models are analyzed by numerical finite difference or finite element procedures. It is necessary in each case to identify a suitable repeating element of the fiber composite and to express its boundary conditions on the basis of symmetry requirements in terms of the external boundary conditions [3.1]. It appears that the hexagonal array was first analyzed in reference 3.4 and the square array in reference 3.5. See reference 3.6 for further references on periodic arrays. It should be noted, however, that the square array is not a suitable model for the usual UDC since it is not transversely isotropic and thus has six independent elastic properties. In particular, the transverse shear modulus depends on the direction of applied shear in the  $x_2 x_3$  plane. On the other hand, the hexagonal array fulfills the transverse isotropy requirement since hexagonal symmetry is equivalent to transverse isotropy.

The only existing model which permits exact analytical determination of effective elastic moduli is the composite cylinder assemblage (CCA) introduced in reference 3.7. To construct the model, imagine that we have at our disposal a collection of composite cylinders each of which consists of a circular fiber core and a concentric matrix shell. The sizes of outer radii  $b_n$  of the cylinders are at our disposal. The size of fiber core radii,  $a_n$ , is restricted by the requirement that in each cylinder the ratio  $a_n/b_n$  is the same, which also implies that matrix and fiber volume fractions are the same in each composite cylinder.

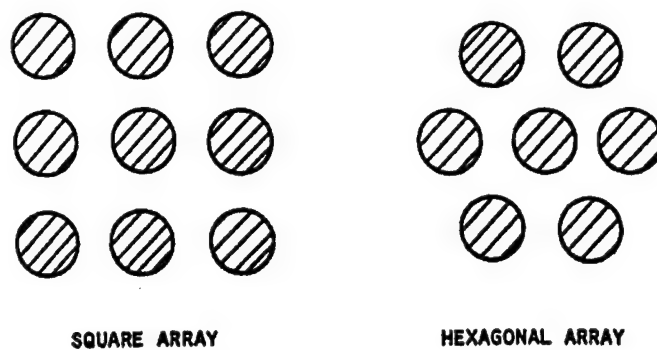


FIGURE 3.7. MODELS FOR NUMERICAL COMPUTATION OF PROPERTIES

It may be shown that for various loadings of interest, each composite cylinder behaves as some equivalent homogeneous cylinder. A hypothetical homogeneous cylindrical specimen is assigned these equivalent properties and is progressively filled out with composite cylinders. Since the radii of the cylinders can be arbitrarily small, the remaining volume can be made arbitrarily small. In the limit, the properties of the assemblage converge to the properties of one composite cylinder. The construction of a CCA is shown schematically in figure 3.8 and the resulting composite in figure 3.9. A desirable feature of the model is the randomness of fiber placement, while an undesirable feature is the large variation of fiber sizes. It will soon become apparent, however, that the latter is not of serious concern.

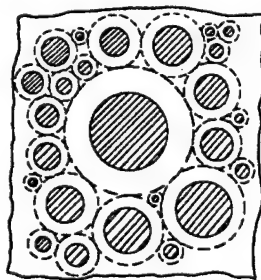


FIGURE 3.8. COMPOSITE CYLINDER ASSEMBLAGE—CONSTRUCTION

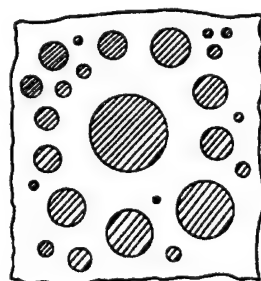


FIGURE 3.9. COMPOSITE CYLINDER ASSEMBLAGE

The analysis of the CCA gives closed form results for the effective properties  $k^*$ ,  $E_L^*$ ,  $n^*$ ,  $v_L^*$ ,  $\ell^*$ ,  $G_L^*$  and close bounds for the properties  $G_T^*$ ,  $E_T^*$ ,  $v_T^*$ . Such results will now be listed for isotropic fibers with the necessary modifications for transversely isotropic fibers. For details of derivation see references 3.1 and 3.8.

$$\begin{aligned} k^* &= \frac{k_m (k_f + G_m) v_m + k_f (k_m + G_m) v_f}{(k_f + G_m) v_m + (k_m + G_m) v_f} \\ &= k_m + \frac{v_f}{1/(k_f - k_m) + v_m/(k_m + G_m)} \end{aligned} \quad (3.13)$$

$$E_L^* = E_m v_m + E_f v_f + \frac{4(v_f - v_m)^2 v_m v_f}{v_m/k_f + v_f/k_m + 1/G_m} \quad (3.14a)$$

$$\approx E_m v_m + E_f v_f \quad (3.14b)$$

The last is an excellent approximation for all UDC.

$$v_L^* \approx v_m v_m + v_f v_f + \frac{(v_f - v_m) (1/k_m - 1/k_f) v_m v_f}{v_m/k_f + v_f/k_m + 1/G_m} \quad (3.15)$$

$$\begin{aligned} G_L^* &= G_m \left[ \frac{G_m v_m + G_f (1 + v_f)}{G_m (1 + v_f) + G_f v_m} \right] \\ &= G_m + \frac{v_f}{1/(G_f - G_m) + v_m/2G_m} \end{aligned} \quad (3.16)$$

As indicated earlier, the result of  $G_T^*$  is a pair of bounds on the actual value. One or the other of these bounds is recommended, depending upon the ratios of the constituent properties. To compute the resulting  $E_T^*$  and  $v_T^*$  use is made of (3.7c,d). When  $G_f > G_m$  and  $k_f > k_m$ , the upper bound is recommended:

$$\begin{aligned}
G_{T(+)}^* - G_T^* &= G_m \left[ 1 + \frac{(1+\beta_m) v_f}{\rho - [1+3\beta_m^2 v_m^2 / (\alpha v_f^3 + 1)] v_f} \right] \\
\alpha &= \frac{\beta_m - \gamma \beta_f}{1 + \gamma \beta_f} & \rho &= \frac{\gamma + \beta_m}{\gamma - 1} \\
\beta_m &= \frac{1}{3 - 4 v_m} & \beta_f &= \frac{1}{3 - 4 v_f} \\
\gamma &= \frac{G_f}{G_m}
\end{aligned} \tag{3.17}$$

When  $G_f < G_m$  and  $k_f < k_m$ , the lower bound is recommended. For this case:

$$G_T^* (-) \sim G_T^* = G_m \left[ 1 + \frac{(1+\beta_m) v_f}{\rho - [1+3\beta_m^2 v_m^2 / (\alpha v_f^3 - \beta_m)] v_f} \right] \tag{3.18}$$

The companion lower bound to (3.17) and the companion upper bound for (3.18) are both given by the same expression:

$$G_T^* (\pm) = G_m \left[ 1 + \frac{v_f}{1/(\gamma - 1) + v_m / (1 + \beta_m)} \right] \tag{3.19}$$

The result (3.18) is of interest for metal matrix composites consisting of carbon and graphite fibers in an aluminum matrix, because in that case the elastic properties  $G_m$  and  $k_m$  of the matrix are larger than the  $G_{Tf}$  and  $k_f$  of the fibers. Note that  $k_m, k_f$  in (3.13) are the isotropic plane strain bulk moduli given by (3.4).

For transversely isotropic fibers, there are the following modifications [3.1 and 3.8]:

For $k^*$	$k_f$ is the fiber transverse bulk modulus	
For $E_L^*, v_L^*$	$E_f = E_{Lf}$ , $v_f = v_{Lf}$ , $k_f$ as above	
For $G_L^*$	$G_f = G_{Lf}$	(3.20)
For $G_T^*$	$G_f = G_{Tf}$ , $\beta_f = k_f / (k_f + 2G_{Tf})$	

A discussion on the bounds for effective elastic moduli of fiber composites is given in an appendix to this chapter.

A rational approximate evaluation of  $G_T^*$  of the CCA model is due to Christensen and Lo [3.2]. They have assumed that any composite cylinder behaves as if it were embedded in the effective medium with effective shear modulus  $G_T^*$ . The result of the rather involved calculation is

$$A (G_T^* / G_m)^2 + 2B (G_T^* / G_m) + C = 0 \quad (3.21)$$

where

$$\begin{aligned} A &= 3v_f v_m^2 (\gamma - 1) (\gamma + \eta_f) \\ &\quad + [\gamma \eta_m + \eta_f \eta_m - (\gamma \eta_m - \eta_f) v_f^3] [v_f \eta_m (\gamma - 1) - (\gamma \eta_m + 1)] \\ B &= -3v_f v_m^2 (\gamma - 1) (\gamma + \eta_f) + \frac{1}{2} [\eta_m \gamma + (\gamma - 1)v_f + 1] [(n_m - 1) (\gamma + \eta_f) \\ &\quad - 2 (\gamma \eta_m - \eta_f) v_f^3] + \frac{1}{2} v_f (\eta_m + 1) (\gamma - 1) [\gamma + \eta_f + (\gamma \eta_m - \eta_f) v_f^3] \\ C &= 3v_f v_m^2 (\gamma - 1) (\gamma + \eta_f) \\ &\quad + [\eta_m \gamma + (\gamma - 1)v_f + 1] [\gamma + \eta_f + (\gamma \eta_m - \eta_f) v_f^3] \\ \eta_m &= 1/\beta_m \quad \eta_f = 1/\beta_f \end{aligned}$$

$\beta_m$ ,  $\beta_f$  and  $\lambda$  were defined in (3.17). In the following, results based on (3.21) will be denoted as EA (Embedding Approximation).

Numerical analysis of the effective elastic properties of the hexagonal array model reveals that their values are extremely close to those predicted by the CCA model as given by the above equations. Examples are shown in table 3.1 and figure 3.10. Also note the close agreement between  $G_T^*$  as predicted by (3.21) and the hexagonal array results in the table. This numerical coincidence is remarkable, since the two models are quite different. If so, the simple exact results (3.13-3.18) are valid also for random distribution of circular fibers of equal diameters (figure 3.11), which is the case of practical interest.

Comparisons of analytical property predictions with experimental results are shown in figures 3.12 and 3.13 for the transverse Young's moduli  $E_T^*$  of boron/epoxy and glass/epoxy. Results based on (3.13-3.17) are denoted CCA and results based on (3.21) are denoted EA. It is seen that the analytical results are close and agree with experimental data.

The simple analytical results given here predict effective elastic properties with sufficient engineering accuracy. They are of considerable practical importance for two main reasons: (a) they permit easy determination of effective properties for a variety of matrix properties, fiber

properties, and volume fractions, and (b) they are the only approach known today for experimental determination of carbon fiber properties.

TABLE 3.1. COMPARISON OF EFFECTIVE ELASTIC PROPERTIES PREDICTED BY CCA ANALYSIS AND HEXAGONAL ARRAY NUMERICAL ANALYSIS

Glass/Epoxy  $E_f = 10.0$  Msi  $E_m = 0.496$  Msi  
 $v_f = 0.20$   $v_m = 0.34$

	CCA	HA	CCA	HA	CCA	HA	CCA	HA
$v_f$	0.50	0.50	0.60	0.60	0.70	0.70	0.80	0.80
$k^*$ , Msi	1.194	1.194	1.459	1.461	1.851	1.865	2.487	2.563
$E_L^*$ , Msi	5.255	5.253	6.206	6.210	7.157	7.160	8.107	8.104
$v_L^*$	0.261	0.262	0.248	0.248	0.235	0.235	0.223	0.223
$G_L^*$ , Msi	0.497	0.495	0.635	0.693	0.844	0.852	1.196	1.308
$G_{T(-)}^*$ , Msi	0.437		0.553		0.729		1.060	
$G_T^*$ , Msi	0.463*	0.463	0.614*	0.611	0.838*	0.850	1.202*	1.264
$G_{T(+)}^*$ , Msi	0.540		0.705		0.944		1.323	

CCA - Composite Cylinder Assemblage (Hashin and Rosen, ref. 3.1, 3.7)

HA - Hexagonal Array (Pickett, ref. 3.4)

\*EA - Embedding Approximation (Christensen and Lo, ref. 3.2)

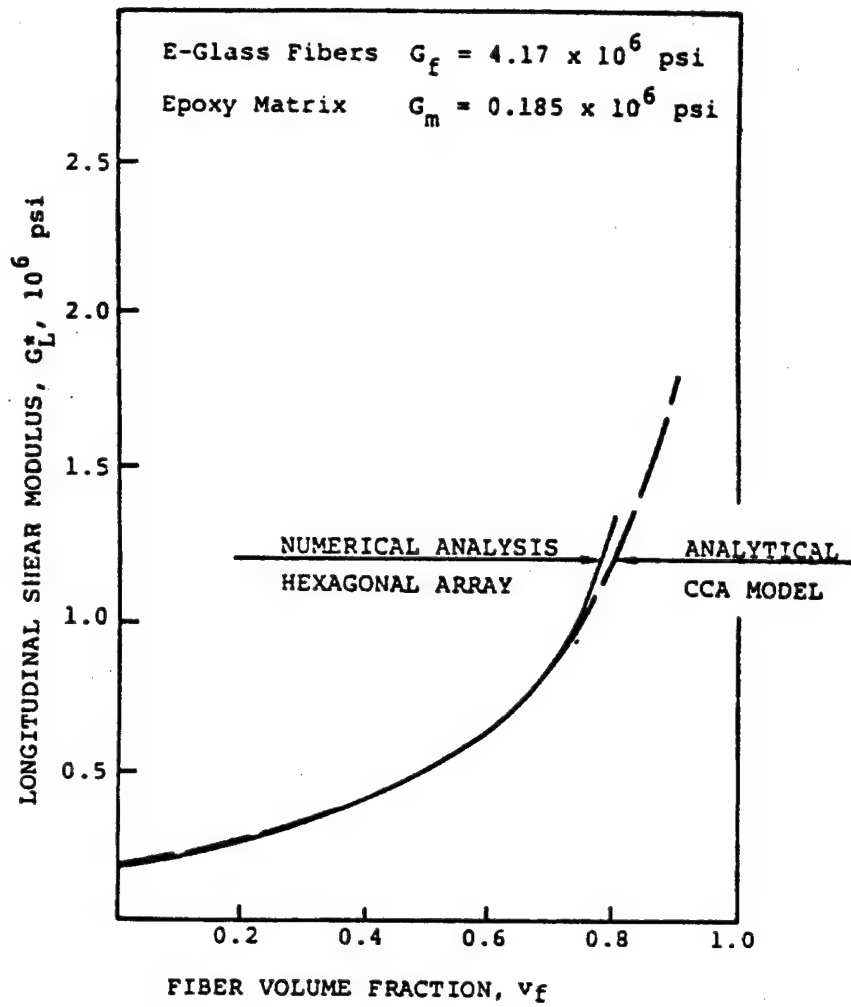


FIGURE 3.10. LONGITUDINAL SHEAR MODULUS,  $G_L^*$ , HEXAGONAL ARRAY OF CIRCULAR FIBERS AND COMPOSITE CYLINDER ASSEMBLAGE

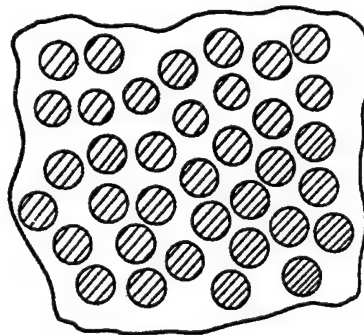


FIGURE 3.11. TRANSVERSE SECTION THROUGH UNIDIRECTIONAL FIBER COMPOSITE

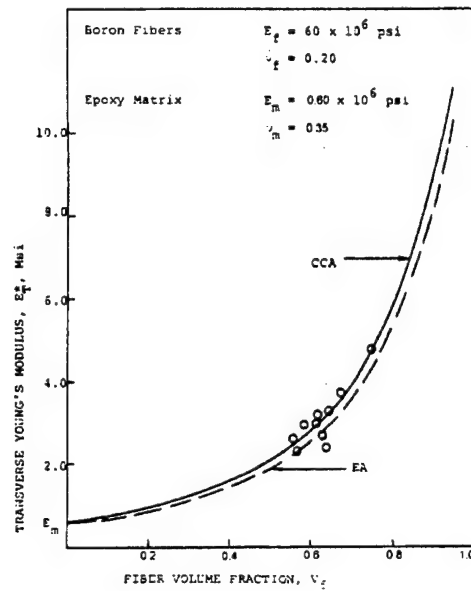


FIGURE 3.12. TRANSVERSE YOUNG'S MODULUS,  $E_T^*$ , OF BORON-REINFORCED EPOXY, COMPARISON OF THEORY AND EXPERIMENT. Experimental data from reference 3.107.

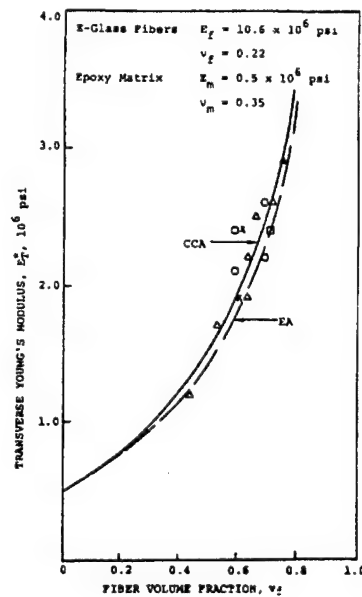


FIGURE 3.13. TRANSVERSE YOUNG'S MODULUS,  $E_T^*$ , OF GLASS-REINFORCED EPOXY COMPARISON OF THEORY AND EXPERIMENT. Experimental data from reference 3.108.



In reference to the previously mentioned reason (a), we note that the variety of matrix properties to be considered does not arise only from choice of different materials but also, and perhaps more importantly, from environmental changes of properties of a specified matrix. Important examples are property changes due to temperature, moisture absorption, fatigue damage accumulation, and radiation. Thus, environmental changes of composite stiffness can be determined by measurement of environmental matrix stiffness changes and computation of such changes for the composite. This avoids a great deal of expensive experimentation.

In reference to the previously mentioned reason (b), we recall that a carbon or graphite fiber has five independent elastic properties (3.5) and that its diameter is of the order of 0.01 mm. It is thus quite impossible to measure directly the elastic properties except for  $E_L$  in the fiber direction. A remaining alternative is to measure the elastic moduli of the matrix and the five effective elastic moduli of the composite and then to compute the five fiber elastic properties from eqs. 3.13-3.17 with the modification (3.20). The current standard method for doing this is to prepare a flat unidirectional fiber composite specimen and to measure the effective elastic properties by ultrasonic wave propagation. The principle of the method is to measure various wave velocities in various directions relative to the fiber direction. Since wave velocities are defined in terms of elastic moduli and density, their measurement determines the elastic moduli. Table 3.2 lists the anisotropic elastic properties of Thornel 50 fiber determined in this fashion by use of epoxy/Thornel 50 specimens.

The fiber properties obtained have then been used to compute the elastic properties of a UDC consisting of aluminum matrix and Thornel 50. Also shown is the comparison between measured and computed composite elastic properties (eq. 3.13-3.16, 3.18) based on the results of reference 3.9. It is seen that the agreement is excellent. Table 3.3 lists the properties of various carbon and graphite fibers obtained by this method, based on the ultrasonic measurements in reference 3.10.

The results given above are sufficiently rigorous and reliable to provide the engineer with a predictive tool for evaluation of effective elastic properties of fiber composites. The expressions are no more complicated than those obtained using various other treatments and approximations, which usually have a limited range of validity. However, such treatments may be of use when the fibers (inclusions) have different geometric shapes and for this reason a short discussion on such approximations is given next.

The self-consistent scheme (SCS), which has been used for two-phase particulate composites, can be readily applied to fiber composites. In one version of this scheme, the circular fiber is considered to be embedded in the equivalent transversely isotropic material, which yields an algebraic equation for determination of all five effective moduli [3.11]. The results considerably overestimate the actual effective moduli. In a generalized version, a composite cylinder in which the fiber and matrix volume fractions are those of the composite is embedded in the equivalent transversely isotropic composite [3.12]. Some of the effective moduli ( $k^*$ ,  $E_L^*$ ,  $\nu_L^*$ ,  $G_L^*$ ) obtained from this approach are identical to those obtained from the CCA results. The results for  $G_T^*$  given in reference 3.12 is not correct; the correct solution has been given by Christensen and Lo [3.2].

TABLE 3.2. ELASTIC PROPERTIES OF GRAPHITE/ALLUMINUM COMPOSITE.  
A comparison of analytical and experimental results.

Fiber - T50 Graphite

$E_L$ ksi	$E_T$ ksi	$k$ ksi	$G_T$ ksi	$G_L$ ksi	$\nu_L$	$\nu_T$
56,300	1040	1015	350	985	0.23	0.486

Matrix - Aluminum 201

$E$ ksi	$G$ ksi	$\nu$
10,300	3870	0.33

Composite - 30% T50/70% Al

$E_L^*$ ksi	$E_T^*$ ksi	$G_T^*$ ksi	$G_L^*$ ksi	$\nu_L^*$	
23,200	4300	1495	2697	0.43	Experimental
24,100	4640	1510	2700	0.41	Analytical

Based on various numerical solutions reported in literature and approximate results from self-consistent schemes [3.11 and 3.12], Halpin and Tsai suggested a set of approximate formulae, called the Halpin-Tsai equations [3.13]. For  $E_L^*$  and  $\nu_L^*$ , they suggest the use of the rule of mixtures ((3.14b) and (3.15)), with the last term on the right-hand side of the latter equation omitted. For  $E_T^*$ ,  $G_L^*$  and  $G_T^*$ , the following approximation is suggested

$$P^* = P_m \frac{1 + \zeta \eta \nu_f}{1 - \eta \nu_f} \quad (3.22a)$$

TABLE 3.3. ELASTIC PROPERTIES OF CARBON AND GRAPHITE FIBERS COMPUTED FROM ULTRASONIC MEASUREMENT OF EFFECTIVE FIBER COMPOSITE MODULI

• English Units

Graphite	$E_L$ ksi	$E_T$ ksi	$k$ ksi	$G_T$ ksi	$G_L$ ksi	$\nu_L$	$\nu_T$
WYB	7830	1810	1640	695	940	0.14	0.31
Thornel 25	20600	1420	1160	550	960	0.23	0.28
Thornel 40	37550	1220	1015	450	960	0.23	0.34
Thornel 50	56300	1130	1015	350	985	0.23	0.45
Thornel 505	58600	1015	960	362	1015	0.37	0.40
Thornel 755	81200	755	930	245	930	0.40	0.55
Carbon							
VYB	6235	1700	2250	940	1045	0.30	-0.10
Exp. PAN	28860	2200	1830	940	1130	0.33	0.16
HTS	26100	1680	1420	640	1060	0.34	0.19
Thornel 400	26400	1900	1860	710	1115	0.26	0.34

• Standard International (SI) Units

Graphite	$E_L$ GN/m <sup>2</sup>	$E_T$ GN/m <sup>2</sup>	$k$ GN/m <sup>2</sup>	$G_T$ GN/m <sup>2</sup>	$G_L$ GN/m <sup>2</sup>	$\nu_L$	$\nu_T$
WYB	53.95	12.47	11.30	4.79	6.48	0.14	0.31
Thornel 25	141.93	9.78	7.99	3.79	6.61	0.23	0.28
Thornel 40	258.72	8.41	6.99	3.10	6.61	0.23	0.35
Thornel 50	387.91	7.79	6.99	2.41	6.79	0.23	0.45
Thornel 505	403.75	6.99	6.61	2.49	6.99	0.37	0.40
Thornel 755	559.47	5.20	6.41	1.69	6.41	0.40	0.55
Carbon							
VYB	42.96	11.71	15.50	6.48	7.20	0.30	-0.10
Exp. PAN	198.85	15.16	12.61	6.48	7.79	0.33	0.16
HTS	179.83	11.58	9.78	4.41	7.30	0.34	0.19
Thornel 400	181.90	13.09	12.82	4.89	7.68	0.26	0.34

where

$$\eta = \frac{p_f/p_m - 1}{p_f/p_m + \zeta} \quad (3.22b)$$

where  $p^*$  denotes the modulus ( $E_T^*$ ,  $G_T^*$ , or  $G_L^*$ ) and  $\zeta$  is a factor which depends on the geometry of inclusions, packing geometry, and loading conditions. This factor is chosen to match the results of numerical calculations for each of the composite moduli reported in literature. It has been found [3.13] that  $\zeta = 1$  for  $G_L^*$  and  $\zeta = 2$  for  $E_T^*$  match the results for a square array of fibers up to a fiber volume fraction of 65 percent. Other values have been suggested for rectangular fiber arrays with different aspect ratios.

Bounds on properties for composites with arbitrary phase geometry are discussed in reference 3.14. Some results are given in appendix to this chapter.

For purposes of laminate analysis, it is important to consider the plane stress version of the effective stress-strain relations. Let  $x_3$  be the normal to the plane of a thin unidirectionally reinforced lamina. The plane stress condition is defined by

$$\bar{\sigma}_{33} = \bar{\sigma}_{13} = \bar{\sigma}_{23} = 0 \quad (3.23)$$

Then from (3.5-3.6)

$$\begin{aligned} \bar{\epsilon}_{11} &= \frac{\bar{\sigma}_{11}}{E_L^*} - \frac{\nu_L^*}{E_L^*} \bar{\sigma}_{22} \\ \bar{\epsilon}_{22} &= -\frac{\nu_L^*}{E_L^*} \bar{\sigma}_{11} + \frac{\bar{\sigma}_{22}}{E_T^*} \\ 2\bar{\epsilon}_{12} &= \frac{\bar{\sigma}_{12}}{G_L^*} \end{aligned} \quad (3.24)$$

The inversion of (3.24) is

$$\begin{aligned} \bar{\sigma}_{11} &= C_{11}^* \bar{\epsilon}_{11} + C_{12}^* \bar{\epsilon}_{22} \\ \bar{\sigma}_{22} &= C_{12}^* \bar{\epsilon}_{11} + C_{22}^* \bar{\epsilon}_{22} \\ \bar{\sigma}_{12} &= 2G_L^* \bar{\epsilon}_{12} \end{aligned} \quad (3.25)$$

where

$$\begin{aligned} C_{11}^* &= \frac{E_L^*}{1 - v_L^{*2} E_T^*/E_L^*} \\ C_{12}^* &= \frac{v_L^* E_T^*}{1 - v_L^{*2} E_T^*/E_L^*} \\ C_{22}^* &= \frac{E_T^*}{1 - v_L^{*2} E_T^*/E_L^*} \end{aligned} \quad (3.26a)$$

The value of  $v_L^*$  for polymeric matrix composites at the usual 60% fiber volume fraction is of the order of 0.25 while the ratio  $E_T^*/E_L^*$  is of the order of 0.1-0.2. Consequently, the denominator is generally almost equal to unity. Hence, the following approximations give reasonable results for such composites.

$$\begin{aligned} C_{11}^* &\approx E_L^* \\ C_{12}^* &\approx v_L^* E_T^* \\ C_{22}^* &\approx E_T^* \end{aligned} \quad (3.26b)$$

### 3.1.2 Thermal Expansion and Moisture Swelling.

The elastic behavior of composite materials discussed in the previous section is concerned with deformations produced by stresses, thus by loads. Deformations are also produced by temperature changes and by absorption of moisture, thus by environmental changes. The two phenomena are similar and, therefore, will be discussed together. A change of temperature in a free body produces thermal strains while moisture absorption produces swelling strains. The relevant physical parameters to quantify these phenomena are thermal expansion coefficients and swelling coefficients.

Fibers have significantly smaller thermal expansion coefficients than do polymeric matrices. The expansion coefficient of glass fibers is  $2.8 \times 10^{-6}$  (in/in $^{\circ}$ F) while a typical epoxy value is  $30 \times 10^{-6}$ . Carbon and graphite fibers are anisotropic in thermal expansion. The expansion coefficients in the fiber direction are mostly very small, either positive or negative of the order of  $0.5 \times 10^{-6}$ . It follows that a UDC will have a very small expansion coefficient in the fiber direction since the fibers will restrain matrix expansion. On the other hand, transverse expansion coefficients will be much larger since the fibers move with the expanding matrix and, thus, provide less restraint to matrix expansion.

These phenomena are of considerable practical importance, in particular, for laminates which are made of unidirectionally reinforced layers. When such a laminate is heated, the free expansion of any layer is prevented by the adjacent laminae since the fiber directions in all layers are different. Therefore, internal stresses develop which may be considerable. To compute these stresses, it is obviously necessary to know the thermal expansion coefficients of the layers. Procedures to determine these coefficients in terms of the elastic properties and the expansion coefficients of component fibers and matrix will be discussed in this section.

A physically similar situation arises in the case of moisture swelling. Polymers absorb moisture in a wet environment and consequently swell. When this swelling is restrained, stresses are produced. If a UDC is placed in a wet environment, the matrix absorbs moisture but, with the exception of Kevlar, the fibers do not. Therefore, the fibers restrain – literally prevent – swelling in the fiber direction but not in the direction transverse to the fibers. Thus, the UDC is very anisotropic with respect to moisture swelling.

When a laminate absorbs moisture, there occurs the same phenomenon as in the case of heating. Free swelling of the layers cannot take place and consequently internal stresses develop which can be computed if the UDC swelling coefficients are known. In this section, we shall also discuss procedures to compute those coefficients.

The thermal expansion coefficients of homogeneous solids are defined by the strains produced by unit change of temperature in bodies which are free of load and, thus, free of stress. The main engineering importance of thermal expansion is in the stresses produced when temperature changes occur under conditions of constraint and, thus, free expansion is prevented.

As will be explained below, the thermal expansion coefficients of a composite are defined by the average strains produced by unit temperature change. It should be noted, however, that in this case free thermal expansion cannot take place on the microscale because the difference of thermal expansion coefficients of the constituents will produce microstresses when the temperature changes. Thus, it is possible to fail a composite material by changing its temperature. The thermal expansion coefficients of a UDC are indispensable for stress analysis of laminates which are subjected to temperature changes.

When an isotropic homogeneous body is subjected to a temperature change  $\Delta T$ , the thermal expansion coefficient  $\alpha$  is defined by

$$e_{ij} = \alpha \Delta T \delta_{ij} \quad (3.27)$$

where  $\delta_{ij}$  is the Kronecker delta

$$\delta_{ij} = \begin{matrix} 1 & i = j \\ 0 & i \neq j \end{matrix}$$

and  $\epsilon_{ij}$  are the stress free strains, which in this case are isotropic, thus equal in all directions. For an anisotropic homogeneous body, (3.27) assumes the form

$$\epsilon_{ij} = \alpha_{ij} \Delta T \quad (3.28)$$

where  $\alpha_{ij}$  is the thermal expansion tensor. For a transversely isotropic body such as a single carbon or graphite fiber, (3.28) is of the form

$$\begin{aligned} \epsilon_{11} &= \alpha_L \Delta T \\ \epsilon_{22} &= \epsilon_{33} = \alpha_T \Delta T \\ \epsilon_{12} &= \epsilon_{23} = \epsilon_{13} = 0 \end{aligned} \quad (3.29)$$

where

$\alpha_L$  - axial expansion coefficient  
 $\alpha_T$  - transverse expansion coefficient

If there are also mechanical strains produced by stresses, then these are given by (3.1b), (3.2c), or (3.5c). It is the fundamental premise of uncoupled thermoelasticity that the mechanical strains and free thermal strains can be superposed to give the effect of simultaneous loading and temperature change.

$$\epsilon_{ij} = \epsilon_{ij}^M + \epsilon_{ij}^\lambda = S_{ijkl} \sigma_{kl} + \alpha_{ij} \Delta T \quad (3.30)$$

Next we consider a free cylindrical specimen of UDC under uniform temperature change  $\Delta T$ . This implies that the boundary temperature of the specimen is changed from  $T$  to  $T+\Delta$ . It may be easily shown that when a composite body is subjected to uniform boundary temperature, the temperature will also be uniform throughout the constituents. On the other hand, the stresses and strains in the phases are nonuniform and complex. The effective thermal expansion coefficients  $\alpha_{ij}^*$  are defined by

$$\bar{\epsilon}_{ij} = \alpha_{ij}^* \Delta T \quad (3.31)$$

where  $\bar{\epsilon}_{ij}$  are the average strains. Note that the average stresses  $\bar{\sigma}_{ij}$  vanish since the specimen is not loaded. (This follows from the average stress theorem [3.1].) If statistical transverse isotropy is assumed, (3.31) is analogous to (3.29) and there remain only the effective axial expansion coefficient  $\alpha_L^*$  and the transverse expansion coefficient  $\alpha_T^*$  (figure 3.14). The stress-strain relations (3.6) in the presence of temperature change  $\Delta T$  then assume the form

$$\begin{aligned}
\bar{\epsilon}_{11} &= \frac{\bar{\sigma}_{11}}{E_L^*} - \frac{\nu_L^*}{E_L^*} \bar{\sigma}_{22} - \frac{\nu_L^*}{E_L^*} \bar{\sigma}_{33} + \alpha_L^* \Delta T \\
\bar{\epsilon}_{22} &= -\frac{\nu_L^*}{E_L^*} \bar{\sigma}_{11} + \frac{\bar{\sigma}_{22}}{E_T^*} - \frac{\nu_T^*}{E_T^*} \bar{\sigma}_{33} + \alpha_T^* \Delta T \\
\bar{\epsilon}_{33} &= -\frac{\nu_L^*}{E_L^*} \bar{\sigma}_{11} - \frac{\nu_T^*}{E_T^*} \bar{\sigma}_{22} + \frac{\bar{\sigma}_{33}}{E_T^*} + \alpha_T^* \Delta T
\end{aligned} \tag{3.32}$$

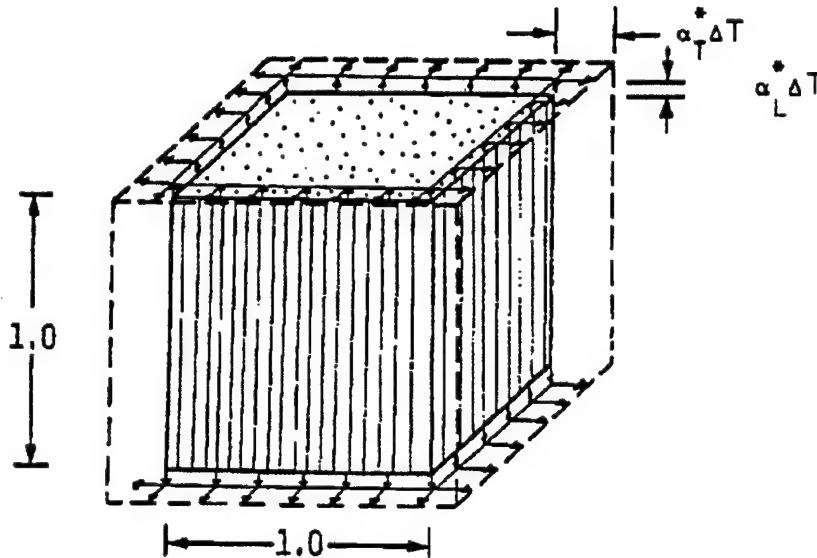


FIGURE 3.14. THERMAL EXPANSION

The definition (3.31) would indicate that in order to compute  $\alpha_{ij}^*$ , it would be necessary to compute the detailed strain fields in the two phases of a composite subjected to uniform temperature rise. Fortunately, however, it is not necessary to proceed by this difficult route. It has been shown by Levin [3.15] in a fundamental paper that there is a unique mathematical relation between the effective thermal expansion coefficients and the effective elastic properties of a two-phase composite. For the general relations, see references 3.1 and 3.16. Here we shall confine ourselves to specific cases of interest for a UDC. When fibers and matrix are isotropic we have



$$\alpha_L^* = \alpha_m + \frac{\alpha_f - \alpha_m}{1/K_f - 1/K_m} \left[ \frac{3(1-2\nu_L^*)}{E_L^*} - \frac{1}{K_m} \right]$$

$$\alpha_T^* = \alpha_m + \frac{\alpha_f - \alpha_m}{1/K_f - 1/K_m} \left[ \frac{3}{2k^*} - \frac{3(1-2\nu_L^*)\nu_L^*}{E_L^*} - \frac{1}{K_m} \right]$$
(3.33)

where

$\alpha_m, \alpha_f$  - matrix, fiber isotropic expansion coefficients

$K_m, K_f$  - matrix, fiber three-dimensional bulk modulus

$E_L^*, \nu_L^*, k^*$  - effective axial Young's modulus, axial Poisson's ratio, transverse bulk modulus

These equations are suitable for glass/epoxy and for boron/epoxy or boron/aluminum composites. They have also been derived in references 3.17 and 3.18.

For carbon and graphite fibers, it is necessary to consider the case of transversely isotropic fibers whose elastic and thermal expansion behavior is characterized by (3.3) and (3.29). This complicates the results considerably (references 3.6 and 3.8):

$$\begin{aligned} \alpha_L^* &= \alpha_m + (\alpha_{Lf} - \alpha_m) [P_{11} (S_{11}^* - S_{11}) + 2P_{12} (S_{12}^* - S_{12})] \\ &\quad + 2(\alpha_{Tf} - \alpha_m) [P_{12} (S_{11}^* - S_{11}) + (P_{22} + P_{23}) (S_{12}^* - S_{12})] \\ \alpha_T^* &= \alpha_m + (\alpha_{Lf} - \alpha_m) \{P_{11}(S_{12}^* - S_{12}) + P_{12}[S_{22}^* + S_{23}^* - (S_{22} + S_{23})]\} \\ &\quad + 2(\alpha_{Tf} - \alpha_m) \{P_{12} (S_{12}^* - S_{12}) + \frac{1}{2} (P_{22} + P_{23}) [S_{22}^* + S_{23}^* - (S_{22} + S_{23})]\} \end{aligned}$$
(3.34)

where

$$\begin{aligned}
P_{11} &= (\Delta S_{22} + \Delta S_{23})/D & P_{12} &= -\Delta S_{12}/D \\
P_{22} + P_{23} &= \Delta S_{11}/D & D &= \Delta S_{11} (\Delta S_{22} + \Delta S_{23}) - 2\Delta S_{12}^2 \\
\Delta S_{11} &= 1/E_{Lf} - S_{11} & \Delta S_{12} &= -\nu_{Lf}/E_{Lf} - S_{12} \\
\Delta S_{22} + \Delta S_{23} &= \frac{1}{2} (1/k_f + 4\nu_f^2/E_{Lf}) - (S_{22} + S_{23}) \\
S_{11} &= 1/E_m & S_{12} &= -\nu_m/E_m \\
S_{22} + S_{23} &= (1-\nu_m)/E_m \\
S_{11}^* &= 1/E_L^* & S_{12}^* &= -\nu_L^*/E_L^* \\
S_{22}^* + S_{23}^* &= \frac{1}{2} (1/k^* + 4\nu_L^{*2}/E_L^*)
\end{aligned}$$

Frequently thermal expansion coefficients of fibers and matrix are functions of temperature. In this case, there are two useful definitions of the expansion coefficient. Assuming that  $T_0$  is the reference state of zero strain (stress free state) and the temperature is raised to  $T$ , we may write the free thermal strains in the forms given below

$$\begin{aligned}
\epsilon_{ij} &= \alpha_{ij}^S(T) \Delta T \\
d\epsilon_{ij} &= \alpha_{ij}^t(T) dT
\end{aligned} \tag{3.35}$$

where  $\alpha_{ij}^S$  are the secant expansion coefficients and  $\alpha_{ij}^t$  are the tangent expansion coefficients. The two expansion coefficients are obviously related in the form

$$\alpha_{ij}^t = \frac{d\alpha_{ij}^S}{dT} \Delta T + \alpha_{ij}^S \tag{3.36}$$

Assuming that elastic properties are also temperature dependent, thermoelastic stress-strain relations such as (3.30) assume the form

$$\epsilon_{ij}(T) = S_{ijk\ell}(T) \sigma_{k\ell} + \alpha_{ij}^S(T) \Delta T \tag{3.37}$$

It is not difficult to show that (3.33-3.34) remain valid for temperature dependent properties if elastic properties are taken at final temperature and secant thermal expansion coefficients from stress-free temperature to the final state are used.

To evaluate the thermal expansion coefficients from (3.33) or (3.34), it is necessary to know the effective elastic properties  $K^*$ ,  $E_L^*$ ,  $\nu_L^*$ . These may be taken as the values predicted by the CCA model as given by (3.13-3.15) with the modification (3.20) when the fibers are transversely isotropic. Comparison of the values thus obtained with a numerical analysis performed for a hexagonal array of T300 fibers in epoxy [3.19] shows that the results obtained are numerically indistinguishable.

The thermal expansion coefficients of carbon and graphite fibers can be measured directly only in the fiber direction, thus obtaining  $\alpha_L$ . Direct measurement of transverse  $\alpha_T$  is not possible because of the minute fiber diameters. Again, the only possible method to evaluate  $\alpha_T$  is to measure  $\alpha_L^*$  and  $\alpha_T^*$  experimentally for a specified composite and to then compute  $\alpha_T$  from (3.34). If (3.34) is written in the form

$$\alpha_L^* = \alpha_m + (\alpha_{Lf} - \alpha_m) a_{11} + (\alpha_{Tf} - \alpha_m) a_{12} \quad (3.38)$$

$$\alpha_T^* = \alpha_m + (\alpha_{Lf} - \alpha_m) a_{21} + (\alpha_{Tf} - \alpha_m) a_{22}$$

it follows that

$$\alpha_{Lf} = \alpha_m + \frac{(\alpha_L^* - \alpha_m)a_{22} - (\alpha_T^* - \alpha_m)a_{12}}{a_{11}a_{22} - a_{12}a_{21}} \quad (3.39)$$

$$\alpha_{Tf} = \alpha_m + \frac{(\alpha_T^* - \alpha_m)a_{11} - (\alpha_L^* - \alpha_m)a_{21}}{a_{11}a_{22} - a_{12}a_{21}}$$

Figures 3.15-3.16 show typical plots of the effective thermal expansion coefficients of glass/epoxy and of graphite/epoxy. Note that for 50 percent volume fraction of fibers, the axial expansion coefficient  $\alpha_L^*$  is practically equal to that of the fibers. Many carbon and graphite fibers have small negative axial expansion coefficients and consequently many composites with such fibers have small negative or practically vanishing axial expansion coefficients. Also, note the interesting phenomenon that for small fiber volume fractions the transverse thermal expansion coefficient becomes larger than the matrix expansion coefficient, which is the maximum constituent expansion coefficient. Table 3.4 lists values of expansion coefficients for typical composites.

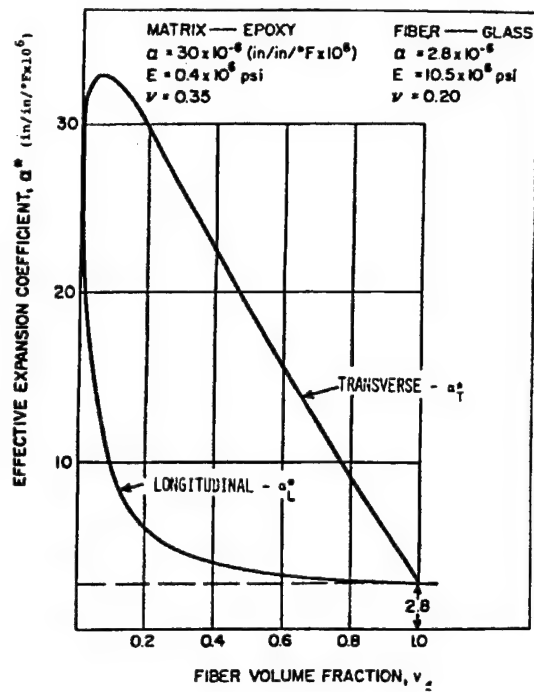


FIGURE 3.15. EFFECTIVE THERMAL EXPANSION COEFFICIENTS—CCA MODEL

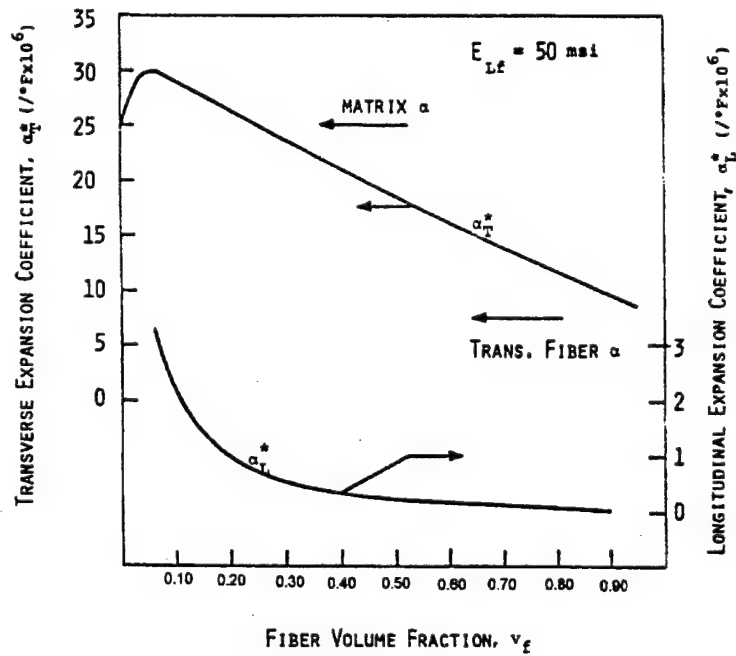


FIGURE 3.16. EFFECT OF FIBER FRACTION ON THERMAL EXPANSION FOR REPRESENTATIVE CARBON/EPOXY COMPOSITE

TABLE 3.4. CALCULATED THERMOELASTIC PROPERTIES FOR TYPICAL UNIDIRECTIONAL FIBER COMPOSITES

Fiber	Matrix	$v_f$	$\rho$ pci	$E_L$ ksi	$E_T$ ksi	$v_L$	$v_T$	$G_{LT}$ ksi	$\alpha_L$ $^{\circ}F \times 10^6$	$\alpha_T$ $^{\circ}F \times 10^6$
T-50	Al	0.3	0.088	24,100	6,380	0.339	0.354	3260	3.56	14.69
HM-1000	Al	0.3	0.089	21,200	6,630	0.322	0.346	3925	4.29	14.34
Pitch	Al	0.3	0.090	19,400	6,330	0.339	0.334	3260	4.50	14.59
T-300	Al	0.3	0.089	16,600	7,650	0.324	0.353	3650	5.19	12.96
T-50	Epoxy	0.3	0.045	17,230	654	0.337	0.421	310	0.14	25.00
HM-1000	Epoxy	0.3	0.047	14,350	705	0.286	0.396	330	0.46	24.80
Pitch	Epoxy	0.3	0.049	12,500	650	0.337	0.419	315	0.29	25.70
T-300	Epoxy	0.3	0.046	9,800	800	0.300	0.380	325	0.23	23.80
T-50	Epoxy	0.7	0.054	39,600	870	0.380	0.432	730	-0.288	13.30
HM-1000	Epoxy	0.7	0.057	32,800	1,060	0.270	0.371	850	-0.074	13.10
Pitch	Epoxy	0.7	0.061	28,500	870	0.380	0.431	725	-0.301	14.90
T-300	Epoxy	0.7	0.056	22,200	1,580	0.300	0.342	810	-0.557	11.60

We now consider the case of deformation due to moisture. When a body which absorbs moisture is placed in a wet environment, moisture will diffuse through the external boundary. The internal moisture concentration  $C$  is defined by the mass of moisture accumulated per unit volume and is initially a function of space and time. Ultimately the moisture concentration will settle down and become time independent. The time dependent stage is called the transient stage while the ultimate time independent stage is the stationary stage. There is complete mathematical analogy between the equations describing heat conduction and moisture diffusion, both in the transient and in the stationary stages. Thus, in the latter stage the concentration  $C$  satisfies the Laplace equation given by

$$C_{,xx} + C_{,yy} + C_{,zz} = 0$$

When a composite with a polymeric matrix is placed in a wet environment, the matrix will begin to absorb moisture. However, the moisture absorption of most fibers used in practice is negligible. Kevlar fibers alone do absorb significant amounts of moisture when exposed to high humidity. The total moisture absorbed by a Kevlar/epoxy composite, however, may not be substantially greater than other epoxy composites.

In most composites, the fibers act as barriers to moisture diffusion, analogous to perfect insulators in heat conduction. After sufficient time has elapsed, the matrix will be in an equilibrium moisture state with uniform concentration on the boundary. After a long time in this stage, the moisture concentration throughout the matrix will also be uniform, thus the same as the boundary concentration. It is customary to define the specific moisture concentration  $c$  by

$$c = C/\rho \quad (3.40)$$

where  $\rho$  is the density. Thus  $c$  is the mass of moisture per unit mass and is thus a non-dimensional number. The swelling strains due to moisture are obviously functions of  $c$  and to a first approximation are given by

$$\epsilon_{ij} = \beta_{ij} c \quad (3.41)$$

where  $\beta_{ij}$  are the swelling coefficients. For an isotropic material, which is the case for all polymeric matrices, (3.41) simplifies to

$$\epsilon_{ij} = \beta c \delta_{ij} \quad (3.42)$$

Thus

$$\begin{aligned} \epsilon_{11} &= \epsilon_{22} = \epsilon_{33} = \beta c \\ \epsilon_{12} &= \epsilon_{23} = \epsilon_{13} = 0 \end{aligned}$$

where  $\beta$  is the isotropic moisture swelling coefficient.

If there are also mechanical stresses and strains, then the swelling strains are superposed on the latter and thus for an isotropic material

$$\begin{aligned} \epsilon_{11} &= \frac{\sigma_{11}}{E} - \frac{\nu}{E} (\sigma_{22} + \sigma_{33}) + \beta c \\ \text{etc.} \end{aligned} \quad (3.43)$$

$$\epsilon_{12} = \frac{\sigma_{12}}{2G}$$

etc.

which are exactly analogous to the thermoelastic stress-strain relations of an isotropic material where  $\beta$  replaces the expansion coefficient and  $c$  the temperature. The swelling coefficients of most fibers are zero since their moisture absorption can be neglected. (Kevlar fiber swelling coefficients are unknown.) It follows that moisture swelling of a unidirectional composite is mathematically analogous to thermal expansion of such a composite with vanishing fiber

expansion coefficients. Therefore, all of the results previously given for thermal expansion can be transcribed to moisture swelling. The effective swelling coefficients  $\beta_{ij}^*$  are defined by the average strains produced in a free sample subjected to uniform unit change of specific moisture concentration in the matrix.

Thus

$$\bar{\epsilon}_{ij} = \beta_{ij}^* c \quad (3.44)$$

where

$$\begin{aligned} \beta_{11}^* &= \beta_L^* & \beta_{22}^* &= \beta_{33}^* = \beta_T^* \\ \beta_{12}^* &= \beta_{23}^* = \beta_{13}^* = 0 \end{aligned} \quad (3.45)$$

For isotropic fibers (e.g., glass) it follows from (3.33) that

$$\begin{aligned} \beta_L^* &= \beta_m \left\{ 1 - \frac{1}{1/K_f - 1/K_m} \left[ \frac{3(1-2\nu_L^*)}{E_L^*} - \frac{1}{K_m} \right] \right\} \\ \beta_T^* &= \beta_m \left\{ 1 - \frac{1}{1/K_f - 1/K_m} \left[ \frac{3}{2k^*} - \frac{3(1-2\nu_L^*)\nu_L^*}{E_L^*} - \frac{1}{K_m} \right] \right\} \end{aligned} \quad (3.46)$$

For transversely isotropic fibers (e.g., carbon and graphite), it follows from (3.34) that

$$\begin{aligned} \beta_L^* &= \beta_m \{ 1 - [(P_{11} + 2P_{12})(S_{11}^* - S_{11}) + 2(P_{12} + P_{22} + P_{23})(S_{12}^* - S_{12})] \} \\ \beta_T^* &= \beta_m \{ 1 - [(P_{11} + 2P_{12})(S_{12}^* - S_{12}) + (P_{12} + P_{22} + P_{23}) \\ &\quad (S_{22}^* + S_{23}^* - S_{22} - S_{23})] \} \end{aligned} \quad (3.47)$$

where the rest of the notation in (3.34) remains the same.

Table 3.5 shows the ratios of longitudinal and transverse swelling coefficients to matrix swelling coefficient for two typical composites as a function of fiber volume fraction. It is seen that the longitudinal swelling coefficients are negligible, while the transverse swelling coefficients are literally constant and larger than matrix swelling coefficients. This seemingly curious phenomenon is explained by the large matrix compressive stresses in the fiber direction due to the restraining effect of fibers on axial swelling. Because of the Poisson effect, these compressive stresses produce substantial transverse strains, which appear as transverse swelling. It should be emphasized that the above is concerned with the case of moisture equilibrium. Since moisture content changes slowly, it is sometimes necessary to predict the moisture swelling coefficients in the transient state. The relations given above can be utilized for this purpose, but the moisture concentration and swelling stress will vary with position. Further, the swelling coefficient for the matrix may not be a constant but a function of the moisture concentration, which is difficult to determine experimentally. To the best of our knowledge, this problem is unresolved at the present time.

TABLE 3.5. EFFECTIVE SWELLING COEFFICIENTS

$v_f$	Glass/Epoxy		T50/Epoxy	
	$\beta_L^*/\beta_m$	$\beta_T^*/\beta_m$	$\beta_L^*/\beta_m$	$\beta_T^*/\beta_m$
0.2	0.160	1.30	0.030	1.34
0.4	0.067	1.34	0.011	1.35
0.6	0.031	1.35	0.005	1.35
0.8	0.011	1.36	0.002	1.35

For discussion of other aspects of moisture absorption and transient and steady state, see reference 3.20, which also contains other interesting survey articles on this subject, and reference 3.21.

Finally, we consider the important question of simultaneous moisture swelling and temperature rise. This is often called hygrothermal behavior. The simplest approach is to assume that thermal expansion strains and moisture swelling strains can be superposed. Thus, for a free specimen

$$\begin{aligned}\bar{\epsilon}_{11} &= \alpha_L^* \Delta T + \beta_L^* c \\ \bar{\epsilon}_{22} = \bar{\epsilon}_{33} &= \alpha_T^* \Delta T + \beta_T^* c\end{aligned}\tag{3.48}$$

In this event, the matrix elastic properties in (3.33-3.34) and in (3.47) may be functions of the end temperature and the equilibrium moisture concentration  $c$ , and this dependence must be known in order to evaluate  $\alpha_L^*$ ,  $\alpha_T^*$ ,  $\beta_L^*$  and  $\beta_T^*$  in (3.48).



### 3.1.3 Viscoelastic Properties.

All polymers exhibit the phenomenon of time dependence. This manifests itself by the increase of deformations with time under constant load (which is called creep) and, conversely, by the decrease of stresses with time under deformation constraints, which is called relaxation. Another important effect of time dependence is the damping of vibrations due to energy dissipation in the polymeric matrix. The significance of all these phenomena increases with rise in temperature.

The effects described are of considerable engineering importance for fiber composite structures, since stresses and deformations determined on the basis of elastic analysis may change considerably with time due to polymeric matrix time dependence. Vibration damping is a beneficial effect which is of particular significance for the higher vibration modes which often become negligible due to damping.

The simplest description of time dependence is linear viscoelasticity. Viscoelastic behavior of polymers manifests itself primarily in shear and is negligible for isotropic stress and strain. This implies that the elastic stress-strain relation

$$\sigma_{11} + \sigma_{22} + \sigma_{33} = 3K (\epsilon_{11} + \epsilon_{22} + \epsilon_{33}), \quad (3.49)$$

where  $K$  is the three-dimensional bulk modulus, remains valid for polymers. When a polymeric specimen is subjected to shear strain  $\epsilon_{12}^0$  which does not vary with time, the stress needed to maintain this shear strain is given by

$$\sigma_{12}(t) = 2G(t) \epsilon_{12}^0 \quad (3.50)$$

and  $G(t)$  is defined as the shear relaxation modulus. When a specimen is subjected to shear stress  $\sigma_{12}^0$  constant in time, the resulting shear strain is given by

$$\epsilon_{12}(t) = \frac{1}{2} g(t) \sigma_{12}^0 \quad (3.51)$$

and  $g(t)$  is defined as the shear creep compliance.

If the applied shear strain is an arbitrary function of time, commencing at time zero, (3.50) is replaced by

$$\sigma_{12}(t) = 2G(t) \epsilon_{12}(0) + 2 \int_0^t G(t-t') \frac{d\epsilon_{12}}{dt'} dt' \quad (3.52)$$

Similarly, for applied shear stress which is a function of time (3.51) is replaced by

$$\epsilon_{12}(t) = \frac{1}{2} g(t) \sigma_{12}(0) + \frac{1}{2} \int_0^t g(t-t') \frac{d\sigma_{12}}{dt'} dt' \quad (3.53)$$

The viscoelastic counterpart of the Young's modulus is obtained by subjecting a cylindrical specimen to axial strain  $\epsilon_{11}^0$  constant in space and time. Then

$$\sigma_{11}(t) = E(t) \epsilon_{11}^0 \quad (3.54)$$

and  $E(t)$  is the Young's relaxation modulus. If the specimen is subjected to axial stress  $\sigma_{11}^0$  constant in space and time then

$$\epsilon_{11}(t) = e(t) \sigma_{11}^0 \quad (3.55)$$

and  $e(t)$  is the Young's creep compliance. This is schematically shown in figure 3.17.

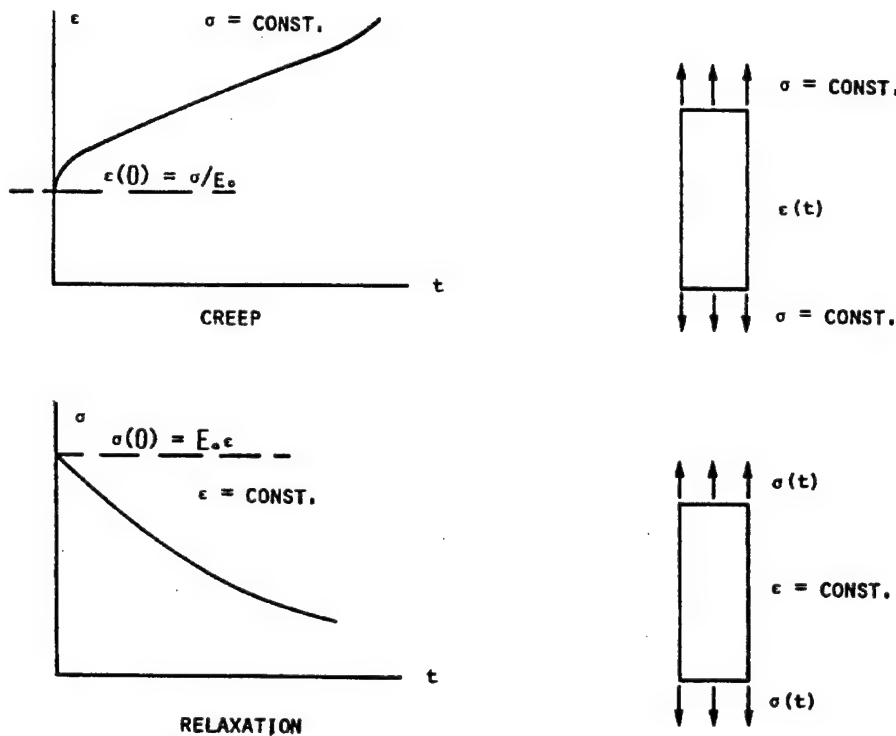


FIGURE 3.17. VISCOELASTICITY

These material properties may change significantly with temperature; the relaxation modulus decreases with temperature and the creep compliance increases with temperature, which implies that stiffness decreases with temperature. The change of creep compliance  $e(t)$  with temperature for an epoxy resin is illustrated in figure 3.18. The initial values of these properties at time zero  $E_m$ —thus at the beginning of deformation—are denoted  $E_0$  and  $e_0$  and are the elastic properties of the matrix. Note that  $E_0 e_0 = 1$ .

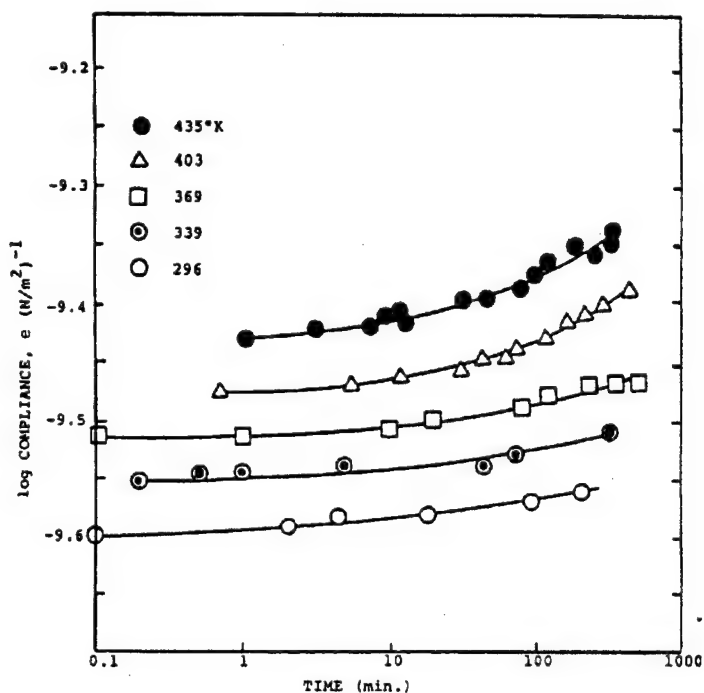


FIGURE 3.18. CREEP COMPLIANCE FOR 5208 RESIN AS A FUNCTION OF TEMPERATURE [3.109]

Obviously  $E(t)$  is related to  $K$  and  $G(t)$ , and  $e(t)$  is related to  $k$  and  $g(t)$ . The relations are not simple and the interested reader is referred to reference 3.22. To write the viscoelastic stress-strain relations for general states of three-dimensional stress and strain, it is customary to separate stress and strain into isotropic (or hydrostatic) and deviatoric parts.

Thus

$$\begin{aligned}
 \sigma_{ij} &= \sigma \delta_{ij} + s_{ij} & \sigma &= \frac{1}{3} (\sigma_{11} + \sigma_{22} + \sigma_{33}) \\
 \epsilon_{ij} &= \epsilon \delta_{ij} + e_{ij} & \epsilon &= \frac{1}{3} (\epsilon_{11} + \epsilon_{22} + \epsilon_{33})
 \end{aligned}
 \tag{3.56}$$

Then

$$\sigma(t) = 3K\epsilon(t)$$

$$S_{ij}(t) = 2G(t)e_{ij}(0) + 2 \int_0^t G(t-t') \frac{\partial e_{ij}}{\partial t'} dt' \quad (3.57)$$

$$e_{ij}(t) = \frac{1}{2} g(t) s_{ij}(0) + \frac{1}{2} \int_0^t g(t-t') \frac{\partial s_{ij}}{\partial t'} dt'$$

The basic problem is to evaluate the effective viscoelastic properties of a unidirectional fiber composite in terms of polymeric matrix viscoelastic properties and the elastic properties of the fibers. (It is assumed that the fibers themselves do not experience any time dependent effect.) This problem has been resolved in general fashion in references 3.23 and 3.24, where it has been shown that the Laplace transforms of the effective relaxation moduli and creep compliances of a composite can be written in terms of expressions for effective elastic moduli in which elastic matrix properties are replaced by Laplace transforms of viscoelastic matrix properties (called the correspondence principle). The main difficulty is the inversion of these Laplace transforms into the time domain. Details and applications of such procedures have been given in reference 3.1. Here we shall only be concerned with some simple illustrative cases.

Detailed analysis shows that the viscoelastic effect in a unidirectional fiber composite is significant only for axial shear, transverse shear, and transverse uniaxial stress. This is schematically illustrated in figures 3.19 and 3.20, and the stress-strain relations in these cases are presented after the figures.

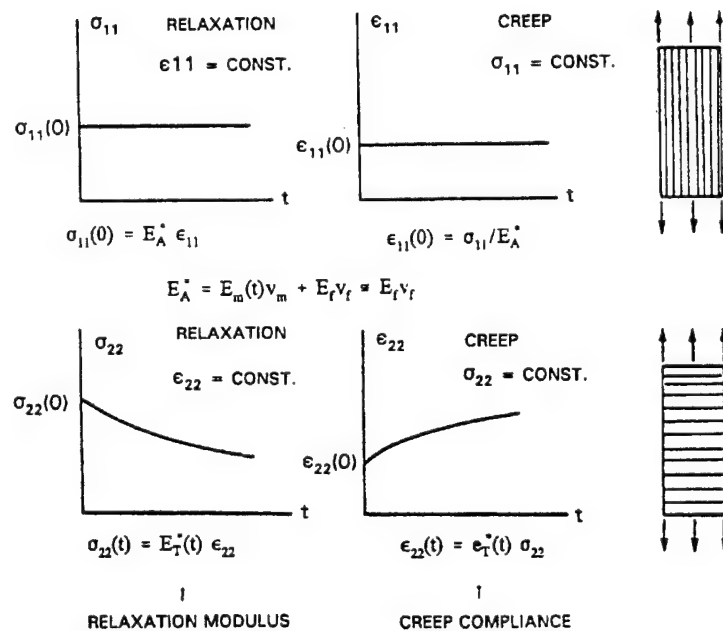


FIGURE 3.19. VISCOELASTICITY OF FIBER COMPOSITES

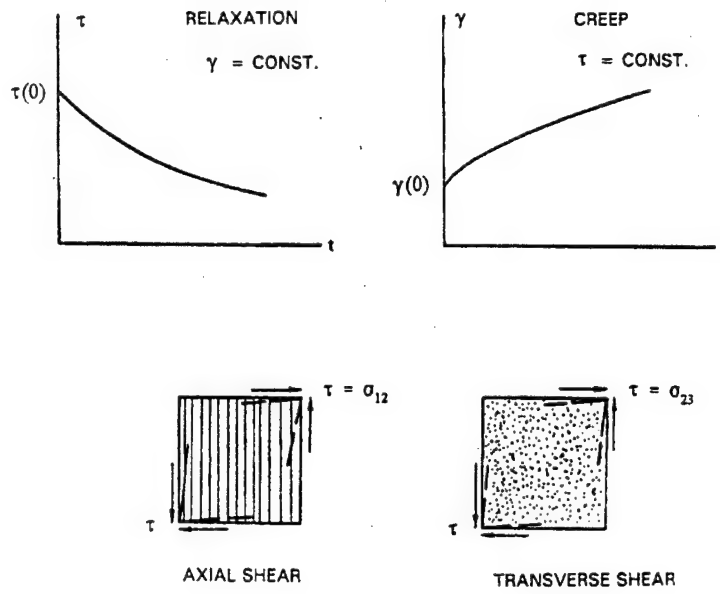


FIGURE 3.20. VISCOELASTICITY IN SHEAR

For average strains  $\bar{\epsilon}_{22}$ ,  $\bar{\epsilon}_{33}$ , and  $\bar{\epsilon}_{12}$  constant in time, the stress relaxation relations are given by

$$\begin{aligned}\bar{\sigma}_{22}(t) &= E_T^*(t) \bar{\epsilon}_{22} & \bar{\sigma}_{12}(t) &= 2G_L^*(t) \bar{\epsilon}_{12} \\ \bar{\sigma}_{23}(t) &= 2G_T^*(t) \bar{\epsilon}_{23}\end{aligned}\tag{3.58}$$

For stresses  $\bar{\sigma}_{22}$ ,  $\bar{\sigma}_{23}$  and  $\bar{\sigma}_{12}$  constant in time, the creep deformations are given by

$$\begin{aligned}\bar{\epsilon}_{22}(t) &= e_T^*(t) \bar{\sigma}_{22} \\ \bar{\epsilon}_{23}(t) &= \frac{1}{2} g_T^*(t) \bar{\sigma}_{23} \\ \bar{\epsilon}_{12}(t) &= \frac{1}{2} g_L^*(t) \bar{\sigma}_{12}\end{aligned}\tag{3.59}$$

where the material properties in (3.58) are effective relaxation moduli and the properties in (3.59) are associated effective creep functions. All other effective properties may be considered elastic. This implies in particular that if a fiber composite is subjected to stress  $\bar{\sigma}_{11}(t)$  in the fiber direction then

$$\begin{aligned}\bar{\sigma}_{11}(t) &\approx E_L^* \bar{\epsilon}_{11}(t) \\ \bar{\epsilon}_{22}(t), \bar{\epsilon}_{33}(t) &\approx -\nu_L^* \bar{\epsilon}_{11}(t)\end{aligned}\tag{3.60}$$

where  $E_L^*$  and  $\nu_L^*$  are the elastic results (3.14-3.15) with matrix properties taken as initial (elastic) matrix properties. Similar considerations apply to the relaxation modulus  $k^*$ .

The simplest case of the viscoelastic properties entering into (3.58-3.59) is the relaxation modulus  $G_L^*(t)$  and its associated creep compliance  $g_L^*(t)$ . A very simple result has been obtained for fibers which are infinitely more rigid than the matrix, reference 3.1. In this case, the elastic result (3.16) reduces to

$$G_L^* = G_m \frac{1+\nu_f}{1-\nu_f}$$

For a viscoelastic matrix, the corresponding results are

$$\begin{aligned}G_L^*(t) &= G_m(t) \frac{1+\nu_f}{1-\nu_f} \\ g_L^*(t) &= g_m(t) \frac{1-\nu_f}{1+\nu_f}\end{aligned}\tag{3.61}$$

This result is an acceptable approximation for glass fibers in polymeric matrix and an excellent approximation for boron fibers in a polymeric matrix. However, the result is not applicable to the case of carbon or graphite fibers in a polymeric matrix since the axial shear modulus of these fibers is not large enough in relation to the matrix shear modulus to justify rigid fiber approximation. In this case, it is necessary to use the correspondence principle mentioned earlier (after equation 3.57). Laplace transform inversion can be carried out by representing the matrix in terms of a viscoelastic spring dashpot model. The interested reader is referred to references 3.1 and 3.23 where details of such analysis have been given.

A somewhat drastic approximation for evaluation of viscoelastic properties of composites has been introduced in reference 3.25 and has been further discussed in reference 3.26. According to the scheme proposed, the effective property at time  $t$  is given by the corresponding effective elastic modulus expression, in which matrix elastic moduli are replaced by matrix relaxation moduli at time  $t$ . Thus  $G_L^*(t)$  for this approximation states that

$$G_L^*(t) \sim G_m(t) \left[ \frac{G_m(t)v_m + G_f(1+v_f)}{G_m(t)(1+v_f) + G_f v_m} \right] \quad (3.62)$$

$$g_L^*(t) \sim 1/G_L^*(t)$$

While the simplicity of this scheme is attractive, the range of its reliability is not established.

The situation for transverse shear is more complicated and involves complicated Laplace transform inversions. An assessment of the effective relaxation modulus  $G_T^*(t)$  can perhaps be obtained by using the previously mentioned approximation illustrated by (3.62). Accordingly, the matrix shear modulus  $G_m$  in (3.17) or in (3.21) is replaced by  $G_m(t)$  and  $v_m$  must be interpreted as  $[3K_m - 2G_m(t)]/2[3K_m + G_m(t)]$ . Within the frame of the same approximation, it then follows from (3.17) that

$$4/E_T^*(t) \sim 1/G_T^*(t) + 1/k^* + 4v_A^{*2}/E_A^* \quad (3.63)$$

We now consider the subject of the effect of polymeric matrix viscoelasticity on steady state vibrations of a UDC. Matrix viscoelasticity is beneficial since it produces damping of free vibrations and attenuation of resonance peaks. It will be recalled that when an elastic structure vibrates at critical frequency, deformations and stresses become, theoretically, infinite. If the structural material is viscoelastic, however, there are finite resonance peaks which rapidly diminish for higher order critical frequencies.

For the purpose of discussion, we first summarize some basic concepts for vibrations of viscoelastic homogeneous materials. For simplicity, we first consider the case of a simple elastic cylindrical test specimen which is subjected to sinusoidally oscillating uniaxial stress in either one of the forms

$$\sigma_c = \sigma_o \cos \omega t \quad \sigma_s = \sigma_o \sin \omega t \quad (3.64)$$

where  $\omega$  is the frequency and  $\sigma_o$  is the amplitude. The strain responses in these two cases are

$$\begin{aligned}\epsilon_c &= \epsilon_o \cos \omega t & \epsilon_s &= \epsilon_o \sin \omega t \\ \epsilon_o &= \sigma_o / E\end{aligned}$$

It is customary to summarize such results by the single relation

$$\begin{aligned}\sigma &= \sigma_o e^{i\omega t} \\ \epsilon &= \frac{\sigma_o}{E} e^{i\omega t}\end{aligned}\tag{3.65}$$

where

$$i = \sqrt{-1}, \quad e^{i\omega t} = \cos \omega t + i \sin \omega t$$

The important feature of these results is that stress and strain vibrations are in phase.

The situation is different for a viscoelastic specimen, in which case stress and strain vibrations will no longer be in phase. It is customary to express this in terms of the complex modulus. If

$$\sigma = \sigma_o e^{i\omega t}$$

then

$$\epsilon = \frac{\sigma_o}{\tilde{E}} e^{i\omega t}\tag{3.66a}$$

$$\tilde{E} = E'(\omega) + iE''(\omega)\tag{3.66b}$$

The complex number  $\tilde{E}$  is defined as the complex modulus. To explain the physical meaning of this seemingly abstruse result, we use the rules for complex numbers to write  $\tilde{E}$  in the form

$$\tilde{E} = |E| e^{i\delta}\tag{3.67}$$

where



$$|E| = \sqrt{E'^2 + E''^2} \quad (3.68a)$$

$$\tan \delta = E''/E' \quad (3.68b)$$

The various quantities are called:  $E'$  = storage modulus,  $E''$  = loss modulus, and  $\tan \delta$  = loss tangent. If (3.67) is introduced into (3.66), it assumes the form

$$\epsilon = \frac{\sigma_o}{|E|} e^{i(\omega t - \delta)}$$

and taking real and imaginary parts we have

$$\epsilon_c = \frac{\sigma_o}{|E|} \cos(\omega t - \delta) \quad (3.69)$$

$$\epsilon_s = \frac{\sigma_o}{|E|} \sin(\omega t - \delta)$$

The strain  $\epsilon_c$  is the response to  $\sigma_c$  as given in (3.64) and the strain  $\epsilon_s$  is the response to  $\sigma_s$ . It is seen that there is a phase lag and the strains are frequency dependent.

The loss tangent (3.68b) is an important quantity for determination of the degree of vibration damping of a viscoelastic material and for computation of structural resonance peaks. It is a small quantity at room temperature, of the order of 0.05, for the epoxies used in composite materials.

In a UDC, the state of stress in the matrix is quite complex and, therefore, the simple description given above for uniaxial stress is not sufficient. It will be recalled that it may generally be assumed that a polymer behaves elastically under isotropic (e.g., hydrostatic) stress and for this situation is characterized by an elastic bulk modulus  $K$  (3.57). This simplification can also be adopted for the case of vibrations. The viscoelastic effect occurs predominantly in shear;

therefore, we define a complex shear modulus  $\tilde{G}$  in complete analogy to the complex Young's modulus discussed above. We may imagine that a thin-walled circular tube is subjected to sinusoidal shear vibration by means of an oscillating torque. The response is an oscillating angle of twist which determines the oscillatory shear strain. In the viscoelastic case, the two are related by the complex shear modulus

$$\begin{aligned} \tilde{G} &= G'(\omega) + iG''(\omega) \\ \tan \delta &= G''/G' \end{aligned} \quad (3.70)$$

It may be noted that  $\tilde{E}$  is related to  $\tilde{G}$  and  $K$  by the usual elastic relation.

$$\tilde{E} = \frac{9K\tilde{G}}{3K + \tilde{G}}$$

The viscoelastic response of a UDC to steady-state vibration is expressed in terms of effective complex moduli. Since the material is anisotropic, it has many such complex moduli, just as it has a variety of effective elastic moduli. A complete discussion is beyond the scope of the present treatment, and the interested reader is referred to reference 3.1. Here we shall confine ourselves to some simple results which are of engineering interest.

The basis for the analytical treatment is a correspondence principle derived in reference 3.27, which states that an effective complex modulus of a composite is determined by the corresponding expression for effective elastic modulus in which constituent elastic properties are replaced by viscoelastic constituent properties in the form of complex moduli. As a simple example for this procedure, we consider the case of oscillatory stress in the fiber direction. In the elastic case, this is characterized by the effective longitudinal Young's modulus  $E_L^*$  which is accurately given by the simple expression (3.14b). The effective complex modulus is then given by

$$\tilde{E}_L^* \approx \tilde{E}_m v_m + E_f v_f \quad (3.71)$$

Where  $\tilde{E}_m$  is represented by (3.66b). Separating into real and imaginary parts, we have

$$E_L^{*'} = E_m' v_m + E_f v_f \quad (3.72)$$

$$E_L^{*''} = E_m'' v_m$$

from which it follows that the loss tangent is

$$\tan \delta^* = \frac{E_L^{*''}}{E_L^{*'}} = \frac{E_m''/E_m'}{1 + E_f v_f / E_m' v_m} \quad (3.73)$$

The numerator is the matrix loss tangent. Since the fibers are much stiffer than the matrix, the ratio in the denominator is a number in the range 25-100 for glass, carbon, and graphite fibers. It is seen, therefore, that the fibers significantly reduce the viscoelastic effect in longitudinal vibrations in the fiber direction, indeed to the point where it is negligible.

Another important case is longitudinal shear oscillations. This case is characterized by a complex modulus,  $\tilde{G}_L^*$  which is obtained by replacement of  $\tilde{G}_m$  by  $G_m$  in (3.16). Separating into real and imaginary parts, we find [3.27]:

$$\begin{aligned} G_L^{*'} &= G_m' \left[ \frac{G_m'(1+v_f) + G_f v_m}{G_m' v_m + G_f(1+v_f)} \right] \\ G_L^{*''} &= G_m'' \left[ \frac{[(G_f + G_m')^2 + v_f(G_f - G_m')^2] v_m}{[G_f v_m + G_m'(1+v_f)]^2} \right] \end{aligned} \quad (3.74)$$

Then the loss tangent is defined by

$$\tan \delta^* = G_L^{*''} / G_L^{*'} \quad (3.75)$$

Evaluation of this loss tangent for glass/epoxy shows that it is about 0.90 of the matrix loss tangent, while for carbon-graphite/epoxy it is about 0.50-0.60 of the matrix loss tangent. This implies that the viscoelastic effect in longitudinal shear is of the order of that of the matrix and thus is significant.

An illuminating case is the transverse vibration of a beam which is made of a UDC with fibers in the beam axis direction. The bending stresses are in the fiber direction and, therefore, do not produce noticeable viscoelastic effect. However, the shear stresses from beam theory are longitudinal and, therefore, produce significant vibration damping.

Longitudinal shear is also produced in torsional vibrations of an axially reinforced cylinder. Figure 3.21 shows a plot of the amplitude of angle of twist versus frequency of forcing torque for such a cylinder made of glass/epoxy. In the case of assumed elastic behavior, there are resonances at critical frequencies as shown. If matrix viscoelasticity is taken into account through complex longitudinal shear modulus, there are finite resonance peaks which are quickly damped out.

Another case of engineering interest is damping due to transverse oscillatory stress as expressed by complex modulus  $E_T^*$ . The results for this case, however, are complicated. The interested reader is referred to reference 3.1.

All polymeric matrix viscoelastic properties such as creep and relaxation functions and complex moduli are significantly temperature dependent. If this temperature dependence is known, all of the results given in this section can be obtained for the temperature of interest by introducing into the results matrix properties at that temperature.

At elevated temperatures the viscoelastic behavior of the polymeric matrix may become nonlinear. In this event, the UDC will also be nonlinearly viscoelastic and all of the results given

are not valid. The problem of analytical determination of nonlinear properties is, of course, much more difficult than the linear problem. Some results have been obtained in reference 3.26.

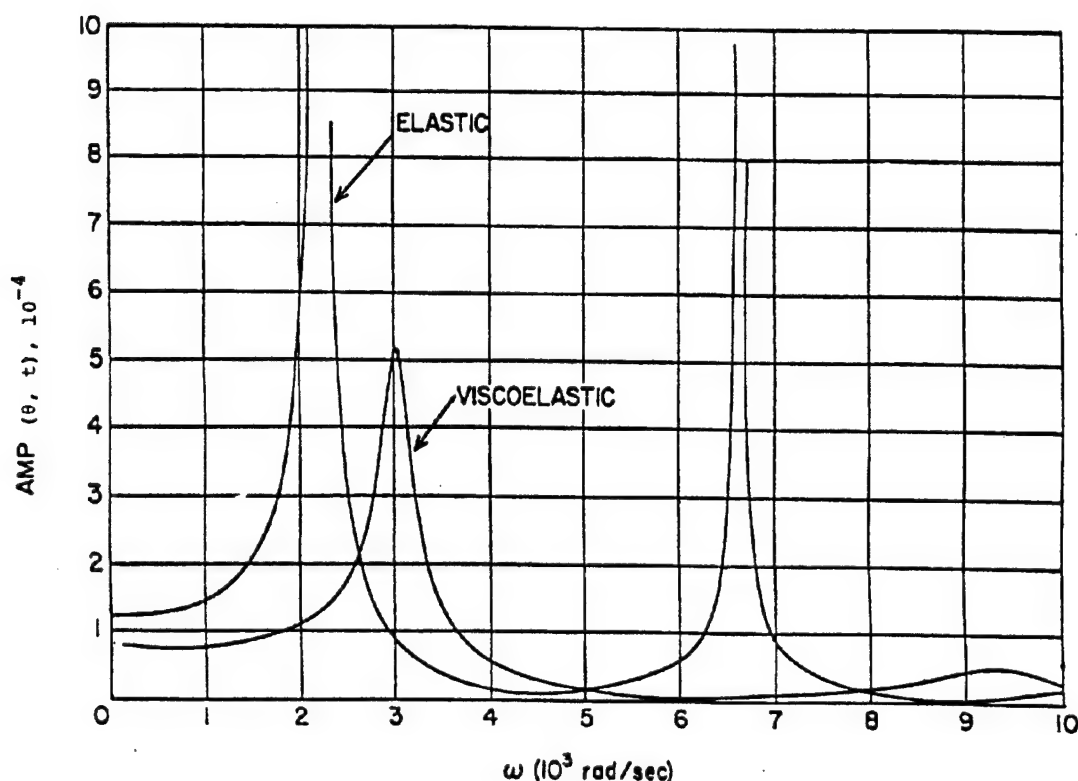


FIGURE 3.21. CALCULATED AMPLITUDE OF ANGLE OF TWIST IN TORSIONAL VIBRATIONS OF A UNIDIRECTIONALLY REINFORCED GLASS/EPOXY CYLINDER [3.1 and 3.27]

Polymers are also known to show some effect of aging. However, if the effects of aging on viscoelastic properties of the matrix are known, the properties of the composite can be evaluated by the procedures discussed earlier.

#### 3.1.4 Conduction and Moisture Diffusion.

We shall discuss here the subject of the conductivity of a UDC. This implies both thermal and electrical conductivity. Since all of the conductivity problems are governed by similar equations, the results obtained also apply to the cases of dielectric and magnetic properties and to steady-state moisture diffusion. The various equivalent physical quantities related to these aspects of composite behavior are listed in table 3.6. The discussion will be given in the language of thermal conductivity.

TABLE 3.6. ANALOGOUS QUANTITIES

Physical Subject	T	$\underline{H} = -\nabla T$
Thermal Conduction	Temperature	Temperature Gradient
Electric Conduction	Electric Potential	Electric Field Intensity
Electrostatics	Electric Potential	Electric Field Intensity
Magnetostatics	Magnetic Potential	Magnetic Field Intensity
Moisture Diffusion	Concentration	Moisture Gradient
$\underline{D}$	$\mu_{ij}$	$\zeta_{ij}$
Heat Flux	Heat Conductivities	Resistivities
Current Density	Electric Conductivities	Resistivities
Electric Induction, Electric Displacement	Dielectric Constants, Permittivities	
Magnetic Induction	Magnetic Permeabilities	
Moisture Flux	Diffusivities	

Let  $T(\underline{x})$  be a steady-state temperature field in a homogeneous body. The temperature gradient is given by

$$H_i = - \frac{\partial T}{\partial x_i} \quad (3.76)$$

and the heat flux vector by

$$D_i = \mu_{ij} H_j \quad (3.77)$$

where  $\mu_{ij}$  is the conductivity tensor. The inverse of (3.77) is

$$H_i = \xi_{ij} D_j \quad (3.78)$$

where  $\xi_{ij}$  is the resistivity tensor. In an isotropic material

$$\begin{aligned} D_i &= \mu H_i \\ H_i &= \xi D_i \\ \xi &= 1/\mu \end{aligned} \quad (3.79)$$

For a transversely isotropic material, e.g., carbon and graphite fibers, with  $x_1$  the axis of transverse isotropy (fiber axis)

$$\begin{aligned} D_1 &= \mu_L H_1 \\ D_2 &= \mu_T H_2 \\ D_3 &= \mu_T H_3 \end{aligned} \quad (3.80)$$

where  $\mu_L$  is longitudinal conductivity and  $\mu_T$  is transverse conductivity.

A simple common example is heat conduction through a slab, figure 3.22, whose faces are maintained at different temperatures  $T$  and  $T + \Delta T$ . Then

$$\begin{aligned} H_1 &= - \frac{\Delta T}{h} \\ D_1 &= \mu_{11} H_1 \end{aligned}$$

where  $\mu_{11}$  is the conductivity coefficient normal to the faces of the slab.

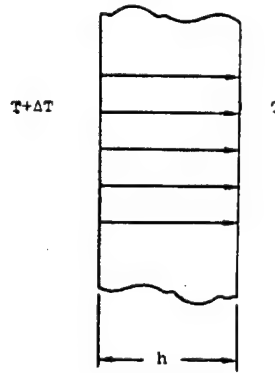


FIGURE 3.22. ONE-DIMENSIONAL HEAT CONDUCTION THROUGH A SLAB

Since a UDC is statistically transversely isotropic, it has two different effective conductivities,  $\mu_L^*$  in the fiber direction and  $\mu_T^*$  transverse to the fibers. The effective constituent relations are analogous to (3.80)

$$\begin{aligned} \bar{D}_1 &= \mu_L^* \bar{H}_1 \\ \bar{D}_2 &= \mu_T^* \bar{H}_2 \quad \bar{D}_3 = \mu_T^* \bar{H}_3 \end{aligned} \quad (3.81)$$

where overbars denote averages over the representative volume element (RVE).

It may be easily shown [3.1] that for isotropic matrices and fibers the axial conductivity  $\mu_L^*$  is given by

$$\mu_L^* = \mu_m v_m + \mu_f v_f \quad (3.82)$$

and for transversely isotropic fibers

$$\mu_L^* = \mu_m v_m + \mu_{Lf} v_f \quad (3.83)$$

where the subscript Lf notation refers to the longitudinal conductivity of the fibers. The results (3.82 and 3.83) are valid for any fiber distribution and any fiber cross sections.

The problem of transverse conductivity is mathematically analogous to the problem of longitudinal shearing [3.1]. It follows that all results for the effective longitudinal shear modulus  $G_L^*$  can be interpreted as results for transverse effective conductivity  $\mu_T^*$ . In particular, for the composite cylinder assemblage model

$$\begin{aligned} \mu_T^* &= \mu_m \left[ \frac{\mu_m v_m + \mu_f (1 + v_f)}{\mu_m (1 + v_f) + \mu_f v_m} \right] \\ &= \mu_m + \frac{v_f}{1/(\mu_f - \mu_m) + v_m/2\mu_m} \end{aligned} \quad (3.84)$$

These results are for isotropic fibers. For carbon and graphite fibers,  $\mu_f$  should be replaced by the transverse conductivity  $\mu_{Tf}$  of the fibers [3.8].

As in the elastic case, there is reason to believe that (3.84) represents with great accuracy all cases of circular fibers which are randomly distributed and are not in contact. The reason is again the numerical coincidence of hexagonal array numerical analysis results with those predicted by (3.84).

To interpret the results for the case of moisture diffusion the quantity  $\mu_m$  is interpreted as the diffusivity of the matrix. Since moisture absorption of fibers is negligible,  $\mu_f$  is set equal to zero. The results are then

$$\begin{aligned} \mu_L^* &= \mu_m v_m \\ \mu_T^* &= \mu_m \left[ \frac{v_m}{1 + v_f} \right] \end{aligned} \quad (3.85)$$

which leads to the interesting relation

$$\mu_L^* / \mu_T^* = 1 + v_f \quad (3.86)$$

### 3.2 FIBER COMPOSITES: STRENGTH AND FAILURE.

The mathematical treatment of the relationships between the strength of a composite and the properties of its constituents is considerably less developed than the analyses for the other physical property relationships discussed in the previous sections of this chapter. One of the reasons for this is that failure is likely to initiate in a local region due to the influence of the local values of constituent properties and geometry in that region. Thus, the high degree of variability of local geometry (e.g., relative locations of adjacent fibers) and of the local strength of the fibers both contribute to the onset of initial localized damage within the composite. This dependence upon local characteristics makes the analysis of the composite failure mechanisms much more complex than the analyses of the physical properties discussed earlier.

The strength of a fiber composite clearly depends upon the orientation of the applied load with respect to the direction in which the fibers are oriented as well as on whether the applied load is tensile or compressive. Therefore, the following strength parameters and corresponding failure modes are of interest.

- a. **Axial Tensile Strength**—This strength is the tensile stress in the fiber direction required for failure. Dispersed fiber breaks are the initial forms of damage which develop in unidirectional brittle fiber composites subjected to such loading. Final failure occurs when such damages join up causing fracture. Depending on the fiber volume fraction, fiber, and matrix and/or interface characteristics, the final failure may involve (a) brittle failure on a section perpendicular to fibers, (b) brittle failure with some fiber pullouts, and (c) such failure on two or more sections with matrix failure or debonding joining the sections. Axial tensile failure of a lamina (UDC) is of great interest, since it often governs the failure of laminates made by stacking layers of different orientations. For this reason numerous studies have been devoted in modeling the tensile failure mechanisms and some of them will be discussed in the following subsections.
- b. **Axial Compressive Strength**—Compressive load carrying capacity of a unidirectional composite in the fiber direction is also of great interest, since it often governs the failure of a laminate. Microbuckling or kinking of slender fibers, which are supported laterally by the matrix, is often the mode of failure under compression and such instability is often influenced by the presence of local or global initial imperfections, fiber waviness, and ductile behavior of the matrix. Transverse splitting of the matrix and/or fiber/matrix debonding due to tensile Poisson strain may also cause initiation of damage and final failure. Compressive failure of the fiber (crushing) or the matrix may also initiate failure in certain systems.
- c. **Matrix Mode Strengths**—The two failure modes mentioned above are called fiber mode failures since they occur due to the destruction of the load carrying capacity of the fibers, although the strengths (especially the compressive strength) can be strongly influenced



by matrix properties. On the other hand, there are three other types of failure which may be caused without fiber failure, and they are discussed next.

- (1) **Transverse Tensile Strength**—Unidirectional brittle matrix composites under transverse tension often fail by the propagation of a single crack parallel to fibers. This type of failure may also involve some fiber/matrix debonding. Transverse cracks may also develop in fibers which are weak in the transverse direction. Fibers with transverse moduli lower than that of the matrix may also act as stress raisers, facilitating the development of transverse cracks in the matrix.
- (2) **Transverse Compressive Strength**—Under transverse compression, failure usually occurs on planes of maximum shear which are parallel to the fibers. However, such failure may often involve fiber/matrix debonding or may also be caused by fiber crushing.
- (3) **Axial Shear Strength**—Under axial shear (often called in-plane shear), failure usually occurs due to matrix shear failure and may also involve fiber/matrix debonding.

It may be noted that the types of matrix failure observed in testing of unidirectional composites do not necessarily lead to final failure in multidirectional laminates. The matrix damage in a layer caused by such failures is usually constrained by the fibers of the neighboring layers and tends to develop at different locations as the load is increased. However, matrix mode strengths are important for quantifying damage initiation and for modeling the growth of such damage as the load on the laminate is increased.

The following sections present discussions on the failure modes and composite-constituent property relationships for the types of loading conditions mentioned above. It may be noted that strength properties of unidirectional composites are strongly influenced by in situ microstructural details, imperfections, and microlevel properties of the constituents including interfaces, which are difficult to measure and quantify. Hence, the results obtained from various models usually yield qualitative results and quantitative trends rather than specific strength predictions. For this reason, testing is essential for the determination of strength properties of unidirectional composites. Because of the large differences between fiber and matrix strengths and because of the anisotropy of the material, various complications may arise in composite testing, and different interacting failure modes may influence the test results. For this reason numerous studies have been devoted to the development of test methods for composites. Selection of one or more suitable test methods is of great importance, but this issue is not addressed in this volume. For a survey of such test methods, interested readers may refer to reference 3.28.

### 3.2.1 Axial Tensile Strength.

One of the most attractive properties of advanced fiber composites is their high tensile strength. The simplest model for the tensile failure of a unidirectional fiber composite subjected to a tensile load in the fiber direction is based upon the elasticity solution for the case of uniform axial strain throughout the composite. Generally, the fibers have a lower strain to failure than

the matrix, and composite fracture occurs at the failure strain of the fibers alone. This results in a composite tensile strength,  $\sigma_L$ , given by

$$\sigma_L = v_f \sigma_f + v_m \sigma_m \quad (3.87)$$

where

$\sigma_f$  - the fiber tensile strength

$\sigma_m$  - the stress in the matrix at a strain equal to the fiber failure strain,  $\sigma_f/E_f$

The problem with this approach is the variability of fiber strength. Nonuniform strength is characteristic of most current high-strength filaments. This is illustrated in figure 3.23, which shows strength distributions for single filaments of two different types of commercial glass fibers. This statistical distribution of single-filament strength is generally considered to result from a distribution of imperfections along the length of these brittle fibers. There are two important consequences of a wide distribution of individual fiber strengths. (Note that the word "fiber" is used to denote a single filament, generally on the order of 10 microns in diameter.) First, all fibers will not be stressed to their maximum value at the same time. Thus, the strength of a group of fibers will not equal the sum of the strengths of the individual fibers; nor will it equal the mean strength of these fibers. The second important factor is that those fibers which break earliest during the loading process will cause perturbations of the stress field in the vicinity of the break, resulting in localized high fiber-matrix interface shear stresses. These shear stresses transfer the load across the interface and also introduce stress concentrations into adjacent unbroken fibers.

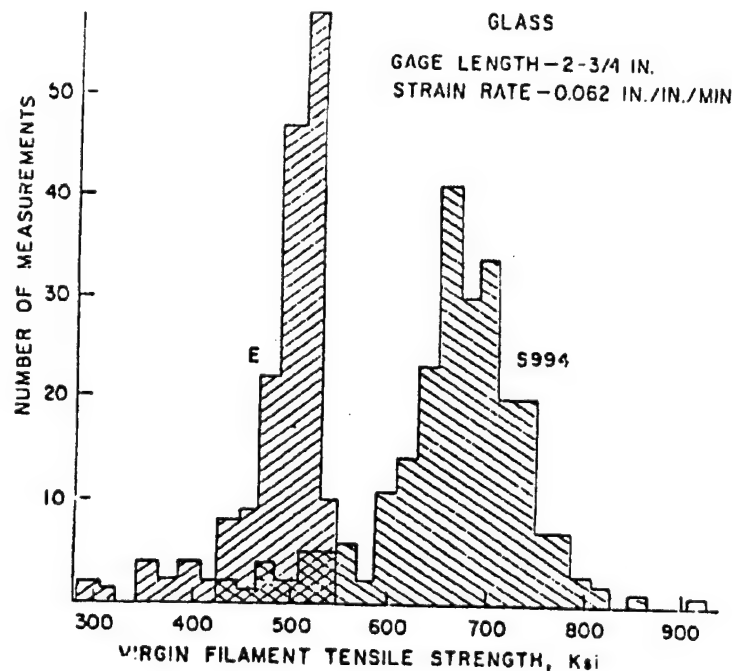


FIGURE 3.23. SINGLE FILAMENT TENSILE STRENGTH

At each local fiber break, the stress in the vicinity of the broken fiber changes so that the axial stress in the fiber vanishes at the fiber break and gradually builds back up along the fiber length to its undisturbed stress value. The general form of the local stress pattern in the fiber is shown schematically in figure 3.24. Here it is seen that the interfacial stress is at maximum close to the fiber break and decays rapidly along the length of the fiber. As a result, the axial fiber stress builds up to its initial undisturbed value over a relatively short dimension.

This stress distribution may cause several possible failure events to occur. The shear stresses may cause a crack to progress along the interface. If the interface is weak, such propagation can be extensive; in this case, the strength of the composite material may differ only slightly from that of a bundle of unbonded fibers. This undesirable mode of failure can be prevented by the attainment of a strong fiber-matrix interface or by the use of a soft ductile matrix which permits the redistribution of the high shear stresses. When the bond strength is high enough to prevent interface failure, the local stress concentrations may cause the fiber break to propagate through the matrix and, in turn, through adjacent fibers. Alternatively, the stress concentration may cause fibers to break prior to the occurrence of failure in the matrix. (If such a crack or such fiber breaks continue to propagate, the strength of the composite may be no greater than that of the weakest fiber.) This failure mode is defined as a weakest-link failure (see section 3.2.1.2). If the matrix and interface are of sufficient strength and toughness to prevent or arrest these failure mechanisms, then continued load increases will produce new fiber failures at other locations in the material, resulting in an accumulation of dispersed internal damage as the loading continues.

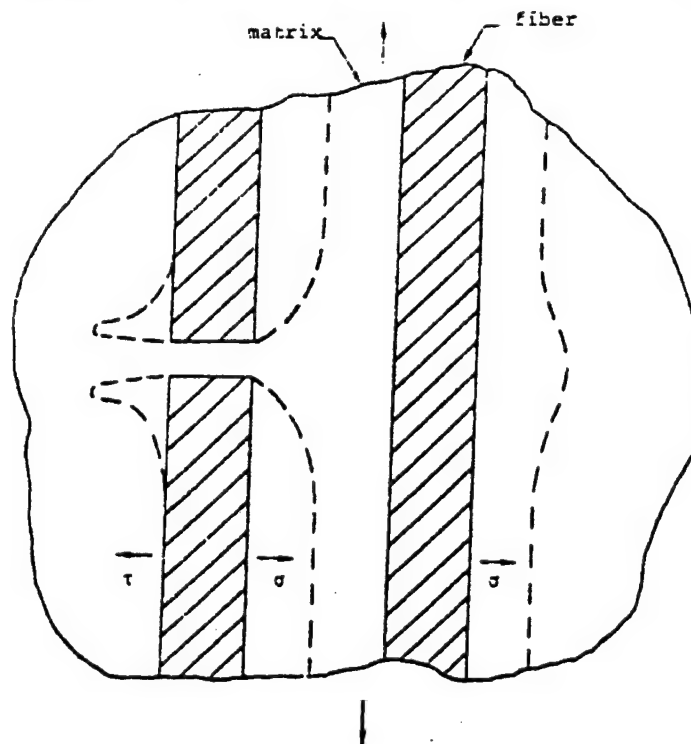


FIGURE 3.24. PERTURBATION OF STRESSES IN THE VICINITY OF A BROKEN FIBER END

It can be expected that all of these effects will occur prior to final failure. That is, local fractures will propagate for some distances along the fibers and normal to the fibers. These fractures will initiate and grow at various points within the composite. Increasing the load will produce a statistical accumulation of dispersed damage regions until a sufficient number of such regions interact to provide a weak surface, resulting in composite tensile failure. Experimental observations of dispersed fiber fractures at relatively low loads and of irregular failure surfaces showing combinations of clusters of broken fibers and axial shear failure planes suggest that this complex failure mechanism represents the practical case in most, if not all, composites of interest.

Contemporary filaments exhibit very high tensile strengths. The objective, when incorporating these filaments into a composite material, is to ensure that this high strength can be utilized. The degree to which this can be done is dependent upon matrix characteristics, which may vary with the service and environmental history of the composite material. Furthermore, new materials are constantly under development to improve composite resistance to temperature, impact, etc. Also, matrix materials are being developed to achieve lower-cost manufacturing processes. An understanding of the influence of these changes upon composite tensile strength appears to be essential.

#### 3.2.1.1 Fiber Strength.

Fiber tensile strength is generally reported as the average strength of a group of fibers of a particular type. In actuality, the strength is rarely obtained by testing single filaments and obtaining a numerical average of their strength values. Generally, a bundle of yarn of such fibers is impregnated with a polymer and loaded to failure. The average fiber strength is then defined by the maximum load divided by the cross-sectional area of the fibers alone. It is important to recognize the difference between these two techniques for measuring fiber strength. At a constant gage length, the strength of single filaments will exhibit a certain amount of dispersion due to fiber imperfections. The probability of finding an imperfection of given severity increases with gage length; hence, the average strength of the fiber can be expected to, and indeed does, decrease with increasing gage length. An example of this effect is shown by the data of figure 3.25. The question of which value of fiber strength influences composite strength can be resolved only by determining the failure mechanism. It will be shown that a characteristic length of the fiber which is effective within the composite can be defined.

It should be emphasized that despite the factors discussed above, the prevalent technique for defining fiber strength in the industry today is to test a strand of fibers impregnated with a low-quality matrix material and to use the failure load to define average strength [3.29].

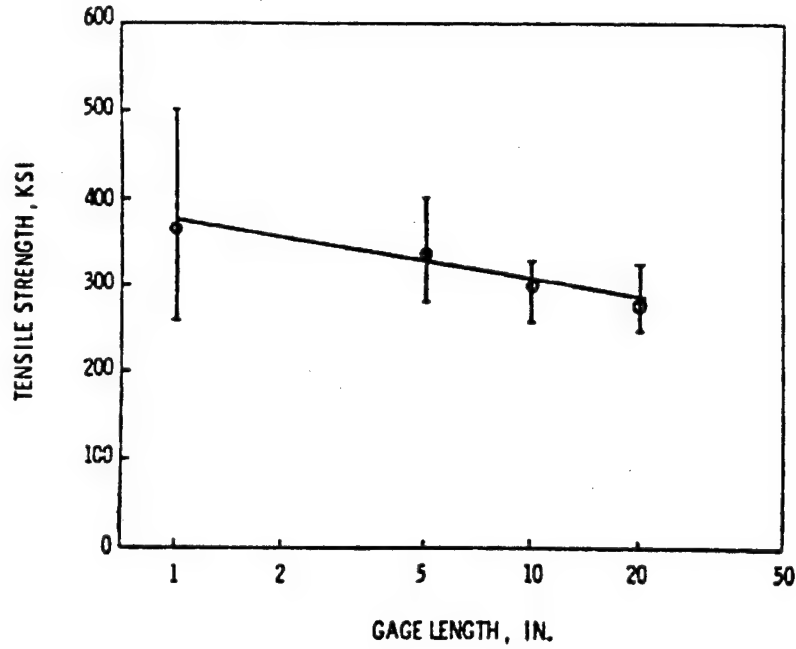


FIGURE 3.25. VARIATION OF MEAN AND RANGE OF INDIVIDUAL FIBER STRENGTH VALUES (BORON FIBER DATA)

It has been found that a Weibull distribution [3.30] provides a good fit to experimental data of the type shown in figure 3.25. The cumulative distribution function for this case can be expressed in the form

$$F(\sigma) = 1 - \exp(-\alpha L \sigma^\beta) \quad (3.88a)$$

and the Weibull strength distribution function is then

$$f(\sigma) = L \alpha \beta \sigma^{\beta-1} \exp(-L \alpha \sigma^\beta) \quad (3.88b)$$

where

$\alpha, \beta$  – two parameters to be fit to the experimental fiber tensile strength data  
 $L$  – the fiber length

For the Weibull distribution of equation (3.88b), the mean strength, can be found to be

$$\bar{\sigma} = (\alpha L)^{-1/\beta} \Gamma\left(1 + \frac{1}{\beta}\right) \quad (3.89)$$

where  $\Gamma$  is the standard gamma function.

The standard deviation,  $s$ , is

$$s = (\alpha L)^{-1/\beta} \left[ \Gamma \left( 1 + \frac{2}{\beta} \right) - \Gamma^2 \left( 1 + \frac{1}{\beta} \right) \right] \quad (3.90)$$

Thus, the coefficient of variation, c.v., for this distribution is given by

$$c.v. = \frac{s}{\bar{\sigma}} = \frac{\Gamma \left( 1 + \frac{2}{\beta} \right) - \Gamma^2 \left( 1 + \frac{1}{\beta} \right)}{\Gamma \left( 1 + \frac{1}{\beta} \right)} \quad (3.91)$$

It is now possible to assign some physical significance to the parameters of the distribution function of equation (3.88b). First of all, it is seen that the coefficient of variation is a function only of the parameter  $\beta$ . Indeed, it can be shown that equation 3.91 is approximated to within 3 percent for  $0.05 \leq c.v. \leq 0.50$ , by

$$c.v. = \beta^{-0.92} \quad (3.92)$$

Thus  $\beta$  is essentially an inverse measure of the coefficient of variation, and for practical fibers

$$\beta \approx \frac{1}{c.v.} \quad (3.93)$$

Also since for  $\beta > 1$ , the value of the gamma function in (3.89) is close to unity, it can be seen that for a unit length

$$\bar{\sigma}_1 \approx \alpha^{-1/\beta} \quad (3.94)$$

Thus the quantity  $\alpha^{-1/\beta}$  may be viewed as a reference stress level. With these definitions, equation 3.89 may be plotted in the form shown in figure 3.26. Here, the tensile strength of single fibers of length  $L$  is shown as a function of some normalized fiber length for different values of  $\beta$ . The upper curve, where  $\beta$  is infinity, applies to a set of fibers having identical strength (standard deviation = 0). For this case, there is no length dependence. For  $\beta$  of 10, which represents approximately a 12 percent coefficient of variation, an order of magnitude change in the fiber length produces about a 20 percent drop in its average strength and, for  $\beta$  of 4, an order of magnitude change in length produces almost a 50 percent drop in strength.

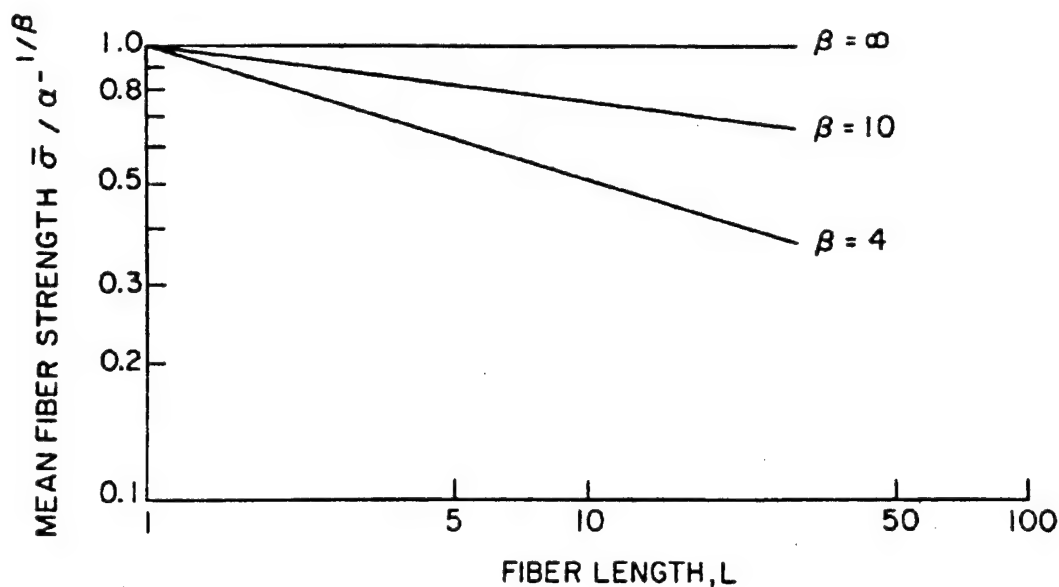


FIGURE 3.26. STRENGTH LENGTH VARIATION OF FIBER STRENGTHS FOLLOWING WEIBULL STATISTICAL DISTRIBUTION FUNCTIONS

#### 3.2.1.2 Weakest-Link Failure.

When a unidirectional composite is loaded in axial tension, scattered fiber breaks occur through the material at various stress levels. It is possible that one of these fiber breaks may trigger a stress wave or initiate a crack in the matrix resulting in localized stress concentrations which cause the fracture of one or more adjacent fibers. In turn, the failure of these fibers may result in additional stress waves or matrix cracks, leading to overall failure. This produces a catastrophic mode of failure associated with the occurrence of one or a small number of isolated fiber breaks. This is referred to as the weakest-link mode of failure. The lowest stress at which this type of failure can occur is the stress at which the first fiber will break. The expressions for the expected value of the weakest element in a statistical population [3.31] have been applied by Zweben [3.32] to determine the expected stress at which the first fiber will break. Assuming that the fiber strength is characterized by a Weibull distribution, the expected first fiber break will occur at a stress

$$\sigma_w = \left( \frac{\beta - 1}{NL\alpha\beta} \right)^{1/\beta} \quad (3.95)$$

where  $N$  is the number of fibers in the material. Thus, (3.95) provides an estimate of the failure stress associated with the weakest-link mode.

It should be noted that the occurrence of the first fiber break is a necessary, but not a sufficient, condition for failure.

In general, it is rare that the occurrence of a single fiber break produces catastrophic failure; however, in very small samples containing fibers having a very narrow dispersion of strength, this is a possible failure mechanism. For practical materials in realistic structure, the calculated weakest-link failure stress is quite small, and in general, failure cannot be expected to occur in this mode.

#### 3.2.1.3 Cumulative-Weakening Failure.

If the weakest-link failure mode does not occur, it is possible to continue loading the composite, and with increasing stress, fibers will continue to break randomly throughout the material. When a fiber breaks, there is a redistribution of stress in the vicinity of the fracture site (figure 3.24). This stress perturbation is the origin of important mechanisms involved in composite failure. When a fiber break occurs, the broken surfaces displace axially, inducing stresses in the matrix and large shear stresses at the fiber-matrix interface. The interface shear stress acting on the broken fiber localizes the axial fiber dimension over which the stress in the broken fiber is greatly reduced. Were it not for some form of interfacial shear stress, a broken fiber would be unable to carry any load and the composite would be, in effect, a bundle of separate fibers from the standpoint of resisting axial tensile loading.

An important function of the matrix is to localize the reduction of fiber stress when a fiber breaks. The axial dimension over which the axial fiber stress is significantly reduced is referred to as the ineffective length,  $\delta$ . It is a significant length parameter involved in the failure of fiber composite materials. The magnitude of  $\delta$  depends on the stress distribution in the region of the fiber break. This distribution is quite complex and is influenced by fiber and matrix elastic properties as well as by any inelastic phenomena such as debonding, matrix fracture, or yield, etc., that may occur. Also, the definition of  $\delta$  is somewhat arbitrary since the stress in the broken fiber is a continuously varying quantity that asymptotically approaches the average stress in unbroken fibers.

The concept of representing this variable stress field and a fiber composite material having distributed fractures by an assemblage of elements of length  $\delta$  was introduced by Rosen [3.33]. In this model, as shown in figure 3.27, the composite may be considered to be a chain of layers of dimension equal to the ineffective length. Any fiber with fractures within this layer will be unable to transmit a load across the layer. The applied load at that cross section is then assumed to be distributed among the unbroken fibers in each layer. (The effective load concentrations, which would introduce a nonuniform redistribution of these loads, are not considered at this point.) A segment of a fiber within one of these layers may be considered as a link in the chain which constitutes an individual fiber. Each layer of the composite is then a bundle of such links, and the composite itself is a series of such bundles, as shown in figure 3.27.



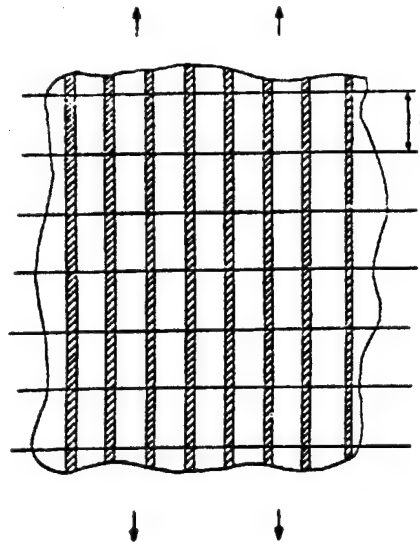


FIGURE 3.27. GEOMETRY OF COMPOSITE FOR STATISTICAL TENSILE FAILURE MODEL

The filaments in each bundle act in parallel, and it is well known that the strength of a bundle of filaments, the strength of whose members are not uniform, is not equal to the mean fiber strength. Following the work of Coleman [3.34], one obtains the results shown in figure 3.28. This shows the variation of bundle strength (again a statistical characterization, so that the bundle strength is in this case measured by the mode of the strength) normalized with respect to the mean strength of individual fibers of the same length as the bundles. This is plotted as a function of the fiber population's coefficient of variation, and it is seen that the general result is that the average strength of the bundle is somewhat less than the average strength of the fibers and is a decreasing function of the coefficient of variation of the fibers.

Treatment of a fiber as a chain of links is appropriate to the hypothesis that fracture is due to local imperfections. The links may be considered to have a statistical strength distribution which is equivalent to the statistical flaw distribution along the fibers. The validity of such a model for the fibers is demonstrated by the length dependence of fiber strength. For this model, it is necessary to define the link dimension,  $\delta$ ; the probability of failure of fiber elements of that length; and then the statistical strength distribution of the assemblage. This analysis leads to the cumulative-weakening mode of failure. The definition of ineffective length is discussed further below. The determination of the link strength distribution is treated in [3.33]. When these are known, the relationship of the strength of the assemblage to the strength of the elements, or links, can be treated by the methods of reference 3.31. The result for fibers having a strength distribution of the form (3.88a) is given in reference 3.33 as

$$\sigma^* = (\alpha \delta \beta e)^{-1/\beta} \quad (3.96)$$

where  $\sigma^*$  is the statistical mode of the composite tensile strength based on fiber area.

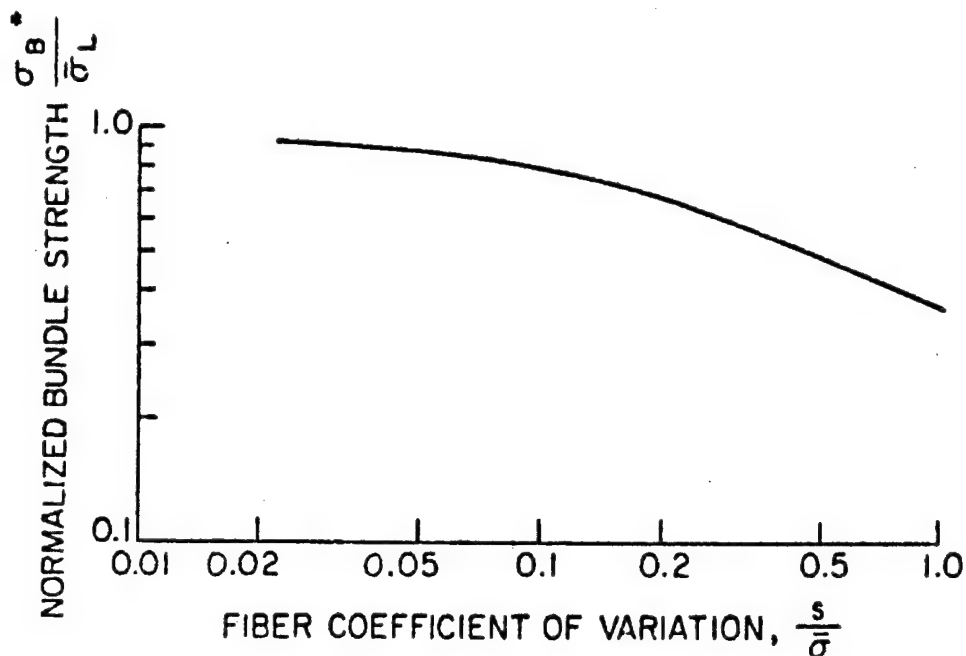


FIGURE 3.28. VARIATION OF FIBER BUNDLE STRENGTH WITH FIBER COEFFICIENT OF VARIATION

As pointed out above, the cumulative-weakening model represents the varying stress near a fiber break by a step function in stress. The model also neglects the possibility of failures involving parts of more than one layer. More importantly, the overstress in unbroken fibers adjacent to the broken fibers has not been considered. This stress concentration increases the probability of failure for these adjacent elements and creates the probability of propagation of fiber breaks. This combination of variable fiber strength and variable fiber stress can be expected to lead to a growth in both the number of damaged regions and in the size of a given damaged region. This is represented schematically in figure 3.29, wherein the cross-hatched regions at the ends of tracks represent the ineffective lengths of the broken groups.

In the situation described above, there exists the possibility that one damaged group may propagate, causing failure, or that the cumulative effect of many smaller damaged groups will weaken a cross section, causing failure. The latter possibility is discussed subsequently. The former possibility, which was proposed by Zweben [3.32], is reviewed below. First, a discussion of the stresses in the vicinity of a broken fiber is in order.

#### 3.2.1.4 Internal Stresses.

The stress field around a broken fiber has been studied by many authors. Among the early studies are those of references 3.35 and 3.36. These or similar stress distributions were used in references 3.33 and 3.37 to define ineffective lengths. More recently, the studies of references 3.38-3.41 have defined stress distributions in two- and three-dimensional unidirectional fiber composites. These results can be used to determine the stresses in unbroken fibers required to assess the probability of propagation.

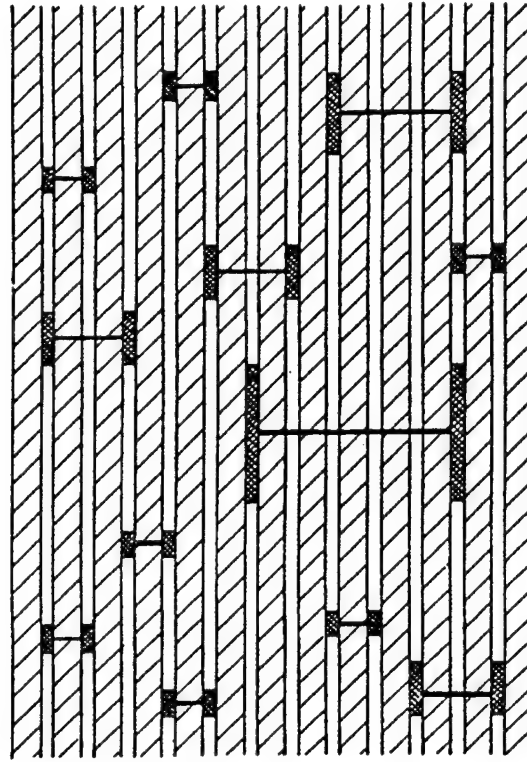


FIGURE 3.29. DISTRIBUTION OF DAMAGE IN A FIBER COMPOSITE MATERIAL RESULTING FROM AN APPLIED TENSILE LOAD

The nature of load concentrations in filamentary composites was studied analytically by Hedgepeth and Van Dyke [3.38, 3.39, and 3.41]. The results of these investigations showed that elastic load concentrations in two-dimensional (planar) arrays of parallel fibers in axial tension are large and increase drastically with the number of adjacent broken filaments. This conclusion was supported by a series of experiments performed by Zender and Deaton [3.42]. Elastic load concentrations for three-dimensional arrays of parallel fibers are much less severe. The effects of fiber debonding, or matrix cracking, and matrix plasticity for the case of one broken fiber was studied in references 3.38 and 3.39. It was found that inelastic effects such as complete debonding and matrix plasticity can significantly reduce load concentration factors. This would serve to reduce the likelihood of fiber break propagation.

A reasonable definition of ineffective length for the case of an elastic, perfectly bonded matrix was proposed by Friedman [3.37]. He defined the ineffective length on each side of the break by taking the area under the curve of stress versus the axial distance from the fracture surface and equating it to a stress distribution in the form of a step function that is zero over the ineffective length and equal to the applied stress everywhere else. The resulting elastic ineffective length,  $\delta_E$ , for a single broken fiber is

$$\delta_E = \left( \frac{E_f}{G_m} \right)^{1/2} \left( \frac{1 - \nu_f^{1/2}}{2\nu_f^{1/2}} \right)^{1/2} d_f \quad (3.97)$$

The effects of an elastic perfectly plastic matrix and interfacial failure on the perturbed region adjacent to a single broken fiber were studied by Hedgepeth and Van Dyke [3.38 and 3.39]. They found that if there is a finite interfacial strength with no postfailure shear transfer across the interface, broken fibers will debond completely when the load is increased only slightly above the fiber fracture load. Experience with real materials indicates that complete debonding is rarely observed and thus the assumption of no postfailure shear transfer appears to be unrealistic. The results for the elastic-plastic matrix material predict a more gradual extension of the perturbed region with increasing stress.

For real materials the postfailure shear transfer probably lies somewhere in between the extremes of zero stress transfer and perfect plasticity (constant shear stress).

For the case of a perfectly plastic matrix material in which the elastic strains are neglected, the plastic ineffective length,  $\delta_p$ , is

$$\delta_p = \frac{\sigma_f}{4\tau_y} d_f \quad (3.98)$$

where

$\sigma_f$  - fiber tensile strength

$\tau_y$  - matrix shear yield strength

$d_f$  - fiber diameter

Generally, the size of the ineffective length, even when inelastic effects are present, is not greater than 100 fiber diameters.

For groups of adjacent broken fibers, Fichter [3.40] studied the variation of the length of the perturbed region with the number of adjacent broken fibers in a two-dimensional (planar) array of fibers with an elastic matrix. He found that the ineffective length of the affected region grows with the number of broken fibers in the group. The effect of inelasticity in the matrix or failure of the interface on ineffective length for groups of arbitrary size was treated in reference 3.43. The indicated size of the ineffective length appears to be orders of magnitude smaller than the linear dimensions of a realistic structure or even of a laboratory test coupon. This is significant since mean fiber strength is length dependent. At these short ineffective lengths, mean fiber tensile strengths are greater than mean strengths at the gage lengths commonly used to evaluate fiber strength (usually 1 or 2 inches). This follows from the length dependence illustrated in figure 3.25.

### 3.2.1.5 Fiber Break Propagation Failure.

The effects of stress perturbations on fibers adjacent to broken ones are of significance. When a fiber breaks, equilibrium requires that the net load on the cross section containing the broken fiber be unchanged. Therefore, the average stress in the remaining fibers must increase. Because of the matrix, the stress redistribution is highly nonuniform. The shear stress that arises in the

matrix when a fiber breaks results in localized increases of average stress in the fibers surrounding the break. In order to differentiate this increase in the average stress over a fiber cross section from the increase at a point, the term "load concentration" is used for the former and the conventional term "stress concentration" for the latter.

The load concentration in the fibers adjacent to a broken one increases the probability that one or more of them will break. When such an event occurs, the load concentration in neighboring fibers intensifies, increasing the probability of additional fiber breaks, and so on. From this description, it is not difficult to identify the propagation of fiber breaks as a mechanism of failure. The probability of occurrence of this mode of failure increases with the average fiber stress because of the increasing number of scattered fiber breaks and the increasing stress level in over stressed fibers.

The case of fiber break propagation mode of failure was studied by Zweben [3.32], who proposed that the occurrence of the first fracture of an overstressed fiber could be used as a measure of the tendency for the fiber breaks to propagate and, hence, as a failure criterion for this mode, at least for small volumes of material. The effects of load concentrations upon fiber propagation in 3D unidirectional composites, as well as upon cumulative-weakening failures, was treated in reference 3.44. In reference 3.45, Zweben reviewed experimental data available for various fiber-matrix systems to support the contention that the first multiple break is a lower bound to strength. Although the first multiple break criterion may provide good correlation with experimental data for small specimens and may be a lower bound on the stress associated with fiber break propagation, it gives very low stresses for large volumes of materials, which appears to conflict with practical experience with composites. There does not appear to be any available reliable data, however, which shed light on the influence of material size on strength.

The approximate model of reference 3.44 for including effects of load concentrations in the cumulative-weakening model was also of limited success. The resulting mathematical expression for composite strength is a sequence in which each term corresponds to a group of broken fibers of increasing size. A very large number of terms is required for convergence. Continuing investigations of procedures for reflecting such statistics have been undertaken by Phoenix and Harlow [3.46]. They have treated the conditional probabilities which result from sequential breaks of adjacent fibers in order to obtain manageable expressions for failure probabilities. Such approaches require assumptions regarding the redistributions of load from the broken fibers. Various such load-sharing rules have been explored. The failure mode remains a cumulative weakening of the material.

#### 3.2.1.6 Cumulative Group Mode Failure.

As multiple broken fiber groups grow, the magnitude of the local axial shear stress increases and axial cracking can occur. This effect has been treated in the failure model [3.43] formulated to incorporate the following three effects which were deemed to be of importance in the tensile failure of high-strength fibrous composites:

1. The variability of fiber strength will result in distributed fiber fractures at stress levels well below the composite strength.

2. Load concentrations in fibers adjacent to broken fibers will influence the growth in size of the crack regions to include additional fibers.
3. High shear stresses will cause matrix shear failure or interfacial debonding which will serve to arrest the propagating crack.

Thus, as the stress level increases from that at which fiber breaks are initiated toward that at which the composite fails, the material will have distributed groups of broken fibers. Each group will have an ineffective length which increases with group size and, after matrix failure, with stress. This situation may be viewed as a generalization of the cumulative-weakening model of reference 3.33, wherein the effect of the isolated breaks was modeled by a chain of bundles model such as that used in reference 3.31.

In practical materials, the problem is complicated by the presence of bundles of various sizes. That is, both the number of broken fibers in a bundle and the ineffective length of that bundle vary. Thus, the basic problems of defining the required input information for the analysis of the chain of bundles model are of increased complexity. The size of the basic element must first be defined and then the probability of failure of that element can be determined.

At stress levels above those required to cause some number of isolated breaks in the composite, there is an increasing probability of occurrence of multiple adjacent breaks as a result of stress concentrations. Thus, at moderate stress levels it will be usual to have a non-negligible probability of existence of a crack containing  $n$  broken fibers, for many values of  $n$ . For each crack size  $n$ , there is a different elastic ineffective length and also different values of both shear load concentration and fiber load concentration factors. Thus, for different size cracks there are different stress levels at which matrix failure initiates and differing distances over which it propagates.

The statistical problem represented by the situation described above is exceedingly complex. Various authors have taken different approaches in an attempt to obtain a reliable model. Phoenix and Harlow have pursued the development of the statistics by focusing their efforts on two- and three-dimensional materials and specified load sharing rules [3.46 and 3.47]. Rosen and Zweben have pursued an approximate model which is based on the definition of a characteristic group size. This group size is determined by an estimate of the size at which growth would be arrested by axial shear cracks. Batdorf [3.48] has utilized simplifying approximations of the statistical functions which result in a propagation failure mode having a defined critical crack size.

Each of these models has severe limitations with regard to the quantitative prediction of tensile strength. However, the models show the importance of variability of fiber strength and of matrix stress-strain characteristics upon composite tensile strength.

#### 3.2.1.7 Fracture Mechanics.

In this discussion of composite failure mechanics, a number of basic modes of failure have been described, including those associated with propagation effects. Yet in the discussion of the analytical treatment of these modes, no mention has been made of classical fracture mechanics.

Since there exists a large, well developed body of knowledge dealing with the failure of homogeneous materials, it is instructive to examine the possibility of applying classical fracture mechanics techniques to analyze the failure of composite materials. A basic principle of classical fracture mechanics is that a crack will grow when the energy required to extend a crack a given amount is equal to the change in strain energy in the body resulting from that crack advance. The implications of this condition for the analysis of the modes of failure treated earlier are discussed below.

First, consider the weakest-link mode of failure in which a single fiber break results in a catastrophic crack propagation. If failure results from a crack that propagates in a continuous manner through both phases, fiber and matrix, it is reasonable to expect that the fracture mechanics approach can be used to describe the process, although it may be necessary to consider propagation through the two phases separately. Additionally, when the crack size becomes large with respect to fiber diameter and interfiber spacing distance, it seems reasonable to expect that the material can be adequately treated as a homogeneous, anisotropic material.

In the case of the fiber break propagation mode, the onset of unstable crack growth is governed by fiber load concentrations and the statistical aspects of material strength. This mode of failure need not result from a crack propagating through the matrix. Thus, the total energy of fracture of the composite has no relation to the condition precipitating fiber break propagation. However, it is reasonable to expect that when the crack grows to some large size, the form of the damage region will become stabilized and will advance through the material without significant change. If this should occur, it is reasonable to believe that it would be possible to relate increments of strain energy to the energy expended in extending the damaged region. It should be emphasized that this type of energy balance, which may be valid when the crack size is large with respect to fiber diameter and spacing, would not be expected to be applicable at the early stages of instability, when the crack is small and the effects of heterogeneity are important.

The remaining modes of failure discussed earlier are associated with failure due to an accumulation of weakened areas. This is not directly related to crack propagation. Therefore, it seems reasonable to assume that classical fracture mechanics has no relevance in this case.

A multiplicity of internal planes of weakness creates the possibility for various failure modes in composites. It appears that the heterogeneity must be considered in the development of failure criteria. After an understanding of failure modes is obtained, it may be possible to formulate effective fracture mechanics parameters for some composites under some, as yet, unknown loading conditions.

#### 3.2.1.8 Concluding Remarks.

Uniaxial tensile strength is one of the most attractive properties of contemporary advanced fiber composites. Despite its importance, however, it is generally viewed in a rudimentary fashion. Thus, manufacturers of fibers persist in measuring the strength of their product by using yarns impregnated with room temperature curing resin systems of uncertain properties. The ratio of the measured tensile strength of a sound unidirectional composite to the tensile strength of this nonuniform impregnated strand is identified as a measure of the efficiency of the composite. The



acceptance of this procedure apparently stems from the fact that, for current test specimen dimensions and materials, this ratio is approximately unity.

It can be expected that when improved materials are developed, they will be treated by improved methods. The statistical methods presented herein provide the basis for such a treatment. Although these methods are not yet adequate for definitive quantitative prediction, they can be very useful for assessment of the relative merits of different materials. The rule of mixtures need no longer be a substitute for an understanding of material behavior. Assessment of merit should utilize both cumulative and propagation type models to define both the relative level of strength and the expected mode of failure.

For preliminary estimates, cumulative weakening (3.96) can be used with an inelastic ineffective length (3.98) to provide an overestimate of the actual value and an indication of the role of the properties of each constituent.

### 3.2.2 Axial Compressive Strength.

For compressive loads applied parallel to the fibers of a unidirectional composite, both strength and stability failures must be considered.

Microbuckling was proposed as a failure mechanism by Dow [3.49]. It was suggested that small wavelength microinstability of the fibers occurs in a fashion analogous to the buckling of a column on an elastic foundation. It has been demonstrated that this will occur even for a brittle material, such as glass. For example, figure 3.30 (from reference 3.50) shows a single E-glass filament embedded in a block of epoxy which has been cooled to produce a compressive strain. The specimen contains a fiber of 0.003 inch in diameter. The photoelastic stress pattern in the epoxy emphasizes the repetitive nature of the deformation pattern for each fiber and supports the contention that the deformations result from an elastic instability.

Analyses of this instability were performed independently in references 3.51 and 3.52. The analyses approximate the problem by treating a layered two-dimensional medium, as shown in figure 3.31. The model consists of plates of thickness  $h$  separated by a matrix of dimension  $2c$ . Each fiber is subjected to a compressive load,  $P$ , and the fiber length is given by the dimension,  $L$ .

Two possibilities are considered for the instability failure mode. First, the fibers may buckle in opposite directions in adjacent fibers, as shown on the left portion of the figure, and the so-called extension mode occurs. This mode receives its name from the fact that the major deformation of the matrix material is an extension of the direction perpendicular to the fibers. The analysis treats the fibers as stiff, relative to the matrix, so that shear deformations in the fiber can be neglected relative to those in the matrix.





FIGURE 3.30. PHOTOELASTIC STRESS PATTERN FOR AN INDIVIDUAL E-GLASS FIBER EMBEDDED IN AN EPOXY MATERIAL

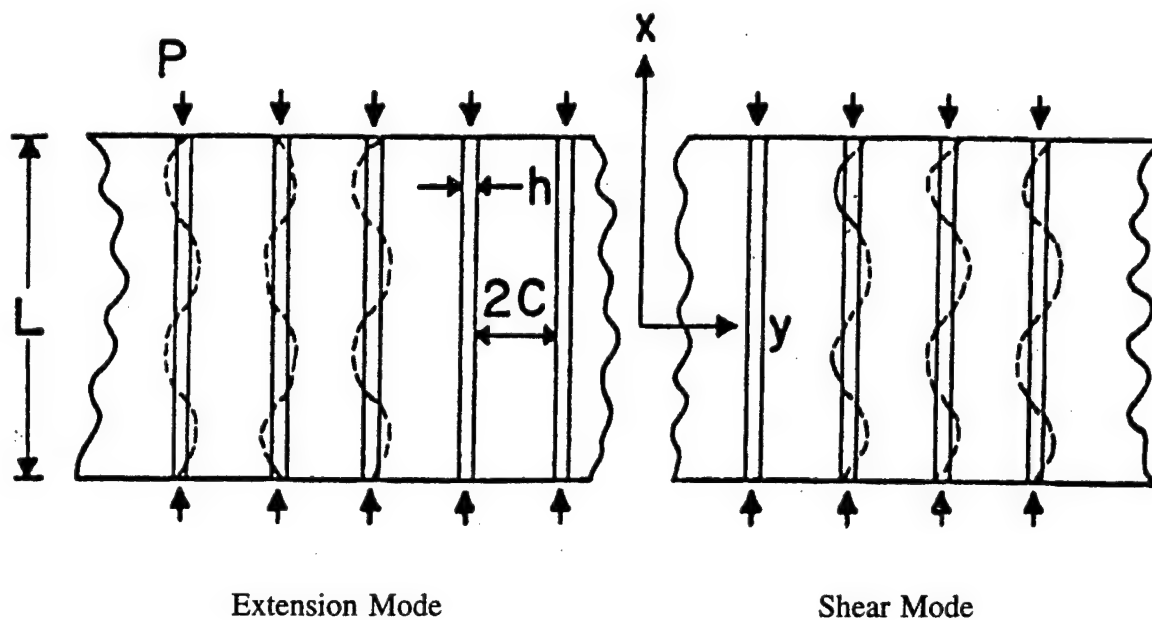


FIGURE 3.31. ANALYTICAL MODEL FOR COMPRESSIVE STRENGTH OF FIBROUS COMPOSITES

The second possibility is shown on the right portion of the figure where adjacent fibers buckle in the same wavelength and in phase with one another, so that the deformation of the matrix material between adjacent fibers is primarily a shear deformation. Hence, the shear mode label is given to this potential mode.

The energy method for evaluation of the buckling stress for these modes has been utilized where the procedure is to consider the composite stressed to the buckling load and then to compare the strain energy in this compressed but straight deformation pattern to a deformation pattern following an assumed buckling shape under the same load. Thus, a change in the strain energy of the composite consisting of the strain energy change in the fiber and in the matrix can be compared to the change in the potential energy associated with the shortening of the distance between the applied loads at the end of the fibers. The condition for instability is given by equating the strain energy change to the work done by the external loads during buckling. It is found that buckling occurs at a relatively short wavelength (10 to 100 fiber diameters).

The results for the compressive strength,  $\sigma_c$ , for the extension mode is given by

$$\sigma_c = 2v_f [(v_f E_m E_f) / 3 (1 - v_f)]^{1/2} \quad (3.99)$$

The results for the shear mode is given by

$$\sigma_c = G_m / (1 - v_f) \quad (3.100a)$$

when the shear modulus of the fiber is high in comparison to the matrix shear modulus. For carbon or Kevlar fibers, the shear modulus is low and a better estimate of  $\sigma_c$  is given by

$$\sigma_c = G^* \quad (3.100b)$$

where  $G^*$  is the composite shear modulus. An estimate of this modulus is given by the inverse rule of the mixtures.

$$\sigma_c = \frac{G_m}{1 - v_f (1 - G_m / G_{Lf})} \quad (3.100c)$$

$G_{Lf}$  being the fiber longitudinal shear modulus. A better estimate is given by (3.16).

These results from (3.99) and (3.100a) are plotted in figure 3.32 for E-glass fibers embedded in an epoxy matrix. The compressive strength of the composite is plotted as a function of the fiber volume fraction,  $v_f$ . The two curves represent the two failure modes considered. It is seen that for the low fiber volume fractions the extension mode yields lower stress, while for high-volume fractions of fibers the shear mode predominates. The compressive strength of typical glass reinforced plastic containing fiber volume fractions on the order of 0.6 to 0.7 is seen to be on the order of 450 to 600 ksi. Values of this magnitude do not appear to have been measured for any realistic specimens. However, the achievement of a strength of half a million psi in a composite of this type would require an average shortening of greater than 5 percent. For the epoxy materials used, such a shortening would result in a decrease in the effective shear stiffness of the binder material because the proportional limit of the matrix would be exceeded. Hence, it is necessary to modify the analysis to consider inelastic deformation of the matrix material. In reference 3.51, a simple approximation to this has been suggested by replacing the binder modulus in the formulas previously shown by a reduced modulus. As an example, a reduced

modulus is assumed which varies linearly for the epoxy from its elastic value at 1 percent strain to a zero value at 5 percent strain. The result of this assumption is the curve labeled inelastic in figure 3.32. Here it is seen that for very high fiber volume fractions the strength is bounded, and although higher than any results obtained to date, they are not unreasonably high.

Another result reported in reference 3.51 is obtained by modeling the matrix as an elastic, perfectly plastic material. For this matrix, the secant modulus at each axial strain value is assumed to govern the instability. These assumptions [3.50] yield the following result, in place of (3.100) for the dominant shear mode:

$$\sigma_c = \left[ \frac{v_f E_f \sigma_y}{3 (1-v_f)} \right]^{1/2} \quad (3.101)$$

where  $\sigma_y$  is the matrix yield stress level in tension or compression.

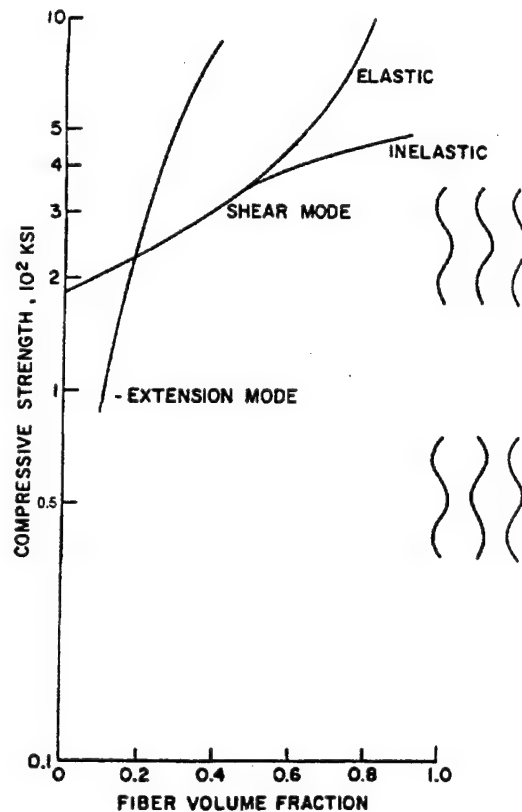


FIGURE 3.32. COMPRESSIVE STRENGTH OF GLASS-REINFORCED EPOXY COMPOSITES

For the generally dominant shear mode, the elastic results of (3.100a) are independent of the fiber modulus, yet the compressive strength of boron/epoxy is much greater than that of glass/epoxy

composites. One hypothesis to explain this is that use of the stiffer boron fibers yields lower matrix strains and less of a strength reduction due to inelastic effects. Thus, the results of (3.101) show a ratio of  $\sqrt{6}$  or 2.4 for the relative strength of boron as compared to glass fibers in the same matrix.

All of the analytical results above indicate that compressive strength is independent of fiber diameter. Yet, different diameter fibers may yield different compressive strengths for composites because large diameter fibers such as boron ( $\sim 0.005$ "D) are better collimated than smaller diameter fibers, such as glass ( $\sim 0.0004$ "D). For small diameter fibers, such as Kevlar and carbon, local out-of-straightness can introduce matrix shear stresses, can cause fiber-matrix debonding, and can produce lower instability stress levels.

Effects of smaller fiber diameter on the reduction in the strength of boron/epoxy systems have been reported in reference 3.53. Recently, detailed calculations of the fiber microbuckling stress with due consideration to fiber waviness and nonlinear response of the matrix subjected to multi-axial stress fields (axial compression, lateral compression, and shear stresses) have been reported in the literature [3.54]. In composites reinforced with fibers having very high axial Young's modulus, axial strains are usually small and some simple results may be obtained by modeling the nonlinear shear response of the composite, provided the wave length of the fiber waviness is large [3.55]. Consider a group of fibers making angle  $\theta_1$  with the direction of the applied axial compressive stress  $\sigma$  (figure 3.33a); for small  $\theta_1$  (imperfection) and shear strain  $\gamma$ ,

$$\tau = \sigma (\theta_1 + \gamma) \quad (3.102)$$

The increases in shear stress and strain with  $\sigma$  are schematically shown in figure 3.33b, where the  $\tau - \gamma$  curve shows the nonlinear shear response of the composite, which is similar in shape to those of common epoxy resin systems reinforced with carbon or glass fibers. The nonlinearity in such systems is usually attributed to progressive cracking parallel to fibers. Equation 3.102 implies that straight lines may be drawn from a point  $-\theta_1$  on the  $\gamma$  axis to the shear stress-strain curve with slopes equal to the applied compressive stress  $\sigma$ , and the ordinate and the abscissa of the point on the  $\tau - \gamma$  curve give the shear stress  $\tau$  and shear strain  $\gamma$ , respectively (as shown by  $\tau_1$  and  $\gamma_1$  for an applied stress  $\sigma_1$ ). It is clear that for a small imperfection ( $\theta_1$ ), a point of instability will be reached, i.e.,  $\sigma$  cannot be increased beyond the value  $\sigma_c$ , which is the slope of the tangent to  $\tau - \gamma$  curve drawn from the point  $-\theta_1$  on the  $\gamma$ -axis (figure 3.33b). For commonly used carbon and glass/epoxy composites, an initial imperfection,  $\theta_1 = 0.04$  radians, yields values of  $\sigma_c$  close to the compressive strength measured from tests. If the  $\tau - \gamma$  curve has a well defined point of deviation from the initial linear response or a yield stress  $\tau_y$  and a low tangent modulus beyond this point (or if the material is elasto-plastic), then

$$\sigma_c = \tau_y / (\theta_1 + \gamma_y) \quad (3.103)$$

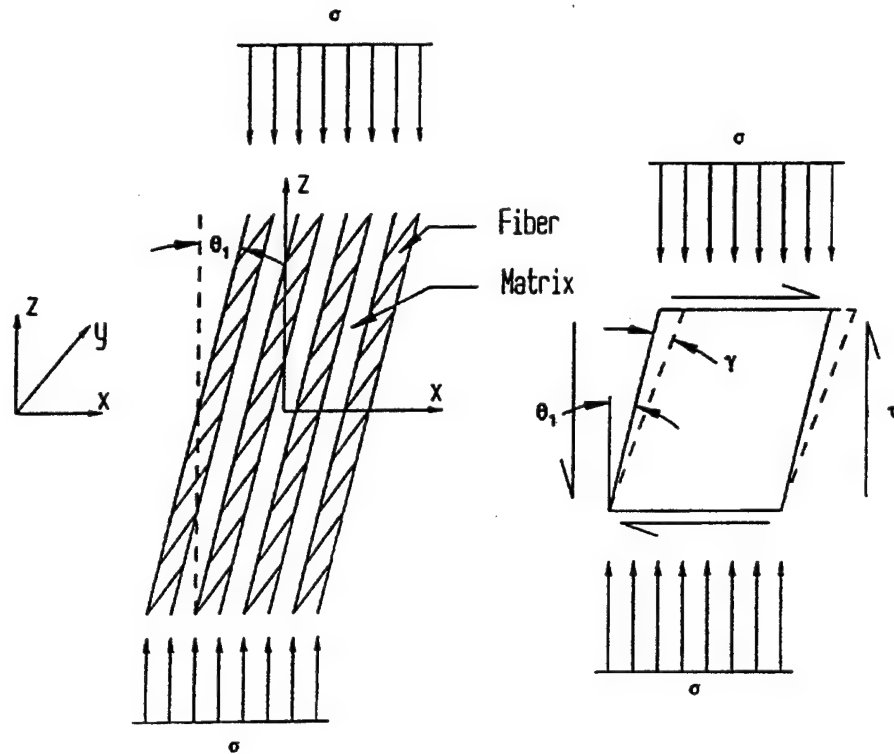


FIGURE 3.33a. AN INCLINED GROUP OF FIBERS UNDER COMPRESSION AND SHEAR STRESS AND STRAIN

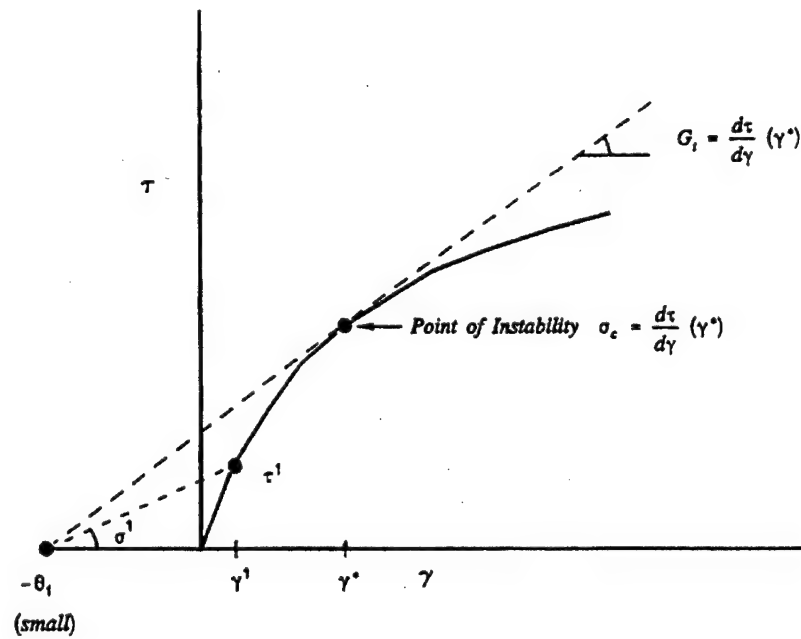


FIGURE 3.33b. INCREASES IN SHEAR STRESS AND POINT OF INSTABILITY FOR SMALL IMPERFECTION

Expected compressive stress-strain responses beyond instability are also discussed in reference 3.55. On the other hand, when  $\theta_1$  is sufficiently large or the brittle matrix composite has a limited shear strain carrying capacity  $\gamma^f$ , shear failure due to debonding (or splitting) may occur as shown in figure 3.33c, the compressive strength being given by

$$\sigma_c = \tau^f / (\theta_1 + \gamma^f) \quad (3.104)$$

where  $\tau^f$  is the shear strength of the composite.

It is clear, therefore, that either instability or shear failure due to debonding may govern the failure under compression. However, it is often difficult to identify the reason for the failure.

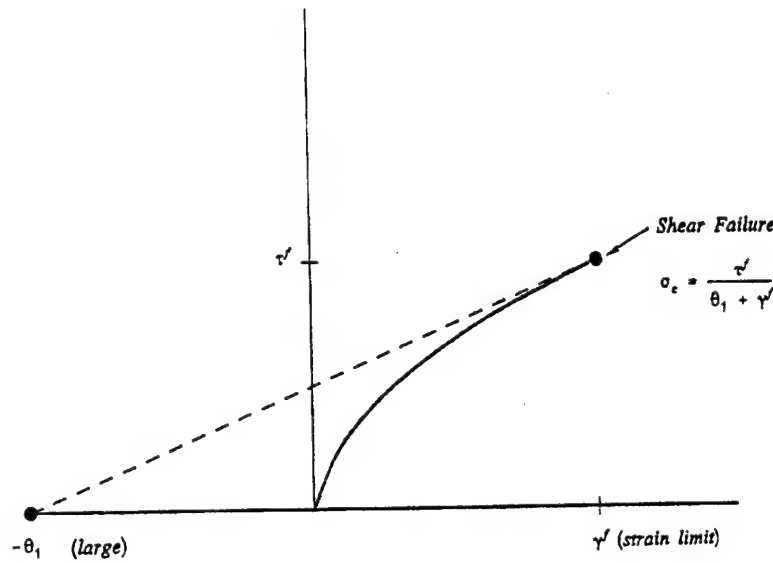


FIGURE 3.33c. SHEAR FAILURE FOR LARGE IMPERFECTIONS

Recent experimental studies [3.56 and 3.57] indicate that kinkband formation may be the reason of failure for some types of composites. Argon [3.58] and Budiansky [3.59] identified the shear yield stress  $\tau_y$ , of the matrix and the initial misalignment angle  $\theta_1$  of the fibers as the parameters controlling the failure by kinkband formation. For elastic, perfectly plastic case, Budiansky derived an equation similar to (3.102) given by

$$\sigma = \tau_y^* / (\theta_1 + \gamma) \quad (3.105)$$

in which

$$\tau_y^* = (\tau_y^2 + \sigma_{Ty}^2 \tan^2 \beta)^{1/2} \quad (3.106)$$

where  $\beta$  is the kinkband orientation and  $\sigma_{Ty}$  is yield stress in the transverse direction. In the case  $\beta = 0$ , the microinstability due to kinking occurs at a stress level

$$\sigma_c = \tau_y / \theta_1 \quad (3.107)$$

when the matrix response is rigid plastic ( $\gamma = 0$ ). One should note the similarity of the result (3.105) when  $\beta = 0$  with that in (3.103) for inelastic microbuckling in presence of imperfections derived on the assumption that the wave length of the fiber waviness is large. Correlations with test data [3.60] for AS4/PEEK material indicate measured and inferred values of  $\theta_1$  to be of the order of  $2.5^\circ$  (0.044 radians). Detailed measurements of fiber misalignments in such composites [3.61] indicate that misalignments  $\theta_1$  are in the range of 0-4 degrees. Therefore, it appears that the models for inelastic microbuckling and plastic kinking yield comparable compressive strengths for similar imperfections. The presence of imperfections (initial or those due to specimen clamping or other constraints addressed in reference 3.57), however, causes significant reduction in strength. Significant reductions are also observed in textile composites with large inherent fiber bundle waviness.

A failure mechanism which has been observed [3.62] for oriented polymeric fibers, such as Kevlar-49, is a kinkband formation at a specific angle to the direction of the compressive stress. A typical formation of slip planes in Kevlar-49 fibers is illustrated in figure 3.34. The formation of kinkbands is mainly attributed to the fibrillar structure of the highly anisotropic fiber and its poor shear strength. Breakup of the fiber into very small diameter fibrils results in the degradation of shear stiffness and hence the compressive strength.



FIGURE 3.34. LOCAL FIBER FAILURE MECHANISMS RESULTING FROM COMPRESSION OF KEVLAR/EPOXY

Other mechanisms of failure such as transverse splitting or debonding due to large tensile Poisson strain [3.63], fiber crushing, or matrix failure under axial compression [3.61] may occur in certain composite systems. The failure criterion for such systems is usually obtained by equating the appropriate strain to a known critical strain governing failure.

The results of the analyses of compressive strength indicate that for the elastic case, the matrix, Young's, or shear modulus is the dominant parameter for commonly used structural composites. For the inelastic case, however, the strength depends upon various other parameters and imperfections. The nature of changes made in matrix properties to improve the compressive strength of composites of a given fiber depends upon the base of reference. In some cases, performance is limited by the binder yield stress or the fiber/matrix interface shear strength; whereas, for other cases, a gain in compressive strength could be achieved by improving the binder modulus. The analytical results provide some guidance for determination of reasonable changes in matrix properties to yield improved composite compressive strength.

### 3.2.3 Matrix Mode Strength.

The remaining failure modes of interest are transverse tension and compression and axial shear. For each of these loading conditions, it is possible to have material failure without fracture of the fibers, hence the terminology "matrix dominated" or "matrix modes of failure".

Micromechanical analyses of these failure modes are complex because, unlike the axial failure modes treated above, for these matrix modes the critical stress states are in the matrix, are highly nonuniform, and are very dependent upon local details of the geometry. As a result, it appears that the most fruitful approaches will be those that consider average states of stress rather than local details.

Under transverse tensile stress, failure may occur within the matrix or along the fiber-matrix interface. It is not expected that composite transverse tensile strengths will be significantly in excess of matrix tensile strength. Indeed, perhaps the addition of fibers will weaken the matrix in this direction due to local stress concentrations or weak interfaces, etc. Various attempts have been made to predict the transverse tensile strength of brittle matrix composites based on local maximum stress, strain, or distortion energy in the matrix which are quantified in terms of stress concentration or strain magnification factor or via detailed stress analyses based on the assumption of a regular arrangement of fibers [3.64]. Other empirical approaches [3.65] have also been proposed.

Under transverse compression, failure may sometimes occur due to crushing of the fiber or the matrix. However, for commonly used epoxy composites, failure usually occurs by sliding (shearing) along planes parallel to fibers (figure 3.35a) in a manner similar to what is observed in homogeneous brittle materials [3.66]. For such materials, the angle  $\phi$  which the failure planes make with the loading direction is  $45^\circ$ , if the Tresca criterion governs failure. However, it is known that for many brittle materials, the Mohr-Coulomb criterion is more appropriate and the angle may differ slightly from  $45^\circ$ , although the compressive strength is usually of the order of twice the shear strength of the material, which is consistent with a  $45^\circ$  failure plane angle. For



composites the strength may be lower than twice the shear strength of the matrix material because of fiber matrix debonding.

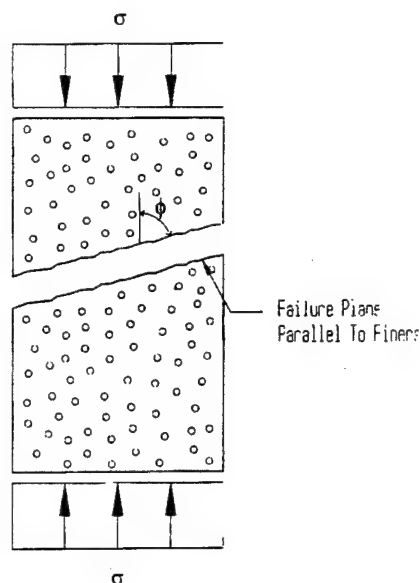


FIGURE 3.35a. SHEAR FAILURE UNDER TRANSVERSE COMPRESSION

Matrix shear failure and fiber matrix debonding also influence the failure mode under in-plane shear (figure 3.35b) and, therefore, it is expected that the shear strength of brittle matrix composites will be less than or equal to the shear strength of the matrix material. It may be noted that the complementary shear stress which acts on planes perpendicular to the fibers is equal in magnitude to that on the planes parallel to fibers (the failure plane shown in figure 3.35b). Thus, there are two types of shearing which are of interest for matrix dominated failures: (1) in a plane which contains the filaments and (2) in a plane normal to the filaments. In the first case, as the following discussion will show, the filaments provide very little reinforcement to the composite, and the shear strength depends upon the shear strength of the matrix material when fiber/matrix debonding does not occur. In the second case, some reinforcement may occur, and at high volume fractions of filaments, it may be substantial. Because the analysis shows that reinforcement does not take place in planes or surfaces parallel to the filaments, these planes may be considered planes of shear weakness. Surfaces of shear weakness do indeed exist in filamentary composites. It is important to recognize that filaments provide little resistance to shearing in any surfaces parallel to them.

For the composites with elastic plastic (ductile) matrices, the theorems of limit analysis of plasticity have been utilized to obtain upper and lower bounds of a composite limit load [3.67]. This is defined as the load at which the matrix yield stress permits composite deformation to increase with no increase in load. This limit load has been defined as composite failure and may be considered as an approximation to the strength of a composite having a ductile matrix. The assumptions are made that the filaments are elastic brittle and that the matrix is elastic, perfectly plastic and obeys the von Mises yield criterion. The procedure is to select admissible stress and velocity fields for construction of the lower and upper bounds, respectively. (Details are presented in reference 3.67). The results show that the yield strength of the matrix in shear is

a lower bound for the composite shear strength and the upper bound depends on the fiber volume fraction approaching a value of  $4/\pi$  times the matrix yield stress when  $v_f$  approaches 1.

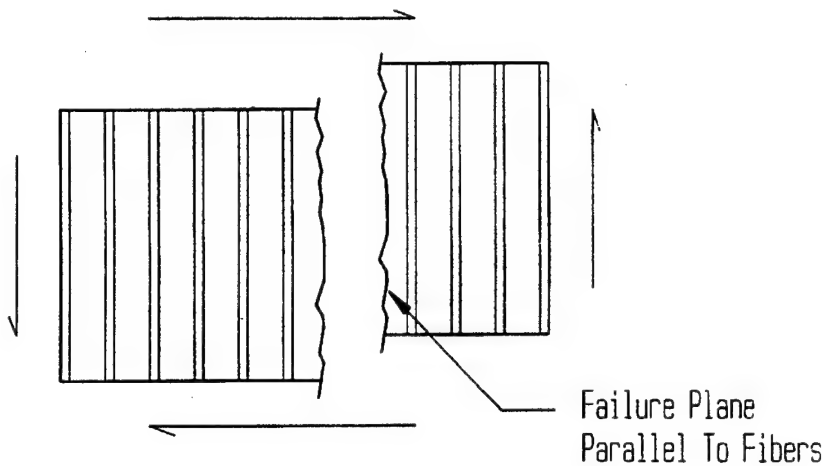


FIGURE 3.35b. SHEAR FAILURE UNDER LONGITUDINAL SHEAR

For transverse shear, the lower bound is the same, but the upper bound rapidly increases from the lower bound (for  $v_f \rightarrow 0$ ) as  $v_f$  is increased. The implication here is that reinforcement against transverse shear may in fact take place, particularly in compression, when the matrix is ductile.

#### 3.2.4 Remarks on Strength Analysis.

The developments of sections 3.2.1, 3.2.2, and 3.2.3 demonstrate that the analytical determination of the ultimate stresses of a unidirectional composite in terms of microstructure and constituent strength characteristics is extremely complex, perhaps to the point of being regarded as an intractable problem. The qualitative treatments discussed provide valuable insights into the problem of strength and guidelines for the development of improved materials, but design values of the ultimate stresses must be determined experimentally. Even such experimental information, however, is not sufficient for characterization of the strength of a UDC, since in most structural applications the material is subjected to states of combined stress. The reason is that the most common structural usage of a UDC is as an element of a laminate. As will be shown later, the state of stress in such a lamina is two or three dimensional and has at least three components:

$\sigma_{11}$  in the fiber direction,  $\sigma_{22}$  transverse to the fibers, and  $\sigma_{12}$  in axial shear. It is necessary, therefore, to determine the strength of a UDC under a state of combined stress. In view of the extreme difficulty of the analytical determination of strength for a single stress component, it is impractical to attempt to resolve the problem for combined stress by microstructural analysis. On the other hand, it is also impractical to resolve the problem by experimentation, since the number of tests required to develop the full failure surface would be enormous and some of the combined stress tests are very difficult to perform. The remaining alternative is to establish the ultimate stress values for single stress components by experiment and construct analytical failure criteria in terms of these values by global considerations. Such failure criteria are often used in predicting failure of a ply (UDC) in a laminate. It should be noted, however, that matrix

dominated failure of a ply does not imply the destruction of the load carrying capacity of the ply, but it indicates onset of damage (local). This issue will be discussed in the next chapter.

### 3.2.5 Strength Under Combined Stress.

The failure of a UDC under single-stress components has been shown to involve a number of very different failure mechanisms. It is now desired to use this knowledge and quantitative experimental data for single stress components to formulate practical failure criteria for combined stresses. For simplicity, the discussion will deal with the case of plane stress. Results for more complicated stress systems will be described subsequently. The stresses considered are averages over an RVE. The fundamental assumption is that there exists a failure criterion of the form

$$F(\sigma_{11}, \sigma_{22}, \sigma_{12}) = 1 \quad (3.108)$$

which characterizes the failure of the UDC. (The "1" on the right side of (3.108) results from normalizing the stresses in terms of the uniaxial strengths of the laminate.) A convenient representation of (3.108) is a surface in stress space with coordinates  $\sigma_{11}$ ,  $\sigma_{22}$ , and  $\sigma_{12}$ , (figure 3.36). Since all failure stresses are finite, the surface must be closed. Each point in stress space represents a state of stress. Points inside the surface indicate no failure, points on the surface indicate failure, and points outside the surface are not realizable stress states. A failure surface can also be expressed in terms of strains. The stress and strain failure surfaces must be connected by the stress-strain relations of the UDC.

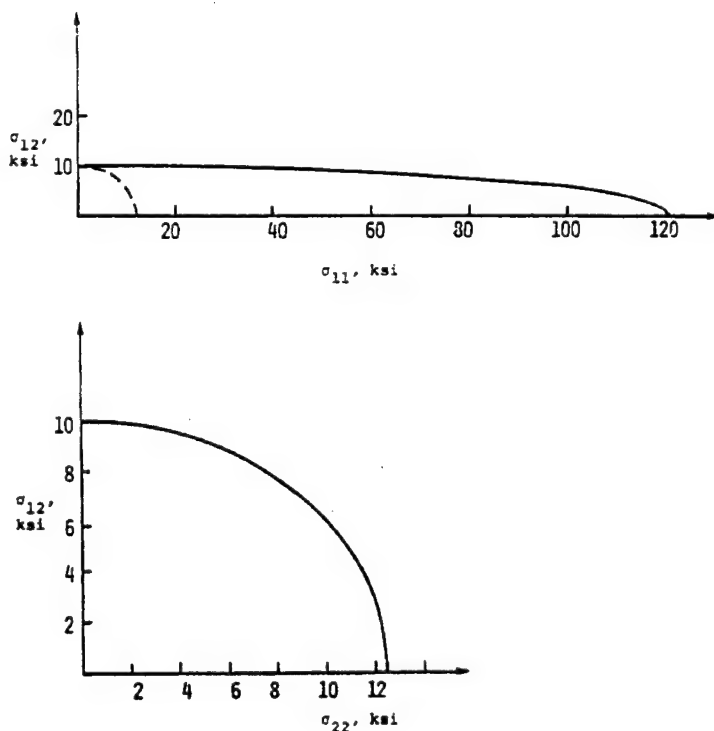


FIGURE 3.36. FAILURE SURFACES IN STRESS SPACE FOR HS GRAPHITE/EPOXY, 60% FIBERS

The most primitive failure criterion consists of the assumption that failure will occur whenever any single stress component reaches its ultimate value, regardless of the values of the other stress components. This maximum stress failure criterion is not realistic, since it disregards the combined effects of stresses on failure. Although it is simple to utilize in practice, such a criterion is usually nonconservative since it often overestimates the strength of the material under combined stress. A similar possibility is the assumption that failure occurs whenever any strain component reaches its ultimate value regardless of the others. This maximum strain criterion is also frequently used, although it is, of course, open to similar criticism. It should be noted, however, that the load carrying capacity of a well designed laminate is usually governed by fiber failure of the principal load bearing laminae, and for this reason, maximum stress or maximum strain criteria used in progressive failure analyses of laminates may yield good estimates of the failure loads of a laminate.

The usual approach to construction of a failure criterion is to assume that it can be represented by a quadratic polynomial in the stresses. The coefficients of the polynomial should be expressed in terms of simple experimental information such as ultimate stresses under individual load components. The various failure criteria which have been proposed all attempt to utilize these basic test data to define a surface of the form (3.108). No fundamental significance should be attached to the choice of a quadratic form.

This should be regarded as the simplest choice which can adequately describe the experimental data. It appears that such an approach was originated simultaneously in references 3.68 and 3.69. A general quadratic failure criterion including linear terms is presented in reference 3.70, a comprehensive general discussion of quadratic failure criteria is given in reference 3.71, and a more recent review of this subject has been addressed in reference 3.72. All of the failure surfaces obtained from the quadratic failure criteria are characterized by smooth curves having continuous slopes because of the fact that the failure criteria are represented in terms of a single polynomial. For example, in the case of plane stress, the general quadratic version of equation 3.108 would be

$$F_{11}\sigma_{11}^2 + F_{22}\sigma_{22}^2 + F_{66}\sigma_{12}^2 + 2F_{12}\sigma_{11}\sigma_{22} + 2F_{16}\sigma_{11}\sigma_{12} + 2F_{26}\sigma_{22}\sigma_{12} + F_1\sigma_{11} + F_2\sigma_{22} + F_6\sigma_{12} = 1 \quad (3.109)$$

The material has different strengths in uniaxial, longitudinal, and transverse tension and compression, but evidently the shear strength is not affected by the sign of the shear stress. It follows that all powers of shear stress in the failure criterion must be even, and therefore, all the terms containing a shear stress to power one must be rejected. Consequently, the criterion (3.109) simplifies to

$$F_{11}\sigma_{11}^2 + F_{22}\sigma_{22}^2 + F_{66}\sigma_{12}^2 + 2F_{12}\sigma_{11}\sigma_{22} + F_1\sigma_{11} + F_2\sigma_{22} = 1 \quad (3.110)$$

Let the ultimate stresses for single stress components be denoted by

- $\sigma_L^{tu}$  - tensile ultimate, fiber direction
- $\sigma_L^{cu}$  - compressive ultimate, fiber direction
- $\sigma_T^{tu}$  - tensile ultimate, transverse to fibers
- $\sigma_T^{cu}$  - compressive ultimate, transverse to fibers
- $\tau_L^u$  - ultimate longitudinal shear stress

These values determine the points on the  $\sigma_{11}$ ,  $\sigma_{22}$ , and  $\sigma_{12}$  axes through which the surface (3.110) must pass. It follows that

$$\begin{aligned}
 F_{11} &= \frac{1}{\sigma_L^{tu} \sigma_L^{cu}} & F_{22} &= \frac{1}{\sigma_T^{tu} \sigma_T^{cu}} \\
 F_1 &= \frac{1}{\sigma_L^{tu}} - \frac{1}{\sigma_L^{cu}} & F_2 &= \frac{1}{\sigma_T^{tu}} - \frac{1}{\sigma_T^{cu}} \\
 F_{66} &= \frac{1}{\left(\tau_L^u\right)^2}
 \end{aligned} \tag{3.111}$$

When the tensile and compressive strengths are equal,  $F_1$  and  $F_2$  are zero and the criterion reduces to a form similar to Von Mises' equation generalized to consider orthotropic material failure (reference 3.73). Modification of this criterion by introducing cutoffs in tension-tension and compression-compression quadrants has also been proposed in reference 3.73.

The constant,  $F_{12}$ , cannot be determined in terms of the ultimate stresses, and it is necessary to perform failure tests under biaxial stress to find this coefficient. Frequently, this coefficient is established by relating (3.110) to the Mises-Hencky yield criterion for isotropic materials. This yields

$$F_{12} = -\frac{1}{2} (F_{11} F_{22})^{1/2}$$

The above failure criterion is the two-dimensional version of the Tsai-Wu criterion [3.70]. Its implementation and use may involve some problems:

1. The coefficient  $F_{12}$  must be determined by biaxial testing. It is necessary to select tension or compression values for both  $\sigma_{11}$  and  $\sigma_{22}$  for these tests. It is reasonable to expect that

$F_{12}$  will have four different values corresponding to these choices. This contradicts the premise of the description of the failure criterion by a single polynomial.

2. Since the coefficients are expressed in terms of both tensile and compressive strengths, it follows that in a biaxial tension-tension test the failure will depend on the compressive ultimate stresses. This is not satisfactory from a physical point of view [3.74].
3. The failure criterion does not address the mechanics of the different failure modes of a UDC and does not specify how the composite fails.

Even with the problems discussed above, this criterion or its modified versions are widely used in industry. The shortcomings 1 and 2, mentioned above, are usually overcome by fitting different polynomials in different quadrants and such an approach may often be a better choice. As regards to the third shortcoming, attempts have been made by many investigators to identify the type of failure by comparing relative contributions of different stresses to the left-hand side of (3.110). However, in view of the diverse failure mechanisms discussed earlier, such an approach may not be a good choice. It is possible to use the identification of the different failure modes of a UDC to lead to physically more realistic and, at the same time, simpler failure criteria. Such an approach is presented in reference 3.75. Testing of a polymer matrix UDC reveals that tensile stress in the fiber direction produces a jagged, irregular failure surface, while tensile stress transverse to the fibers produces a smooth, straight failure surface (figures 3.37 and 3.38). The underlying microstructural phenomena are as follows.

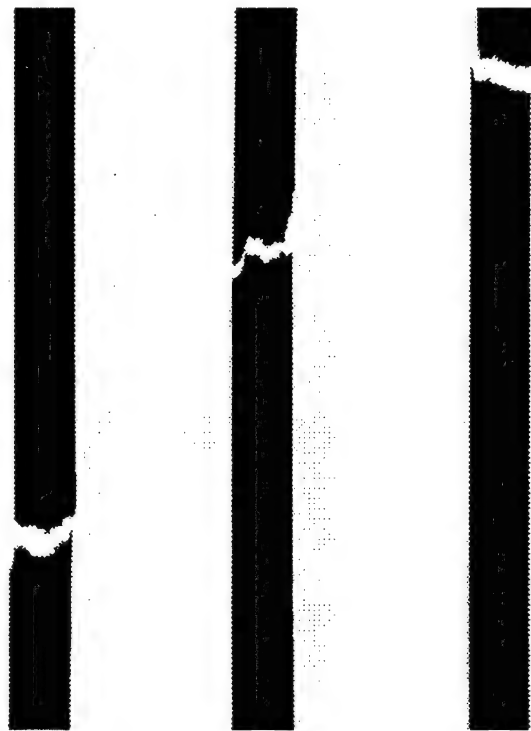


FIGURE 3.37. TYPICAL FAILURE OF [0] BORON/EPOXY LAMINATES SUBJECTED TO LONGITUDINAL TENSION-TENSION FATIGUE LOADING

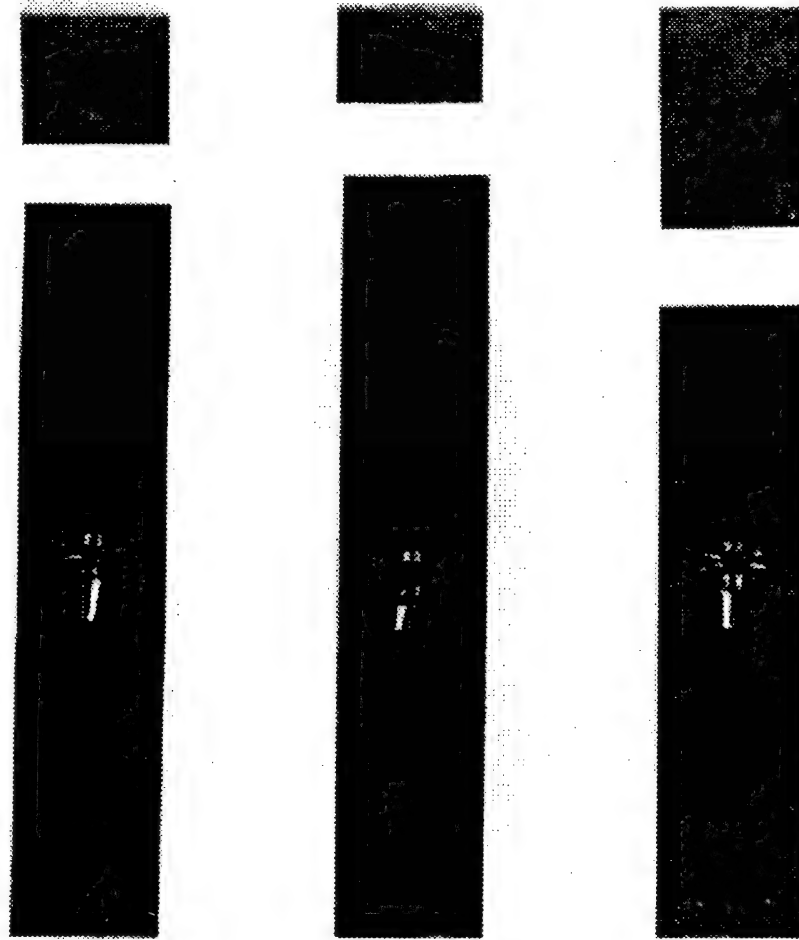


FIGURE 3.38. TYPICAL FAILURE OF UNIDIRECTIONAL BORON/EPOXY LAMINATES  
SUBJECTED TO TRANSVERSE TENSION-TENSION FATIGUE LOADING

In the case of tension in the fiber direction, fibers break progressively at random places leading to small cracks perpendicular to fibers and also longitudinal cracks along the fibers (figure 3.39). The load carrying capacity in the fiber direction deteriorates because of the cracks cutting the fibers until a sufficient number coalesce to result in catastrophic failure. Such failure will be identified as the tensile fiber mode. Since, in this mode, the carrying capacity deterioration is due to cracks created by fiber breaks, and since transverse stress  $\sigma_{22}$  has no effect on such cracks (although it may affect load transfer after cracking), it is assumed that the tensile mode is only dependent on the stresses  $\sigma_{11}$  and  $\sigma_{12}$ .

In the case of compressive  $\sigma_{11}$ , failure is due to fiber buckling, as has been discussed in section 3.2.2. The fibers buckle in the shear mode, and therefore, it may again be assumed that the transverse stress  $\sigma_{22}$  has little effect on the compressive failure. Thus, in this compressive fiber mode, failure again depends primarily on  $\sigma_{11}$  and also on  $\sigma_{12}$ . The dependence of  $\sigma_{12}$  is not known and arguments may be offered for and against, including it in the failure criterion.

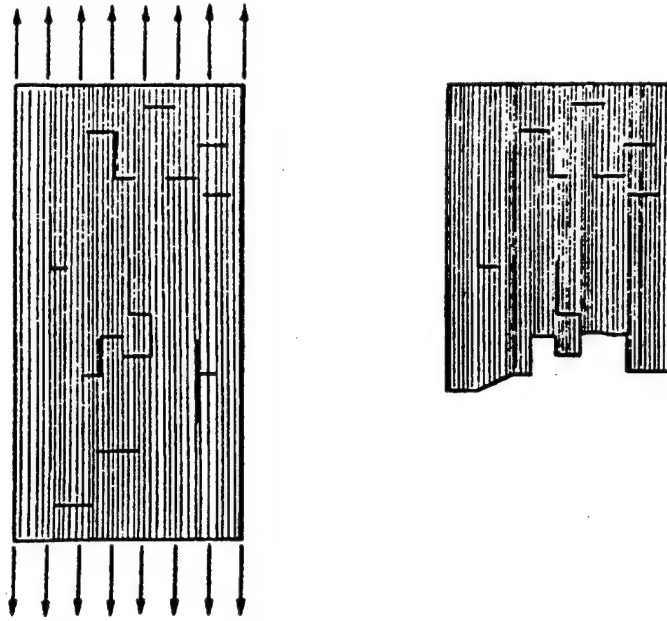


FIGURE 3.39. TENSILE FIBER FAILURE MODE

In the case of tension transverse to the fibers, failure occurs by the sudden growth of a crack in the fiber direction, figure 3.40. The phenomenon is so abrupt that it is extremely difficult to detect its initiation and extension. This failure mode will be called the tensile matrix mode. Since stress in the fiber direction has no effect on a crack in the fiber direction, the axial stress does not enter into this failure mode, which is thus dependent only on  $\sigma_{22}$  and  $\sigma_{12}$ .

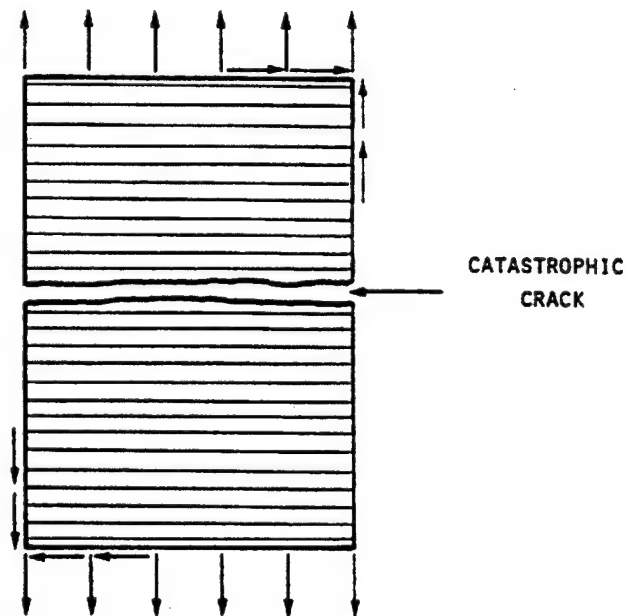


FIGURE 3.40. TENSILE MATRIX FAILURE MODE



For compressive stress transverse to the fibers, failure occurs on some plane parallel to the fibers, not necessarily normal to the direction of  $\sigma_{22}$ . This is called the compressive matrix mode and is produced by normal stress and shear stress on the failure plane. Again, the stress  $\sigma_{11}$  does not affect the failure.

Each of the failure modes described can be modelled separately by a quadratic polynomial. (For details, see reference 3.75 in which the general case of three-dimensional stress is considered.) This results in four individual failure criteria.

It should be noted that the choice of stress components included in each of these criteria and the particular mathematical form used are subjects which are not fully resolved at this point in time. The following criteria appear to be a reasonable set which satisfy the desire to deal separately with different modes of failure.

#### Fiber Modes

Tensile

$$\left( \frac{\sigma_{11}}{\sigma_L^{tu}} \right)^2 + \left( \frac{\sigma_{12}}{\tau_L^u} \right)^2 = 1 \quad (3.112a)$$

Compressive

$$\left( \frac{\sigma_{11}}{\sigma_L^{cu}} \right)^2 + \left( \frac{\sigma_{12}}{\tau_L^u} \right)^2 = 1 \quad (3.112b)$$

#### Matrix Modes

Tensile

$$\left( \frac{\sigma_{22}}{\sigma_T^{tu}} \right)^2 + \left( \frac{\sigma_{12}}{\tau_L^u} \right)^2 = 1 \quad (3.113a)$$

Compressive

$$\left( \frac{\sigma_{22}}{2\tau_T^u} \right)^2 + \left[ \left( \frac{\sigma_T^{cu}}{2\tau_T^u} \right)^2 - 1 \right] \frac{\sigma_{22}}{\sigma_T^{cu}} + \left( \frac{\sigma_{12}}{\tau_L^u} \right)^2 = 1 \quad (3.113b)$$

Note that  $\sigma_T^u$  in (3.113b) should be taken with its absolute value. The ultimate transverse shear  $\sigma_{23} = \tau_T^u$  is very difficult to measure. However, a reasonable approximation for this quantity is the ultimate shear stress for the polymeric matrix. For any given state of stress, one of each of (3.112) and (3.113) is chosen according to the signs of  $\sigma_{11}$  and  $\sigma_{22}$ . The stress components are introduced into the appropriate pair and whichever criterion is satisfied first is the operative criterion.

The advantages of this approach are as follows:

1. The failure criteria are expressed in terms of the components of ultimate stresses. No biaxial test results are needed.
2. The failure mode is identified by the criterion which is satisfied first.

The last feature is of fundamental importance for analysis of fiber composite structural elements since it permits identification of the nature of initial damage. Moreover, in conjunction with a finite element analysis, it is possible to identify the nature of the failure in elements, modify their stiffness accordingly, and proceed with the analysis to predict new failure, etc.

A convenient method to examine the failure criteria experimentally is by means of off-axis specimens, figure 3.41. In such a specimen, the stresses are given by

$$\begin{aligned}\sigma_{11} &= \sigma \cos^2 \theta \\ \sigma_{22} &= \sigma \sin^2 \theta \\ \sigma_{12} &= \sigma \sin \theta \cos \theta\end{aligned}\tag{3.114}$$

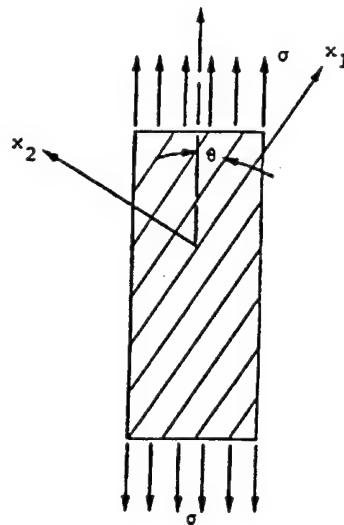


FIGURE 3.41. OFF-AXIS SPECIMEN

Testing in tension shows [3.76] that for very small reinforcement angles, specimens fail in the fiber mode, while for increased angles they fail in the matrix mode. This is shown schematically in figure 3.42. The angle  $\theta_o$  separating the two modes is obtained when (3.112) and (3.113) are satisfied simultaneously in terms of (3.114). This leads to

$$\tan^2 \theta_o = \frac{\sigma_T^{tu}}{\sigma_L^{tu}} \quad (3.115)$$

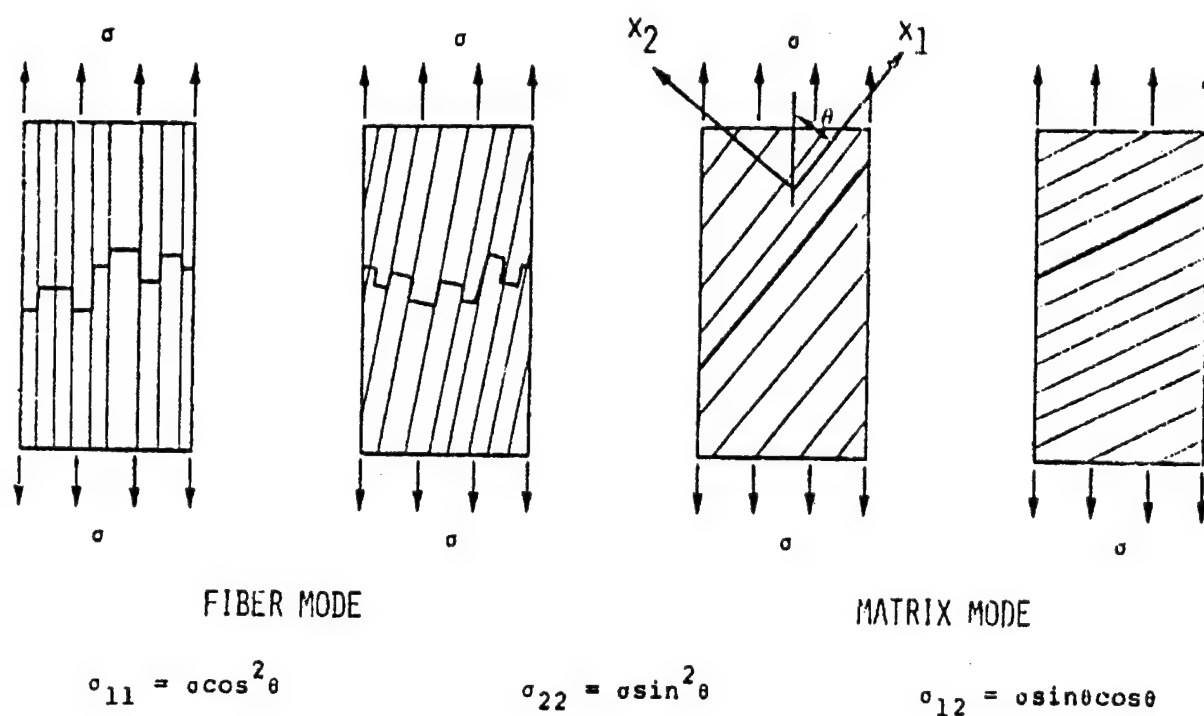


FIGURE 3.42. FAILURE MODES—OFF-AXIS SPECIMENS

Figure 3.43 shows comparison of the prediction of the failure criteria (3.112a) and (3.113a) with experimental data for glass/epoxy off-axis specimens [3.77] showing excellent agreement. For a general state of average three-dimensional stress, the failure criteria are [3.75].

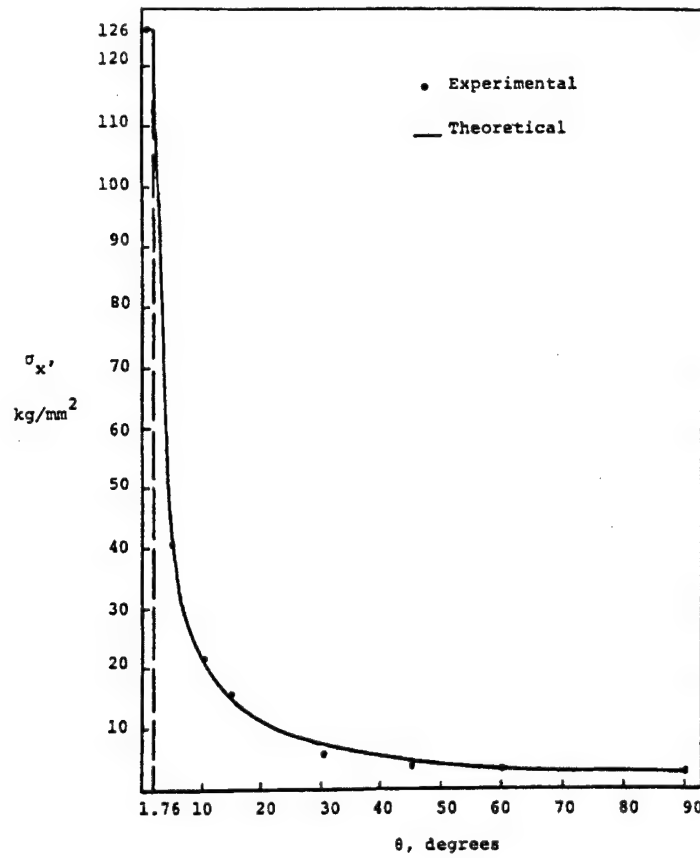


FIGURE 3.43. STATIC OFF-AXIS STRENGTH VERSUS ANGLE

### Fiber Modes

$$\left( \frac{\sigma_{11}}{\sigma_T^{tu}} \right)^2 + \frac{\sigma_{12}^2 + \sigma_{13}^2}{(\tau_L^u)^2} = 1 \quad \sigma_{11} > 0$$

(3.116)

$$\left( \frac{\sigma_{11}}{\sigma_T^{cu}} \right)^2 + \frac{\sigma_{12}^2 + \sigma_{13}^2}{(\tau_L^u)^2} = 1 \quad \sigma_{11} > 0$$

### Matrix Modes

$$\left( \frac{\sigma_{22} + \sigma_{33}}{\sigma_T^{tu}} \right)^2 + \frac{\sigma_{23}^2 - \sigma_{22}\sigma_{33}}{\left( \tau_T^u \right)^2} + \frac{\sigma_{12}^2 + \sigma_{13}^2}{\left( \tau_L^u \right)^2} = 1$$

$$\sigma_{22} + \sigma_{33} > 0$$

(3.117)

$$\left[ \left( \frac{\sigma_T^{cu}}{2\tau_T^u} \right)^2 - 1 \right] \frac{\sigma_{22} + \sigma_{33}}{\sigma_T^{cu}} + \left( \frac{\sigma_{22} + \sigma_{33}}{2\tau_T^u} \right)^2 + \frac{\sigma_{23}^2 - \sigma_{22}\sigma_{33}}{\left( \tau_T^u \right)^2}$$

$$+ \frac{\sigma_{12}^2 + \sigma_{13}^2}{\left( \tau_L^u \right)^2} = 1 \quad \sigma_{22} + \sigma_{33} < 0$$

It has been pointed out earlier that failure of a ply in a laminate which is predicted by the use of a failure criterion of the types discussed in this section does not always imply the failure of the laminate (or the ply under consideration), but it indicates onset of damage. Some authors have attempted to obtain failure criteria which are better suited for practical design [3.74] of laminates. Laminates usually fail after the development of a significant amount of subcritical damages, which will be addressed in the next chapter.

#### 3.2.6 Fatigue Failure.

Understanding the response of composites to repeated load applications is of primary importance since aeronautical structures are subjected to many load cycles during their lifetime. Local areas of damage may be initiated by cyclic loading. Such localized damage may also exist as a result of deficiencies of the fabrication process or as a result of unanticipated events in service, such as foreign object impact. Damage resulting from all of these causes may be expected to propagate as a result of subsequent cyclic loading. This increase in the amount of damage may lead to a loss in structural performance and eventually to failure.

For metal structures, fatigue problems have been approached with some success by use of the methodology of fracture mechanics. In metal fatigue, failure consists of the initiation and propagation of one dominant crack. Over the years, there has emerged a fracture mechanics design procedure for fatigue of metal aeronautical structures which is based on periodic inspection and monitoring of visible cracks [3.78]. As will be discussed below, there are significant differences between the fatigue failure processes in metals and those in fiber

composites. This requires new design procedures, which have not yet been established in a definitive form, for fiber composite structures.

It is again emphasized that in the design process of a fiber composite structure the laminate configuration and also the constituents of the UDC are design variables. Clearly, it is prohibitively expensive to obtain the necessary laminate fatigue data by testing all possible candidate laminates for all loading conditions of interest. It, therefore, becomes necessary to either severely limit the number of alternatives to be examined or to develop an analytical procedure. Again, it appears desirable to assess the fatigue characteristics of a laminate for general loading conditions in terms of the fatigue characteristics of the unidirectional material and the laminate geometry. The fatigue responses of the UDC under different loading modes are determined experimentally. Therefore, the present discussion is concerned with fatigue failure of UDC. Just as in the case of static failure (sections 3.2.1-3.2.5), here the point of view is adopted that the complexities of the microstructural failure process prohibit quantitative analytical determination of fatigue failure in terms of the microcharacteristics of the composite. The observed nature of microfailures is of great qualitative importance, however, primarily for the detection and description of different failure modes.

#### 3.2.6.1 Uniaxial Loading—Axial Tension-Tension Fatigue (Basic Concepts and Phenomenological Considerations).

In the traditional fatigue test, a specimen is subjected to uniform sinusoidal cyclic stress, figure 3.44.

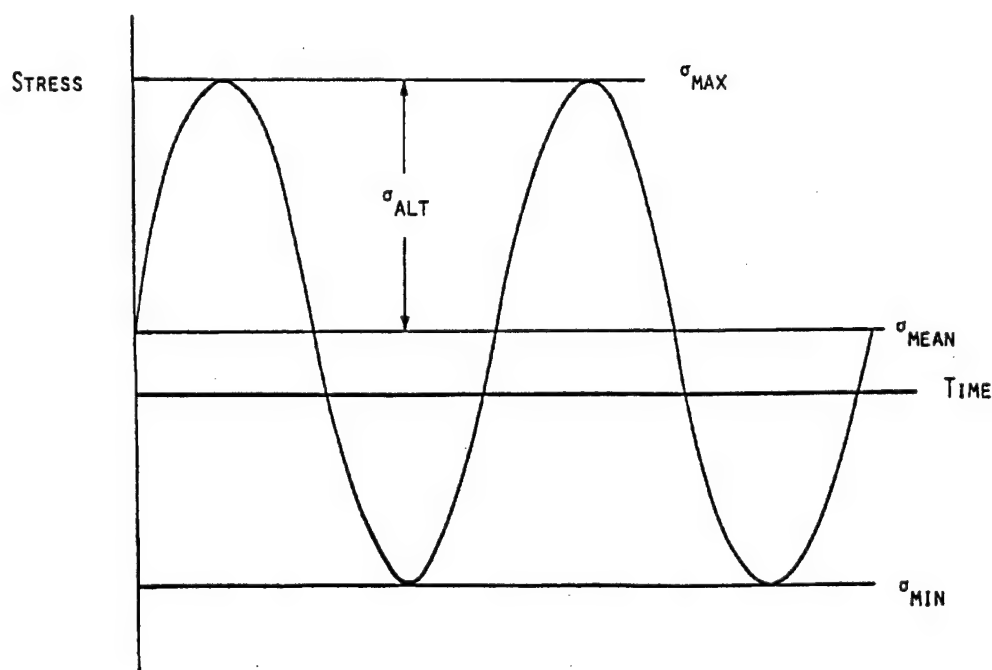


FIGURE 3.44. UNIFORM SINUSOIDAL CYCLIC STRESS FOR FATIGUE TESTING

The mean,  $\sigma^m$ , and alternating,  $\sigma^a$ , parts of the cyclic stress are defined by

$$\sigma^m = \frac{1}{2} (\sigma_{\max} + \sigma_{\min})$$

$$\sigma^a = \frac{1}{2} (\sigma_{\max} - \sigma_{\min})$$
(3.118)

and the stress amplitude ratio by

$$R = \sigma_{\min} / \sigma_{\max}$$
(3.119)

The magnitude and the algebraic sign of this ratio characterize the general type of load combinations being applied. This is illustrated in figure 3.45 for various kinds of sinusoidal cyclings.

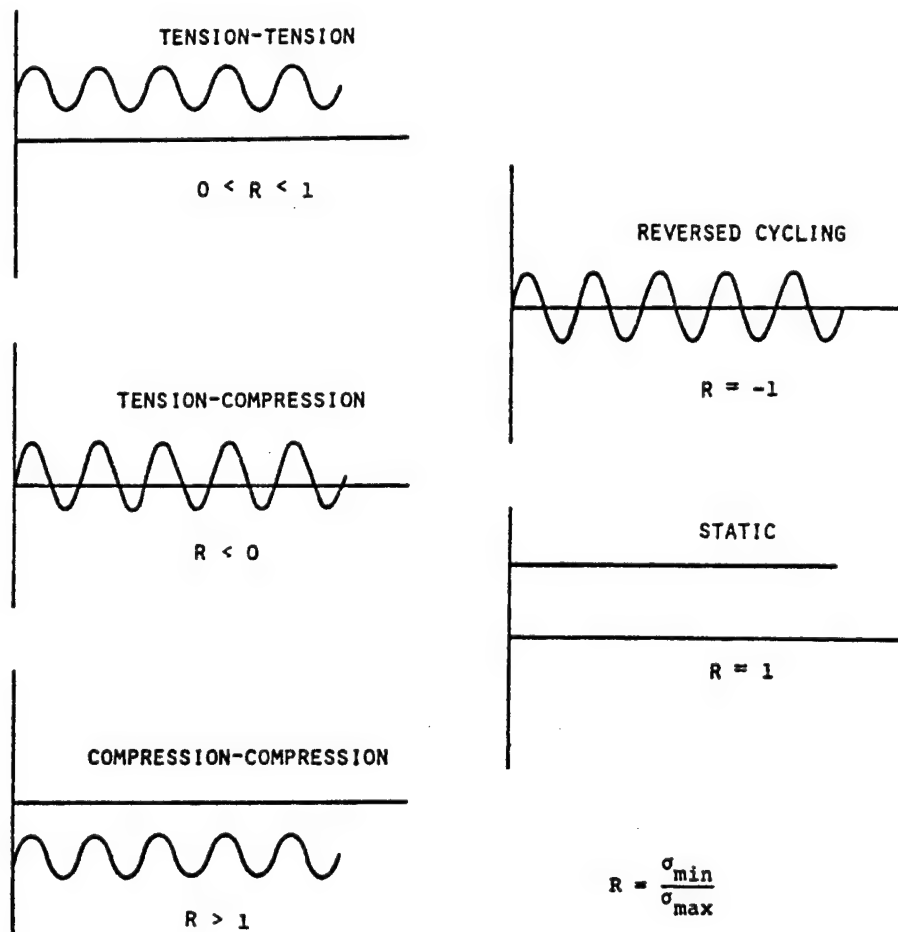


FIGURE 3.45. CLASSIFICATION OF FATIGUE CYCLES

The most common fatigue characterization is a plot of number of cycles to failure—also called lifetime—versus the maximum amplitude in a constant sinusoidal cycling. This is known as the S-N curve and is generally presented for stress ratios,  $R$ , of either zero or one. Since lifetimes may attain millions of cycles and since most of the fatigue damage develops towards the end of the lifetime, it is convenient to plot  $\log N$  versus amplitude and sometimes versus  $\log$  amplitude. An example of an S-N curve, for cyclic stress of graphite/epoxy in the fiber direction, is shown in figure 3.46. Notice the relatively small decrease in maximum stress over the range in lifetime out to  $10^5$  cycles. It should be remembered that sinusoidal loading is characterized by two numbers, e.g.,  $\sigma^a$  and  $\sigma^m$ , or alternatively, by  $\sigma^m$  and  $R$ . The relative effect of different loadings is shown in figure 3.47 for a carbon/epoxy composite. The tension-tension curve ( $R = 0.1$ ) illustrates the characteristic insensitivity of the UDC to repeated tensile loadings in the fiber direction. This is in contrast to the axial compression results ( $R = 10$ ) which demonstrate significant fatigue degradation. For both loading conditions, however, the maximum stress values are substantially greater than the results obtained for a good aluminum alloy. The figure also contains a representative result for compressive cyclic loading transverse to the fibers. In this mode, the S-N curve is flat but substantially below all the other curves.

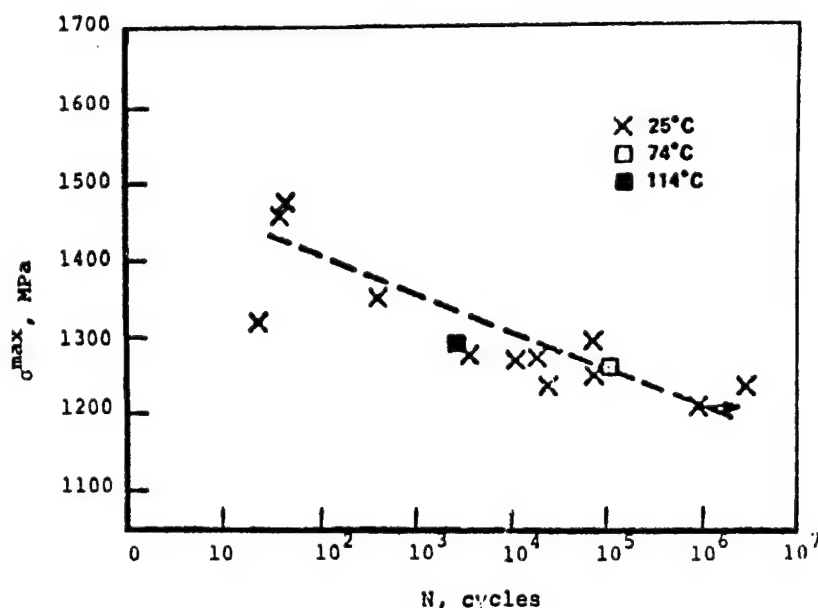


FIGURE 3.46. S-N CURVE FOR CYCLIC STRESS OF GRAPHITE/EPOXY COMPOSITE IN THE FIBER DIRECTION

An intrinsic characteristic of fatigue failure is large scatter in lifetime data (e.g., figure 3.46), which implies that repeated tests of the same cyclic loading produce very different lifetimes. This scatter is due to the complexity of developing microdamages under cyclic loading, which is different in detail for every specimen tested. Such scatter is inherent to fatigue for all materials and must be considered in the analytical methodology.



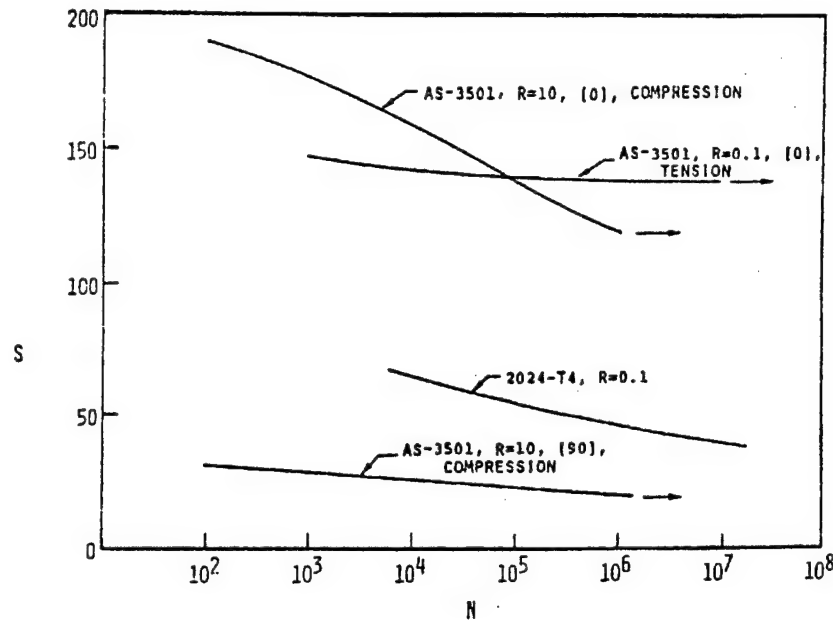


FIGURE 3.47. TYPICAL S-N CURVES SHOWING THE EFFECT OF DIFFERENT LOADINGS ON CARBON/EPOXY COMPOSITES

Since most of the experience in fatigue failure has been accumulated for metals, it is of importance to point out some fundamental differences between fatigue failure of metals and composites. Metals are polycrystalline aggregates. During stress cycling, microdamage develops in the form of microcracks and plastifications of single crystals, the latter being known as persistent slip bands (PSB). At some stages of the cycling, a crack develops which grows with continued cycling until the specimen fails. These two stages are known as initiation and propagation. This is shown schematically in figure 3.48. At the present time, the fraction of lifetime spent in initiation cannot be predicted. In the propagation stage, however, the growth of the crack with cycling can be reasonably well predicted [3.79]. The use of a crack growth law along with a measured or assumed size of the existing crack forms the basis for design methods for fatigue of metals. These methods take into account possible crack locations and characteristics of available inspection methods to define safe inspection periods.

For the case of a UDC, the nature of damage growth is quite different. The microstructure consists of a polymeric matrix containing stiff, strong fibers. The material is very anisotropic and cracks propagate easily in the matrix along surfaces parallel to the fibers. When a unidirectional specimen is cycled under tension-tension loading in the fiber direction, damage accumulates in the form of random fiber ruptures which are the source of small cracks in the matrix, figure 3.39. More and more cracks develop both perpendicular and parallel to the fibers with additional cycling until some of these coalesce to produce catastrophic failure. The failure surface is jagged and irregular, as suggested in figure 3.39 and illustrated in figure 3.37. The failure mode is similar to the static tensile fiber mode discussed in section 3.2.1. For some fibers, it may happen that failure will occur by propagation of one sudden transverse crack. Observations of this mode are rare.

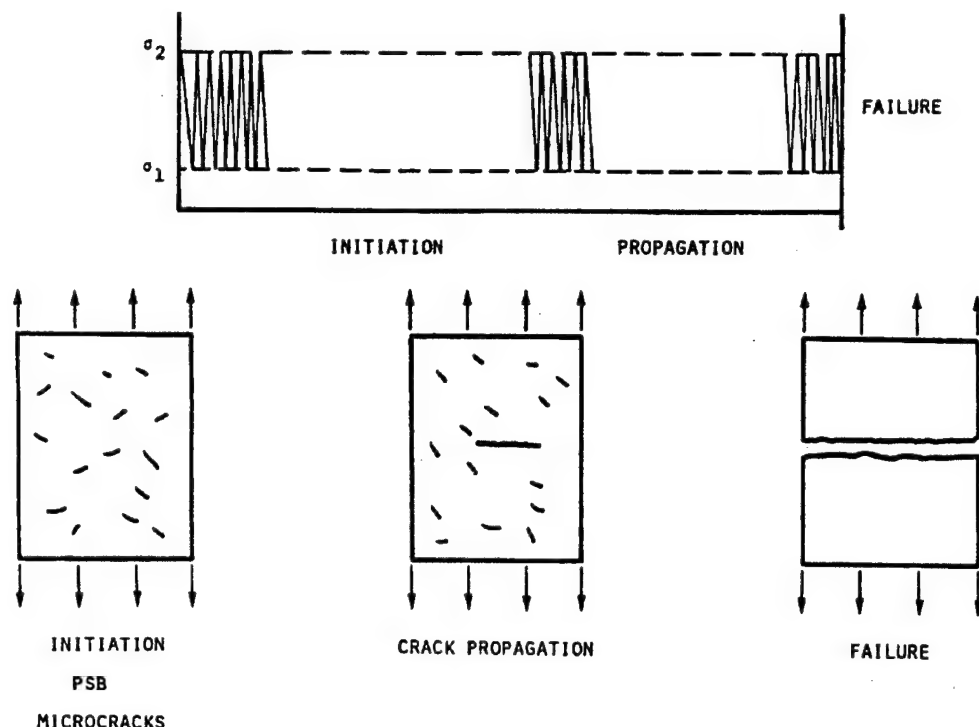


FIGURE 3.48. SCHEMATIC ILLUSTRATION OF METAL FATIGUE

This damage accumulation mechanism of fatigue failure will be called the tension-tension fiber mode. Its main characteristics are (1) failure occurs because of fiber rupture, and (2) the entire lifetime consists of damage initiation.

When the cycling is other than tension-tension, the situation is less clear. It may be argued that for tension-compression cycling the same phenomena should be expected because of the tension component. The matter of the failure mechanism in compression-compression cycling is an open question. It is possible that fibers will buckle at a cyclic load much lower than a static buckling load because of deterioration of the matrix shear modulus due to cycling and/or due to the opening of longitudinal cracks at fiber-matrix interfaces. Careful experimentation is needed to uncover the governing mechanisms.

As in the static case, the second primary failure mode consists of a sudden cracking in a plane along the fibers and is called the matrix mode. This is shown schematically in figure 3.40, and is illustrated for the tension-tension loading of a boron/epoxy composite in figure 3.38. Pending thorough experimental investigation, it seems reasonable to expect that, in the cases of tension-compression and compression cycling, the directionality of the fibers will lead to the same kind of plane matrix failure mode.

The main characteristics of the matrix tensile failure mode are (1) failure occurs by cracking parallel to the fibers, and (2) the crack propagates quickly; thus a major part of the fatigue life consists of initiation. However, for tough durable (or ductile) matrices, propagation of cracks may occur at a much slower rate than in brittle matrices.

The S-N curve describes the relation between maximum cyclic stress amplitude and lifetime for a single cyclic stress component having a specified stress ratio. It has been introduced in the investigation of fatigue of metal structures where there are many cases of a single component cyclic stress. Even under multiaxial stress states, failure in metal structures often occurs due to propagation of a crack perpendicular to the direction of largest principal tensile stress. For a given stress ratio,  $R$ , of a single stress component, the S-N curve defines the lifetime,  $N$ , as a function of the maximum applied stress,  $S$ . Another useful format for presentation of fatigue data is the Goodman diagram, illustrated in figure 3.49, which presents various combinations of uniaxial mean and alternating stress for failure at a specified lifetime. By virtue of equations 3.118 and 3.119, it is clear that constant values of  $R$  are represented by straight lines through the origin. Thus, different regimes of fatigue loading, as shown in figure 3.45, can be located as shown in figure 3.49. This format is convenient for interpolation for different values of stress ratio. Representative uniaxial fatigue data for several UDC materials are presented in figure 3.50.

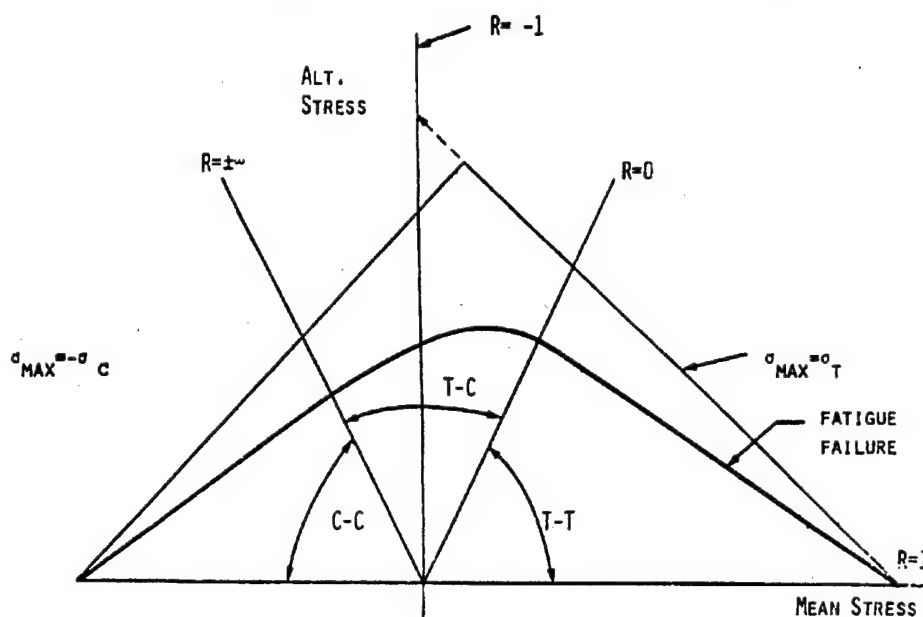


FIGURE 3.49. CHARACTERISTICS OF THE GOODMAN DIAGRAM

In practical metal structures, it is to be expected that fatigue failure will occur first in the vicinity of a discontinuity which causes a stress concentration. Appropriate S-N curves may be of value for predicting the onset of such failure. Following such an initial crack, the dominant effect may become the subsequent growth of that crack. As indicated earlier, metal fatigue failures are ascribed to fracture following a stable crack growth. Thus, design methods require the definition of an appropriate crack growth law. It has been customary in metal fatigue to use notched specimens for this purpose.

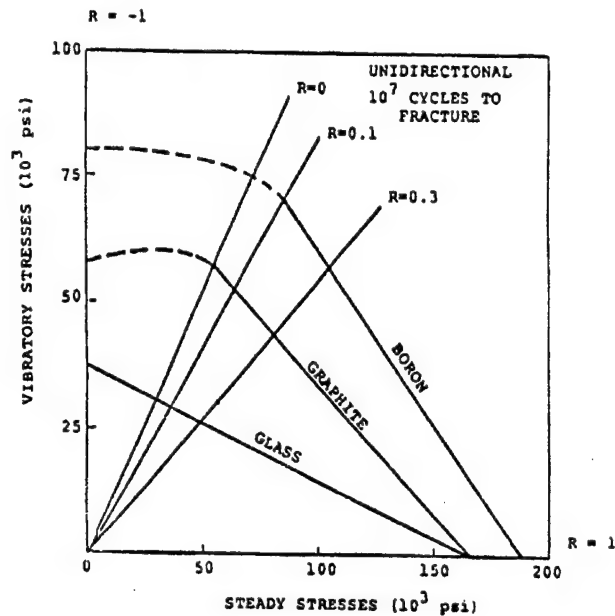


FIGURE 3.50. GOODMAN DIAGRAM FOR REPRESENTATIVE UNIDIRECTIONAL COMPOSITES

In a plain specimen, the stress in the test section is uniform and equal to the applied stress. Thus a dominant crack may start at any place in the test section. In a notched specimen, there is significant magnification (stress concentration) of applied stress at the notch, where the state of stress is locally uniaxial tension. Thus, a fatigue crack will develop and grow at this location. The notched specimen, however, does not provide useful information for the fatigue characteristics of a UDC, since it initiates different kinds of fatigue failure. A common case is the propagation of a crack along the fibers, and not a crack parallel to the notch as in metals. This situation is much more complicated in a laminate, where a notch produces a complicated state of three-dimensional stress which must be found numerically by the use of complex computer programs. Therefore, notched specimens are not usually helpful for determination of fatigue characteristics of fiber composites. Many experimental and modeling studies have been performed to determine the fatigue behaviors of various unidirectional composites. A majority of these studies have been devoted to tension-tension fatigue in the fiber direction, since a well designed laminate contains laminae whose fiber directions coincide with the principal loading directions, and therefore the fatigue behavior in the fiber direction of the individual laminae usually governs the life of such laminates, although there are other factors which influence the laminate performance. This issue will be addressed in the next chapter. Research on axial tension-tension fatigue of polymer matrix composites started in the early 1960's and results from some of these studies are discussed next. A survey on this topic can be found in reference 3.80.

#### 3.2.6.1.1 Damage Growth.

Fatigue damage in a UDC subjected to tension-tension fatigue usually starts with the development of dispersed matrix microcracks or isolated fiber breaks, depending on the applied stress level. In polymer matrix composites, the bond at the fiber/matrix interface is not very strong and debonds develop at such interfaces near matrix cracks or fiber breaks blunting their growth.

Therefore, as cycling continues, additional cracks or breaks and debonds develop at different locations causing some loss in stiffness and residual strength. A better understanding of the effects of such complex damage growth patterns can be obtained from the so-called fatigue-life diagrams shown schematically in figure 3.51 [3.81], where the band widths indicate expected scatter in test data. These diagrams are strain-life plots originally suggested in reference 3.82.

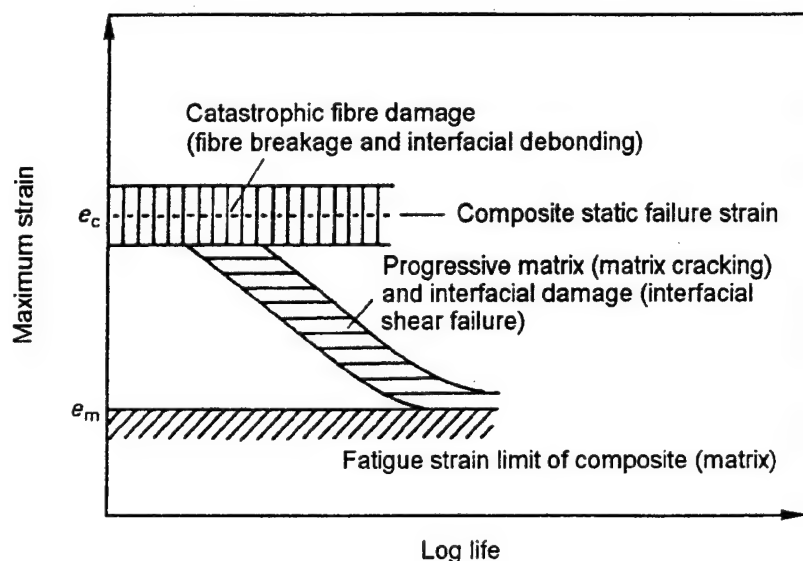


FIGURE 3.51. STRAIN-LIFE DIAGRAMS SHOWING VARIOUS REGIONS OF DIFFERENT TENSILE FATIGUE DAMAGE MECHANISMS (Proposed in references 3.81 and 3.82)

The upper band centered at composite static failure strain,  $\epsilon_c$ , shows the region where the dominant failure mechanism is progressive fiber breaks and debond growth and final catastrophic failure producing a jagged failure surface joining such breaks discussed earlier. If the fibers do not show any loss in strength with cycling, the band is expected to be horizontal. However, there may be some influence of progressive damage growth due to cycling and the phenomenon called static fatigue (or time under load effect), due to which the band may have a small slope. The band with a large slope corresponds to the region of progressive damage growth in the form of matrix microcracks and debonding, but the final failure involves fiber breaks. The horizontal line below the sloping band is the endurance strain limit ( $\epsilon_m$ ) of the matrix, below which matrix microcrack development is very limited. The patterns of damage growth in different regions have been observed in tests with glass/epoxy composites [3.83]. It should be noted that the concept is an idealization and mixed modes of damages usually occur at the junctions of the bands. Also, for high modulus carbon fiber composites, the endurance strain limit of the matrix is close to or higher than the composite static failure strain and in such materials the sloping band region is small or absent. This concept has been illustrated in reference 3.81 with test data for glass fiber reinforced and carbon fiber reinforced epoxy matrix composites. A value of 0.6 percent for the endurance strain limit of epoxy matrix has been used for this purpose. The phenomenological concept just discussed indicates that fiber, matrix, and interface (or interphase) properties have

strong influences on the fatigue performance of different types of composites and these influences are discussed in the following paragraphs.

#### 3.2.6.1.2 Effects of Constituents.

Effects of fiber type as reported in references 3.84 and 3.85 are shown in figures 3.52 and 3.53. In figure 3.52, the maximum stress is normalized to the static strength of the composite so that effect of fatigue on composites with different static strengths can be compared in the same plot. The figure clearly shows the increasing slope of the sloping bands with increasing composite failure strain. It should be noted that S-glass fiber composites have a normalized stress versus log-life curve, which is similar to that of E-glass reinforced materials, but S-glass composites have a much higher static strength as compared to E-glass reinforced materials and retain this superiority up to 10 million cycles [3.82]. Figure 3.53 shows that various carbon fiber composites show very similar fatigue behaviors. Normalized stress versus log-life curve for a crossply E-glass composite is also shown in figure 3.52. The slope of the curve is much higher than that of the unidirectional material because of additional damage development in the  $90^\circ$  plycracks and delaminations, which will be discussed in the next chapter. Figure 3.54 [3.84] compares the slope of the normalized stress log-life curves of various systems with different fiber moduli, which shows that the slope for crossply carbon fiber composites is very close to that of the unidirectional material, since the loads carried by the  $90^\circ$  layers (which are transferred to the  $0^\circ$  layers due to damage in the  $90^\circ$  plies) are very small and do not change the fatigue behavior of  $0^\circ$  layers.

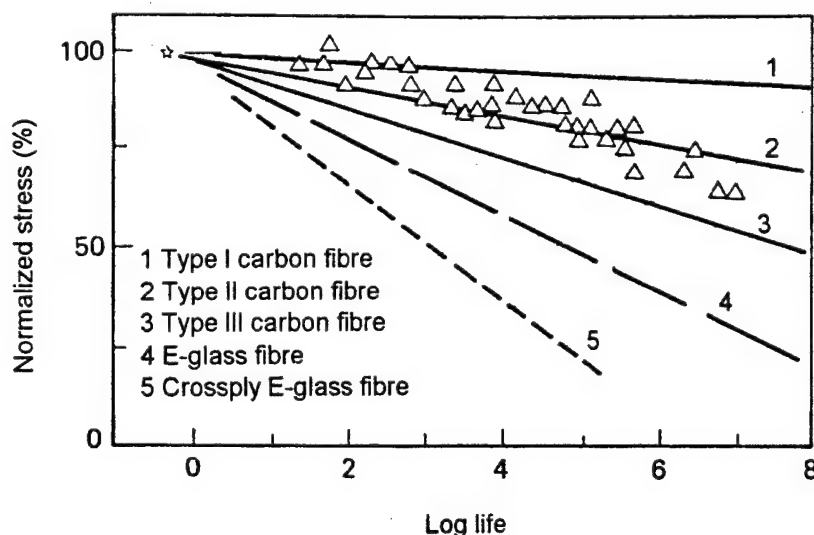


FIGURE 3.52. EFFECTS OF FIBER TYPE ON STRESS VERSUS LOG-LIFE CURVES OF UNIDIRECTIONAL COMPOSITES [3.84]

Effects of matrix material on the fatigue behavior have also been studied by various investigators. Early studies have shown that glass-reinforced epoxy matrix composites show superior fatigue performance as compared to phenolic, polyester, and silicone matrices [3.86]. This superiority may be attributed to the inherent toughness, durability, and compatibility of the epoxy matrix

with glass fibers. More recent studies on E-glass strands and composites with polyester, epoxy, and toughened epoxy matrices [3.86, 3.87, and 3.88] appear to show that fatigue performance of glass fiber composites is fiber dominated; however, their fatigue performance with different matrices may be improved with residual surface compression. Test data for carbon fiber composites with standard and toughened epoxies and thermoplastic matrices such as PEEK and J-Polymer are also reported in literature. Results from different investigators are sometimes contradictory. It appears, however, that use of tough matrices may not always result in improved or comparable fatigue performance of carbon fiber composites as compared to those with epoxy matrices, which are usually not very sensitive to fatigue loading [3.80]. It is likely that fiber/matrix interface conditions play a more dominant role, and new surface treatments of fibers are needed when tough matrix materials are used to obtain improved fatigue response.

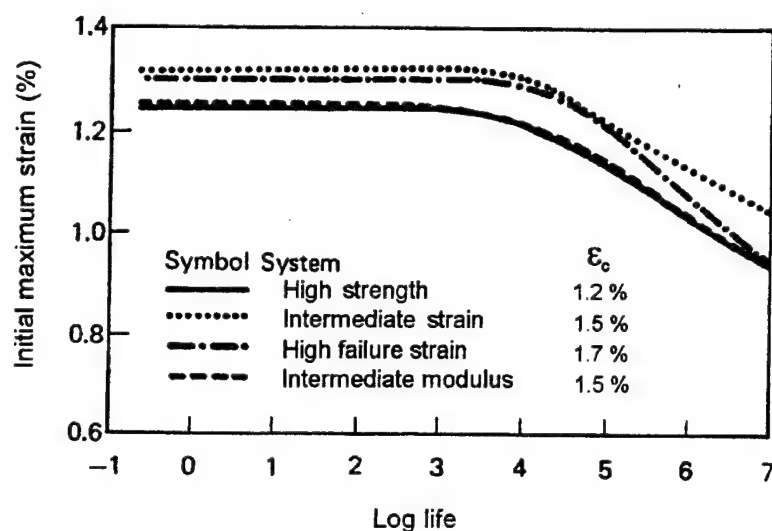


FIGURE 3.53. STRAIN LOG-LIFE CURVES FOR UNIDIRECTIONAL COMPOSITES [3.85]

Effects of fiber surface treatments on flexural fatigue of E-glass/epoxy composites were studied in reference 3.89. Coated fiber composites had a higher static shear strength as compared to those with uncoated fibers and it was concluded that glass fiber composites with a stronger interface will show improved fatigue resistance. This conclusion may be correct for flexural fatigue where transverse shear stresses play a role on damage growth and failure. It is not certain, however, that a strong interface will always improve the axial fatigue performance. Studies on the influence of interphase properties on fatigue of carbon fiber composites [3.90] indicate that a strong interphase results in transverse crack propagation across fibers causing premature composite failure. Whereas a very weak interphase may cause extensive fiber matrix debonding, interphases of intermediate strength may lead to optimum composite performance between the two extreme conditions. A considerable amount of research is being devoted to find how such a condition can be obtained for various types of composites.

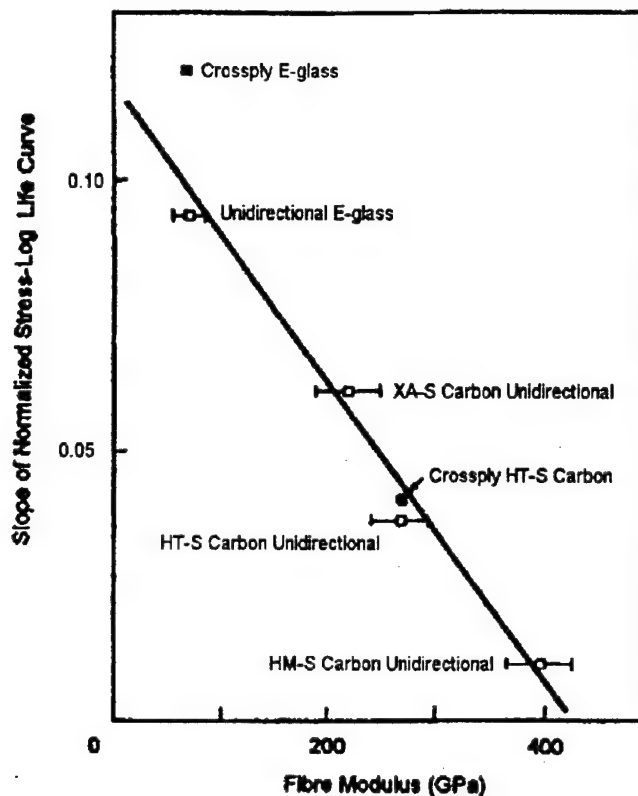


FIGURE 3.54. SLOPES OF NORMALIZED STRESS LOG-LIFE CURVES VERSUS FIBER MODULUS

#### 3.2.6.1.3 Phenomenological Models.

The S-N curves discussed earlier represent the number of cycles for certain constant stress amplitudes after which the material will fail. If load cycling is stopped before failure occurs and the material is loaded statically till failure occurs, the stress to cause failure is called the residual strength. Residual strength usually decreases with load cycling. When residual strength matches the stress amplitude, failure occurs. Various models have been proposed to model residual strength degradation and fatigue life [3.91-3.93]. If Weibull distributions can be used to describe the fatigue strength and fatigue life and they obey "the strength-life equal rank assumption", i.e., a specimen with higher strength has a longer fatigue life, then the degradation of residual strength with load cycling or sequence of loading can be estimated. The model discussed in reference 3.91 predicts that, as assumed in Miner's rule which is discussed later, the residual strength does not depend on the load sequence although the fatigue life is influenced by the sequence of load cycling. In some materials, static strength is maintained almost to final failure by fatigue, and "sudden death" models appear to be better suited for such cases [3.94]. A simple model based on linear fits to the S-N curve and "damage lines" (stress amplitude versus remaining life curves) plotted on a semi-log scale (S versus log N, N being the number of cycles) has been proposed in reference 3.95. In these models, it is assumed that damage development influences the residual strength but the type of damage need not be defined or known. However, such models are often useful for estimating the effects of load sequence (cumulative damage). In other



models, use has been made of various types of damage functions [3.96]. For certain types of composites, stiffness loss is an important parameter and it can be used as a measure of damage [3.97]. Another model, which is based on a more realistic damage pattern, assumes that damage growth rate depends on the statistical distribution of flaws along the fiber length as well as the growth of fiber/matrix debonds. During fatigue cycling, fiber/matrix debonds grow from a fiber fracture site. A length, called the "positively affected length", in adjacent fibers grows with increasing debond length and the probability of failure of these fibers within this length increases. If one of the nearest fibers fails, the result is two fiber fractures joined by a debond. As this process continues, more fibers are broken and the damage zone increases in size. This zone is called the fatal crack, which consists of fiber fractures linked by debonds of various lengths. Based on certain assumptions about the distribution of these debond lengths and the mean debond length, the following results are obtained (the details can be found in reference 3.98), for the residual strength  $\sigma_{rs}$  after  $N$  cycles with maximum stress  $\sigma_{max}$  and the fatigue life  $N_f$

$$\sigma_{rs} = \sigma_{ss} \left[ 1 - \frac{N}{A} \left( \frac{\sigma_{max}}{\sigma_{ss}} \right)^b \right] \quad (3.120)$$

$$N_f = A \left( 1 - \frac{\sigma_{max}}{\sigma_{ss}} \right) \left( \frac{\sigma_{ss}}{\sigma_{max}} \right)^b \quad (3.121)$$

where  $A$  and  $b$  are constants and  $\sigma_{ss}$  is the static tensile strength.

### 3.2.6.2 Combined Cyclic Stress.

As discussed earlier, a lamina in a laminate is subjected to a multiaxial stress state, which may be assumed to be that of plane stress. Phenomenological models have been proposed to model lamina fatigue failure under such conditions. However, usefulness of such models to predict laminate performance is questionable, since damage growth in a lamina in a laminate occurs in a constrained fashion (as in static failure, discussed earlier). A discussion on such models is, however, included here for completeness.

In order to discuss fatigue under combined cyclic stress, it is necessary to introduce the concept of a fatigue failure criterion for such a stress state. This is a generalization of the failure criterion for combined static stress discussed in section 3.2.5. In the general case of three-dimensional cyclic stress, each stress component has a mean component,  $\sigma_{ij}^m$ , and an alternating component,  $\sigma_{ij}^a$ , as in (3.118). In addition, the stress cycles are not necessarily in phase and may have phase lags,  $\lambda_{ij}$ . Suppose that the lifetime,  $N$ , under such stress cycling is defined by the quantities cited. Then the relation among all of these is written as

$$F(\sigma_{ij}^m, \sigma_{ij}^a, \lambda_{ij}, N) = 1 \quad (3.122)$$

Nothing seems to be known about such a general relation.

Even if it is assumed that there are no phase lags (this is the case when the applied cyclic loads are in phase and the material is linear elastic), establishment of a general failure criterion in terms of means and alternating stresses is a formidable problem. The only existing work in the literature seems to be for the case of one stress component and is purely empirical. In this case, it is customary to plot the experimentally obtained pairs of  $\sigma_{ij}^m$  and  $\sigma_{ij}^a$  which lead to the same lifetime. This is called a Goodman diagram and was discussed in the preceding section.

To simplify matters further, it is assumed that all stress components have the same ratio,  $R$ . Thus from (3.118 and 3.119)

$$\begin{aligned} \sigma_{ij}^{\min} / \sigma_{ij}^{\max} &= R \\ \sigma_{ij}^m &= \sigma_{ij}^{\max} (1 + R) \\ \sigma_{ij}^a &= \sigma_{ij}^{\max} (1 - R) \end{aligned} \quad (3.123)$$

Inserting this into (3.122) we obtain

$$F(\sigma_{ij}^{\max}, R, N) = 1 \quad (3.124)$$

The case described occurs in practice when all cyclic loads are in phase and cycle with the same ratio,  $R$ .

Just as in the case of static failure criteria, it is convenient to represent (3.124) as a surface in stress space where in the present case the stress variables are  $\sigma_{ij}^{\max}$  (which will be called simply  $\sigma_{ij}$ ). Suppose that  $R$  has some fixed value. Then (3.124) may be interpreted as a family of surfaces, each of which is associated with a different  $N$  (figure 3.55). Each surface is the locus of all cyclic stress states which produce fatigue after same lifetime  $N$ . This description ignores scatter and, therefore,  $N$  must be interpreted in some mean sense. The static failure criterion is a special case,  $N = 0$ . At the other extremity there are stress states of such low amplitudes that fatigue failure does not occur. This defines the fatigue (or endurance) limit region in figure 3.55, which is a generalization of the usual fatigue (or endurance) limit of an S-N curve. It should be noted that the family of surfaces is for a fixed  $R$ ; a different family will be associated with a different  $R$ .

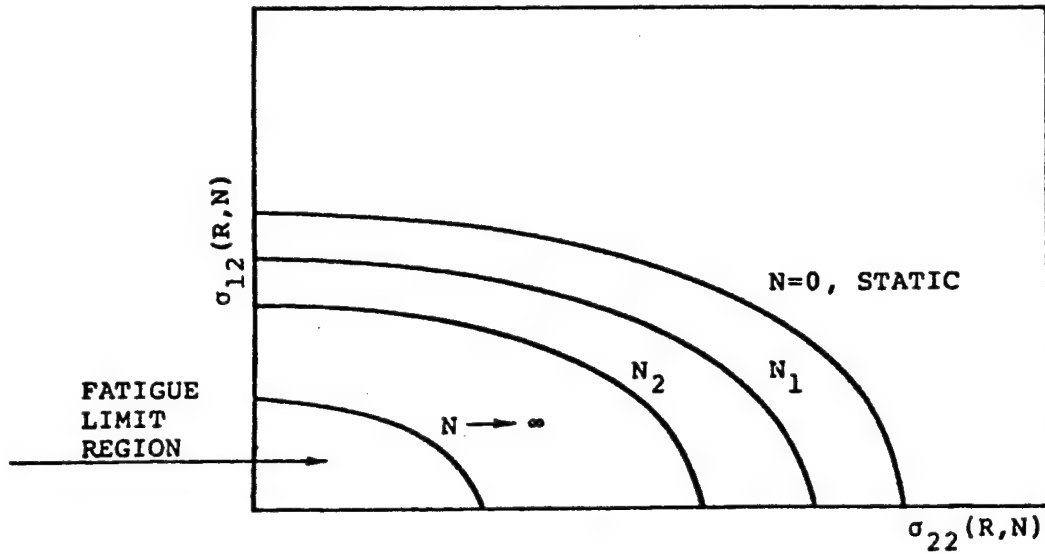


FIGURE 3.55. FATIGUE FAILURE SURFACE FAMILY

As in the static case, the failure surfaces will be described in terms of quadratics in the stress amplitudes  $\sigma_{ij}$ . Since the surfaces vary with  $N$  and  $R$ , the coefficients of the quadratics must also be functions of  $N$  and  $R$ . This approach will be applied to the case of plane cyclic stress. The problem may be posed in the following fashion: For specified  $R$ , the S-N curves are given for cyclic stress in the fiber direction, transverse to the fibers and in shear. What is the S-N curve for the combined state of cyclic stress? This is illustrated in figure 3.56. As in the static case, the approach is to describe fiber and matrix failure modes by different quadratic polynomials. The outcome of this procedure is:

Fiber mode

$$\left[ \frac{\sigma_{11}}{\sigma_L^f(R, N)} \right]^2 + \left[ \frac{\sigma_{12}}{\tau_L^f(R, N)} \right]^2 = 1$$

(3.125)

Matrix mode

$$\left[ \frac{\sigma_{22}}{\sigma_T^f(R, N)} \right]^2 + \left[ \frac{\sigma_{12}}{\tau_L^f(R, N)} \right]^2 = 1$$

where  $\sigma_L^f(R, N)$ ,  $\sigma_T^f(R, N)$ , and  $\tau_L^f(R, N)$ , are the S-N curve stresses in the fiber direction, transverse to the fibers, and in shear, figure 3.56. For details, see references 3.77 and 3.98.

Applications of the model to the failure of unidirectional materials under off-axis loading are also discussed in these works.

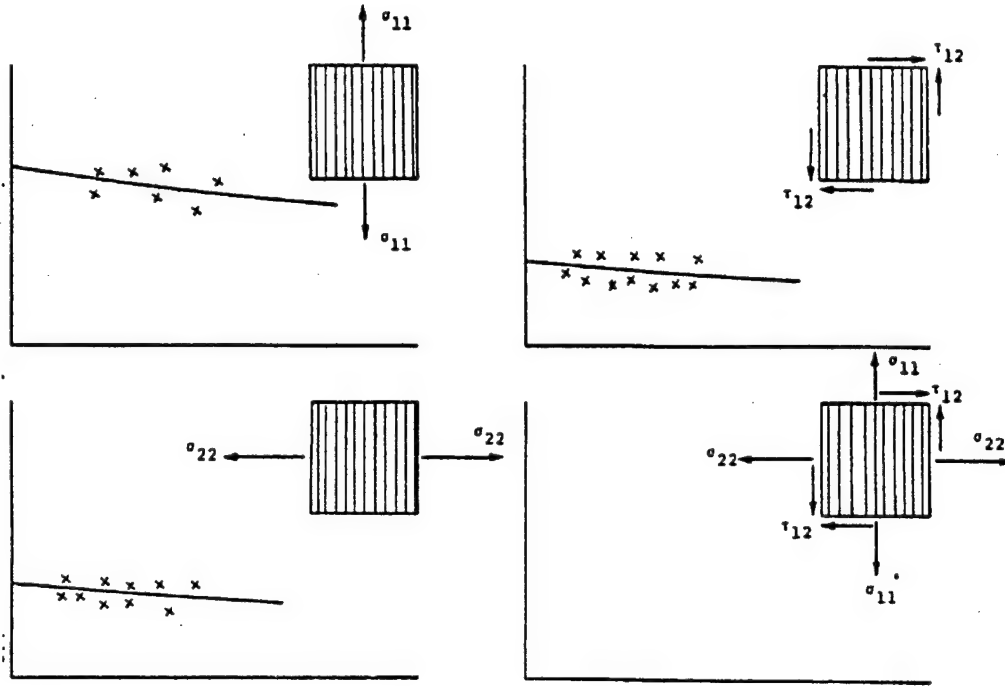


FIGURE 3.56. COMBINED CYCLIC STRESS PROBLEM

Fatigue failure criteria for a general three-dimensional state of cyclic stress (all components with the same  $R$ ) have been given in reference 3.98. These results are

$$\left( \frac{\sigma_{11}}{\sigma_L^f} \right)^2 + \frac{\sigma_{12}^2 + \sigma_{13}^2}{(\tau_L^f)^2} = 1 \quad (3.126)$$

$$\left( \frac{\sigma_{22} + \sigma_{33}}{\sigma_T^f} \right)^2 + \frac{\sigma_{23}^2 - \sigma_{22}\sigma_{33}}{(\tau_T^f)^2} + \frac{\sigma_{12}^2 + \sigma_{13}^2}{(\tau_L^f)^2} = 1$$

where  $\sigma_L^f(R, N)$ ,  $\sigma_T^f(R, N)$ ,  $\tau_L^f(R, N)$ , and  $\tau_T^f(R, N)$  are the S-N curve stresses: normal stress in the fiber direction, normal stress transverse to the fibers, longitudinal shear stress, and transverse shear stress. There is as yet no known method to obtain the last one experimentally, but a reasonable approximation is to assume that it is equal to matrix cyclic shear failure stresses.

The problem of residual strength for combined states of stress does not appear to have received attention in the literature. The subject of residual strength will be addressed more fully in chapter 4.

### 3.2.6.3 Cumulative Damage.

Another central problem of fatigue failure is known as the cumulative damage problem, which has been mentioned in section 3.2.6.4. Most fatigue testing is conducted for the case of constant amplitude cycling resulting in the S-N curve. Constant amplitude cycling, however, only rarely occurs in practice. As an example, consider the wing of an airplane. During takeoff, maneuvering, cruising, and landing, the wing is subjected to very different aerodynamic loads. Variable weather conditions result in gust loads of different intensities. It is thus seen that the loads are significantly variable in time and that the wing is subjected to a program of cyclic loading. The problem that arises is to predict the lifetime of a structural member which is subjected to a cyclic loading program of variable amplitude; e.g., figure 3.57. This has become known as the cumulative damage problem.

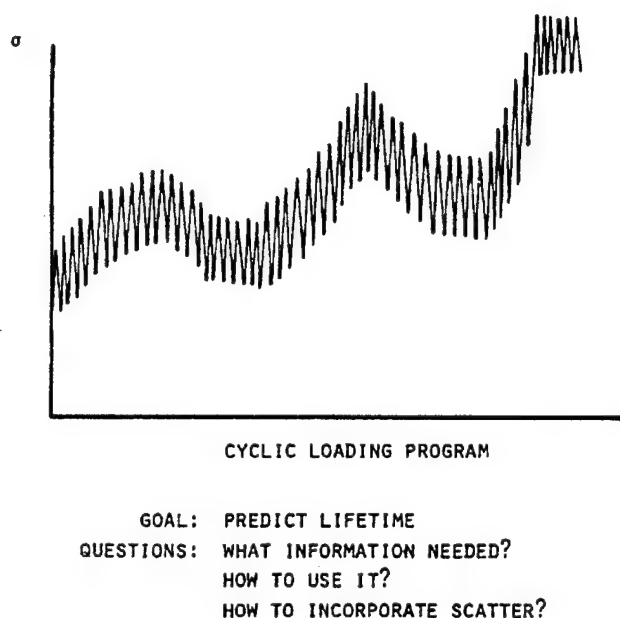


FIGURE 3.57. CUMULATIVE DAMAGE PROBLEM

It should be emphasized that there is little hope to treat the cumulative damage problem on the basis of the microstructure of a UDC since the failure process consisting of damage accumulation and terminating in catastrophic failure is much too complex and unpredictable to be handled by analytical means. At the present time, the only viable approach seems to consist of lifetime prediction under complex cyclic load in terms of lifetime test data for simple cyclic loading; e.g., in terms of the usual S-N curves for specimens. From this point of view, the problem has been the subject of numerous theoretical and experimental investigations in the context of metal fatigue. For a review of this subject, see references 3.79 and 3.99.

The simplest and most well known procedure for lifetime evaluation is an empirical formula which has become known as Miner's Rule or the Palmgren-Miner Rule and will be referred to here as the PM rule. Consider a cyclic loading program where the amplitude varies in jumps from one constant value to another. Let the number of cycles applied at amplitude  $\sigma_i$  be  $n_i$  and

let  $N_i(\sigma_i)$  be the lifetime under constant amplitude cycling as defined by the S-N curve. The PM rule asserts that

$$\sum_i \frac{n_i}{N_i(\sigma_i)} = \frac{n_1}{N_1} + \frac{n_2}{N_2} + \dots = 1 \quad (3.127)$$

This defines the last  $n_i$  which terminates at failure, and thus the total lifetime is

$$L = \sum_i n_i \quad (3.128)$$

The procedure is illustrated in figure 3.58.

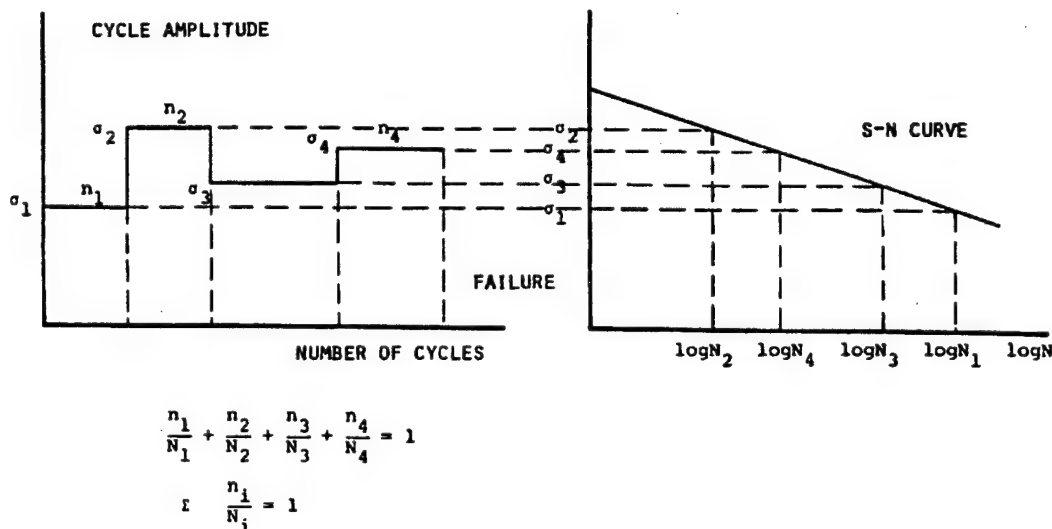


FIGURE 3.58. PALMGREN-MINER RULE

Experience with metal fatigue has shown that the simple PM rule is not reliable. The major problem is that since it is a linear superposition rule, it cannot take into account a sequence of loading effects. For example, if the loading is two stage, i.e., first  $n_1$  cycles at amplitude  $\sigma_1$  and then  $n_2$  cycles to failure at amplitude  $\sigma_2 > \sigma_1$ , then the total lifetime is  $n_1 + n_2$  cycles. If the sequence of loading is reversed and  $\sigma_2$  is first applied for  $n_2$  cycles, then the PM rule would predict the same total lifetime,  $n_1 + n_2$ . Experience with metal fatigue shows, however, that the sequence of loading does significantly affect the lifetime: Generally, the lifetime is larger for low-high than for high-low, two-stage cycling.

Many alternative cumulative damage approaches have been proposed for metals [3.79 and 3.99], generally on an empirical or semiempirical basis. A general cumulative damage theory, based

on the concept of damage curves and an equivalent cyclic loading postulate, has been developed in reference 3.100. A cumulative damage theory based on residual strength degradation has been proposed in reference 3.91. A definitive theory, however, is not available at the present time, either for metals or for composites. Consequently, many engineers still continue to use the simple PM rule in spite of its severe limitations.

Most of the cumulative damage work is concerned with one-component cyclic stress. It is again emphasized that this is not of great interest for UDC since the layers in a laminate are at least in states of plane cyclic stress. It is necessary, therefore, to construct a cumulative damage theory for UDC under combined states of cyclic stress. The theory should also account for the difference between the behavior of an individual layer and that in a laminate. Such a theory is not available at the present time.

#### 3.2.6.4 Concluding Remarks.

The subject of fatigue failure of fiber composites is still under development. It is clear, however, that fatigue failure mechanisms of composites differ significantly from those of metals. Further, the widely used carbon fiber, polymeric composites have demonstrated excellent fatigue characteristics when loaded in the fiber direction. Utilization of these properties will be discussed in chapter 4.

Since damage growth in laminates occurs in a constrained fashion, much of the current research on fatigue of composites is concerned with laminates, rather than unidirectional specimens. In view of the enormous diversity of candidate laminates, theories relating laminate fatigue failure to the behavior of the unidirectional layers are clearly needed, and therefore, the constrained damage growth in the unidirectional material merits some attention. Many interesting and important fatigue studies have been performed. The reader is referred to the chapters on fatigue of composites in the proceedings of the ASTM composite conferences of recent years [3.101 to 3.107].

## REFERENCES

- 3.1. Hashin, Z., Theory of Fiber Reinforced Materials, NASA CR-1974 (1972).
- 3.2. Christensen, R.M. and Lo, K.H., "Solutions for Effective Shear Properties in Three-Phase Sphere and Cylinder Models," J. Mechanics and Physics of Solids Vol. 27 No. 4 (1979).
- 3.3. Hill, R., Theory of Mechanical Properties of Fiber Strengthened Materials, I. Elastic Behavior, J. Mech. Phys. Solids, Vol. 12, pp. 199-212 (1964).
- 3.4. Pickett, G., AFML TR-65-220 (1965) and in Fundamental Aspects of Fiber Reinforced Plastic Composites, Schwartz, R.T. and Schwartz, H.S., Eds., pp. 13-27, Wiley-Interscience (1968).
- 3.5. Adams, D.F., Doner, D.R., and Thomas, R.L., AFML TR-67-96 (1967). Also, J. Composite Mats., Vol. 1, pp. 4-17, pp. 152-165 (1967).
- 3.6. Sendekyj, G.P., Elastic Behavior of Composites, in Mechanics of Composite Materials, Vol. II, Sendekyj, G.P., Ed., Academic Press (1974).
- 3.7. Hashin, Z. and Rosen, B.W., The Elastic Moduli of Fiber Reinforced Materials, J. Appl. Mech., Vol. 31, pp. 223-232 (1964).
- 3.8. Hashin, Z., Analysis of Properties of Fiber Composites with Anisotropic Constituents, J. Appl. Mech., Vol. 46, pp. 543-550 (1979).
- 3.9. Blessing, C.V. and Elban, W.L., Aluminum Matrix Composite Elasticity Measured Ultrasonically, J. Appl Mech., Vol. 48, pp. 965-966 (1981).
- 3.10. Smith, R.E., Ultrasonic Elastic Constants of Carbon Fibers and Their Composites, J. Appl. Phys., Vol. 43, pp. 2555-2561 (1972).
- 3.11. Hill, R., Theory of Mechanical Properties of Fiber Strengthened Materials - III. Self-Consistent Model, J. Mech. Phys. Solids, Vol. 13, pp. 189-198 (1965).
- 3.12. Hermans, J.J., The Elastic Properties of Fiber Reinforced Materials When the Fibers Are Aligned, Proc. Koninklijke Nederlandse Akademik Van Wetenschappen, Series B, Vol. 70, pp. 1-9 (1967).
- 3.13. Ashton, J.E., Halpin, J.C., and Petit, P.H., Primer on Composite Materials, Chap. 5, Technomic (1969).
- 3.14. Hashin, Z., On Elastic Behavior of Fiber Reinforced Materials at Arbitrary Transverse Phase Geometry, J. Mech. Phys. Solids, Vol. 13, pp. 119-134 (1965).



- 3.15. Levin, V.M., On the Coefficients of Thermal Expansion of Heterogeneous Materials, Mekh. Tverd. Tela, Vol. 1, pp. 84-88 (1967) English Translation: Mechanics of Solids, Vol. 1, pp. 58-61 (1967).
- 3.16. Rosen, B.W. and Hashin, Z., Effective Thermal Expansion Coefficients and Specific Heats of Composite Materials, Int. J. Engng. Sci., Vol. 8, pp. 157-173 (1970).
- 3.17. Schapery, R.A., Thermal Expansion Coefficients of Composite Materials Based on Energy Principles, J Composite Mats., Vol. 2, p. 380 (1968).
- 3.18. Rosen, B.W., Thermal Expansion Coefficients of Composite Materials, Ph.D. Dissertation, Univ. of Pennsylvania (1968).
- 3.19. Ishikawa, T., Koyama, K., and Kobayashi, S., Thermal Expansion Coefficients of Unidirectional Composites, J. Composite Mats., Vol. 12, pp. 153-168 (1978).
- 3.20. Springer, G.S., Environmental Effects on Epoxy Matrix Composites, in ASTM STP 674, Tsai, S.W., Ed., pp. 291-311 (1979).
- 3.21. Tsai, S.W. and Hahn, H.T., Introduction to Composite Materials, Technomic (1980).
- 3.22. Christensen, R.M., Theory of Viscoelasticity, Academic Press (1971).
- 3.23. Hashin, Z., Viscoelastic Behavior of Heterogeneous Media, J. Appl. Mech., Vol. 32, pp. 630-636 (1965).
- 3.24. Hashin, Z., Viscoelastic Fiber Reinforced Materials, AIAA J., Vol. 4 pp. 1411-1417 (1966).
- 3.25. Schapery, R.A., Stress Analysis of Viscoelastic Composite Materials, J. Composite Mats., Vol. 1, pp. 228-267 (1967).
- 3.26. Schapery, R.A., Viscoelastic Behavior of Composites, in Mechanics of Composite Materials, Vol. II, Sendeckyi, G.P., Ed., Academic Press 1974.
- 3.27. Hashin, Z., Complex Moduli of Viscoelastic Composites I. General Theory and Application to Particulate Composites. II Fiber Reinforcement Materials, Int. J. Solids Structures, Vol. 6, pp. 539-552; pp. 797-807 (1970).
- 3.28. Chatterjee, S.N., Adams, D., and Oplinger, D., Test Methods for Composites - A Status Report, Volumes I, II, III, DOT/FAA/CT-93/17, June 1993.
- 3.29. Standard Test Method for Tensile Properties of Glass Fiber Strands, Yarns, and Rovings Used in Reinforced Plastics, ASTM D2343.
- 3.30. Weibull, W., A Statistical Distribution Function of Wide Applicability, Journal of Applied Mechanics, Vol. 18, pp. 293-296 (1951).

- 3.31. Gucer, D.E. and Garland, J., Comparison of the Statistics of Two Fracture Modes, J. Mech. Phys. Solids, pp. 365-373 (1962).
- 3.32. Zweben, C., Tensile Failure Analysis of Fibrous Composites, AIAA J., Vol. 6, pp. 2325- 2331 (1968).
- 3.33. Rosen, B.W., Tensile Failure of Fibrous Composites, AIAA J., Vol. 2, pp. 1982-1991 (1964).
- 3.34. Coleman, B.D., On the Strength of Classical Fibers and Fiber Bundles, J. Mech. Phys. Solids, Vol. 7, pp. 60-70 (1958).
- 3.35. Cox, H.L., The Elasticity and Strength of Paper and Other Fibrous Materials, British J. Appl. Phys. (1951).
- 3.36. Dow, N.F., Study of Stresses Near A Discontinuity In a Filament-Reinforced Composite Material, General Elec. Co. Space Sciences Lab., TIS R63D61, August 1963.
- 3.37. Flom, D.B., Mazzio, V.F., and Friedman, E., Whisker Reinforced Resin Composites, Air Force Report, AFML TR-66-362 (1967).
- 3.38. Hedgepeth, J.M. and Van Dyke, P., Local Stress Concentrations in Imperfect Filamentary Composite Materials, J. Composite Mats., Vol. 1, pp. 294-309 (1967).
- 3.39. Van Dyke, P. and Hedgepeth, J.M., Stress Concentrations from Single-Filament Failures in Composite Materials, Textile Research, Vol. 39, pp. 618-626 (1969).
- 3.40. Fichter, W.B., Stress Concentration Around Broken Filaments in a Filament-Stiffened Sheet, NASA TN D-5453 (1969).
- 3.41. Hedgepeth, J.M., Stress Concentrations in Filamentary Structures, NASA TN D-882, May 1961.
- 3.42. Zender, G.W. and Denton, J.W., Strength of Filamentary Sheets with One or More Fibers Broken, NASA TN D-1619 (1963).
- 3.43. Rosen, B.W. and Zweben, C.H., Tensile Failure Criteria for Fiber Composite Materials, NASA CR-2057, August 1972.
- 3.44. Zweben, C. and Rosen, B.W., A Statistical Theory of Material Strength with Application to Composite Materials, J. Mech. Phys. Solids, Vol. 18, pp. 180-206 (1970).
- 3.45. Zweben, C., A Bounding Approach to the Strength of Composite Materials, Eng. Frac. Mech., Vol. 4, pp. 1-8 (1972).

- 3.46. Harlow, D.G. and Phoenix, S.L., The Chain of Bundles Probability Model for the Strength of Fibrous Materials. I. Analysis and Conjectures. II. A Numerical Study of Convergence, J. Composites Mats., Vol. 12, pp. 195-214, pp. 300-313 (1978).
- 3.47. Smith, R.L., Phoenix, S.L., Greenfield, M.R., Henstenburg, R.L., and Pohs, R.L., Lower Tail Approximations for the Probability of Failure of Three-Dimensional Fibrous Composites with Hexagonal Geometry, Proc. Royal Soc., London, A388 (1983).
- 3.48. Batdorf, S.B., Fracture Statistics of Brittle Materials with Intergranular Cracks, Third International Conference on Structural Mechanics in Reactor Technology, London, September 1975.
- 3.49. Dow, N.F. and Fruntfest, I.J., Determination of Most Needed Potentially Possible Improvements in Materials for Ballistic and Space Vehicles, GE-TIS 60SD389, June 1960.
- 3.50. Rosen B.W., Strength of Uniaxial Fibrous Composites, in Mechanics of Composite Materials, Pergamon Press (1970).
- 3.51. Rosen, B.W., Mechanics of Composite Strengthening, in Fiber Composite Materials, Am. Soc. for Metals, Metals Park, Ohio (1965).
- 3.52. Schuerch, H., Prediction of Compressive Strength in Uniaxial Boron Fiber-Metal Matrix Composite Materials, AIAA J., Vol. 4 (1966).
- 3.53. Davis, J.G., Jr., Compressive Strength of Fiber Reinforced Composite Materials, ASTM STP 580, p. 364 (1974).
- 3.54. Caiazzo, A.A., Sullivan, B.J., and Rosen, B.W., Analysis of Micromechanical and Microstructural Effects on Compression Behavior of Unidirectional Composites, J. Reinforced Plastics and Composites, V. 12, pp. 457-469 (1993).
- 3.55. Chatterjee, S.N. and McLaughlin, P.V., Inelastic Shear Instability in Composite Materials Under Compression, in Proc. Third Engineering Mechanics Division Specialty Conference, ASCE, Austin, TX, pp. 649-652, September 17-19, 1979.
- 3.56. Hahn, H.T. and Williams, J.G., Compressive Failure Mechanisms in Unidirectional Composites, ASTM STP 893, p. 115 (1986).
- 3.57. Camponeschi, E.T., Jr., Gillespie, J.W., Jr., and Wilkins, D.J., Kink-Band Failure Analysis of Thick Composites in Compression, J. Composite Mats., Vol. 27, pp. 471-490 (1993).
- 3.58. Argon, A.S., Fracture of Composites, in Treatise of Materials Science and Technology, Vol. 1, Academic Press, New York (1972).
- 3.59. Budiansky, B., Micromechanics, Computers and Structures, Vol. 16, pp. 3-12 (1983).

- 3.60. Jelf, P.M. and Fleck, N.A., Compression Failure Mechanisms in Unidirectional Composites, J. Composite Mats., Vol. 26, pp. 2706-2726 (1992).
- 3.61. Yurgatis, S.W., Measurement of Small Angle Fiber Misalignments in Continuous Fiber Composites, Composites Sci. & Tech., Vol. 30, pp. 279-293 (1987).
- 3.62. Kulkarni, S.V., Rice, J.S., and Rosen, B.W., An Investigation of the Compressive Strength of Kevlar 49/Epoxy Composites, Composites, Vol. 6, pp. 217-225 (1975).
- 3.63. Broutman, L.J., Glass-Resin Joint Strengths and Their Effect on Failure Mechanisms in Reinforced Plastics, Modern Plast., April 1965.
- 3.64. Greszczuk, L.B., Theoretical and Experimental Studies on Properties and Behavior of Filamentary Composites, Society of Plastics Industry, 21st Annual Conference, Washington, DC (1966).
- 3.65. Nielson, L.E., Mechanical Properties of Polymers and Composites, Vol. 2, Marcel Dekker, New York, p. 407 (1974).
- 3.66. Collings, T.A., Transverse Compressive Behavior of Unidirectional Carbon Fiber Reinforced Plastics, Composites, Vol. 5, p. 108 (1974).
- 3.67. Shu, L.S. and Rosen, B.W., Strength of Fiber Reinforced Composites by Limit Analysis Method, J. Composite Mats., Vol. 1, p. 366 (1967).
- 3.68. Tsai, S.W., Strength Characteristics of Composite Materials, NASA CR-224 (1965).
- 3.69. Ashkenazi, E.K., Zavod. Lab., Vol. 30, pp. 285-287 (1964), Mekh. Polim, Vol. 1, pp. 60-70 (1965).
- 3.70. Tsai, S.W. and Wu, E.M., A General Theory of Strength for Anisotropic Materials, J. Composite Mats., Vol. 5, p. 58 (1971).
- 3.71. Wu, E.M., Phenomenological Anisotropic Failure Criterion, in Mechanics of Composite Materials, Sendeckyi, G.P., Ed., Academic Press (1974).
- 3.72. Sun, C.T., Quinn, B., Tao, J., and Oplinger, D.W., "Comparative Evaluation of Failure Analysis Methods for Composite Laminates," FAA Technical Report DOT/FAA/AR-95/109 (1996)
- 3.73. Norris, C.B., Strength of Orthotropic Materials Subject to Combined Stresses, Report No. 1816, U.S. Forest Products Laboratory, Madison, WI, May 1962.
- 3.74. Hart-Smith, L.J., Some Observations on the Analysis of In-Plane Matrix Failures in Fibrous Composite Laminates, ASTM STP 1156, pp. 363-380 (1993).

- 3.75. Hashin, Z., Failure Criteria for Unidirectional Fiber Composites, J. Appl. Mech., Vol. 47, pp. 329-334 (1980).
- 3.76. Tsai, S.W., Strength Theories of Filamentary Structures, in Fundamental Aspects of Fiber Reinforced Plastic Composites, Schwartz, R.T. and Schwartz H.S., Eds., Wiley-Interscience (1968).
- 3.77. Hashin, Z. and Rotem, A., A Fatigue Failure Criterion for Fiber Reinforced Materials, J. Composite Mats., Vol. 7, p. 444 (1973).
- 3.78. Pellini, W.S., Principles of Structural Integrity Technology, ONR, Arlington, VA (1976).
- 3.79. Frost, N.E., Marsh, K.J., and Pook, L.P., Metal Fatigue, Oxford University Press (1974).
- 3.80. Konur, O. and Mathews, F.L., Effect of the Properties of the Constituents on the Fatigue Performance of Composites: A Review, Composites, Vol. 20, pp. 317-328 (1989).
- 3.81. Talreja, R., Fatigue of Composite Materials and Fatigue-Life Diagrams, Proc. Royal Soc. London, A378, pp. 461-475 (1981).
- 3.82. Boller, K.H., Fatigue Fundamentals for Composite Materials, ASTM STP 460, pp. 217-235 (1969).
- 3.83. Dharan, C.K.H., Fatigue Failure in Glass Fiber Polymer Matrix Composites, J. Mater. Sci., Vol. 10, pp. 1665-1670 (1975).
- 3.84. Jones, C.J., Dickson, R.F., Adam, T., Reiter, H., and Harris, B., The Environmental Fatigue Behavior of Reinforced Plastics, Proc. Royal Soc. London, A369, pp. 315-338 (1984).
- 3.85. Curtis, P., An Investigation of Tensile Fatigue Behavior of Carbon Fiber Composite Laminates, ICCM6 Proceedings, Imperial College of Science and Technology, London, Elsevier Applied Science Publishers, Vol. 4, pp. 54-64 (1987).
- 3.86. Boller, K.H., Fatigue Characteristics of Reinforced Plastic Laminates Subjected to Axial Loading, Mod. Plast., Vol. 41, p. 145 (1964).
- 3.87. Mandel, J.F., Huang, D.D., and McGary, F.J., Tensile Fatigue Performance of Glass Fiber Dominated Composites, Comp. Tech. Rev., Vol. 3, pp. 96-102 (1981).
- 3.88. Mandel, J.F., McGary, F.J., Hsiah, A.J.Y., and Li, C.G., Tensile Fatigue of Glass Fibers and Composites with Conventional and Surface Compressed Fibers, Polym. Comp., Vol. 6, pp. 168-174 (1985).

- 3.89. Shih, G.C. and Elbert, L.J., Effect of Interface on Fatigue Performance of Unidirectional Fiberglass Reinforced Composites, Comp. Sci. Tech., Vol. 28, pp. 137-161 (1987).
- 3.90. Drazl, L.T. and Rich, M.J., Effect of Graphite Fiber/Epoxy Adhesion on Composite Fracture Behavior, ASTM STP 864, pp. 16-26 (1985).
- 3.91. Yang, J.N. and Jones, D.L., Load Sequence Effects on the Fatigue of Unnotched Composite Materials, ASTM STP 723, pp. 213-232 (1981).
- 3.92. Hahn, H.T. and Hwang, D.G., Fatigue Characterization of a Graphite/Epoxy Laminate Through Proof Testing, ASTM STP 787, pp. 247-273 (1982).
- 3.93. Chou, P.C. and Croman, R., Residual Strength in Fatigue Based on the Strength-Life Equal Rank Assumption, J. Composite Mats., Vol. 12, pp. 177-194 (1978).
- 3.94. Rotem, A., Fatigue and Residual Strength of Composite Laminates, Eng. Fracture Mech., Vol. 25, pp. 819-827 (1986).
- 3.95. Hwang, W. and Han, K.S., Cumulative Damage Models and Multistress Fatigue Life Prediction, J. Composite Mats., Vol. 20, pp. 125-153 (1986).
- 3.96. Hwang, W. and Han, K.S., Fatigue of Composites - Fatigue Modulus Concept and Life Prediction, J. Composite Mats., Vol. 20, pp. 154-165 (1986).
- 3.97. Ogin, S.L., A Model for the Fatigue Life and Residual Strength of Unidirectional and Crossply Composites; Which Fail by "Wearout," Paper No. 15, The Plastics and Rubber Institute, Third International Conference on Fiber Reinforced Composites, Liverpool, U.K., March 23-25 1988.
- 3.98. Hashin, Z., Fatigue Failure Criteria for Unidirectional Fiber Composites, J. Appl. Mech., Vol. 48, pp. 846-852 (1981).
- 3.99. Leve, H. L., Cumulative Damage Theories, in Metal Fatigue: Theory and Design, Madayag, A.F., Ed., Wiley (1969).
- 3.100. Hashin, Z. and Rotem, A., A Cumulative Damage Theory of Fatigue Failure, Mats. Sci. Engng., Vol. 34, pp. 147-160 (1978).
- 3.101. Composite Materials: Testing and Design, (Second Conference), STP 497, ASTM (1971).
- 3.102. Composite Materials: Testing and Design, (Third Conference), STP 546, ASTM (1974).
- 3.103. Fatigue of Composite Materials, STP 569, ASTM (1975).
- 3.104. Composite Materials: Testing and Design, (Fourth Conference), STP 617, ASTM (1977).

- 3.105. Fatigue of Filamentary Composite Materials. STP 636. ASTM (1977).
- 3.106. Composite Materials: Testing and Design, (Fifth Conference), STP 674, ASTM (1979).
- 3.107. Fatigue of Fibrous Composite Materials, STP 723, ASTM (1981).
- 3.108. Whitney, J.M. and Riley, M.B., Elastic Properties of Fiber-Reinforced Composite Materials, AIAA J., Vol. 4, p. 1537 (1966).
- 3.109. Tsai, S.W., Structural Behavior of Composite Materials, NASA CR-71 (1964).
- 3.110. Kibler, K.G. and Carter, H.G., Viscoelastic Parameters of Measurements, ASTM STP 674, Tsai, S.W., Ed., pp. 282-288 (1979).

## APPENDIX TO CHAPTER 3—GENERAL BOUNDS FOR EFFECTIVE ELASTIC MODULI

The effective elastic moduli depend in principle on the details of the internal geometry of the composite. Since such details are never known in practice, there are two avenues of approach: the first is to analyze a model that is known in detail, which has been discussed in section 3.1.1; the second is to construct upper and lower bounds on the effective properties in terms of partial information. The most rudimentary items of geometrical information are the volume fractions of the constituents and macrotransverse isotropy of the material. Bounds in terms of such information have been established for UDC in references 3.3 and 3.14. The approach is to define the effective elastic constants by strain energy expressions utilizing stresses and strains separately. (This definition is equivalent to defining elastic constants as ratios of average stresses to average strains.) Then extremum principles are employed to bound the strain energy and thereby bound the elastic moduli. Since the treatment is quite involved, only final results will be given here. Let the matrix material be denoted 1 and the fiber material 2. Upper and lower bounds are identified by subscripts (+) and (−), respectively. Then, for isotropic matrix and fibers

$$v_L^*(\pm) = v_1 v_1 + v_2 v_2 + \frac{(v_2 - v_1) (1/k_1 - 1/k_2) v_1 v_2}{v_1/k_2 + v_2/k_1 + 1/G_1} \quad (\text{A3.1})$$

$$v_L^*(\mp) = v_1 v_1 + v_2 v_2 + \frac{(v_2 - v_1) (1/k_2 - 1/k_1) v_1 v_2}{v_1/k_2 + v_2/k_1 + 1/G_2} \quad (\text{A3.2})$$

The upper subscript signs in the left of (A3.1) and (A3.2) apply when

$$(v_1 - v_2) (k_1 - k_2) > 0$$

and the lower subscript signs apply when

$$(v_1 - v_2) (k_1 - k_2) < 0$$

The first case usually applies for a polymer UDC since the matrix Poisson's ratio is larger than that of fiber, and the matrix  $k$  is smaller than that of fiber. Bounds for the other moduli follow:

$$k_{(-)}^* = k_1 + \frac{v_2}{1/(k_2 - k_1) + v_1/(k_1 + G_1)} \quad (\text{A3.3})$$

$$k_{(+)}^* = k_2 + \frac{v_1}{1/(k_1 - k_2) + v_2/(k_2 + G_2)}$$



$$G_{T(-)}^* = G_1 + \frac{v_2}{1/(G_2 - G_1) + v_1(k_1 + 2G_1)/2G_1(k_1 + G_1)} \quad (A3.4)$$

$$G_{T(+)}^* = G_2 + \frac{v_1}{1/(G_1 - G_2) + v_2(k_2 + 2G_2)/2G_2(k_2 + G_2)}$$

$$G_{L(-)}^* = G_1 + \frac{v_2}{1/(G_2 - G_1) + v_1/2G_1} \quad (A3.5)$$

$$G_{L(+)}^* = G_2 + \frac{v_1}{1/(G_1 - G_2) + v_2/2G_2}$$

The above results apply to isotropic fibers. When the fibers are transversely isotropic (carbon and graphite), the bound modification is given by the modifications given in (3.20). Bounds (A3.1-A3.3) have been derived in reference 3.3 and bounds (A3.5) in reference 3.14. The modification to transversely isotropic fibers has been given in references 3.1 and 3.8. It should be emphasized that the bounds are valid for statistically transversely isotropic materials of arbitrary fiber distribution.

Bounds for  $E_T^*$  are given in terms of the above bounds by

$$\frac{4}{E_{T(-)}^*} = \frac{1}{G_{T(-)}^*} + \frac{1}{k_{(-)}^*} + \frac{4v_{L(+)}^{*2}}{E_L^*} \quad (A3.6)$$

$$\frac{4}{E_{T(+)}^*} = \frac{1}{G_{T(+)}^*} + \frac{1}{k_{(+)}^*} + \frac{4v_{L(-)}^{*2}}{E_L^*}$$

where

$$E_L^* = E_1 v_1 + E_2 v_2 \quad (A3.7)$$

It is of interest to note that all bounds except for (A3.4) are composite cylinder assemblage solutions. For details see references 3.1 and 3.8. Note that (3.19) is the equivalent of the lower bound (A3.4).

The bounds (A3.1) and (A3.2) are extremely close for all UDC and are for all practical purposes both equal to the volume average. The bounds (A3.6) are not particularly close for glass/polymer or boron/polymer UDC but their modifications for transversely isotropic fibers are extremely close for carbon/polymer and graphite/polymer UDC. The reason is that the moduli  $k$ ,  $G_{Tf}$ , and  $G_{Lf}$  of these fibers are much lower in relation to polymer modulus than are the  $k_f$  and  $G_f$  of glass

and boron fibers. Table A3.1 lists the bounds for T50/epoxy. It is seen that the bounds are so close that they actually yield the correct results.

TABLE A3.1. BOUNDS FOR ELASTIC PROPERTIES OF GRAPHITE EPOXY,  
ARBITRARY TRANSVERSE PHASE GEOMETRY

Epoxy Matrix	Graphite Fibers	
$E = 500$	$E_L = 50,000$	$G_L = 300$
$G = 185$	$E_T = 1400$	$\nu_L = 0.20$ (Moduli in ksi)
$k = 612$	$G_T = 540$	$\nu_T = 0.30$
$\nu = 0.35$	$k = 1000$	

$\nu$	$E_L^*$ ksi	$\nu_{A(-)}^*$	$\nu_{A(+)}^*$	$k_{(-)}^*$ ksi	$k_{(+)}^*$ ksi	$G_{T(-)}^*$ ksi	$G_{T(+)}^*$ ksi	$E_{T(-)}^*$ ksi	$E_{T(+)}^*$ ksi	$\nu_{T(-)}^*$	$\nu_{T(+)}^*$	$G_{L(-)}^*$ ksi	$G_{L(+)}^*$ ksi
0	500	0.35	0.35	612	612	185	185	500	500	0.35	0.35	185	185
0.20	10400	0.315	0.318	671	679	222	228	663	679	0.484	0.497	203	204
0.40	20300	0.283	0.287	734	745	268	281	783	813	0.443	0.466	223	225
0.60	30200	0.253	0.257	811	821	331	347	937	971	0.398	0.423	246	248
0.80	40100	0.226	0.228	898	903	415	431	1132	1164	0.350	0.369	272	272
1.00	50000	0.20	0.20	1000	1000	540	540	1400	1400	0.30	0.30	300	300

## CHAPTER 4. LAMINATES

*Where order in variety we see  
And where, through all things differ, all agree.*

Alexander Pope  
Windsor Castle

The properties of unidirectional composites described in the previous chapter have been shown to be decidedly different from those of conventional metallic materials. The primary difference from an analytical viewpoint results from the material anisotropy. These materials typically have exceptional properties in the direction of the reinforcing fibers while properties perpendicular (transverse) to the fibers are poor to mediocre. Thus, with the exception of one-dimensionally loaded members (e.g., truss members), unidirectional composites would be expected to perform poorly with respect to conventional materials. The problem then is how to best utilize the exceptional fiber directional properties while minimizing the effects of the low transverse properties. One obvious solution is to utilize the approach taken in the manufacture of plywood.

Plywood, as is well known, is made up of layers or plies of wood bonded together with the wood grain in each ply oriented perpendicularly to the adjacent plies. By orienting the plies of wood in this way, the lesser properties of the wood perpendicular to the grain are augmented by the superior properties in the direction of the wood grain. At the same time, however, the superior properties in the grain direction cannot be fully utilized due to the presence of the perpendicular plies.

This bonding together of individual plies is used with unidirectional composites to form laminates. The plies or laminae are oriented such that the effective properties of the laminate match the loading environment. Lamination theory is used to tailor the laminate effective material properties to correspond to performance requirements.

Lamination theory can be considered a form of structural analysis. Here, however the structural material is being designed. This adds another level of effort to the design process but at the same time allows the structural material to be tailored to match the loadings. Thus, if a 2:1 biaxial loading environment is prescribed, the structural laminate used can be designed for a 2:1 strength. In this fashion, the amount of material is minimized in a way which is not possible with conventional materials.

This chapter starts with a treatment of the stress-strain relations of the unidirectional fiber composite in the form appropriate for analysis of thin plies of the material. In the following section the analysis is developed for an assemblage of plies, i.e., a laminate. The stress-strain relations for a thin laminated plate are developed for the case of plate membrane forces and bending moments.

For purposes of structural analysis, it is desirable to represent a laminate by a set of effective stiffnesses, just as a homogeneous plate is defined by its extensional and bending stiffnesses.

The calculation of these laminate mechanical properties is defined and illustrated in section 4.4. Also in that section, the analysis is expanded to include treatment of laminate expansion resulting from temperature and moisture changes.

Section 4.5 addresses the calculation of temperature and moisture distributions through the thickness of a laminate. With this information, and the definition of applied loads or deformations, the stresses in each ply can be calculated. Procedures for doing this are presented and illustrated in section 4.6.

Up to this point, the chapter deals with what may be classified as the elastic response of the laminate to external load and environment. The remaining sections address laminate failure resulting from static, cyclic, and impact loading conditions, respectively.

#### 4.1 TERMINOLOGY.

Lamination theory, as with all technical endeavors, involves a certain amount of specialized terminology or nomenclature. In order that the reader of this text not be confused by the use of this terminology, some of the more frequently used terms are described in the Glossary of Terms and Acronyms.

#### 4.2 LAMINA STRESS-STRAIN RELATIONS.

A laminate is composed of unidirectionally reinforced laminae oriented in various directions. Each lamina is the type of UDC discussed in chapter 3. Therefore, the elastic stress-strain relations of the lamina are described by equation 3.6. These stress-strain relations will be written here in matrix form using a different notation for elastic properties. With  $x_1$  in the fiber direction,  $x_2$  transverse to the fibers in the plane of the lamina, and  $x_3$  normal to the plane of the lamina (see figure 3.2), the material properties define the lamina properties as follows:

$$\begin{aligned} E_1 &= E_L^* & \nu_{12} &= \nu_L^* \\ E_2 &= E_3 = E_T^* & \nu_{23} &= \nu_T^* \\ G_{12} &= G_L^* & G_{23} &= G_T^* \end{aligned} \quad (4.1)$$

Furthermore, the laminae, at this point, are treated as effective homogeneous transversely isotropic materials and the strains are written without overbars. Thus:

$$\begin{Bmatrix} \epsilon_{11} \\ \epsilon_{22} \\ \epsilon_{33} \\ 2\epsilon_{23} \\ 2\epsilon_{13} \\ 2\epsilon_{12} \end{Bmatrix} = \begin{bmatrix} 1/E_1 & -\nu_{12}/E_1 & -\nu_{13}/E_1 & 0 & 0 & 0 \\ -\nu_{12}/E_1 & 1/E_2 & -\nu_{23}/E_2 & 0 & 0 & 0 \\ -\nu_{13}/E_1 & -\nu_{23}/E_2 & 1/E_3 & 0 & 0 & 0 \\ 0 & 0 & 0 & 1/G_{23} & 0 & 0 \\ 0 & 0 & 0 & 0 & 1/G_{13} & 0 \\ 0 & 0 & 0 & 0 & 0 & 1/G_{12} \end{bmatrix} \begin{Bmatrix} \sigma_{11} \\ \sigma_{22} \\ \sigma_{33} \\ \sigma_{23} \\ \sigma_{13} \\ \sigma_{12} \end{Bmatrix} \quad (4.2)$$

where account has been taken of the symmetry relations

$$\frac{\nu_{21}}{E_2} = \frac{\nu_{12}}{E_1} = \frac{\nu_{31}}{E_3} = \frac{\nu_{13}}{E_1} \quad \frac{\nu_{23}}{E_2} = \frac{\nu_{32}}{E_3}$$

The literature on laminates frequently considers the case of orthotropic laminae, which involve nine elastic properties instead of the present five of the transversely isotropic material. In the orthotropic case the stress-strain relations (4.2) are replaced by

$$\begin{Bmatrix} \epsilon_{11} \\ \epsilon_{22} \\ \epsilon_{33} \\ 2\epsilon_{23} \\ 2\epsilon_{13} \\ 2\epsilon_{12} \end{Bmatrix} = \begin{bmatrix} 1/E_1 & -\nu_{12}/E_1 & -\nu_{13}/E_1 & 0 & 0 & 0 \\ -\nu_{12}/E_1 & 1/E_2 & -\nu_{23}/E_2 & 0 & 0 & 0 \\ -\nu_{13}/E_1 & -\nu_{23}/E_2 & 1/E_3 & 0 & 0 & 0 \\ 0 & 0 & 0 & 1/G_{23} & 0 & 0 \\ 0 & 0 & 0 & 0 & 1/G_{13} & 0 \\ 0 & 0 & 0 & 0 & 0 & 1/G_{12} \end{bmatrix} \begin{Bmatrix} \sigma_{11} \\ \sigma_{22} \\ \sigma_{33} \\ \sigma_{23} \\ \sigma_{13} \\ \sigma_{12} \end{Bmatrix} \quad (4.3)$$

The orthotropic case is of limited practical interest. It has been used in the case of boron fiber reinforced laminae, which typically contain only a few fibers, or even only one fiber, through the thickness. Such a lamina is not a composite material in the sense described in chapter 3, which requires the concept of representative volume elements containing a multitude of fibers.

It has been common practice in the analysis of laminates to utilize engineering shear strains ( $u_{,y} + v_{,x}$ ) rather than tensor shear strains  $(u_{,y} + v_{,x})/2$ . Thus, the factor of 2 has been introduced into the stress-strain relations of (4.2) and (4.3). The relationship between tensor and engineering shear strains is

$$\begin{Bmatrix} 2\epsilon_{23} \\ 2\epsilon_{13} \\ 2\epsilon_{12} \end{Bmatrix} = \begin{Bmatrix} \gamma_{23} \\ \gamma_{13} \\ \gamma_{12} \end{Bmatrix}$$

The most important state of stress in a lamina is plane, i.e.,

$$\sigma_{13} = \sigma_{23} = \sigma_{33} = 0 \quad (4.4)$$

since it occurs for both in-plane loading and bending at sufficient distance from the laminate edges. In this case (4.2) reduces to

$$\begin{Bmatrix} \epsilon_{11} \\ \epsilon_{22} \\ 2\epsilon_{12} \end{Bmatrix} = \begin{bmatrix} 1/E_1 & -\nu_{12}/E_1 & 0 \\ -\nu_{12}/E_1 & 1/E_2 & 0 \\ 0 & 0 & 1/G_{12} \end{bmatrix} \begin{Bmatrix} \sigma_{11} \\ \sigma_{22} \\ \sigma_{12} \end{Bmatrix} \quad (4.5)$$

which may be written as

$$\{\epsilon_\ell\} = [S] \{\sigma_\ell\}$$

Here (S), the compliance matrix, relates the stress and strain components in the principal material directions. These are called lamina coordinates and are denoted in the condensed notation by the subscript  $\ell$ . These equations are equivalent to equations in chapter 3, section 3.24.

The three parts of (4.5) relate the in-plane strain components to the three in-plane stress components. For this plane stress state, the three additional strains can be found to be

$$\epsilon_{23} = \epsilon_{13} = 0$$

$$\epsilon_{33} = -\sigma_{11} \frac{\nu_{13}}{E_1} - \sigma_{22} \frac{\nu_{23}}{E_2}$$

and thus the complete state of stress and strain is determined.

The relations (4.5) can be inverted to yield

$$\{\sigma_i\} = [S]^{-1} \{\epsilon_i\}$$

or

(4.6)

$$\{\sigma_i\} = [Q] \{\epsilon_i\}$$

The matrix (Q) is defined as the inverse of the compliance matrix and is known as the reduced lamina stiffness matrix. Its terms can be shown to be given by

$$[Q] = \begin{bmatrix} Q_{11} & Q_{12} & 0 \\ Q_{12} & Q_{22} & 0 \\ 0 & 0 & Q_{66} \end{bmatrix} \quad (4.7a)$$

$$Q_{11} = \frac{E_1}{1 - \nu_{12}^2 E_2 / E_1}$$

$$Q_{22} = \frac{E_2}{1 - \nu_{12}^2 E_2 / E_1}$$

(4.7b)

$$Q_{12} = \frac{\nu_{12} E_2}{1 - \nu_{12}^2 E_2 / E_1}$$

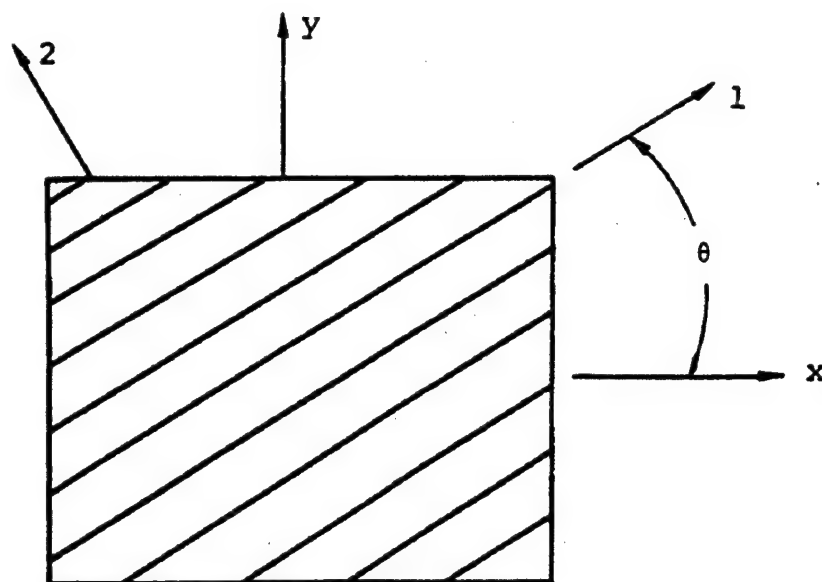
$$Q_{66} = G_{12}$$

The notation used for the (Q) matrix results from the procedure discussed in chapter 3 for simplified engineering representation of the fourth-rank stiffness tensor. Each pair of subscripts of the stiffness components is replaced by a single subscript according to the following scheme:

$$\begin{array}{lll} 11 \rightarrow 1 & 22 \rightarrow 2 & 33 \rightarrow 3 \\ 23 \rightarrow 4 & 31 \rightarrow 5 & 12 \rightarrow 6 \end{array}$$

The reduced stiffness and compliance matrixes (4.7) and (4.5) relate stresses and strains in the principal material directions of the material. In order to define the material response in directions other than those material coordinates, it is necessary to develop transformation relations for the material stiffnesses.

In figure 4.1, two sets of coordinate systems are depicted. The 1-2 coordinate system corresponds to the principal material directions for a lamina, while the x-y coordinates are arbitrary and related to the 1-2 coordinates through a rotation about the axis out of the plane of the figure.



1,2 Principal Material Coordinates  
 x,y Laminate, or Arbitrary Coordinates

FIGURE 4.1. COORDINATE SYSTEMS

The angle  $\theta$  is defined as the rotation from the arbitrary x-y system to the material 1-2 system. ( $\theta$  is positive for a counterclockwise rotation).

The transformation of stresses from the 1-2 system to the x-y system follows the rules for transformation of tensor components. Thus

$$\begin{Bmatrix} \sigma_{xx} \\ \sigma_{yy} \\ \sigma_{xy} \end{Bmatrix} = \begin{bmatrix} m^2 & n^2 & -2mn \\ n^2 & m^2 & 2mn \\ mn & -mn & m^2 - n^2 \end{bmatrix} \begin{Bmatrix} \sigma_{11} \\ \sigma_{22} \\ \sigma_{12} \end{Bmatrix} \quad (4.8)$$

or

$$\{\sigma_x\} = [\theta] \{\sigma_l\}$$

where  $m = \cos\theta$ ,  $n = \sin\theta$

In these relations, the subscript x is used as shorthand to refer to the laminate coordinate system.

The same transformation matrix ( $\theta$ ) can also be used for the tensor strain components. However, since the engineering shear strains have been utilized, a different transformation matrix is required. Thus



$$\begin{Bmatrix} \epsilon_{xx} \\ \epsilon_{yy} \\ 2\epsilon_{xy} \end{Bmatrix} = \begin{bmatrix} m^2 & n^2 & -mn \\ n^2 & m^2 & mn \\ 2mn & -2mn & m^2 - n^2 \end{bmatrix} \begin{Bmatrix} \epsilon_{11} \\ \epsilon_{22} \\ 2\epsilon_{12} \end{Bmatrix} \quad (4.9)$$

or

$$\{\epsilon_x\} = [\psi] \{\epsilon_l\}$$

Both equations 4.8 and 4.9 can be inverted to yield

$$\{\sigma_l\} = [\theta]^{-1} \{\sigma_x\}$$

and

$$\{\epsilon_l\} = [\psi]^{-1} \{\epsilon_x\}$$

where

$$[\theta]^{-1} = \begin{bmatrix} m^2 & n^2 & 2mn \\ n^2 & m^2 & -2mn \\ -mn & mn & m^2 - n^2 \end{bmatrix}$$

and

$$[\psi]^{-1} = \begin{bmatrix} m^2 & n^2 & mn \\ n^2 & m^2 & -mn \\ -2mn & 2mn & m^2 - n^2 \end{bmatrix}$$

comparing (4.11) with (4.8) and (4.9) it can easily be seen that in this particular case, the inverse of each transformation matrix can be found simply by substituting negative angles for the various terms within the matrix.

Given the transformations for stress and strain to arbitrary coordinate systems, the relations between stress and strain in the laminate system can be determined. Substituting equations 4.10 and 4.11 into 4.6 yields

$$\{\sigma_t\} = [\theta]^{-1} \{\sigma_x\} = [Q] \{\epsilon_t\} = [Q][\psi]^{-1} \{\epsilon_x\} \quad (4.12)$$

or

$$\{\sigma_x\} = [\theta] [Q] [\psi]^{-1} \{\epsilon_x\}$$

or

$$\{\sigma_x\} = [\bar{Q}] \{\epsilon_x\} \quad (4.13)$$

The reduced stiffness matrix,  $(\bar{Q})$ , relates the stress and strain components in the laminate coordinate system. Here

$$[\bar{Q}] = [\theta] [Q] [\psi]^{-1} \quad (4.14)$$

The terms within  $(\bar{Q})$ , are defined by the appropriate matrix multiplication to be

$$\begin{aligned} \bar{Q}_{11} &= Q_{11}m^4 + Q_{22}n^4 + 2m^2n^2 (Q_{12} + 2Q_{66}) \\ \bar{Q}_{12} &= m^2n^2(Q_{11} + Q_{22} - 4Q_{66}) + (m^4 + n^4) Q_{12} \\ \bar{Q}_{16} &= [Q_{11}m^2 - Q_{22}n^2 - (Q_{12} + 2Q_{66})(m^2 - n^2)] mn \\ \bar{Q}_{22} &= Q_{11}n^4 + Q_{22}m^4 + 2m^2n^2 (Q_{12} + 2Q_{66}) \\ \bar{Q}_{26} &= [Q_{11}n^2 - Q_{22}m^2 + (Q_{12} + 2Q_{66})(m^2 - n^2)] mn \\ \bar{Q}_{66} &= (Q_{11} + Q_{22} - 2Q_{12})m^2n^2 + Q_{66}(m^2 - n^2)^2 \\ \bar{Q}_{21} &= \bar{Q}_{12} \\ \bar{Q}_{61} &= \bar{Q}_{16} \\ \bar{Q}_{62} &= \bar{Q}_{26} \end{aligned} \quad (4.15)$$

where the subscript 6 has been retained in keeping with the discussion following equation 4.7. Thus

$$[\bar{Q}] = \begin{bmatrix} \bar{Q}_{11} & \bar{Q}_{12} & \bar{Q}_{16} \\ \bar{Q}_{21} & \bar{Q}_{22} & \bar{Q}_{26} \\ \bar{Q}_{16} & \bar{Q}_{26} & \bar{Q}_{66} \end{bmatrix} \quad (4.16)$$

A feature of the  $(\bar{Q})$  matrix which is immediately noticed as being dissimilar to previous constitutive relations is that  $(\bar{Q})$  is fully populated. The additional terms which have appeared in  $(\bar{Q})$  - namely  $\bar{Q}_{16}$ , and  $\bar{Q}_{26}$  - relate shear strains to extensional loading and vice versa. This effect of a shear strain resulting from an extensional stress is depicted graphically in figure 4.2.

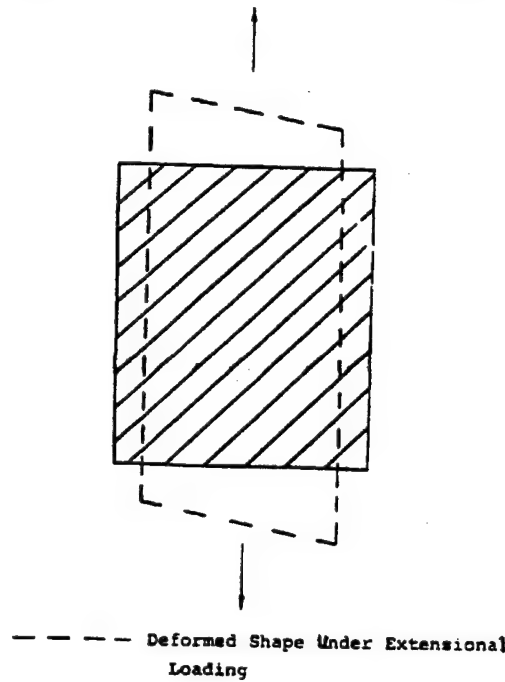


FIGURE 4.2. EXTENSIONAL-SHEAR COUPLING

Referring to equation 4.15, each of the extensional-shear coupling terms can be seen to contain a sine-cosine multiplier term. Obviously, if either  $\sin\theta$  or  $\cos\theta$  is zero, the extensional-shear coupling terms are zero. For the product  $\sin\theta \cos\theta$  to be zero, the angle  $\theta$  must be  $0^\circ$  or  $90^\circ$ . Physically, this means that the fibers are either parallel or perpendicular to the loading direction. For this case, extensional-shear coupling does not occur in an orthotropic material, since the loadings are in the principal material directions (equation 4.5).

The procedure used to develop the transformed stiffness matrix can also be used to find a transformed compliance matrix. Thus

$$\begin{aligned}
\{\epsilon_i\} &= [S] \{\sigma_i\} \\
\{\epsilon_x\} &= [\psi] [S] [\theta]^{-1} \{\sigma_x\} \\
\{\epsilon_x\} &= [\bar{S}] [\sigma_x]
\end{aligned} \tag{4.17}$$

The relations between the terms in  $(\bar{S})$  and  $(S)$  are developed by a procedure identical to that for the relations between  $(\bar{Q})$  and  $(Q)$ .

Noting that the stress-strain relations are now defined in the laminate coordinate system, lamina stiffnesses can also be defined in this system. Thus expanding the last of equation 4.17

$$\begin{Bmatrix} \epsilon_{xx} \\ \epsilon_{yy} \\ 2\epsilon_{xy} \end{Bmatrix} = \begin{bmatrix} \bar{S}_{11} & \bar{S}_{12} & \bar{S}_{16} \\ \bar{S}_{21} & \bar{S}_{22} & \bar{S}_{26} \\ \bar{S}_{16} & \bar{S}_{26} & \bar{S}_{66} \end{bmatrix} \begin{Bmatrix} \sigma_{xx} \\ \sigma_{yy} \\ \sigma_{xy} \end{Bmatrix}$$

The engineering constants for the material can be defined by specifying the conditions for an experiment. Thus, the ratio  $\sigma_{xx}/\epsilon_{xx}$ , for  $\sigma_{yy} = \sigma_{xy} = 0$  is the Young's modulus in the x direction. For this same stress state,  $-\epsilon_{yy}/\epsilon_{xx}$  is the Poisson's ratio. In this fashion, the lamina stiffnesses in the coordinate system of equation 4.17 are found to be

$$\begin{aligned}
E_x &= \frac{1}{\bar{S}_{11}} \\
E_y &= \frac{1}{\bar{S}_{22}} \\
G_{xy} &= \frac{1}{\bar{S}_{66}} \\
\nu_{xy} &= -\bar{S}_{21}/\bar{S}_{11} = -\bar{S}_{12}/\bar{S}_{11}
\end{aligned} \tag{4.18}$$

It is sometimes desirable to obtain elastic constants directly from the reduced stiffnesses,  $(\bar{Q})$ , by utilizing equation 4.13. In the general case where the  $\bar{Q}_{ij}$  matrix is fully populated, this can be accomplished by using equation 4.18 and the solution for  $\bar{S}_{ij}$  as functions of  $\bar{Q}_{ij}$  obtained from the inverse relationship of the two matrices. An alternate approach is to evaluate extensional properties for the case of zero shear strain,  $\epsilon_{xy} = 0$ , as opposed to the previous case of zero shear stress,  $\sigma_{xy} = 0$ . For zero shear strain it is found that, in terms of the transformed stiffness matrix terms (4.16), the elastic constants are

$$\begin{aligned}
 E_x &= \bar{Q}_{11} - \frac{\bar{Q}_{12}^2}{\bar{Q}_{22}} \\
 E_y &= \bar{Q}_{22} - \frac{\bar{Q}_{12}^2}{\bar{Q}_{11}}
 \end{aligned}
 \tag{4.19}$$

$$\begin{aligned}
 \nu_{xy} &= \frac{\bar{Q}_{12}}{\bar{Q}_{22}} \\
 \nu_{yx} &= \frac{\bar{Q}_{21}}{\bar{Q}_{22}}
 \end{aligned}$$

Also, when extensional strains are assumed to be zero, the shear stiffness is given by

$$G_{xy} = \bar{Q}_{66}$$

Referring to the terms in the  $(\bar{Q})$  matrix (4.15) and the stiffness relations (4.19), it can be seen that, in general, the elastic constants in an arbitrary coordinate system are functions of all of the elastic constants in the principal material directions as well as the angle of rotation.

The variation of elastic modulus  $E_x$  as obtained by the use of (4.18) (the values will differ if (4.19) is used) with angle of rotation is depicted in figure 4.3 for a typical graphite/epoxy material. For demonstration purposes, two different shear moduli have been used in generating the figure. The differences between the two curves demonstrate the effect of the principal material shear modulus on the transformed extensional stiffness.

Examining the figure, it can be seen that the two curves are identical at  $\theta = 0^\circ$  and  $\theta = 90^\circ$ . This is as expected since at these angles the extensional stiffness  $E_x$  is simply  $E_1$  or  $E_2$ . Between the two end points, substantial differences are present. For the smaller shear modulus, from approximately  $50^\circ$  to just less than  $90^\circ$ , the extensional stiffness is less than the  $E_2$  value. This is a very interesting result, indicating that for these angles the material stiffness is more strongly governed by the principal material shear modulus than by the transverse extensional stiffness.

The curves of figure 4.3 can also be used to determine the modulus  $E_y$ . This is accomplished simply by reversing the angle scale. Thus, the values shown at  $0^\circ$  correspond to  $E_y$  at  $90^\circ$  and the values at  $90^\circ$  correspond to  $E_y$  at  $0^\circ$ .

With the transformed stress-strain relations, it is now possible to develop an analysis for an assemblage of plies, i.e., a laminate. Thus, we proceed to lamination theory.

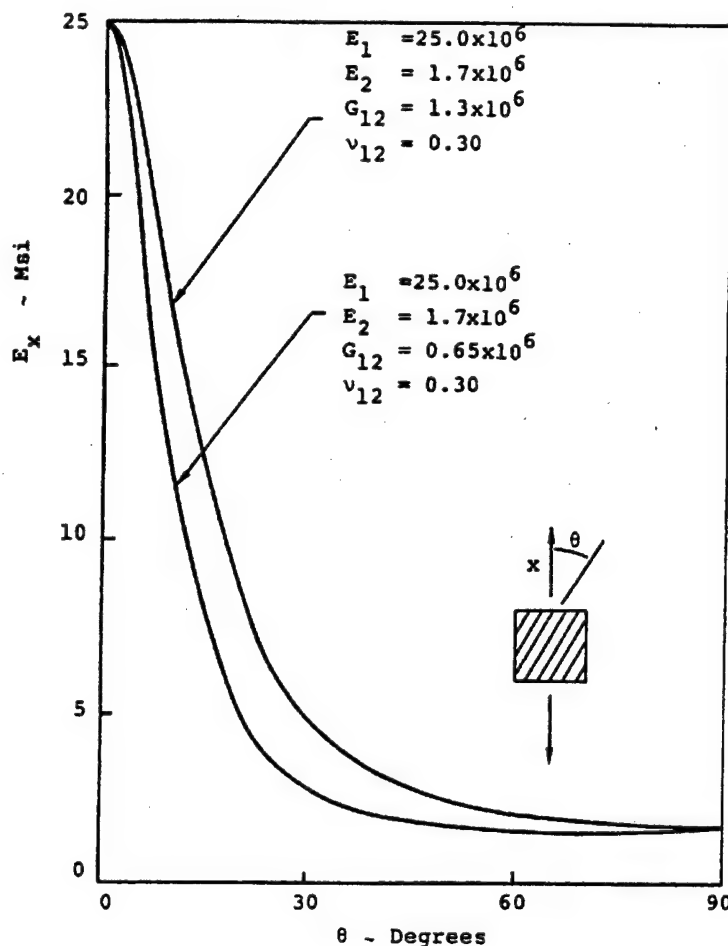


FIGURE 4.3. VARIATION OF  $E_x$  WITH ANGLE AND  $G_{12}$  FOR TYPICAL GRAPHITE/EPOXY MATERIALS

#### 4.3 LAMINATION THEORY.

The development of procedures to evaluate stresses and deformations of laminates is crucially dependent on the fact that the thicknesses of laminates are very much smaller than the in-plane dimensions. Typical thickness values for individual plies range between 0.005" and 0.010". Consequently, aerospace laminates using from 8 to 50 plies are still generally thin plates and, therefore, can be analyzed on the basis of the usual simplifications of thin plate theory.

Analysis of isotropic thin plates is an old and established field in which it has become customary to analyze the cases of in-plane loading and bending separately. The former case is described by plane stress elastic theory and the latter by classical plate bending theory. This separation is possible since the two loadings are uncoupled; when both occur, the result is given by superposition. In the case of anisotropic laminates, in-plane loading and bending, in general, are coupled and have to be treated together. It is only for symmetric laminate stacking sequences that uncoupling occurs. Consequently, lamination theory will first be developed for the general case and then simplifications will be introduced.

1. The thickness of the plate is much smaller than the in-plane dimensions.
2. The deformations of the plate surface are small compared to the plate thickness.
3. Normals to the undeformed plate surface remain normal to the deformed plate surface.
4. Vertical deflection does not vary through the thickness.
5. Stress, normal to the plate surface is negligible.

$$\begin{aligned} u_z &= u_z^o(x, y) \\ u_x &= u_x^o(x, y) - z \frac{\partial u_z}{\partial x} \\ u_y &= u_y^o(x, y) - z \frac{\partial u_z}{\partial y} \end{aligned} \quad (4.20)$$

The diagram illustrates the coordinate system and layer numbering for a laminate. The top part shows a 3D view of a rectangular laminate with a coordinate system (X, Y, Z) and a small cube representing a ply. The bottom part shows a cross-section of the laminate with multiple layers numbered 1 to K. The total thickness is labeled as 2h. The mid-surface is indicated. The Z-axis is vertical, and the X and Y axes are horizontal.

FIGURE 4.4. LAMINATE CONSTRUCTION

Writing the linear strain displacement relations

$$\begin{aligned}\epsilon_{xx} &= \frac{\partial u_x}{\partial x} & \epsilon_{yy} &= \frac{\partial u_y}{\partial y} \\ \epsilon_{xy} &= \frac{1}{2} \left( \frac{\partial u_x}{\partial y} + \frac{\partial u_y}{\partial x} \right)\end{aligned}\tag{4.21}$$

and performing the required partial differentiations

$$\begin{aligned}\epsilon_{xx} &= \frac{\partial}{\partial x} \left[ u_x^o - z \frac{\partial u_z}{\partial x} \right] \\ \epsilon_{yy} &= \frac{\partial}{\partial y} \left[ u_y^o - z \frac{\partial u_z}{\partial y} \right] \\ \epsilon_{xy} &= \frac{1}{2} \left\{ \frac{\partial}{\partial y} \left[ u_x^o - z \frac{\partial u_z}{\partial x} \right] + \frac{\partial}{\partial x} \left[ u_y^o - z \frac{\partial u_z}{\partial y} \right] \right\}\end{aligned}\tag{4.22}$$

yields

$$\begin{aligned}\epsilon_{xx} &= \epsilon_{xx}^o + z \kappa_{xx} \\ \epsilon_{yy} &= \epsilon_{yy}^o + z \kappa_{yy} \\ 2\epsilon_{xy} &= 2\epsilon_{xy}^o + 2z \kappa_{xy}\end{aligned}\tag{4.23}$$

or

$$\{\epsilon_x\} = \{\epsilon^o\} + z \{\kappa\}$$

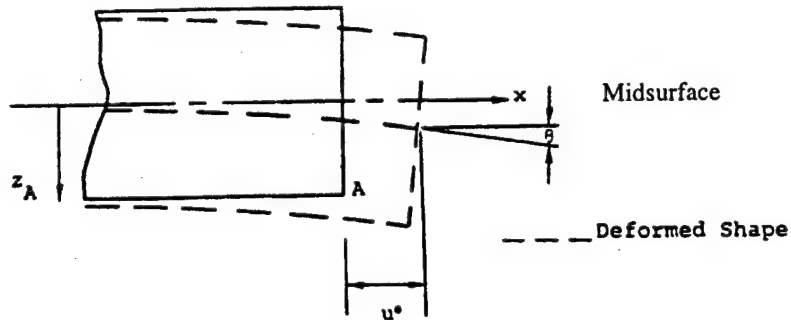
where

$$\{\epsilon^o\} = \begin{Bmatrix} \frac{\partial u_x^o}{\partial x} \\ \frac{\partial u_y^o}{\partial y} \\ \left( \frac{\partial u_x^o}{\partial y} + \frac{\partial u_y^o}{\partial x} \right) \end{Bmatrix}\tag{4.24}$$



$$\{\kappa\} = \begin{Bmatrix} -\frac{\partial^2 u_z}{\partial x^2} \\ -\frac{\partial^2 u_z}{\partial y^2} \\ -2\frac{\partial^2 u_z}{\partial x \partial y} \end{Bmatrix} \quad (4.25)$$

Thus, the strain at any point in the plate is defined as the sum of midsurface strain,  $\epsilon^0$ , and a curvature,  $(\kappa)$ , multiplied by the distance from the midsurface (see figure 4.5).



Total Displacement at A:

$$u = u^0 + \theta z_A$$

Strain at A:

$$\epsilon = \frac{\partial u}{\partial x} = \frac{\partial u^0}{\partial x} + z_A \frac{\partial \theta}{\partial x} = \epsilon^0 + z_A \kappa$$

FIGURE 4.5. PLATE DEFORMATIONS AND STRAINS

For convenience, as is usual in plate theory, stress and moment resultants will be used rather than stresses for the remainder of the development (see figure 4.6). The stress resultants are defined as

$$\{N\} = \begin{Bmatrix} N_{xx} \\ N_{yy} \\ N_{xy} \end{Bmatrix} = \int_{-h}^h \{\sigma_x\} dx \quad (4.26)$$

and the moment resultants are defined as

$$\{M\} = \begin{Bmatrix} M_{xx} \\ M_{yy} \\ M_{xy} \end{Bmatrix} = \int_{-h}^h \{\sigma_x\} z dx \quad (4.27)$$

where the integrations are carried out over the plate thickness. These integrations are graphically depicted in figure 4.7.

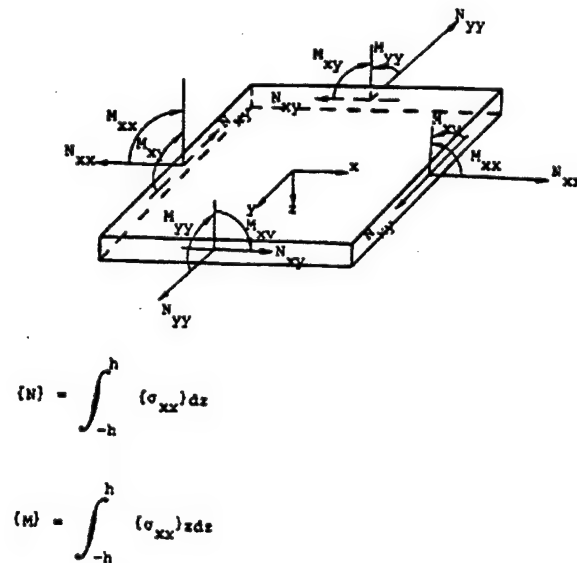


FIGURE 4.6. STRESS AND MOMENT RESULTANTS

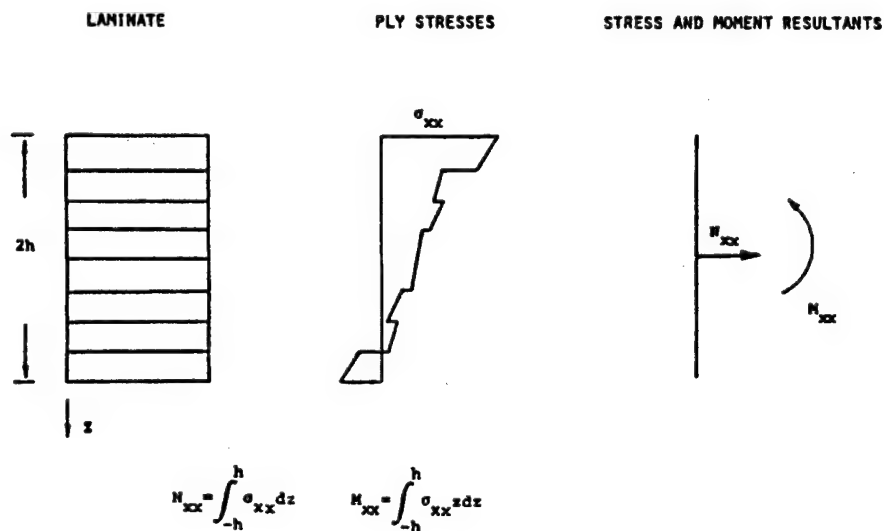


FIGURE 4.7. STRESSES AND STRESS AND MOMENT RESULTANTS

Noting equations 4.13 and 4.23, relations between the stress and moment resultants and the midplane strains and curvatures can be written as

$$\{N\} = \int_{-h}^h \{\sigma_x\} dz = \int_{-h}^h [\bar{Q}] (\{\epsilon^o\} + z \{\kappa\}) dz \quad (4.28)$$

$$\{M\} = \int_{-h}^h \{\sigma_x\} z dz = \int_{-h}^h [\bar{Q}] (\{\epsilon^o\} + z \{\kappa\}) z dz \quad (4.29)$$

The integrals can be separated into their component parts, yielding

$$\{N\} = \int_{-h}^h [\bar{Q}] \{\epsilon^o\} dz + \int_{-h}^h [\bar{Q}] \{\kappa\} z dz \quad (4.30)$$

$$\{M\} = \int_{-h}^h [\bar{Q}] \{\epsilon^o\} z dz + \int_{-h}^h [\bar{Q}] \{\kappa\} z^2 dz \quad (4.31)$$

Since the transformed lamina stiffness matrices are constant within each lamina and the midplane strains and curvatures are constant with respect to the  $z$  coordinate, the integrals in equations 4.30 and 4.31 can be replaced by summations yielding

$$\{N\} = \sum_{i=1}^N [\bar{Q}]^i (z_i - z_{i-1}) \{\epsilon^o\} + \frac{1}{2} \sum_{i=1}^N [\bar{Q}]^i (z_i^2 - z_{i-1}^2) \{\kappa\} \quad (4.32)$$

$$\{M\} = \frac{1}{2} \sum_{i=1}^N [\bar{Q}]^i (z_i^2 - z_{i-1}^2) \{\epsilon^o\} + \frac{1}{3} \sum_{i=1}^N [\bar{Q}]^i (z_i^3 - z_{i-1}^3) \{\kappa\} \quad (4.33)$$

where  $N$  is the total number of plies;  $z_i$  is defined as in figure 4.4 and superscript  $i$  denotes a property of the  $i^{\text{th}}$  ply. Note that  $z_i - z_{i-1}$  is equal to the thickness of the  $i^{\text{th}}$  ply.

Introducing three matrices equivalent to the three different summations shown in equations 4.32 and 4.33, the relations can be written as

$$\{N\} = [A] \{\epsilon^o\} + [B] \{\kappa\}$$

$$\{M\} = [B] \{\epsilon^o\} + [D] \{\kappa\}$$

or

$$\begin{Bmatrix} N \\ M \end{Bmatrix} = \begin{bmatrix} A & | & B \\ B & | & D \end{bmatrix} \begin{Bmatrix} \epsilon^o \\ \kappa \end{Bmatrix} \quad (4.34)$$

where the stiffness matrix is composed of the following 3x3 matrices:

$$\begin{aligned}
 [A] &= \sum_{i=1}^N [\bar{Q}]^i (z_i - z_{i-1}) \\
 [B] &= \frac{1}{2} \sum_{i=1}^N [\bar{Q}]^i (z_i^2 - z_{i-1}^2) \\
 [D] &= \frac{1}{3} \sum_{i=1}^N [\bar{Q}]^i (z_i^3 - z_{i-1}^3)
 \end{aligned} \tag{4.35}$$

where the reduced lamina stiffnesses for the  $i^{\text{th}}$  ply are found from equation 4.15 using the principal ply properties and orientation angle of each ply in turn. Thus, the constitutive relations for a laminate in terms of stress and moment resultants have been developed.

In examining the relations 4.34, the first interesting feature revealed is a coupling between bending and extension. The (B) matrices relate stress resultants to bending curvatures and moment resultants to midplane strains. Thus, for a general laminate, the application of a stress resultant produces curvatures and application of a bending moment produces extensional strain. This feature is known as bending-extensional coupling.

In typical structural laminates, bending-extensional coupling is eliminated by proper specification of the stacking sequence. Stacking sequence refers to the order in which the various plies are put together. Noting the relations for computing the (B) matrix (4.35), it can be seen that if the plies are arranged in an even  $z$  function (symmetric about the midplane) the (B) matrix is eliminated. Thus, if the laminate is designed with identically oriented plies at equal distances from the midsurface, bending-extensional coupling is eliminated.

There are other forms of coupling inherent in the relations (4.34). In order to examine these various couplings, it is necessary to evaluate individual terms in the (A), (B), and (D) matrices. The most general form of these matrices combined as in (4.34) is

$$\begin{bmatrix}
 A_{11} & A_{12} & A_{16} & B_{11} & B_{12} & B_{16} \\
 A_{21} & A_{22} & A_{26} & B_{21} & B_{22} & B_{26} \\
 A_{16} & A_{26} & A_{66} & B_{16} & B_{26} & B_{66} \\
 B_{11} & B_{12} & B_{16} & D_{11} & D_{12} & D_{16} \\
 B_{21} & B_{22} & B_{26} & D_{21} & D_{22} & D_{26} \\
 B_{16} & B_{26} & B_{66} & D_{16} & D_{26} & D_{66}
 \end{bmatrix}$$

It can be seen that, in general, the (A), (B), and (D) matrices are fully populated. Thus, there is coupling between membrane extension and membrane shear ( $A_{16}$ ,  $A_{26}$ ) and coupling between bending and twisting ( $D_{16}$ ,  $D_{26}$ ). Both of these forms of coupling can be eliminated by judicious ply orientation and stacking sequence selection, but in some cases, this selection may be impractical. Extensional-shear coupling can be eliminated by specifying a balanced construction. Balance indicates that for every  $+\theta$  ply, there is a  $-\theta$  ply. These plies do not have to be adjacent to satisfy this requirement.

When bending-twisting coupling is undesirable, it can be eliminated but only by using a unidirectional or crossply construction. Unidirectional construction implies that all layers have the same orientation, which is aligned with the loading direction. A crossply laminate has plies oriented at  $0^\circ$  and  $90^\circ$  only, again oriented with the loading direction. It is also possible to limit the effect of bending-twisting coupling by other means. If a symmetric laminate is constructed with many plies and plies with the same angular orientation are not grouped together, the magnitude of the  $D_{16}$  and  $D_{26}$  terms will be reduced with respect to the other terms in the (D) matrix. Thus, while the bending-twisting coupling is not eliminated, its effect is reduced. In certain applications such coupling may be desirable.

#### 4.4 LAMINATE PROPERTIES.

The previous section presented the development of the relations between the middle surface strains and curvatures and the membrane stress and moment resultants. The elastic stiffnesses in these relationships are functions of the ply elastic constants and the ply orientations and arrangement or stacking sequence. In the present section, these results will be utilized to calculate plate bending and extensional stiffnesses suitable for use in structural analysis. The effects of orientation variables upon plate properties will also be treated.

In addition to the mechanical loading conditions treated thus far in this chapter, for practical structures it is necessary to understand the effects of temperature changes upon laminate behavior. Thus, the thermal expansion characteristics of laminates will be presented. Further, for polymeric matrix composites, it has been found that high moisture content causes dimensional changes. This effect is treated in this section to define effective swelling coefficients.

In the previous section, it was shown that, in general, laminates exhibit coupling between bending and extension. Elimination of this coupling was shown to be possible through the specification of midplane symmetric construction. This leads to a natural division of laminates into symmetric and nonsymmetric categories.

Prior to discussion of these two laminate categories, typical laminate notation will be described. A shorthand notation has been devised and is in common use. The basis for the notation comes from the fact that structural laminates typically have repeating groups of plies and pairs of plies at  $+\theta$  and  $-\theta$  angles. Utilizing these groupings, the laminate construction

$$[0/0/45/-45/90/90/-45/45/0/0]$$

can be specified as

$$[0_2/\pm 45/90]_s$$

The numerical subscript indicates the number of adjacent identical plies. Adjacent balanced angle plies are lumped together, and the subscript *s* indicates that the pattern is repeated in reverse order forming a symmetric laminate. The multiplier subscript is also used to denote multiple groups of plies. Thus, the laminate

$$[45/-45/0/0/45/-45/0/0/0/0/-45/45/0/0/-45/45]$$

is specified as

$$[\pm 45/0_2]_{2s}$$

When the central ply of a symmetric laminate is not repeated, this is denoted by an overbar. Thus, the laminate

$$[45/-45/0/0/90/0/0/-45/45]$$

is specified as

$$[\pm 45/0_2/\overline{90}]_s$$

There are additional conventions which can be designated, but those shown here generally are sufficient.

#### 4.4.1 Symmetric Laminates.

As has been stated, a symmetric laminate does not exhibit coupling between extension and bending. This leads to considerable simplification for the designer of composites in that symmetric constructions behave somewhat similarly to conventional materials.

Recalling equation 4.34 and noting that for this case the (B) matrix is zero, the relations can be rewritten as

$$\begin{Bmatrix} N_{xx} \\ N_{yy} \\ N_{xy} \end{Bmatrix} = \begin{bmatrix} A_{11} & A_{12} & A_{16} \\ A_{12} & A_{22} & A_{26} \\ A_{16} & A_{26} & A_{66} \end{bmatrix} \begin{Bmatrix} \epsilon_{xx}^o \\ \epsilon_{yy}^o \\ 2\epsilon_{xy}^o \end{Bmatrix}$$

and

(4.36)

$$\begin{Bmatrix} M_{xx} \\ M_{yy} \\ M_{xy} \end{Bmatrix} = \begin{bmatrix} D_{11} & D_{12} & D_{16} \\ D_{12} & D_{22} & D_{26} \\ D_{16} & D_{26} & D_{66} \end{bmatrix} \begin{Bmatrix} \kappa_{xx} \\ \kappa_{yy} \\ 2\kappa_{xy} \end{Bmatrix}$$

Since the extensional and bending behavior are uncoupled, effective laminate elastic constants can be readily determined. Inversion of the stress resultant midplane strain relations yields

$$\{\epsilon^o\} = [A]^{-1} \{N\} = [a] \{N\}$$

from which the laminate elastic constants are seen to be

$$\begin{aligned} E_x &= \frac{1}{2ha_{11}} & G_{xy} &= \frac{1}{2ha_{66}} \\ E_y &= \frac{1}{2ha_{22}} & \nu_{xy} &= -\frac{a_{12}}{a_{11}} \end{aligned} \quad (4.37)$$

where the divisor  $2h$  corresponds to the laminate thickness.

Noting that the  $(A)$  matrix is comprised of  $(\bar{Q})$  matrices from each layer in the laminate, it is obvious that the laminate elastic properties are functions of the angular orientation of the plies. This is illustrated in figure 4.8 for a typical high modulus graphite/epoxy system. The lamina properties for this material are listed in table 4.1 and will be referred to in later examples. The laminae are oriented in  $+\theta$  pairs in a symmetric, balanced construction, creating what is called an angle-ply laminate.

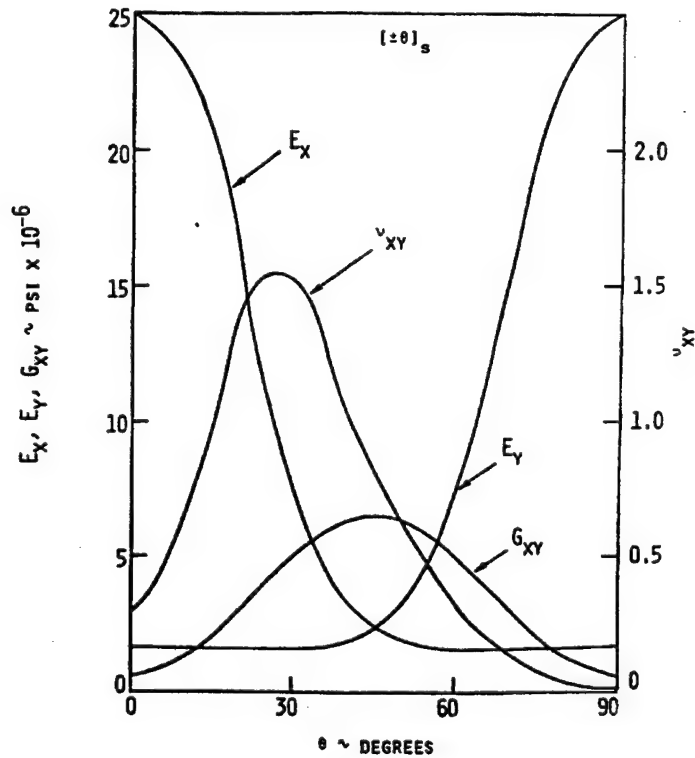


FIGURE 4.8. LAMINATE ELASTIC CONSTANTS FOR HM-GRAPHITE/EPOXY

Figure 4.8 shows the variation of the extensional modulus of angle-ply laminates, which is similar to but slightly different from that shown for the off-axis material (figure 4.3) due to the

effects of extensional-shear coupling. In an off-axis material, extensional loadings produce shear deformations in addition to extensional deformations. In an angle-ply laminate, the shear deformations are eliminated through internal constraints. Since the shear strains are eliminated, the material exhibits higher effective stiffnesses. The effects of shear-extensional coupling are more fully discussed below.

TABLE 4.1. PROPERTIES OF A HIGH-MODULUS GRAPHITE/EPOXY LAMINA

$E_1 = 25.0 \times 10^6$ psi	$\alpha_1 = -0.30 \times 10^{-6}$ in/in/°F
$E_2 = 1.7 \times 10^6$ psi	$\alpha_2 = 19.5 \times 10^{-6}$ in/in/°F
$G_{12} = 0.65 \times 10^6$ psi	
$\nu_{12} = 0.30$	
$\rho = 0.056$ pci	
$\sigma_L^u = 110.0 \times 10^3$ psi	$\sigma_L^{cu} = 110.0 \times 10^3$ psi
$\sigma_T^u = 4.0 \times 10^3$ psi	$\sigma_T^{cu} = 20.0 \times 10^3$ psi
$\tau_L^u = 9.0 \times 10^3$ psi	
$\nu_f = 0.60$	
Ply thickness 0.0052 in.	

Two other features are noteworthy in figure 4.8. These are the variation of shear modulus and Poisson's ratio. The shear modulus is equal to the unidirectional value for  $\theta = 0^\circ$  and  $\theta = 90^\circ$ . The shear modulus rises sharply and reaches a maximum at  $\theta = 45^\circ$ . The peak at  $45^\circ$  can be explained by noting that shear is equivalent to a combined state of equal tension and compression loads oriented at  $45^\circ$ . Thus, the shear loading on a  $(\pm 45)_s$  laminate is equivalent to tensile and compressive loading on a  $(0/90)_s$  laminate. Effectively, the fibers are aligned with the loading directions and, hence, the large shear stiffness.

An even more interesting effect is seen in the variation of Poisson's ratio. The peak value in this example is greater than 1.5. In an isotropic material, this would be impossible. In an orthotropic material, the isotropic restrictions do not hold and a Poisson's ratio greater than one is valid and realistic. In fact, large Poisson's ratios are typical for laminates constructed of unidirectional materials with the plies oriented at approximately  $\pm 30^\circ$ . This effect can readily be explained with the use of figure 4.9.

Depicted in figure 4.9 are two separate loadings on a  $+30^\circ$  lamina. When a positive  $N_{xx}$  load is applied, the deformed shape contains a positive  $\epsilon_{xx}$  and a negative  $\epsilon_{xy}$ . In the  $(\pm 30)_s$  laminate, the shear strain is constrained by the presence of the  $-30^\circ$  plies. This results in an internal shear load which eliminates the shear strain. The large Poisson's ratio is a result of this internal shear load. Noting the second part of figure 4.9, a compressive  $N_{yy}$  load is seen to promote a positive  $\epsilon_{xy}$ . Because of material symmetries, the application of a positive  $N_{xy}$  would produce a compressive  $\epsilon_{yy}$ . Therefore, the positive internal shear load required to constrain the shear strains developed by the positive  $N_{xx}$  in the first part of figure 4.9 produces a compressive  $\epsilon_{yy}$ . Thus,



the Poisson strain is made up of two components: first, the applied tensile  $N_{xx}$  produces a compressive  $\epsilon_{yy}$  and second, the induced positive  $N_{xy}$  produces a compressive  $\epsilon_{yy}$ . Thus, the large Poisson's ratio is simply a function of extensional-shear coupling in the individual laminae.

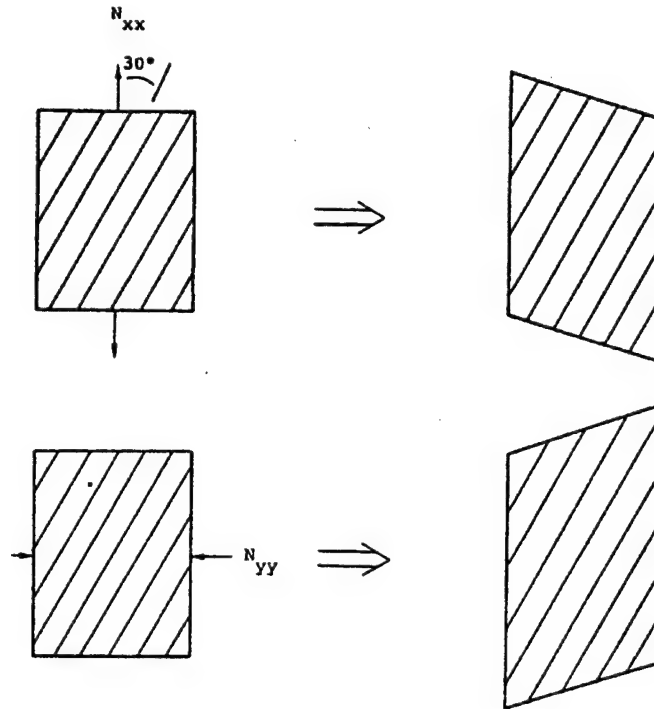


FIGURE 4.9. EXTENSIONAL-SHEAR COUPLING AND POISSON'S RATIO

Because of the infinite variability of the angular orientation of the individual laminae, one would assume that a laminate could be constructed having a stiffness which behaves isotropically in the plane of the laminate by utilizing a large number of plies having small, equal differences in their orientation. It can be shown that a symmetric, quasi-isotropic laminate can also be constructed with as few as six plies, three plies above and three below the midplane. The simplest quasi-isotropic laminate is  $(0/\pm 60)_s$ . A general rule for describing a quasi-isotropic laminate states that the angles between plies are equal to  $\pi/N$ , where  $N$  is an integer greater than or equal to 3, and there is an identical number of plies of each orientation, in a symmetric laminate. For plies of a given material, all such quasi-isotropic laminates will have the same elastic properties, regardless of the value of  $N$ .

As was stated, a quasi-isotropic laminate has in-plane stiffnesses which follow isotropic relationships. Thus,

$$E_x = E_y = E_\theta$$

where the subscript  $\theta$  indicates any arbitrary angle. Additionally,

$$G_{xy} = \frac{E_x}{2(1+\nu_{xy})}$$

There are two items which must be remembered with respect to quasi-isotropic laminates. First and foremost, only the elastic in-plane properties are isotropic; the strength properties, in general, will vary with direction. This will be discussed in a later section. The second item is that two equal moduli  $E_x = E_y$  do not necessarily indicate quasi-isotropy. This second item is graphically demonstrated in table 4.2, where three laminates each have identical  $E_x$  and  $E_y$  moduli.

The first two laminates in table 4.2 are actually the same. If one rotates the  $(0/90)_s$  laminate  $45^\circ$ , it is easily seen that it becomes a  $(\pm 45)_s$  laminate. Note that the extensional moduli of these laminates are not the same and that the shear modulus in each laminate is not related to the extensional moduli and Poisson's ratio. For these laminates, the  $\pi/N$  relation has not been satisfied and they are not quasi-isotropic.

The third laminate has plies oriented at  $45^\circ$  to each other but there are not equal numbers of plies at each angle. This laminate is also not quasi-isotropic. This can be verified by computing a shear modulus using the isotropic relation.

TABLE 4.2. ELASTIC PROPERTIES OF LAMINATES

	$E_x = E_y$ $10^6$ psi	$\nu_{xy}$	$G_{xy}$ $10^6$ psi
$[0^\circ/90^\circ]_s$	13.41	0.038	0.65
$[\pm 45^\circ]_s$	2.38	0.829	6.46
$[0^\circ/90^\circ/+45^\circ/-45^\circ/90^\circ/0^\circ]_s$	10.97	0.213	2.59

(see table 4.1 for lamina properties)

The discussion of symmetric laminates has thus far centered on membrane behavior. It has been shown that symmetric laminates can be constructed which are very well behaved in the membrane sense. The bending behavior of symmetric laminates is considerably more complex, primarily due to the arrangement of the plies through the thickness of the laminate. Before proceeding with the discussion of laminate bending, it will be helpful to examine a numerical example which will serve to illustrate the preceding discussion.

The laminate to be studied is a  $(0/\pm 45/90)_s$  construction (figure 4.10) fabricated from high modulus graphite/epoxy with material properties specified in table 4.1. This laminate will also be used in subsequent discussions in the text in an effort to give the reader a step-by-step understanding of the laminate analysis process.

		$z_0$	$(-4 t_{PLY})$	$= -0.0208$
	0 (1)	$z_1$	$(-3 t_{PLY})$	$= -0.0156$
	45 (2)	$z_2$	$(-2 t_{PLY})$	$= -0.0104$
	-45 (3)	$z_3$	$(-t_{PLY})$	$= -0.0052$
	90 (4)	$z_4$	—————	MIDSURFACE
	90 (5)	$z_5$	$(t_{PLY})$	$= 0.0052$
	-45 (6)	$z_6$	$(2 t_{PLY})$	$= 0.0104$
	45 (7)	$z_7$	$(3 t_{PLY})$	$= 0.0156$
	0 (8)	$z_8$	$(4 t_{PLY})$	$= 0.0208$

FIGURE 4.10. LAMINATE EXAMPLE

The first objective is to determine the laminate extensional stiffness matrix (A). It has been shown in equation 4.35 that the (A) matrix is composed of the lamina ( $\bar{Q}$ ) matrices and that the ( $\bar{Q}$ ) matrices are simply transformed (Q) matrices (4.14). Thus, the example must begin with the determination of the transformed lamina stiffness ( $\bar{Q}$ ) matrices.

Since each ply in this laminate is the same material, the (Q) matrix for each layer is the same. Referring to equation 4.7, the lamina stiffness matrix in the principal material directions is

$$[Q] = \begin{bmatrix} \frac{E_1}{\Delta} & \frac{\nu_{12}E_2}{\Delta} & 0 \\ & \frac{E_2}{\Delta} & 0 \\ sym & & G_{12} \end{bmatrix} \quad \Delta = 1 - \frac{E_2}{E_1} \nu_{12}^2$$

$$= \begin{bmatrix} 25.15 \times 10^6 & 5.13 \times 10^5 & 0 \\ & 1.71 \times 10^6 & 0 \\ sym & & 6.20 \times 10^5 \end{bmatrix} \text{ psi}$$

The various plies within the laminate are oriented in different directions, and therefore, the lamina stiffness matrices must be transformed into the laminate or reference coordinate system. The transformed lamina stiffness matrices are found through the use of equation 4.15. Thus, for the two plies oriented at  $0^\circ$

$$\begin{aligned}
 m &= \cos(0) = 1 & n &= \sin(0) = 0 \\
 \bar{Q}_{11} &= Q_{11} (1)^4 + Q_{22} (0)^4 + 2 (1)^2 (0)^2 (Q_{12} + Q_{66}) \\
 &= Q_{11} \\
 \bar{Q}_{12} &= Q_{12} & \bar{Q}_{16} &= Q_{16} & \bar{Q}_{22} &= Q_{22} \\
 \bar{Q}_{26} &= Q_{26} & \bar{Q}_{66} &= Q_{66}
 \end{aligned}$$

$$[\bar{Q}] = \begin{bmatrix} 25.15 \times 10^6 & 5.13 \times 10^5 & 0 \\ & 1.71 \times 10^6 & 0 \\ \text{sym} & & 6.50 \times 10^5 \end{bmatrix} \text{ psi}$$

It is obvious that the transformation through  $0^\circ$  leaves  $(\bar{Q}) = (Q)$ . For the two plies oriented at  $45^\circ$ , the transformed stiffnesses are found as

$$\begin{aligned}
 m &= \cos(45^\circ) = \frac{\sqrt{2}}{2} & n &= \sin(45^\circ) = \frac{\sqrt{2}}{2} \\
 \bar{Q}_{11} &= Q_{11} \left(\frac{\sqrt{2}}{2}\right)^4 + Q_{22} \left(\frac{\sqrt{2}}{2}\right)^4 + 2 \left(\frac{\sqrt{2}}{2}\right)^2 \left(\frac{\sqrt{2}}{2}\right)^2 (Q_{12} + 2Q_{66}) \\
 &= 25.15 \times 10^6 \left(\frac{1}{4}\right) + 1.710 \times 10^6 \left(\frac{1}{4}\right) + \\
 &\quad 2 \left(\frac{1}{2}\right) \left(\frac{1}{2}\right) (5.131 \times 10^5 + 1.30 \times 10^6) \\
 &= 7.62 \times 10^6 \text{ psi}
 \end{aligned}$$

$$\bar{Q}_{12} = \left(\frac{\sqrt{2}}{2}\right)^2 \left(\frac{\sqrt{2}}{2}\right)^2 (Q_{11} + Q_{22} - 4Q_{66}) + Q_{12} \left[ \left(\frac{\sqrt{2}}{2}\right)^4 + \left(\frac{\sqrt{2}}{2}\right)^4 \right]$$

$$= 6.32 \times 10^6 \text{ psi}$$

$$\bar{Q}_{16} = 5.86 \times 10^6 \text{ psi}$$

$$\bar{Q}_{22} = 7.62 \times 10^6 \text{ psi}$$

$$\bar{Q}_{26} = 5.86 \times 10^6 \text{ psi}$$

$$\bar{Q}_{66} = 6.45 \times 10^6 \text{ psi}$$

$$[\bar{Q}] = \begin{bmatrix} 7.62 \times 10^6 & 6.32 \times 10^6 & 5.86 \times 10^6 \\ & 7.62 \times 10^6 & 5.86 \times 10^6 \\ \text{sym} & & 6.45 \times 10^6 \end{bmatrix} \text{ psi}$$

In the plies oriented at  $-45^\circ$ ,

$$m = \cos(-45^\circ) = \frac{\sqrt{2}}{2} \quad n = \sin(-45^\circ) = -\frac{\sqrt{2}}{2}$$

$$[\bar{Q}] = \begin{bmatrix} 7.62 \times 10^6 & 6.32 \times 10^6 & -5.86 \times 10^6 \\ & 7.62 \times 10^6 & -5.86 \times 10^6 \\ \text{sym} & & 6.45 \times 10^6 \end{bmatrix} \text{ psi}$$

Note that the only difference between the  $+45^\circ$  and  $-45^\circ$  transformed stiffness matrices is the sign of the shear-extensional coupling terms  $\bar{Q}_{16}$ ,  $\bar{Q}_{26}$ ,  $\bar{Q}_{61}$ ,  $\bar{Q}_{62}$ . Finally, the transformations for the  $90^\circ$  plies yield

$$m = \cos (90^\circ) = 0 \quad n = \sin (90^\circ) = 1$$

$$[\bar{Q}] = \begin{bmatrix} 1.71 \times 10^6 & 5.13 \times 10^5 & 0 \\ & 25.15 \times 10^6 & 0 \\ \text{sym} & & 6.50 \times 10^5 \end{bmatrix} \text{ psi}$$

which is the same as ( $\bar{Q}$ ) for the  $0^\circ$  plies with the  $\bar{Q}_{11}$  and  $\bar{Q}_{22}$  terms interchanged.

Now that the transformed lamina stiffness matrices have been computed, the laminate stiffness can be determined. Recalling the relations for (A) (4.35),

$$[A] = \sum_{i=1}^N [\bar{Q}]^i (z_i - z_{i-1})$$

$$= \sum_{i=1}^N [\bar{Q}]^i (t_{Ply}^i)$$

$$A_{11} = \sum_{i=1}^N \bar{Q}_{11}^i (t_{Ply}^i)$$

$$\begin{aligned} &= 25.15 \times 10^6 (0.0052) + 7.62 \times 10^6 (0.0052) + \\ &\quad 7.62 \times 10^6 (0.0052) + 1.71 \times 10^6 (0.0052) + \\ &\quad 1.71 \times 10^6 (0.0052) + 7.62 \times 10^6 (0.0052) + \\ &\quad 7.62 \times 10^6 (0.0052) + 25.15 \times 10^6 (0.0052) \\ &= 4.38 \times 10^5 \text{ lb/in} \end{aligned}$$

$$\begin{aligned} A_{12} &= 2 (0.0052) [5.131 \times 10^5 + 2 (6.32 \times 10^6) + 5.131 \times 10^5] \\ &= 1.42 \times 10^5 \text{ lb/in} \end{aligned}$$

$$\begin{aligned} A_{16} &= 2 (0.0052) [0.0 + 5.86 \times 10^6 - 5.86 \times 10^6 + 0.0] \\ &= 0.0 \text{ lb/in} \end{aligned}$$

$$A_{22} = 4.38 \times 10^5 \text{ lb/in}$$

$$A_{26} = 0.0 \text{ lb/in}$$

$$A_{66} = 1.48 \times 10^5 \text{ lb/in}$$

Note that the extensional-shear coupling terms in the  $45^\circ$  and  $-45^\circ$  plies have canceled each other in the laminate (A) matrix. This explains why balanced laminates do not exhibit extensional-shear coupling.

In order to determine effective elastic constants for this laminate, it is necessary to invert the (A) matrix. Though it has not been shown explicitly, the (B) matrix for this laminate is zero and thus the extensional and bending moduli are uncoupled. Later sections describe how the presence of a (B) matrix can be handled.

$$[a] = [A]^{-1} = \begin{bmatrix} 4.38 \times 10^5 & 1.42 \times 10^5 & 0.0 \\ & 4.38 \times 10^5 & 0.0 \\ \text{sym} & & 1.48 \times 10^5 \end{bmatrix}^{-1} \text{ in/lb}$$

$$[a] = \begin{bmatrix} 2.55 \times 10^{-6} & -8.29 \times 10^{-7} & 0.0 \\ & 2.55 \times 10^{-6} & 0.0 \\ \text{sym} & & 6.76 \times 10^{-6} \end{bmatrix} \text{ in/lb}$$

Referring to equation 4.37

$$E_x = \frac{1}{2ha_{11}} = \frac{1}{2(0.0208)(2.55 \times 10^{-6})} = 9.42 \times 10^6 \text{ psi}$$

$$E_y = 9.42 \times 10^6 \text{ psi}$$

$$G_{xy} = 3.55 \times 10^6 \text{ psi}$$

$$\nu_{xy} = 0.325$$

Since the laminate selected for this example is quasi-isotropic, the in-plane moduli follow the isotropic relationships.

The first complication which arises in the treatment of laminate bending deals with the relationships between membrane, (A), and bending, (D), elastic properties. In composite laminates there is generally no direct relationship between extensional and bending stiffnesses. This is unlike the case of a homogeneous material wherein bending stiffness, D, and extensional stiffness, A, are related by

$$D = \frac{A(2h)^2}{12}$$

In determining the membrane stiffnesses (A), the position of the ply through the thickness of the laminate does not matter. This can be seen by examining the expression for (A) (4.35). It is seen that the multiplier on the  $\bar{Q}$  terms is simply the ply thickness. The relations for the bending stiffnesses are functions of the third power of the distance of the ply from the midsurface, and therefore, the position of the plies through the thickness is critical. The effects of ply position in a unit thickness laminate are shown in table 4.3.

TABLE 4.3. EXTENSIONAL AND BENDING STIFFNESSES

	$[0/\pm 60]_s$	$[\pm 60/0]_s$	$[60/0/-60]_s$	Homogeneous Laminate
$A_{11}$	$1.05 \times 10^7$	$1.05 \times 10^7$	$1.05 \times 10^7$	$1.05 \times 10^7$
$A_{12}$	$3.42 \times 10^6$	$3.42 \times 10^6$	$3.42 \times 10^6$	$3.42 \times 10^6$
$A_{22}$	$1.05 \times 10^7$	$1.05 \times 10^7$	$1.05 \times 10^7$	$1.05 \times 10^7$
$A_{66}$	$3.55 \times 10^6$	$3.55 \times 10^6$	$3.55 \times 10^6$	$3.55 \times 10^6$
$D_{11}$	$1.55 \times 10^6$	$3.36 \times 10^5$	$7.42 \times 10^5$	$8.75 \times 10^5$
$D_{12}$	$1.50 \times 10^5$	$3.92 \times 10^5$	$3.12 \times 10^5$	$2.85 \times 10^5$
$D_{16}$	$4.74 \times 10^4$	$9.50 \times 10^4$	$1.42 \times 10^5$	0.0
$D_{22}$	$4.69 \times 10^5$	$1.20 \times 10^6$	$9.59 \times 10^5$	$8.75 \times 10^5$
$D_{26}$	$1.42 \times 10^5$	$2.81 \times 10^5$	$4.22 \times 10^5$	0.0
$D_{66}$	$1.63 \times 10^5$	$4.04 \times 10^5$	$3.23 \times 10^5$	$2.96 \times 10^5$

Lamina properties from table 4.1; unit thickness laminate units'  $A_{ij}$ -lb/in,  $D_{ij}$ -in-lb

The three laminates shown in table 4.3 are all quasi-isotropic. The membrane properties are isotropic and identical for each of the laminates. The bending stiffnesses can be seen to be a strong function of the thickness position of the plies. Additionally, bending stiffness calculations



based on homogeneity ( $D_{ij} = A_{ij} \frac{(2h)^2}{12}$ ) do not correspond to lamination theory calculations.

Thus, the simple relations between bending and extensional stiffnesses are lost and lamination theory must be used for bending properties. This table also demonstrates that quasi-isotropy holds only for extensional stiffnesses.

Another complication seen in table 4.3 involves the presence of the bending-twisting coupling terms,  $D_{16}$ ,  $D_{26}$ . The corresponding extensional-shear coupling terms are zero because of the presence of pairs of layers at  $+60^\circ$  and  $-60^\circ$  orientations. Noting that the bending-twisting terms can be of the same order of magnitude as the principal bending terms,  $D_{11}$ ,  $D_{22}$ ,  $D_{66}$ , it can be seen that the bending-twisting effect can be severe.

It was stated previously that bending-twisting terms can be reduced; this effect is demonstrated in table 4.4. Each of the laminates has 16 plies oriented at  $+60$  and  $-60$ . The differences between the laminates are due to the distribution of plies through the thickness. It is clearly evident that the bending-twisting terms are reduced as the plies at different orientations are distributed more uniformly through the thickness of the laminate. At the same time, the primary bending stiffnesses remain constant. Obviously, in a thick laminate the optimum configuration has the plies at different orientations distributed through the thickness unless, of course, the bending-twisting coupling is desired due to design considerations.

TABLE 4.4. BENDING-TWISTING COUPLING

Laminate	$D_{11}$	$D_{22}$	$D_{12}$	$D_{16}$	$D_{26}$	$D_{66}$
$[+60_4/-60_4]_s$	$2.60 \times 10^5$	$1.24 \times 10^6$	$3.88 \times 10^5$	$1.65 \times 10^5$	$4.74 \times 10^5$	$4.20 \times 10^5$
$[+60_2/-60_2]_{2s}$	$2.60 \times 10^5$	$1.24 \times 10^6$	$3.88 \times 10^5$	$8.25 \times 10^4$	$2.37 \times 10^5$	$4.20 \times 10^5$
$[\pm 60]_{4s}$	$2.60 \times 10^5$	$1.24 \times 10^6$	$3.88 \times 10^5$	$4.12 \times 10^4$	$1.19 \times 10^5$	$4.20 \times 10^5$

Ply thickness 0.0625 in lamina properties from table 4.1.  $D_{ij}$ -in-lb

Returning to the numerical example, the next step is to determine the laminate (B) and (D) matrices. It was stated previously that the (B) matrix is zero and this will now be demonstrated. Recalling from equation 4.35 the relation for (B),

$$[B] = \frac{1}{2} \sum_{i=1}^N [\bar{Q}^{(i)}] (z_i^2 - z_{i-1}^2)$$

$$\begin{aligned} B_{11} = & \frac{1}{2} \{ \bar{Q}_{11}^{(1)} [(-0.0156)^2 - (0.0208)^2] + \\ & \bar{Q}_{11}^{(2)} [(-0.0104)^2 - (0.0156)^2] + \\ & \bar{Q}_{11}^{(3)} [(-0.0052)^2 - (-0.0104)^2] + \\ & \bar{Q}_{11}^{(4)} [(0.0)^2 - (-0.0052)^2] + \\ & \bar{Q}_{11}^{(5)} [(0.0052)^2 - (0.0)^2] + \\ & \bar{Q}_{11}^{(6)} [(0.0102)^2 - (0.0052)^2] + \\ & \bar{Q}_{11}^{(7)} [(0.0156)^2 - (0.0102)^2] + \\ & \bar{Q}_{11}^{(8)} [(0.0208)^2 - (0.0156)^2] \} \end{aligned}$$

But,

$$\bar{Q}_{11}^{(1)} = \bar{Q}_{11}^{(8)}$$

$$\bar{Q}_{11}^{(2)} = \bar{Q}_{11}^{(7)}$$

$$\bar{Q}_{11}^{(3)} = \bar{Q}_{11}^{(6)}$$

$$\bar{Q}_{11}^{(4)} = \bar{Q}_{11}^{(5)}$$

Therefore

$$\begin{aligned} B_{11} = & \frac{1}{2} \{ \bar{Q}_{11}^1 [(0.0156)^2 - (0.0156)^2 + (0.0208)^2 - (0.0208)^2] \\ & + \bar{Q}_{11}^2 [(0.0156)^2 - (0.0156)^2 + (0.0104)^2 - (0.0104)^2] \\ & + \bar{Q}_{11}^3 [(0.0104)^2 - (0.0104)^2 + (0.0052)^2 - (0.0052)^2] \\ & + \bar{Q}_{11}^4 [(0.0)^2 - (0.0)^2 + (0.0052)^2 - (0.0052)^2] \\ & = 0.0 \end{aligned}$$

and

$$B_{12} = B_{16} = B_{22} = B_{26} = B_{66} = 0.0$$

Thus, for a symmetric laminate,  $(B) = 0$ .

The bending stiffnesses are found from equation 4.35 as

$$\begin{aligned} [D] &= \frac{1}{3} \sum_{i=1}^N [\bar{Q}]^i (z_i^3 - z_{i-1}^3) \\ D_{11} &= \frac{1}{3} \{ \bar{Q}_{11}^1 [(-0.0156)^3 - (0.0208)^3] + \\ &\quad \bar{Q}_{11}^2 [(-0.0104)^3 - (0.0156)^3] + \\ &\quad \bar{Q}_{11}^3 [(-0.0052)^3 - (-0.0104)^3] + \\ &\quad \bar{Q}_{11}^4 [(0.0)^3 - (-0.0052)^3] + \\ &\quad \bar{Q}_{11}^5 [(0.0052)^3 - (0.0)^3] + \\ &\quad \bar{Q}_{11}^6 [(0.0104)^3 - (0.0052)^3] + \\ &\quad \bar{Q}_{11}^7 [(0.0156)^3 - (0.0104)^3] + \\ &\quad \bar{Q}_{11}^8 [(0.0208)^3 - (0.0156)^3] \} \\ &= \frac{2}{3} [\bar{Q}_{11}^1 (5.2025 \times 10^{-6}) + \bar{Q}_{11}^2 (2.67155 \times 10^{-6}) \\ &\quad + \bar{Q}_{11}^3 (9.84256 \times 10^{-7}) + \bar{Q}_{11}^4 (1.40608 \times 10^{-7})] \\ &= 106.0 \\ [D] &= \begin{bmatrix} 106.0 & 17.2 & 6.59 \\ 17.2 & 26.9 & 6.59 \\ 6.59 & 6.59 & 18.1 \end{bmatrix} \text{ in-lb} \end{aligned}$$

The  $(D)$  matrix is seen to be fully populated even though the laminate is balanced and symmetric. The presence of the bending-twisting coupling terms is due to the different distances from the midsurface of the  $45^\circ$  and  $-45^\circ$  plies.

The full laminate stiffness matrix has been found to be

$$\left[ \begin{array}{ccc|ccc} \frac{A}{B} & - & \frac{B}{D} \\ \hline \end{array} \right] =$$

$4.38 \times 10^5$	$1.42 \times 10^5$	$0.0$	$0.0$	$0.0$	$0.0$
$1.42 \times 10^5$	$4.38 \times 10^5$	$0.0$	$0.0$	$0.0$	$0.0$
$0.0$	$0.0$	$1.48 \times 10^5$	$0.0$	$0.0$	$0.0$
<hr style="border-top: 1px dashed black;"/>					
$0.0$	$0.0$	$0.0$	$106.0$	$17.2$	$6.59$
$0.0$	$0.0$	$0.0$	$17.2$	$26.9$	$6.59$
$0.0$	$0.0$	$0.0$	$6.59$	$6.59$	$18.1$

$[A]$  lb/in;  $[D]$  in-lb

#### 4.4.2 Unsymmetric Laminates.

The use of laminates which are not midplane symmetric introduces some fundamental difficulties for the designer and analyst. The first and foremost of these is related to how one defines the membrane and bending stiffnesses of such a material. Because this type of laminate bends when subjected to membrane loading, how is an extensional modulus defined? Conversely, since the material extends when subjected to a bending load, how is a bending stiffness defined? Basically, there are two approaches to defining these elastic constants. A membrane stiffness can be derived either with zero curvatures or with zero bending moments and a bending stiffness can be defined with either zero membrane strains or zero membrane forces. In both cases, the stiffness defined will be greater when the bending-extensional coupling is restrained. The nature of the problem can sometimes help the designer to determine which approach to utilize.

In order to define stiffnesses of unsymmetric laminates with constrained bending-extensional coupling, it is necessary to use zero curvatures for extension and zero midplane strains for bending. Writing the full constitutive relations

$$\{N\} = [A] \{\epsilon^0\} + [B] \{\kappa\} \quad (4.38)$$

$$\{M\} = [B] \{\epsilon^0\} + [D] \{\kappa\}$$

the extensional stiffness can be found by substituting  $\{\kappa\} = 0$ ; thus

$$\{N\} = [A] \{\epsilon^0\} \quad (4.39)$$

and the bending stiffness can be found, substituting  $\{\epsilon^0\} = 0$

$$\{M\} = [D] \{\kappa\} \quad (4.40)$$

These relations are identical to those used in symmetric laminates and, therefore, the constrained stiffnesses are identical to those of symmetric laminates. It must be recognized, however, that moment resultants are required to develop the zero curvatures in equation 4.39 and stress resultants are required to develop the zero midplane strains in equation 4.40.

The moment resultants which are developed due to the prescribed zero curvatures can easily be determined. Solving equation 4.39 for the resulting midplane strains yields

$$\{\epsilon^0\} = [A]^{-1} \{N\} \quad (4.41)$$

Substituting these into the second of equation 4.38, and remembering that the curvatures are zero, yields

$$\{0\} = [B] \{\epsilon^0\}$$

or (4.42)

$$\{M\} = [B] [A]^{-1} \{N\}$$

Stress resultants developed due to midplane strain restraint can be found similarly. Thus,

$$\{\kappa\} = [D]^{-1} \{M\} \quad (4.43)$$

$$\{N\} = [B] \{\kappa\}$$

or

$$\{N\} = [B] [D]^{-1} \{M\} \quad (4.44)$$

Defining stiffnesses without constraining the bending-extensional coupling requires a little more effort. Referring to equation 4.37, the extensional stiffnesses can be found by specifying that  $\{M\} = 0$ . Therefore

$$\{0\} = [B] \{\epsilon^0\} + [D] \{\kappa\} \quad (4.45)$$

The curvatures can then be found to be

$$\{\kappa\} = - [D]^{-1} [B] \{\epsilon^0\} \quad (4.46)$$

Substituting these into the first of equation 4.38 yields

$$\{N\} = [A] \{\epsilon^0\} + [B] (-[D]^{-1} [B] \{\epsilon^0\})$$

or

$$\{N\} = ([A] - [B] [D]^{-1} [B]) \{\epsilon^0\} \quad (4.47)$$

or

$$\{N\} = [A^*] \{\epsilon^0\}$$

The effective laminate elastic constants (moduli and Poisson's ratio) can now be found using the relations (4.37) and the  $(A^*)$  matrix.

An effective bending stiffness matrix can be determined similarly by specifying  $\{N\} = 0$ . Thus

$$\{0\} = [A]^{-1} [B] \{\kappa\} \quad (4.48)$$

Now the midplane strains are seen to be

$$\{\epsilon^0\} = -[A]^{-1} [B] \{\kappa\} \quad (4.49)$$

and the second of relations (4.38) is rewritten as

$$\{M\} = (-[B] [A]^{-1} [B] + [D]) \{\kappa\}$$

or

$$\{M\} = [D^*] \{\kappa\} \quad (4.50)$$

yielding an effective bending stiffness matrix,  $(D^*)$ .

As stated earlier, the stiffness properties computed on the basis of constrained bending-extensional coupling are higher than those computed without this constraint. It can be shown that constrained properties are identical to symmetric properties. These two features are demonstrated in table 4.5, where elastic properties are listed with  $(M \neq 0)$  and without  $(M = 0)$  the constraint of the bending-extensional coupling effects. The laminate modelled is  $(0/\pm 45/90)$ ; hence, it is unsymmetric. The properties computed with zero curvature are seen to be quasi-isotropic. The properties computed with the moment resultants equal to zero are seen not to be quasi-isotropic, which is a result of the lack of symmetry. Also, the stiffnesses are considerably lower than the zero curvature properties in this particular case.

TABLE 4.5. BENDING EXTENSIONAL COUPLING EFFECTS ON STIFFNESS OF A (0/±45/90) GRAPHITE/EPOXY LAMINATE

$E_x$ (Msi)	$E_y$ (Msi)	$\nu_{xy}$	$G_{xy}$ (Msi)	$\frac{E_x}{2(1+\nu_{xy})}$ (Msi)	
9.42	9.42	0.325	3.55	3.55	$\{\kappa\} = 0$ $\{M\} \neq 0$
3.79	3.79	0.422	3.00	1.33	$\{\kappa\} \neq 0$ $\{M\} = 0$

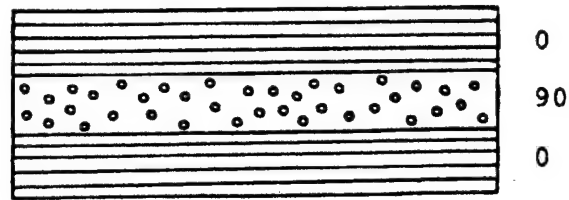
(See table 4.1 for lamina properties)

#### 4.4.3 Thermal Expansion.

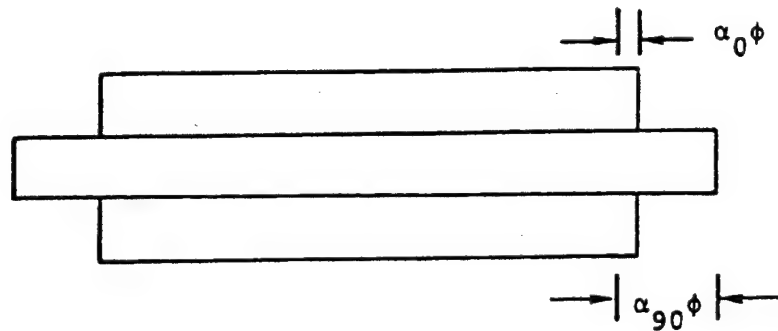
As the use of composite materials becomes more commonplace, they are subjected to mechanical and environmental loading conditions which are increasingly more severe and with the advent of high-temperature resin systems, the range of temperatures over which the composite system can be used has increased. Thus, it is necessary to understand the response of laminates to temperature and moisture as well as to applied loads. Previously, laminate extensional and bending stiffnesses were determined; in this section, laminate conductivities and expansivities will be defined.

The resulting thermoelastic (or hygro-thermoelastic) properties will be used subsequently for structural analysis in realistic environments. The results of such analyses will be the definition of stress and moment resultants throughout the structure. The use of these stress and moment resultants, in conjunction with the local through-the-thickness temperature (and/or moisture) gradients, to find laminate stresses will be treated in section 4.6.

The presence of stresses induced by free thermal expansion is new to the designer and analyst of conventional materials. The mechanism which produces such stresses is qualitatively described in figure 4.11, in which it can be seen that free laminae and bonded laminae (laminate) expand differently. In the direction shown, the 0° plies will develop tensile stress while the 90° ply will develop compressive stress due to the differences between the laminae and laminate thermal expansion coefficients. This effect is similar to heating a conventional material and providing constraints such that thermal expansion strains cannot develop.



#### HEATING OF FREE LAMINAE



#### HEATING OF LAMINATE

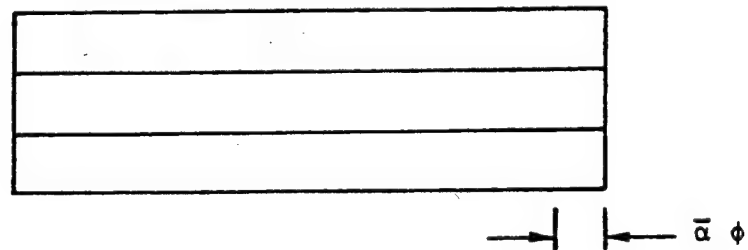


FIGURE 4.11. THERMALLY INDUCED LOADS

In order to quantitatively determine the laminate thermal expansion coefficients and thermally induced stresses, it is necessary to begin at the ply level. The thermoelastic relations for strain in the principal material directions are

$$\{\epsilon_t\} = \{\epsilon_t^M\} + \{\alpha_t\} \Delta T$$

or

$$\{\epsilon_t\} = \{\epsilon_t^M\} + \{\epsilon_t^T\}$$

(4.51)



The vector  $\{\alpha_i\}$  represents the free thermal expansion coefficients of a ply. The individual components are

$$\{\alpha_i\} = \begin{Bmatrix} \alpha_1 \\ \alpha_2 \\ 0 \end{Bmatrix} \quad (4.52)$$

and  $\Delta T$  represents a change in temperature. The thermal strains,  $\{\alpha_i\} \Delta T$ , are denoted by the superscript T and are lamina free thermal expansions. They produce no stress in an unconstrained lamina. The mechanical strains in (4.51) are denoted by the superscript M. The thermal expansion coefficients  $\alpha_1$  and  $\alpha_2$  are the effective coefficients and  $\alpha_L^*$  and  $\alpha_T^*$ , respectively, and are discussed in chapter 3.

Expressing the mechanical strain terms in terms of stresses, (4.51) yields

$$\{\epsilon_i\} = [S] \{\sigma_i\} + \{\alpha_i\} \Delta T \quad (4.53)$$

Inversion of these relations gives

$$\{\sigma_i\} = [S]^{-1} \{\epsilon_i\} - [S]^{-1} \{\alpha_i\} \Delta T$$

or

$$\{\sigma_i\} = [Q] \{\epsilon_i\} - \{\Gamma_i\} \Delta T \quad (4.54)$$

where

$$\{\Gamma_i\} = [Q] \{\alpha_i\}$$

By carrying out the indicated multiplication, the components in the thermal stress coefficient vector ( $\Gamma_i$ ) can be shown to be

$$\{\Gamma_i\} = \begin{Bmatrix} \frac{E_1 \alpha_1 + \nu_{12} E_2 \alpha_2}{\Delta} \\ \frac{E_2 \alpha_2 + \nu_{12} E_1 \alpha_1}{\Delta} \\ 0 \end{Bmatrix} \quad (4.55)$$

where

$$\Delta = 1 - \frac{E_2}{E_1} \nu_{12}^2$$

The vector  $\{\Gamma_i\} \Delta T$  physically represents a correction to the stress vector which results from the full constraint of the free thermal strains in a lamina.

Both the thermal expansion vector,  $\{\alpha_i\} \Delta T$ , and thermal stress vector,  $\{\Gamma_i\} \Delta T$ , can be transformed to an arbitrary coordinate system using the relations developed for stress and strain transformation, equations 4.8 and 4.9. Thus,

$$\{\epsilon_x^T\} = [\psi] \{\epsilon_i^T\} = [\psi] \{\alpha_i\} \Delta T = \{\alpha_x\} \Delta T$$

and (4.56)

$$\{\sigma_x\} = [\theta] \{\sigma_i\} = [\theta] [Q] \{\epsilon_i\} - [\theta] \{\Gamma_i\} \Delta T$$

or (4.57)

$$\{\sigma_x\} = [\bar{Q}] \{\epsilon_x\} - \{\Gamma_x\} \Delta T$$

Therefore

$$\{\alpha_x\} = [\psi] \{\alpha_i\} = \begin{Bmatrix} \alpha_1 m^2 + \alpha_2 n^2 \\ \alpha_1 n^2 + \alpha_2 m^2 \\ 2(\alpha_1 - \alpha_2)mn \end{Bmatrix} = \begin{Bmatrix} \alpha_x \\ \alpha_y \\ \alpha_{xy} \end{Bmatrix} \quad (4.58)$$

$$\{\Gamma_x\} = [\theta] \{\Gamma_i\} = \begin{Bmatrix} \Gamma_1 m^2 + \Gamma_2 n^2 \\ \Gamma_1 n^2 + \Gamma_2 m^2 \\ (\Gamma_1 - \Gamma_2)mn \end{Bmatrix} = \begin{Bmatrix} \Gamma_x \\ \Gamma_y \\ \Gamma_{xy} \end{Bmatrix} \quad (4.59)$$

and  $m = \cos \theta$ ,  $n = \sin \theta$ .

In both equations 4.58 and 4.59, shear terms have appeared due to the transformation. This is similar to the extensional-shear coupling developed in the transformed lamina stiffnesses. The presence of shear thermal expansions and stresses indicates that heating of an off-axis lamina will produce shear strains.

With the transformed thermal expansion and stress vectors, it is now possible to develop thermoelastic relations. Following directly the development of equations 4.26 - 4.34 and using equation 4.57 the membrane relations are

$$\{N\} = \int_{-h}^h \{\sigma_x\} dz = \int_{-h}^h ([\bar{Q}] \{\epsilon_x\} - \{\Gamma_x\} \Delta T) dz$$

or

$$\{N\} = \int_{-h}^h ([\bar{Q}] (\{\epsilon^0\} + z \{\kappa\}) - \{\Gamma_x\} \Delta T) dz$$

or

$$\{N\} = [A] \{\epsilon^0\} + [B] \{\kappa\} + \{N^T\} \quad (4.60)$$

where

$$\{N^T\} = - \int_{-h}^h \{\Gamma_x\} \Delta T dz \quad (4.61)$$

Similarly, the bending relations are

$$\{M\} = \int_{-h}^h \{\sigma_x\} z dz = \int_{-h}^h ([\bar{Q}] \{\epsilon_x\} - \{\Gamma_x\} \Delta T) z dz$$

or

$$\{M\} = \int_{-h}^h ([\bar{Q}] (\{\epsilon^0\} + z \{\kappa\}) - \{\Gamma_x\} \Delta T) z dz$$

or

$$\{M\} = [B] \{\epsilon^0\} + [D] \{\kappa\} + \{M^T\} \quad (4.62)$$

where

$$\{M^T\} = - \int_{-h}^h \{\Gamma_x\} \Delta T z dz \quad (4.63)$$

The integral relations for the thermal stress resultant vector ( $N^T$ ) and thermal moment resultant vector ( $M^T$ ) can be evaluated only when the change in temperature variation through the thickness is known. For the case of uniform temperature change through the thickness of the laminate, the term  $\Delta T$  is constant and can be factored out of the integration, yielding

$$\{N^T\} = -\Delta T \sum_{i=1}^N \{\Gamma_x\}^i (z_i - z_{i-1})$$

$$\{M^T\} = -\frac{1}{2} \Delta T \sum_{i=1}^N \{\Gamma_x\}^i (z_i^2 - z_{i-1}^2)$$

With the relations (4.60) and (4.62) it is possible to determine effective laminate coefficients of thermal expansion and thermal curvature. These quantities are the extension and curvature changes resulting from a uniform temperature distribution.

Noting that for free thermal effects the laminate is not subjected to any forces or moments, i.e.,  $\{N\} = \{M\} = 0$ , the relations (4.60) and (4.62) are written as

$$\{0\} = [A] \{\epsilon^0\} + [B] \{\kappa\} + \{N^T\} \quad (4.64)$$

$$\{0\} = [B] \{\epsilon^0\} + [D] \{\kappa\} + \{M^T\}$$

Defining a free the thermal expansion vector as

$$\{\alpha_x\} = \{\epsilon^0\} \frac{1}{\Delta T} \quad (4.65)$$

and a free thermal curvature vector as

$$\{\delta_x\} = \{\kappa\} \frac{1}{\Delta T} \quad (4.66)$$

the relations (4.64) are written as

$$\{0\} = [A] \{\alpha_x\} \Delta T + [B] \{\delta_x\} \Delta T + \{N^T\}$$

$$\{0\} = [B] \{\alpha_x\} \Delta T + [D] \{\delta_x\} \Delta T + \{M^T\}$$

After suitable matrix manipulations, the following expressions for thermal expansion,  $\alpha_x$ , and thermal curvature,  $\delta_x$ , are found:

$$\{\alpha_x\} = \frac{1}{\Delta T} [L_1]^{-1} ([B] [D]^{-1} \{M^T\} - \{N^T\}) \quad (4.67)$$

$$\{\delta_x\} = \frac{1}{\Delta T} [L_2]^{-1} ([B] [A]^{-1} \{N^T\} - \{M^T\}) \quad (4.68)$$

where

$$[L_1] = [A] - [B] [D]^{-1} [B]$$

$$[L_2] = [D] - [B] [A]^{-1} [B]$$

The relations (4.67) and (4.68) are seen to be complicated expressions containing the (A), (B) and (D) matrices. In many practical cases, the laminates of interest are symmetric, which simplifies the expressions considerably. For symmetric laminates, the bending-extensional coupling vanishes (i.e., (B) = 0), and the relations (4.67) and (4.68) are reduced to the form

$$\{\alpha_x\} = -\frac{1}{\Delta T} [A]^{-1} \{N^T\} \quad (4.69)$$

$$\{\delta_x\} = -\frac{1}{\Delta T} [D]^{-1} \{M^T\}$$

Examination of the relations for (M<sup>T</sup>), equation 4.63, shows that the symmetry which eliminates the (B) matrix also eliminates the (M<sup>T</sup>) vector. Thus

$$\{\delta_x\} = \{0\} \quad (4.70)$$

and no curvatures occur due to uniform temperature changes in symmetric laminates.

The relations for (α<sub>x</sub>) are functions of the (A) matrix, and as a result, the laminate thermal expansion coefficients are functions of the ply orientations. For illustration, the thermal expansion coefficients of the laminate treated in the example of the previous section will be determined.

In order to determine the laminate thermal expansion coefficients, it is again necessary to return to the laminae principal material coordinates. In this coordinate system, the free thermal expansion vector for each ply is identical and can be written directly. Referring to table 4.1, the thermal expansion vector in the principal material directions is

$$\{\alpha_i\} = \begin{Bmatrix} \alpha_1 \\ \alpha_2 \\ 0 \end{Bmatrix} = \begin{Bmatrix} -0.30 \times 10^{-6} \\ 19.5 \times 10^{-6} \\ 0.0 \end{Bmatrix} \quad \text{in/in/}^\circ\text{F}$$

Noting equations 4.54 and 4.55, the lamina thermal stress vector is

$$\{\Gamma_t\} = [Q] \{\alpha_t\}$$

$$\{\Gamma_t\} = \begin{bmatrix} 25.15 \times 10^6 & 5.13 \times 10^5 & 0.0 \\ & 1.71 \times 10^6 & 0.0 \\ \text{sym} & & 6.50 \times 10^5 \end{bmatrix} \begin{Bmatrix} -0.30 \times 10^{-6} \\ 19.5 \times 10^{-6} \\ 0.0 \end{Bmatrix}$$

$$= \begin{Bmatrix} 2.46 \\ 33.2 \\ 0.0 \end{Bmatrix} \text{ psi/}^\circ\text{F}$$

Transformation of the lamina thermal stress vector to the reference or laminate coordinate system is performed for each ply according to the relations (4.59). Thus, for the  $0^\circ$  plies

$$m=1 \quad n=0$$

$$\{\Gamma_x\} = [\theta] \{\Gamma_t\} = \{\Gamma_t\} = \begin{Bmatrix} 2.46 \\ 33.2 \\ 0.0 \end{Bmatrix} \text{ psi/}^\circ\text{F}$$

for the  $45^\circ$  plies

$$m = \frac{\sqrt{2}}{2} \quad n = \frac{\sqrt{2}}{2}$$

$$\{\Gamma_x\} = \begin{Bmatrix} 17.83 \\ 17.83 \\ -15.37 \end{Bmatrix} \text{ psi/}^\circ\text{F}$$

for the  $-45^\circ$  plies

$$m = \frac{\sqrt{2}}{2} \quad n = -\frac{\sqrt{2}}{2}$$

$$\{\Gamma_x\} = \begin{Bmatrix} 17.83 \\ 17.83 \\ 15.37 \end{Bmatrix} \text{ psi/}^\circ\text{F}$$

and finally for the  $90^\circ$  plies

$$m = 0 \quad n = 1$$

$$\{\Gamma_x\} = \begin{Bmatrix} 33.2 \\ 2.46 \\ 0.0 \end{Bmatrix} \text{ psi/}^\circ\text{F}$$

In order to determine the thermoelastic constitutive relations (4.60), the thermal stress resultant vector ( $N^T$ ) is determined using equation 4.61 and assuming a uniform temperature change.

$$\{N^T\} = -\Delta T \sum_{i=1}^N \{\Gamma_x\}^i (z_i - z_{i-1})$$

or

$$\{N^T\} = -\Delta T \sum_{i=1}^N \{\Gamma_x\}^i t_{ply}^i$$

and

$$N_{xx}^T = -2(0.0052) [(2.46+17.83+17.83+33.2)] \Delta T \text{ lb/in}$$

$$= -0.742\Delta T \text{ lb/in}$$

$$N_{yy}^T = -0.742\Delta T \text{ lb/in}$$

$$N_{xy}^T = 0.0 \text{ lb/in}$$

or

$$\{N^T\} = \Delta T \begin{Bmatrix} -0.742 \\ -0.742 \\ 0.0 \end{Bmatrix} \text{ lb/in}$$

Since the laminate under consideration here is symmetric, the (B) matrix and thermal moment resultant vector ( $M^T$ ) are zero. The laminate thermal expansion vector is determined utilizing the relation (4.69). Thus

$$\{\alpha_x\} = -\frac{1}{\Delta T} [A]^{-1} \{N^T\} = -\frac{1}{\Delta T} [a] \{N^T\}$$

$$\{\alpha_x\} = -\frac{1}{\Delta T} \begin{bmatrix} 2.55 \times 10^{-6} & -8.29 \times 10^{-7} & 0.0 \\ -8.29 \times 10^{-7} & 2.55 \times 10^{-6} & 0.0 \\ 0.0 & 0.0 & 6.76 \times 10^{-6} \end{bmatrix} \begin{Bmatrix} -0.742\Delta T \\ -0.742\Delta T \\ 0.0 \end{Bmatrix}$$

$$\{\alpha_x\} = \begin{Bmatrix} 1.28 \times 10^{-6} \\ 1.28 \times 10^{-6} \\ 0.0 \end{Bmatrix} \text{ in/in/}^\circ\text{F}$$

The laminate is seen to have equal thermal expansion coefficients in the x and y coordinate directions. The equal, orthogonal expansion coefficients, along with the zero shear thermal expansion coefficient, are sufficient for the laminate to be isotropic in thermal expansion in the plane of the laminate. This will be described more fully later in this section and a simpler, but more restricted, method for computing the laminate thermal properties will be described.

The variation of one term in the thermal expansion vector for a symmetric angle-ply laminate is shown in figure 4.12 to illustrate the effect of laminae orientation. At  $\theta = 0$ , the term  $\alpha_x$  is simply the axial lamina coefficient of thermal expansion, and at  $\theta = 90$ ,  $\alpha_x$  equals the lamina transverse thermal expansion coefficient. An interesting feature of the curve is the large negative value of  $\alpha_x$  in the region of  $30^\circ$ . Referring to figure 4.8, it is seen that the value of Poisson's ratio also behaves peculiarly in the region around  $30^\circ$ . The odd variation of both the coefficient of thermal expansion and Poisson's ratio stems from the magnitude and sign of the shear-extensional coupling present in the individual lamina.



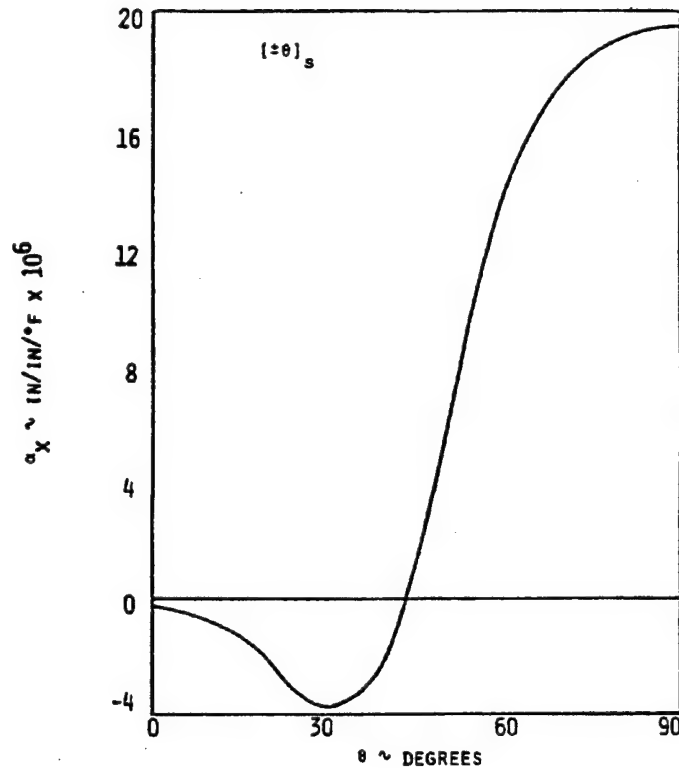


FIGURE 4.12. THERMAL EXPANSION COEFFICIENTS FOR HM-GRAPHITE/EPOXY

Referring to figure 4.13, it can be seen that the free thermal expansion of the  $+30^\circ$  ply produces a shear strain. In the laminate, however, this shear strain does not develop due to the constraint of the  $-30^\circ$  plies. Noting figure 4.9, it can be seen that an internally developed negative  $N_{xy}$  will produce the required shear constraint while at the same time generating a negative  $\epsilon_{xx}$ . The negative strain in the x direction corresponds to a large portion of the laminate thermal expansion coefficient  $\alpha_x$ . Thus, the extensional-shear coupling in the laminae is responsible for the large negative thermal expansion coefficients.

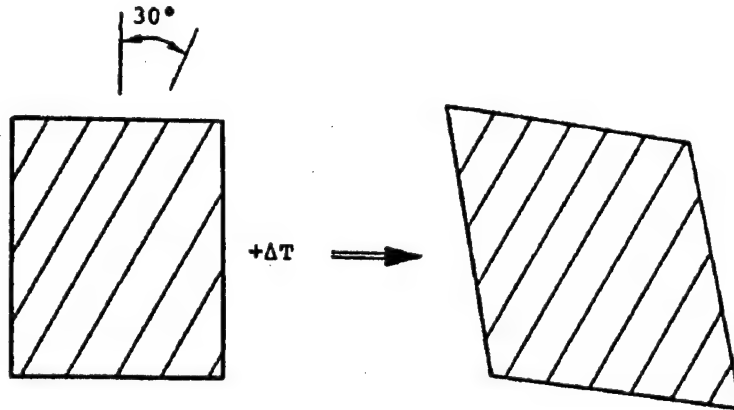


FIGURE 4.13. SHEAR THERMAL EXPANSION EFFECTS

Previously, certain classes of laminates were shown to have isotropic stiffnesses in the plane of the laminate. Similarly, laminates can be specified which are isotropic in thermal expansion within the plane of the laminate. The requirements for thermal expansion isotropy are considerably less restrictive than for elastic constants. In fact, any laminate which has two identical, orthogonal thermal expansion coefficients and a zero shear thermal expansion coefficient is isotropic in thermal expansion. Thus,  $(0/90)_s$  and  $(\pm 45)_s$  laminates are isotropic in thermal expansion even though they are not quasi-isotropic for elastic stiffnesses.

Laminates which are isotropic in thermal expansion have thermal expansions of the form

$$\{\alpha_x\} = \begin{Bmatrix} \alpha_x \\ \alpha_y \\ \alpha_{xy} \end{Bmatrix} = \begin{Bmatrix} \alpha^* \\ \alpha^* \\ 0 \end{Bmatrix} \quad (4.71)$$

where the term  $\alpha^*$  can be shown to be a function of lamina properties only, as follows:

$$\alpha^* = \alpha_1 + \frac{(\alpha_2 - \alpha_1)(1 + \nu_{12})}{1 + 2\nu_{12} + \frac{E_1}{E_2}}$$

Thus, all laminates of the same material which are isotropic in thermal expansion have identical expansion coefficients.

#### 4.4.4 Moisture Expansion.

The term hygro-elastic refers to the phenomenon in resin matrix composites when the matrix absorbs and desorbs moisture from and to the environment. The primary effect of moisture sorption is a volumetric change in the laminae. When a lamina absorbs moisture, it expands and when moisture is lost, the lamina contracts. Thus, the effect is very similar to thermal expansion.

In a lamina, a free moisture expansion coefficient vector can be defined as

$$\{\epsilon_i\} = \{\beta_i\} \Delta c \quad (4.72)$$

where

$$\{\beta_i\} = \begin{Bmatrix} \beta_1 \\ \beta_2 \\ 0 \end{Bmatrix}$$

and  $\Delta c$  is moisture change by weight. Noting that the relation (4.72) is identical to thermal expansion with  $\{\beta_i\}$  substituted for  $\{\alpha_i\}$  and  $\Delta c$  substituted for  $\Delta T$ , it can easily be seen that all of the relations developed for thermal effects can be used for moisture effects. It is required only that the substitutions mentioned be performed.

The procedure required to determine moisture gains or losses will be described in a later section. The analytical procedures detailed here allow for the prediction of moisture induced stresses when the percent moisture change is known for the laminae. As with the thermoelastic analysis, only elastic effects have been treated.

#### 4.4.5 Conductivity.

The conductivity (thermal or moisture) of a laminate in the direction normal to the surface is equal to the transverse conductivity of a unidirectional fiber composite. This follows from the fact that normal conductivity for all plies is identical and unaffected by the ply orientation.

The in-plane conductivities will be required for certain problems involving spatial variations of temperature and moisture. For a given uniform state of moisture in a laminate, the effective thermal conductivities in the  $x(\mu_x)$  and  $y(\mu_y)$  directions can be obtained by methods entirely analogous to those used for stiffnesses in section 4.3:

$$\mu_x = \frac{1}{2h} \sum_{i=1}^N (\mu_1 m^2 + \mu_2 n^2) t_{PLY}^i \quad (4.73)$$

$$\mu_y = \frac{1}{2h} \sum_{i=1}^N (\mu_1 n^2 + \mu_2 m^2) t_{PLY}^i \quad (4.74)$$

where

$\mu_1 =$	ply conductivity in the fiber direction
$\mu_2 =$	ply conductivity transverse to the fibers
$m =$	$\cos \theta^i$
$n =$	$\sin \theta^i$
$\theta^i =$	orientation of ply $i$
$t_{ply}^i =$	thickness of ply $i$
$N =$	the number of plies
$2h =$	laminate thickness

The results apply to symmetric as well as the unsymmetric laminates. The results for moisture conductivity are identical.

#### 4.5 THERMAL AND HYGROSCOPIC ANALYSIS.

This section is concerned with the distribution of temperature and moisture through the thickness of a laminate. The mathematical descriptions of these two phenomena are identical and the physical effects are similar. Some of these aspects have already been discussed in sections 3.1.4 and 4.4.5.

Moisture swelling and thermal mismatch effects occur at several levels in a fiber composite. In a unidirectional laminate, for example, residual stresses occur because of differential thermal expansion between the matrix and fibers. For present purposes, however, a free lamina (modelled as a homogeneous anisotropic material) may be considered to undergo stress-free deformation due to temperature change or moisture swelling. In a laminate, stress-free deformation is constrained by adjacent layers and this produces internal stresses. In addition to the swelling-induced stresses, temperature and moisture content also affect the properties of the material. These effects are primarily related to matrix dominated strength properties. Figure 4.14 [4.1] indicates that for this typical graphite/epoxy system, moisture has little or no effect on stiffness. Figures 4.15 and 4.16 [4.1] show a large variation in strength with the exception of axial tension. In each of these figures, the presence of moisture is seen to decrease the elevated temperature strengths of the material while having no detrimental effect or increasing the lower temperature strengths.

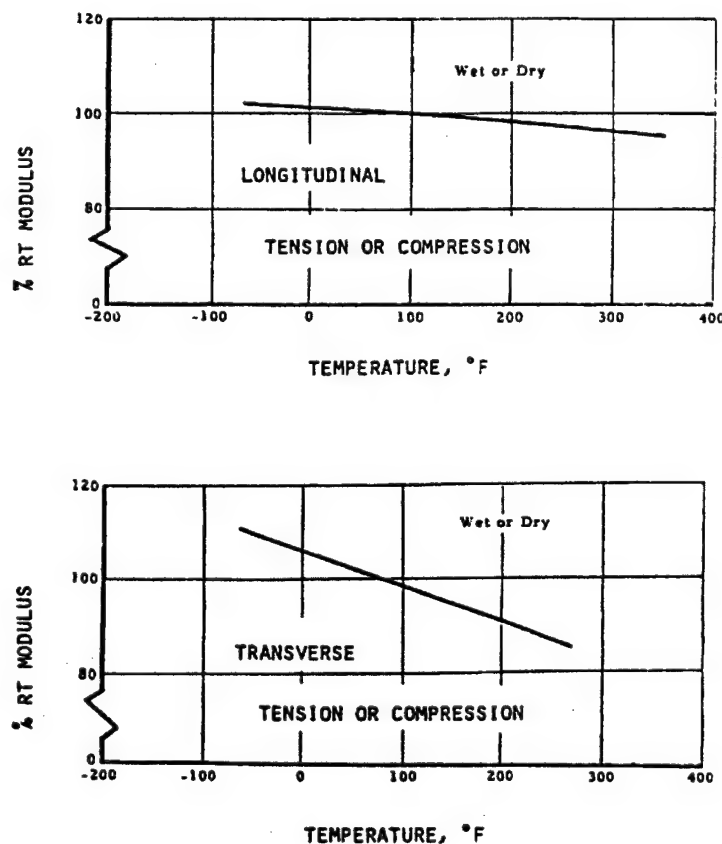


FIGURE 4.14. EFFECTS OF MOISTURE AND TEMPERATURE ON LAMINA STIFFNESS

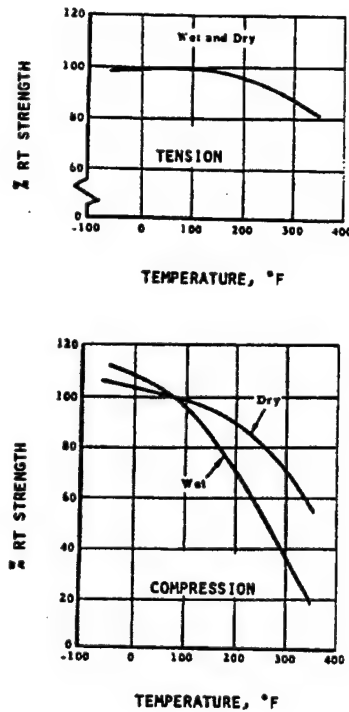


FIGURE 4.15. EFFECTS OF MOISTURE AND TEMPERATURE ON LAMINA LONGITUDINAL STRENGTH

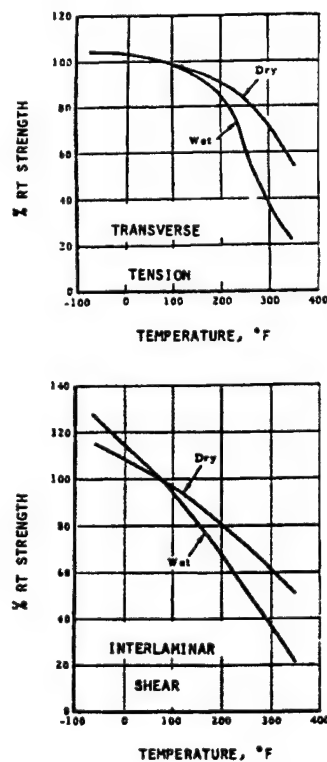


FIGURE 4.16. EFFECTS OF MOISTURE AND TEMPERATURE ON LAMINA MATRIX DOMINATED STRENGTHS

The principal strength degrading effect is related to a change in the glass transition temperature of the matrix material. As moisture is absorbed, the temperature at which the matrix changes from a glassy state to a viscous state decreases. Thus, the elevated temperature strength properties decrease with increasing moisture. Limited data suggest, however, that this process is reversible. When the moisture content of the composite is decreased, the glass transition temperature increases and the original strength properties return.

In all of these figures, wet indicates that the material is fully saturated. This condition corresponds to a state of equilibrium with the environment where the relative humidity is nearly 100%. The equilibrium moisture content at full saturation for typical epoxy composite systems ranges from about a 1.0% to 2.5% weight gain.

All of these considerations also apply in the case of temperature rise in the sense that the matrix and therefore the laminae lose stiffness and strength when the temperature rises.

Therefore, again, this effect is primarily important for the matrix dominated properties such as  $E_T$ ,  $G_L$ ,  $\sigma_T^u$ ,  $\sigma_T^{cu}$ , and  $\tau_L^u$ .

The differential equation governing time dependent moisture sorption of an orthotropic homogeneous material is given by

$$D_1 \frac{\partial^2 c}{\partial x_1^2} + D_2 \frac{\partial^2 c}{\partial x_2^2} + D_3 \frac{\partial^2 c}{\partial x_3^2} = \frac{\partial c}{\partial t} \quad (4.75)$$

where

$t$	=	time
$x_1, x_2, x_3$	=	coordinates in principal material directions
$c$	=	specific moisture concentration (see section 3.1.2)
$D_1, D_2, D_3$	=	moisture diffusivity coefficients

Equation 4.75 is based on Fick's law of moisture diffusion and is entirely analogous to the equation governing time dependent heat conduction with temperature replacing concentration  $c$  and thermal diffusivities  $\mu_1$ ,  $\mu_2$ , and  $\mu_3$  replacing the moisture diffusivities. For a transversely isotropic lamina with  $x_1$  in the fiber direction,  $x_2$  in the transverse direction and  $x_3 = z$  in the direction normal to the lamina, we have

$$\begin{aligned} D_1 &= D_L \\ D_2 &= D_3 = D_T \end{aligned} \quad (4.76)$$

These quantities are analogous to the thermal conductivities of a unidirectional fiber composite and have been discussed in section 3.1.4.

An important special case is one-dimensional diffusion or conduction through the thickness of a lamina. In this case (4.75) reduces to

$$D_T \frac{\delta^2 c}{\delta z^2} = \frac{\delta c}{\delta t} \quad (4.77)$$

This equation also applies to moisture diffusion or thermal conduction through a laminate in the direction normal to its laminae planes, since all laminae are homogeneous in the  $z$  direction with equal diffusion coefficients,  $D_T = D_z$ .

Equation 4.77 is applicable to the important problem of time dependent moisture diffusion through a laminate where the two faces are in different moisture environments. After a sufficiently long time has elapsed, the concentration settles down to a time independent, so-called stationary, state. In this state, since  $c$  is no longer time dependent, (4.77) simplifies to

$$\frac{d^2 c}{dz^2} = 0$$

Thus  $c$  is a linear function of  $z$  and if the laminate faces are in environments with constant saturation concentrations  $c_1$  and  $c_2$  then

$$c = \frac{1}{2} [(c_2 - c_1) z/h + c_2 + c_1] \quad (4.78)$$

where the laminate thickness is  $2h$  and  $z$  originates in the middle surface.

In the important case where  $c_2 = c_1$ , (4.78) reduces to

$$c = c_1 = \text{constant} \quad (4.79)$$

The above discussion of moisture also applies to heat conduction.

Solutions to the time dependent problem (4.77) are readily available and considerable work has been performed in the area of moisture sorption by Springer [4.2]. The most interesting feature of the solutions to equation 4.77 relates to the magnitude of the coefficient  $D_z$ . The coefficient  $D_z$  is a measure of how fast moisture diffusion can occur. In typical epoxy matrix systems,  $D$  is of the order of  $10^{-8} \left(\frac{\text{in}^2}{\text{s}}\right)$  to  $10^{-10} \left(\frac{\text{in}^2}{\text{s}}\right)$ . The diffusion coefficient is sufficiently small, so that full saturation of a resin matrix composite may require months or years to occur even when subjected to 100% relative humidity.

A correlation between analytical and experimental investigations is presented in figure 4.17. The effects of elevated temperature on the rate of diffusion and maximum moisture content are clearly evident. Additionally, reference 4.3 indicates that applied stress may cause variation in moisture diffusion. Obviously, the diffusion of moisture, thermal effects, and loading are coupled, and an

analysis including all of the effects would be desirable. The development of such a solution, however, has been precluded by its complexity.

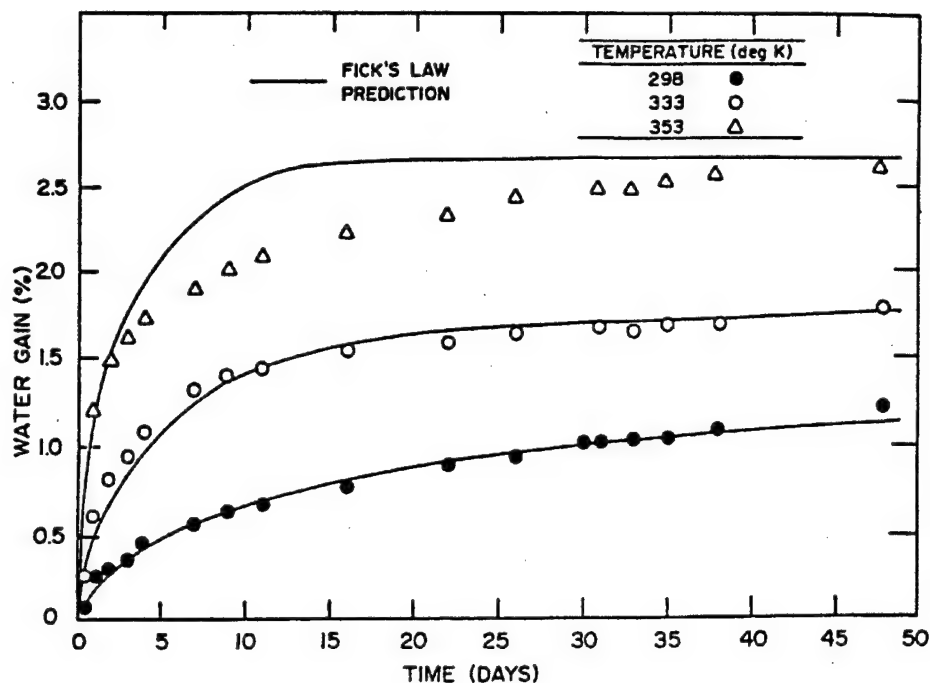


FIGURE 4.17. MOISTURE AS A FUNCTION OF EXPOSURE TIME FOR SP-313 CROSSPLY LAMINATE [4.3]

The approach typically taken for design purposes is to assume a worst case scenario. If the material is assumed to be fully saturated, it is possible to compute reduced allowable strengths. This is a conservative approach, as typical service environments do not generate full saturation. It is utilized since it allows for inclusion of the effects of moisture in a relatively simple fashion. It is to be expected that as the design data base and analytical methodologies mature, more physically realistic methods will be developed. At present, however, the conservative approach is appropriate.

In the case of heat conduction, the time required to achieve the stationary state, an analog of saturation, is extremely rapid compared to characteristic times for moisture diffusion, and thus the transient time dependent state is typically of no practical importance for laminates. There are, of course, rapid heating situations in which transient thermal response may be of importance.

#### 4.6 LAMINATE STRESS ANALYSIS.

The physical properties defined in section 4.4 enable any laminate to be represented by an equivalent homogeneous anisotropic plate or shell element for the purpose of structural analysis. The procedures to be used for this analysis will be discussed in Volume II. The results of such analyses will be the definition of stress resultants, bending moments, temperature, and moisture at any point on the surface defining the plate. (Temperature and moisture distributions through



the thickness of the plate will also be defined when they exist.) With this definition of the local values of the state variables, the analyst next performs a laminate analysis to determine the state of stress in each lamina in order to assess margins for each critical design condition.

#### 4.6.1 Stresses due to Mechanical Loads.

In order to determine stresses in the individual plies, it is necessary to use the laminate midplane strain and curvature vectors. Writing the laminate constitutive relations

$$\begin{Bmatrix} N \\ - \\ M \end{Bmatrix} = \begin{bmatrix} A & B \\ --- & --- \\ B & D \end{bmatrix} \begin{Bmatrix} \epsilon^0 \\ - \\ \kappa \end{Bmatrix} \quad (4.80)$$

it can be seen that a simple inversion of the 6X6 stiffness matrix will yield the required relations for  $(\epsilon^0)$  and  $(\kappa)$ . Thus

$$\begin{Bmatrix} \epsilon^0 \\ - \\ \kappa \end{Bmatrix} = \begin{bmatrix} A & B \\ --- & --- \\ B & D \end{bmatrix}^{-1} \begin{Bmatrix} N \\ - \\ M \end{Bmatrix} \quad (4.81)$$

Given the strain and curvature vectors, the total strain in the laminate can be written as

$$\{\epsilon_x\}^i = \{\epsilon^0\} + z \{\kappa\} \quad (4.82)$$

The strains at any point through the laminate thickness are now given as the superposition of the midplane strains and the curvatures multiplied by the distance from the midplane. Thus, the strain field at the center of ply  $i$  in a laminate can be seen to be

$$\{\epsilon_x\}^i = \{\epsilon^0\} + \frac{1}{2} \{\kappa\} (z^i + z^{i+1}) \quad (4.83)$$

where the term

$$\frac{1}{2} (z^i + z^{i+1})$$

corresponds to the distance from the midplane to the center of ply  $i$ . It is possible to define curvature induced strains at a point through the laminate thickness simply by specifying the distance to the point in question from the midplane.

The strains defined in equation 4.83 correspond to the arbitrary laminate coordinate system. These strains can be transformed into the principal material coordinates for this ply utilizing the transformations developed previously (4.10). Thus

$$\{\epsilon_i\}^i = [\Psi^i]^{-1} \{\epsilon_x\}^i \quad (4.84)$$

where the superscript  $i$  indicates which ply and, therefore, which angle of orientation is to be used. The orientations of different plies may be different, and therefore, it is necessary to utilize the transformation matrix corresponding to the proper ply orientation.

With the strains in the principal material coordinates defined, stresses in these same coordinates are written using the lamina reduced stiffness matrix (4.6). Thus

$$\{\sigma_i\}^i = [Q^i] \{\epsilon_i\}^i \quad (4.85)$$

Again, it is important that the stiffness matrix used correspond to the correct ply, as each ply may be of a different material.

The stresses in the principal material coordinates can be determined without the use of principal material strains. Using the strains defined in the laminate coordinates (4.83) and the transformed lamina stiffness matrix (4.13, 4.15, and 4.16), stresses in the laminate coordination system are written as

$$\{\sigma_x\}^i = [\bar{Q}^i] \{\epsilon_x\}^i \quad (4.86)$$

and these stresses are then transformed to the principal material coordinates using the relations (4.10). Thus

$$\{\sigma_i\}^i = [\theta^i]^{-1} \{\sigma_x\}^i \quad (4.87)$$

For the case of symmetric laminates and membrane loading, the curvature vector is zero. This implies that the laminate coordinate strains are identical in each ply and equal to the midplane strains. However, the differing angular orientation of the various plies will promote different stress and strain fields in the principal material coordinates of each ply.

For the purpose of illustrating the stress analysis procedures, it is now appropriate to return to the laminate example considered in section 4.4.1 (figure 4.10). The applied loadings to be used in this example are

$$\{N\} = \begin{Bmatrix} N_{xx} \\ 0.0 \\ 0.0 \end{Bmatrix} lb/in; \quad \{M\} = \begin{Bmatrix} 0.0 \\ 0.0 \\ 0.0 \end{Bmatrix} in-lb/in$$

Since the  $(0/\pm 45/90)_s$  laminate is symmetric and only membrane loadings are applied, the curvatures are zero and the membrane response is uncoupled from the bending response. Thus, the membrane relations can be written directly:

$$\{N\} = [A] \{\epsilon^0\}$$

The solution for the midplane strain vector is found by inversion

$$\begin{aligned} \{\epsilon^0\} &= [A]^{-1} \{N\} \\ \begin{Bmatrix} \epsilon_{xx}^0 \\ \epsilon_{yy}^0 \\ 2\epsilon_{xy}^0 \end{Bmatrix} &= \begin{bmatrix} 2.55 \times 10^{-6} & -8.29 \times 10^{-7} & 0.0 \\ -8.29 \times 10^{-7} & 2.55 \times 10^{-6} & 0.0 \\ 0.0 & 0.0 & 6.76 \times 10^{-6} \end{bmatrix} \begin{Bmatrix} N_{xx} \\ 0.0 \\ 0.0 \end{Bmatrix} \\ &= N_{xx} \begin{Bmatrix} 2.55 \times 10^{-7} \\ -8.29 \times 10^{-7} \\ 0.0 \end{Bmatrix} \text{ in/in} \end{aligned}$$

Since the curvature vector ( $\kappa$ ) is zero, the strains in each ply in the laminate coordinate system are identical to the midplane strains. Thus

$$\{\epsilon_x\}^i = \{\epsilon^0\}$$

Stresses in the laminate coordinate system can be computed for each ply using the relations

$$\{\sigma_x\}^i = [\bar{Q}^i] \{\epsilon_x\}^i$$

For the  $0^\circ$  plies

$$\begin{aligned} \begin{Bmatrix} \sigma_{xx} \\ \sigma_{yy} \\ \sigma_{xy} \end{Bmatrix} &= \begin{bmatrix} 25.15 \times 10^6 & 5.131 \times 10^5 & 0.0 \\ 5.131 \times 10^5 & 1.71 \times 10^6 & 0.0 \\ 0.0 & 0.0 & 0.65 \times 10^5 \end{bmatrix} \begin{Bmatrix} 2.55 \times 10^{-6} \\ -8.29 \times 10^{-7} \\ 0.0 \end{Bmatrix} N_{xx} \\ &= N_{xx} \begin{Bmatrix} 63.7 \\ -0.11 \\ 0.0 \end{Bmatrix} \text{ psi} \end{aligned}$$

In the 45° plies

$$\{\sigma_x\} = \begin{bmatrix} 7.62 \times 10^6 & 6.32 \times 10^6 & 5.86 \times 10^6 \\ 6.32 \times 10^6 & 7.62 \times 10^6 & 5.86 \times 10^6 \\ 5.86 \times 10^6 & 5.86 \times 10^6 & 6.45 \times 10^6 \end{bmatrix} \begin{Bmatrix} 2.55 \times 10^{-6} \\ -8.29 \times 10^{-7} \\ 0.0 \end{Bmatrix} N_{xx}$$

$$= N_{xx} \begin{Bmatrix} 14.20 \\ 9.80 \\ 10.10 \end{Bmatrix} \text{ psi}$$

In the -45° plies

$$\{\sigma_x\} = N_{xx} \begin{Bmatrix} 14.20 \\ 9.80 \\ -10.10 \end{Bmatrix} \text{ psi}$$

In the 90° plies

$$\{\sigma_x\} = N_{xx} \begin{Bmatrix} 3.94 \\ -19.54 \\ 0.0 \end{Bmatrix} \text{ psi}$$

One should note that for a chosen value of  $N_{xx}$  equal to unity (i.e., 1 lb/inch), the layer stresses are equal to those given by the numerical figures within the brackets in the expressions given above. For this value of  $N_{xx}$  ( $= 1$ ), the average stress in the eight-ply laminate of total thickness 0.0416 inch is 24.04 psi. The layer stresses given above are in laminate coordinates.

With stresses defined in the laminate coordinate system, the appropriate transformations will determine the principal material coordinate stresses

$$\{\sigma_t\}^i = [\theta^i]^{-1} \{\sigma_x\}^i$$

In the  $0^\circ$  plies

$$\begin{Bmatrix} \sigma_{11} \\ \sigma_{22} \\ \sigma_{12} \end{Bmatrix} = \begin{bmatrix} m^2 & n^2 & 2mn \\ n^2 & m^2 & -2mn \\ -mn & mn & m^2 - n^2 \end{bmatrix} \begin{Bmatrix} 63.7 \\ -0.11 \\ 0.0 \end{Bmatrix} N_{xx}$$

$$m = \cos(0) = 1$$

$$n = \sin(0) = 0$$

$$\{\sigma_i\} = N_{xx} \begin{Bmatrix} 63.7 \\ -0.11 \\ 0.0 \end{Bmatrix} \text{psi}$$

In the  $45^\circ$  plies

$$m = \frac{\sqrt{2}}{2} \quad n = \frac{\sqrt{2}}{2}$$

$$\{\sigma_i\} = \begin{bmatrix} \frac{1}{2} & \frac{1}{2} & 1 \\ \frac{1}{2} & \frac{1}{2} & -1 \\ -\frac{1}{2} & \frac{1}{2} & 0 \end{bmatrix} \begin{Bmatrix} 14.20 \\ 9.80 \\ 10.10 \end{Bmatrix} N_{xx} \text{psi}$$

$$\{\sigma_i\} = N_{xx} \begin{Bmatrix} 22.10 \\ 1.90 \\ -2.20 \end{Bmatrix} \text{psi}$$

In the  $-45^\circ$ plies

$$m = \frac{\sqrt{2}}{2} \quad n = -\frac{\sqrt{2}}{2}$$

$$\{\sigma_t\} = N_{xx} \begin{Bmatrix} 22.10 \\ 1.90 \\ 2.20 \end{Bmatrix} \text{ psi}$$

In the  $90^\circ$  plies

$$m = 0$$

$$n = 1$$

$$\{\sigma_t\} = N_{xx} \begin{Bmatrix} -22.10 \\ 3.94 \\ 0.0 \end{Bmatrix} \text{ psi}$$

The stresses in the principal material coordinates can be found in a different fashion described below. The principal material coordinate strains can be determined using the relations

$$\{\epsilon_t\}^i = [\psi^i]^{-1} \{\epsilon_x\}^i$$

Then the principal material coordinate stresses are found using the lamina constitutive relations

$$\{\sigma_t\}^i = [Q^i] \{\epsilon_t\}^i$$

The resulting principal material coordinate stresses are identical using either approach.

#### 4.6.2 Stresses due to Temperature and Moisture.

In section 4.4.3, equations for the thermoelastic response of composite laminates were developed. It was indicated that thermal loading in laminates will cause stresses within the plies even when the laminate is allowed to expand freely. The stresses are induced because of a mismatch in thermal expansion coefficients between plies oriented in different directions.

It should be pointed out that composite laminates are usually manufactured at a temperature higher than room temperature. An estimate of residual stresses in a laminate at room temperature (or any other temperature) may be obtained assuming that the laminate is stress free at a temperature close to the processing or curing temperature. These stresses may have some influence on failure of laminates.

In order to determine the magnitude of thermally induced stresses, the thermoelastic constitutive relations (4.60 and 4.62) are required. Noting that free thermal effects require that  $\{N\} = \{M\} = 0$ , these relations are written as

$$\begin{Bmatrix} 0 \\ - \\ 0 \end{Bmatrix} = \begin{bmatrix} A & | & B \\ \hline & & \\ B & | & D \end{bmatrix} \begin{Bmatrix} \epsilon^0 \\ - \\ \kappa \end{Bmatrix} + \begin{Bmatrix} N^T \\ - \\ M^T \end{Bmatrix} \quad (4.88)$$

Inverting these relations yields the free thermal strain and curvature vectors for the laminate

$$- \begin{bmatrix} A & | & B \\ \hline & & \\ B & | & D \end{bmatrix}^{-1} \begin{Bmatrix} N^T \\ - \\ M^T \end{Bmatrix} = \begin{Bmatrix} \epsilon^0 \\ - \\ \kappa \end{Bmatrix} \quad (4.89)$$

Proceeding as before, the strain field in any ply is written as

$$\{\epsilon_x\}^i = \{\epsilon^0\} + z^i \{\kappa\} \quad (4.90)$$

Recalling equation 4.57, stresses in the laminate coordinates are written as

$$\{\sigma_x\}^i = [\bar{Q}^i] \{\epsilon_x\}^i - \{\Gamma_x\}^i \Delta T^i \quad (4.91)$$

which can then be transformed to the principal material coordinates. Thus

$$\{\sigma_t\}^i = [\theta^i]^{-1} \{\sigma_x\}^i \quad (4.92)$$

As was shown for mechanically induced loadings, the stresses can be found in an alternate fashion. Transforming the strains of equation 4.90 directly yields

$$\{\epsilon_t\}^i = [\psi^i]^{-1} \{\epsilon_x\}^i \quad (4.93)$$

Recalling equation 4.54, stresses in the principal material coordinates are written as

$$\{\sigma_t\}^i = [Q^i] \{\epsilon_t\}^i + \{\Gamma_t\}^i \Delta T \quad (4.94)$$

Returning to the laminate example problems, stresses due to thermal loadings can now be determined. For this example, a uniform temperature change  $\Delta T$  is applied. Since the temperature is uniform and the laminate is symmetric, the midplane strain vector is simply

$$\{\epsilon^0\} = \{\alpha_x\} \Delta T = \Delta T \begin{Bmatrix} 1.28 \times 10^{-6} \\ 1.28 \times 10^{-6} \\ 0.0 \end{Bmatrix}$$

and the curvature vector ( $\kappa$ ) is zero.

The strains in each ply in the laminate coordinates are

$$\{\epsilon_x\}^i = \{\epsilon^0\}$$

Stresses in the laminate coordinates are found using the thermoelastic constitutive relations

$$\{\sigma_x\}^i = [\bar{Q}^i] \{\epsilon_x\}^i - \{\Gamma_x\}^i \Delta T$$

In the  $0^\circ$  plies

$$\{\sigma_x\} = \begin{bmatrix} 25.15 \times 10^6 & 5.131 \times 10^5 & 0.0 \\ 5.131 \times 10^5 & 1.71 \times 10^6 & 0.0 \\ 0.0 & 0.0 & 6.5 \times 10^5 \end{bmatrix} \begin{Bmatrix} 1.28 \times 10^{-6} \\ 1.28 \times 10^{-6} \\ 0.0 \end{Bmatrix} \Delta T$$

$$- \begin{Bmatrix} 2.46 \\ 33.2 \\ 0.0 \end{Bmatrix} \Delta T$$

$$\{\sigma_x\} = \Delta T \begin{Bmatrix} 30.4 \\ -30.4 \\ 0.0 \end{Bmatrix} \text{ psi}$$



In the 45° plies

$$\{\sigma_x\} = \begin{bmatrix} 7.62 \times 10^6 & 6.32 \times 10^6 & 5.86 \times 10^6 \\ 6.32 \times 10^6 & 7.62 \times 10^6 & 5.86 \times 10^6 \\ 5.86 \times 10^6 & 5.86 \times 10^6 & 6.45 \times 10^6 \end{bmatrix} \begin{Bmatrix} 1.28 \times 10^{-6} \\ 1.28 \times 10^{-6} \\ 0.0 \end{Bmatrix} \Delta T$$

$$\{\sigma_x\} = \Delta T \begin{Bmatrix} 0.0 \\ 0.0 \\ 30.4 \end{Bmatrix} \text{ psi} - \begin{Bmatrix} 17.83 \\ 17.83 \\ -15.37 \end{Bmatrix} \Delta T$$

In the -45° plies

$$\{\sigma_x\} = \Delta T \begin{Bmatrix} 0.0 \\ 0.0 \\ -30.4 \end{Bmatrix} \text{ psi}$$

In the 90° plies

$$\{\sigma_x\} = \Delta T \begin{Bmatrix} -30.4 \\ 30.4 \\ 0.0 \end{Bmatrix} \text{ psi}$$

Transforming these stresses into the principal material coordinates yields

$$0^\circ \text{ plies} \quad \{\sigma_l\} = \Delta T \begin{Bmatrix} 30.4 \\ -30.4 \\ 0.0 \end{Bmatrix} \text{ psi}$$

$$45^\circ \text{ plies} \quad \{\sigma_i\} = \Delta T \begin{Bmatrix} 30.4 \\ -30.4 \\ 0.0 \end{Bmatrix} \text{ psi}$$

$$-45^\circ \text{ plies} \quad \{\sigma_i\} = \Delta T \begin{Bmatrix} 30.4 \\ -30.4 \\ 0.0 \end{Bmatrix} \text{ psi}$$

$$90^\circ \text{ plies} \quad \{\sigma_i\} = \Delta T \begin{Bmatrix} 30.4 \\ -30.4 \\ 0.0 \end{Bmatrix} \text{ psi}$$

Examination of the principal material coordinate stresses reveals that all plies have identical stress fields in this example. This is related to the fact that the laminate is isotropic in thermal expansion. A simplified method for computing ply stresses in laminates which are isotropic in thermal expansion will be discussed later in this section.

Some interesting physical interpretations can be obtained by restricting the discussion to uniform temperature fields and symmetric laminates. In the presence of these restrictions, the coupling matrix, (B), and the thermal moment resultant vector,  $\{M^T\}$ , vanish and

$$\{\epsilon^0\} = \{\alpha_x\} \Delta T$$

and

$$\{\kappa\} = \{0\}$$

The strains in the laminate coordinates are identical in each ply. Thus

$$\{\epsilon_x\}^i = \{\epsilon^0\} = \{\alpha_x\} \Delta T \quad (4.95)$$

Recalling equation 4.57, laminate coordinate stresses are written as

$$\{\sigma_x\}^i = [\bar{Q}^i] \{\epsilon_x\}^i + \{\Gamma_x\}^i \Delta T$$

or

$$\{\sigma_x\}^i = [\bar{Q}^i] \{\alpha_x\} \Delta T + \{\Gamma_x\}^i \Delta T \quad (4.96)$$

The terms  $\{\Gamma_x\}$  can be written as

$$\begin{aligned}\{\Gamma_x\}^t &= [\theta^t] \{\Gamma_t\}^t = [\theta^t] [Q^t] \{\alpha_t\}^t \\ &= [\theta^t] [Q^t] [\psi^t]^{-1} \{\alpha_x\}^t \\ &= [\bar{Q}^t] \{\alpha_x\}^t\end{aligned}\tag{4.97}$$

Therefore

$$\{\sigma_x\}^t = [\bar{Q}^t] (\{\alpha\} - \{\alpha_x\}^t) \Delta T\tag{4.98}$$

These relations indicate that stresses induced by the free thermal expansion of a laminate are related to the differences between the laminate and ply thermal expansion vectors. Thus, the stresses are proportional to the difference between the amount the ply would freely expand and the amount the laminate will allow it to expand.

A further simplification can be found if the laminate under investigation is isotropic in thermal expansion. It can be shown for this class of laminates, subjected to a uniform temperature change, that the stresses in the principal material coordinates are identical in every ply. The stress vector can be shown to be

$$\{\sigma_t\} = \frac{E_{11} (\alpha_{22} - \alpha_{11}) \Delta T}{1 + 2\nu_{12} + \frac{E_{11}}{E_{22}}} \begin{Bmatrix} 1 \\ -1 \\ 0 \end{Bmatrix}\tag{4.99}$$

where it can be seen that the transverse direction stress is equal and opposite to the fiber direction stress. This is of importance because unidirectional transverse material strengths are typically an order of magnitude lower than fiber direction strengths.

A similar development can be generated for moisture induced stresses. All of the results of this section apply when the moisture swelling coefficients,  $(\beta_t)$ , are substituted for the thermal expansion coefficients,  $(\alpha_t)$ .

#### 4.6.3 Netting Analysis.

Another approach to the calculation of ply stresses is sometimes used for membrane loading of laminates. This procedure is netting analysis and, as the name implies, treats the laminate as a net; i.e., all loads are carried in the fibers while the matrix material is present only to hold the geometric position of the fibers.

Since only the fibers are assumed to load in this analytical model, stress-strain relations in the principal material directions can be written as

$$\sigma_{11} = E_1 \epsilon_{11}$$

or

$$\epsilon_{11} = \frac{1}{E_1} \sigma_{11} \quad (4.100)$$

and

$$E_2 = G_{12} = \sigma_{22} = \sigma_{12} = 0$$

The transformation for stress and strain are considerably simplified due to the restriction that only one component of stress and strain exists in the principal material directions. Thus

$$\{\sigma_x\} = \begin{Bmatrix} \sigma_{xx} \\ \sigma_{yy} \\ \sigma_{xy} \end{Bmatrix} = \sigma_{11} \begin{Bmatrix} m^2 \\ n^2 \\ mn \end{Bmatrix} \quad (4.101)$$

or

$$\{\sigma_x\} = \sigma_{11} \{\theta_N\}$$

and

$$\{\epsilon_x\} = \begin{Bmatrix} \epsilon_{xx} \\ \epsilon_{yy} \\ 2\epsilon_{xy} \end{Bmatrix} = \epsilon_{11} \begin{Bmatrix} m^2 \\ n^2 \\ 2mn \end{Bmatrix} \quad (4.102)$$

or

$$\{\epsilon_x\} = \epsilon_{11} \{\psi_N\}$$

where  $m = \cos\theta$  and  $n = \sin\theta$ . It is interesting that in the arbitrary coordinate system, three components of stress and strain can exist, while in the principal material directions only fiber direction stresses and strains exist.

The transformation vector  $(\theta_N)$  in equations 4.101 and  $(\psi_N)$  in 4.102 are simply the first columns of the transformation matrices defined earlier (4.8 and 4.9). The netting analysis transformation

is a special case of that used in lamination theory. Noting the similarities between lamination theory and netting analysis, a transformed stiffness matrix for netting analysis can be written directly. Referring to equations 4.15 and noting that only the  $Q_{11}$  terms exist, the transformed netting analysis stiffness matrix can be written as

$$\{\sigma_x\} = [\bar{Q}_N] \{\epsilon_x\} \quad (4.103)$$

where

$$[\bar{Q}_N] = E_1 \begin{bmatrix} m^4 & m^2 n^2 & m^3 n \\ m^2 n^2 & n^4 & n^3 m \\ m^3 n & n^3 m & m^2 m^2 \end{bmatrix} \quad (4.104)$$

Utilizing equation 4.103, a laminate membrane stiffness matrix can be defined as before. Thus

$$\{N\} = \int_{-h}^h \{\sigma_x\} dz = \sum_{i=1}^N [\bar{Q}_N]^i (z_i - z_{i-1}) \{\epsilon^0\} = [A_N] \{\epsilon^0\} \quad (4.105)$$

The laminate stiffnesses predicted with a netting analysis will be smaller than those predicted using lamination theory. This is due to exclusion of the transverse and shear stiffnesses from the formulation. This effect is demonstrated in table 4.6 for a quasi-isotropic laminate comprised of high modulus graphite/epoxy. The stiffness properties predicted using a netting analysis are on the order of 10% smaller than lamination theory predictions. Experimental work has consistently shown that lamination theory predictions are more realistic.

TABLE 4.6. LAMINATE ELASTIC CONSTANTS

Analysis	$E_x$ psi	$E_y$ psi	$G_{xy}$ psi	$\nu_{xy}$
Lamination Theory	$9.42 \times 10^6$	$9.42 \times 10^6$	$3.55 \times 10^6$	0.325
Netting Analysis	$8.33 \times 10^6$	$8.33 \times 10^6$	$3.13 \times 10^6$	0.333

Unit Thickness HM - Graphite/Epoxy

Although the stiffness predictions using netting analyses are of limited value, the analysis can be used as an approximation of the response of a composite in which the matrix has been damaged. In this sense it may be considered a worst case analysis and is frequently used to predict ultimate strengths of composite laminates. This will be discussed more fully in the section on Strength and Failure.

#### 4.6.4 Interlaminar Stresses.

The analytical procedures which have been developed in this chapter can be used to predict stresses within each lamina in a laminate. The stresses predicted are plain due to the assumed state of plane stress. There are cases where the assumption of plane stress is not valid and a three-dimensional stress analysis is required.

An example of such a case exists at certain free edges in laminates where stress free boundary conditions must be imposed. To illustrate this, consider the laminate shown in figure 4.18. When this laminate is subjected to a membrane loading in the  $x$  direction, Poisson's ratio mismatches between the  $0^\circ$  plies and the  $\pm 60^\circ$  plies will introduce a stress in the  $y$  direction in each ply. In addition, shear-extension coupling effects will generate equal but opposite shear stresses in the  $60^\circ$  and  $-60^\circ$  plies. Referring to figure 4.18, it can be seen that all  $\sigma_y$  and  $\sigma_{xy}$  stresses must vanish at  $y = \pm b$  in order that the stress free boundary conditions be satisfied. These conditions cannot be satisfied with lamination theory; a three-dimensional analysis is required.

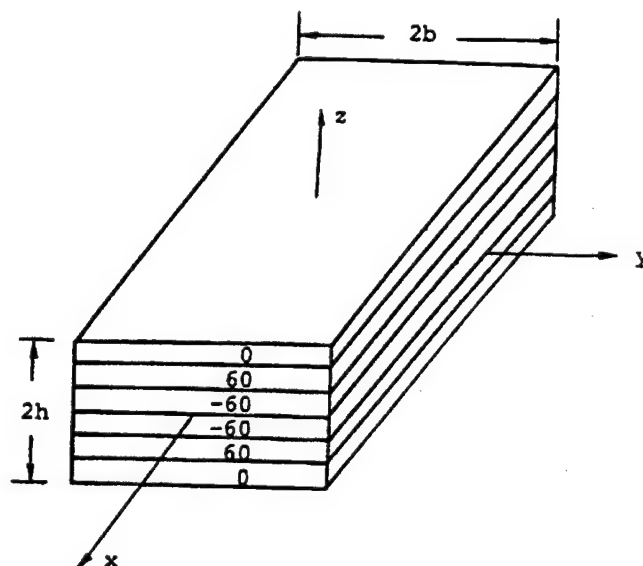


FIGURE 4.18. LAMINATE CONSTRUCTION, INTERLAMINAR STRESS EXAMPLE

Using equilibrium and symmetry considerations, it is, however, possible to visualize the other components of stress which arise at the free edge. In figure 4.19, lamination theory stresses are shown for the uniaxial loading discussed above. As indicated in figure 4.19, the laminate analysis satisfies equilibrium in the  $y$  direction but not the conditions at the free boundary. Thus, additional forces are required to satisfy the boundary conditions. For example, in the  $0^\circ$  plies, a compressive  $\sigma_y$  is predicted using lamination theory. This does not satisfy the boundary condition locally. A second, self-equilibrating set of edge stresses may be regarded as a superposed stress field which brings the lamination theory stresses to the necessary boundary values. Thus, an interlaminar shear stress  $\sigma_{yz}$  develops between the  $0^\circ$  and  $60^\circ$  plies. This introduces an  $x$  moment disequilibrium even though the  $y$  direction force equilibrium has been

satisfied. In order to achieve x moment equilibrium, a couple is needed. The required couple develops as an interlaminar normal stress distribution which in figure 4.20 is seen to be compressive at  $y = b$ . In order that a couple develop, the normal stress must change sign as the distance from the free edge increases.

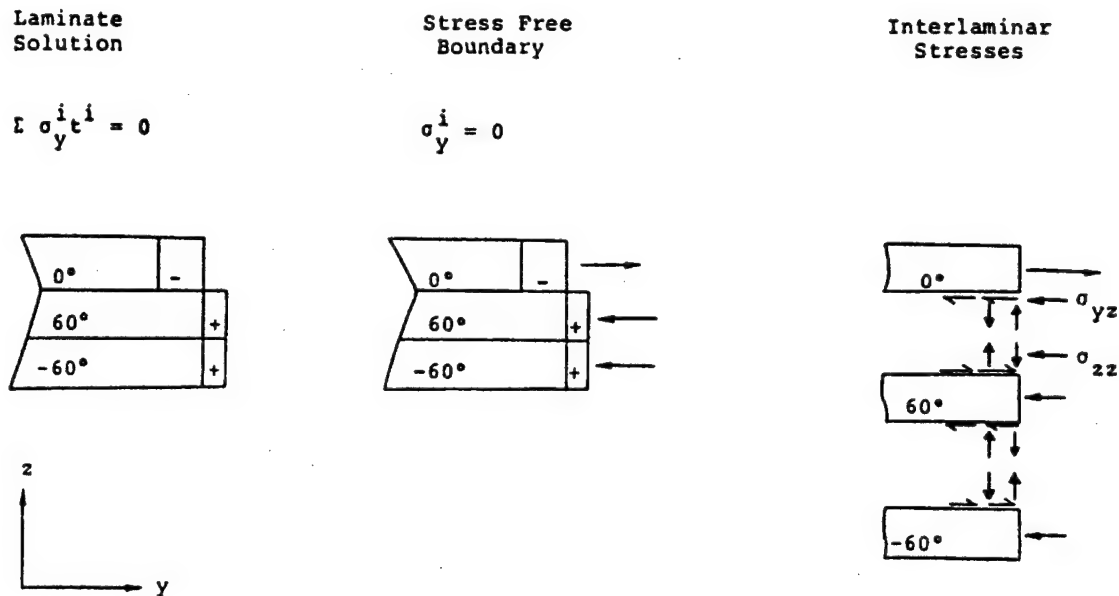


FIGURE 4.19. EQUILIBRIUM AND BOUNDARY CONDITIONS

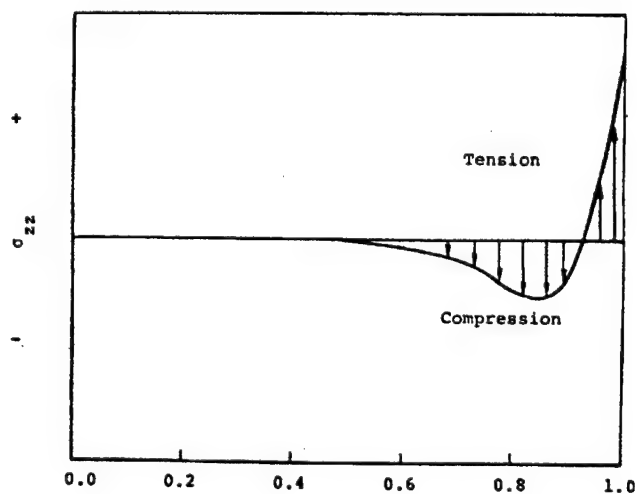


FIGURE 4.20. INTERLAMINAR NORMAL STRESSES AND MOMENT EQUILIBRIUM

In figure 4.21, a similar situation exists with respect to the in-plane shear stresses  $\sigma_{xy}$ . At the free edge  $y = b$ , these stresses must vanish. Therefore, the other component of interlaminar shear stress,  $\sigma_{xz}$ , develops, and the stress free boundary conditions are satisfied. In each case, it is seen that lamination theory satisfies strain compatibility and equilibrium while the interlaminar stresses satisfy the stress free boundary conditions.

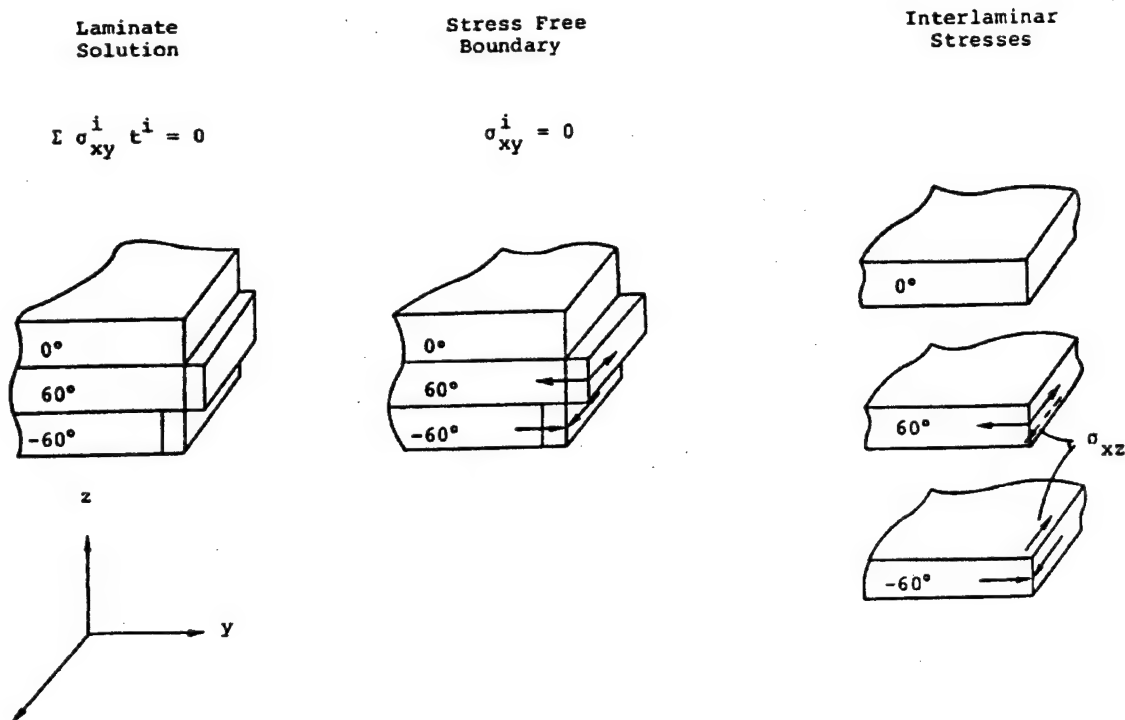


FIGURE 4.21. X EQUILIBRIUM AND BOUNDARY CONDITIONS

The elasticity solution to predict edge stresses was developed by Pipes and Pagano [4.4]. Because of the complexity of the problem, numerical solution techniques were used.

Figure 4.22 shows results published in reference 4.4. The laminate is of  $(\pm 45)_s$  configuration. The only ply stresses which develop according to lamination theory are  $\sigma_{xx}$  and  $\sigma_{xy}$ . There are no Poisson contraction induced stresses, as the  $45^\circ$  and  $-45^\circ$  plies have identical values for  $\nu_{xy}$ . In figure 4.22, a quantitative evaluation of the effects described in figure 4.21 is illustrated. The in-plane shear stress  $\sigma_{xy}$  is zero at the free edge  $y = b$  while the interlaminar shear stress  $\sigma_{xz}$  is maximum there.

One feature which is not apparent in the qualitative depiction in figure 4.21 is the variation of  $\sigma_{xx}$ . The difference between lamination theory and the three-dimensional solution is seen to diminish as the distance from the free edge increases. These results indicate that the variations are a boundary layer effect [4.4]. All of the stress components which are introduced or modified near the free edge vanish at a distance of approximately the plate thickness from the edge. Near the free edge, all six components of stress exist due to the physical three-dimensionality of the problem. It may be seen from figure 4.22 that the extensional stress  $\sigma_{xx}$  and the in-plane shear stress  $\sigma_{xy}$  both reduce from the laminate theory solution as the free edge is approached. It may be noted that  $\sigma_{xy}$  has to be zero at the edge. The interlaminar shear stress  $\sigma_{xz}$  (at and near the



interface between  $+45^\circ$  and  $-45^\circ$  plies), however, shows a rapid increase near the edge. Of the three stress components not shown in figure 4.22, the interlaminar shear stress  $\sigma_{yz}$  and the extensional stress  $\sigma_{zz}$  are small over a large range of  $y/b$  and they are of significance very near the edge. It has been shown that some of the interlaminar stress components ( $\sigma_{zz}$  and  $\sigma_{xz}$  in this problem) can be shown to be singular (approach infinity) because of the mixed boundary conditions present (stress-free condition at the free edge and displacement as well as traction continuities at the  $+45/-45$  interface), provided of course, that each of the plies is modeled as a homogeneous elastic material [4.5]. Severity of such stress intensification will possibly reduce due to the presence of the resin rich layer, but some of the stresses will reach high values near the edge. Such stress peaks can cause interlaminar damages which may grow catastrophically or in a constrained fashion. Fracture mechanics based approaches can be employed to examine such damage growth possibilities, but the types of the interlaminar stress fields are also useful for design purposes such that damage growth can be avoided. This aspect is discussed in the following paragraphs.

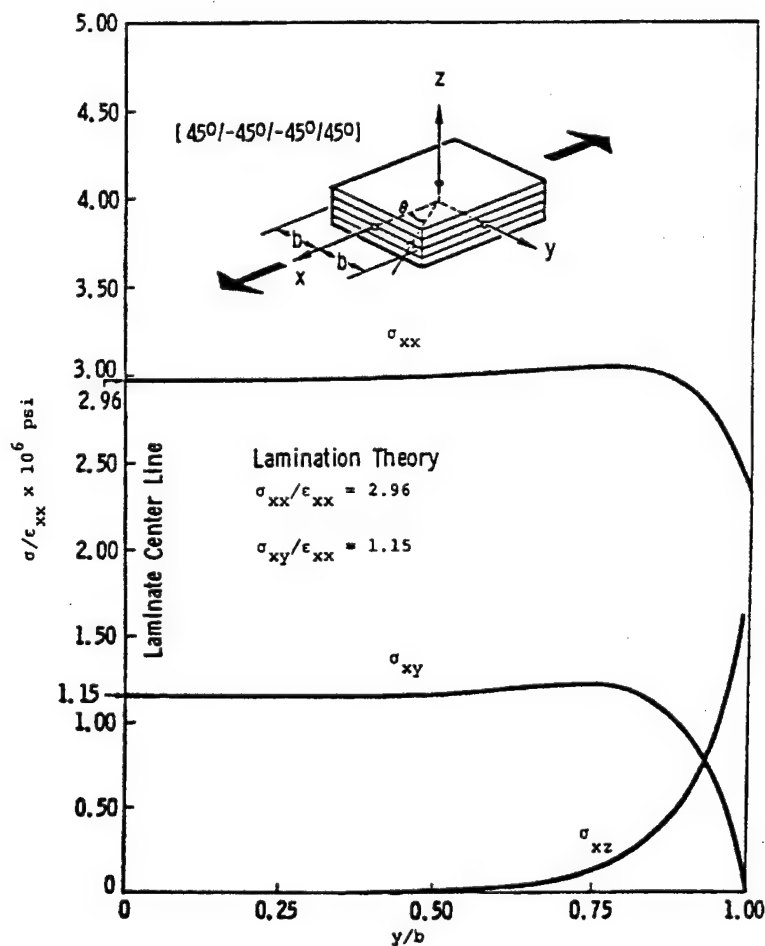


FIGURE 4.22. INTERLAMINAR STRESS NORMALIZED WITH RESPECT TO THE APPLIED STRAIN [4.4]

In figures 4.23 and 4.24 [4.6], results of three-dimensional analyses for two laminates are shown. Here the configurations are both crossply such that only the  $\sigma_{zz}$  and  $\sigma_{yz}$  interlaminar stress components are significant. Figure 4.23 depicts interlaminar normal stresses which demonstrate the couple which was qualitatively described in figures 4.19 and 4.21. A noteworthy feature in these figures is that the results for the  $(0/90)_s$  laminate are exactly opposite to the results for the  $(90/0)_s$  laminate. This response of the two laminates can be explained by referring back to figure 4.19. Examining only the outermost ply, it is obvious that the sign of the  $\sigma_{yy}$  stress component will be different if the ply is oriented at  $0^\circ$  rather than  $90^\circ$ . This reverses the sign of the interlaminar shear stress  $\sigma_{yz}$  which, in turn, reverses the direction of the moment disequilibrium which is balanced by  $\sigma_{zz}$  stresses. If the sign of the applied loading  $\epsilon_{xx}$  were reversed, then these stress curves would reverse and the  $(0/90)_s$  response in compression would be identical to the  $(90/0)_s$  tensile response.

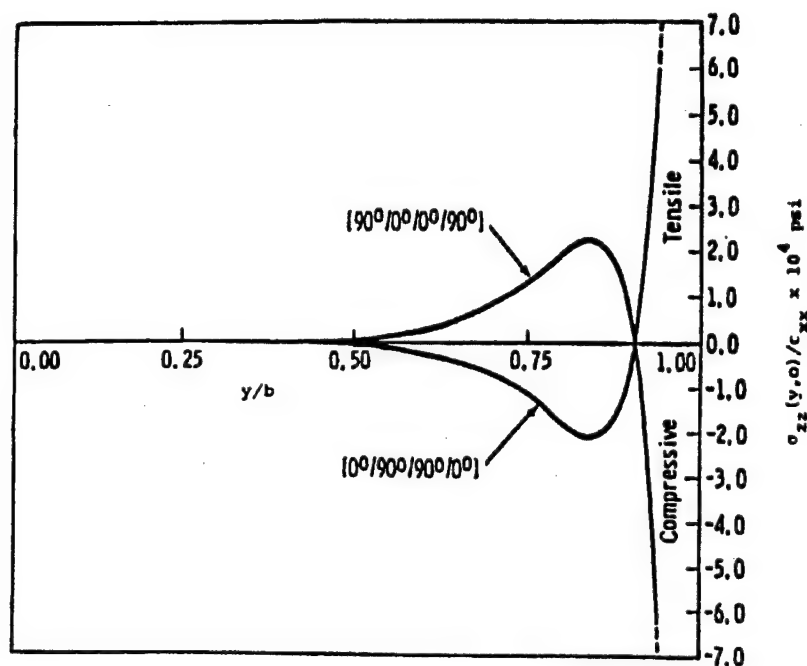


FIGURE 4.23. INTERLAMINAR NORMAL STRESSES AND STACKING SEQUENCE NORMALIZED WITH RESPECT TO THE APPLIED STRAIN [4.6]

The sign of the interlaminar normal stress at the free edge can be of great importance. As can be inferred from the previous discussions, large Poisson's ratio mismatch between plies produces large interlaminar normal stresses. If these stresses are tensile, the laminate may split between plies or delaminate under membrane loading. Obviously, if the laminate is designed such that expected loadings will produce only compressive interlaminar normal stresses at the free edges, then delamination will not occur.

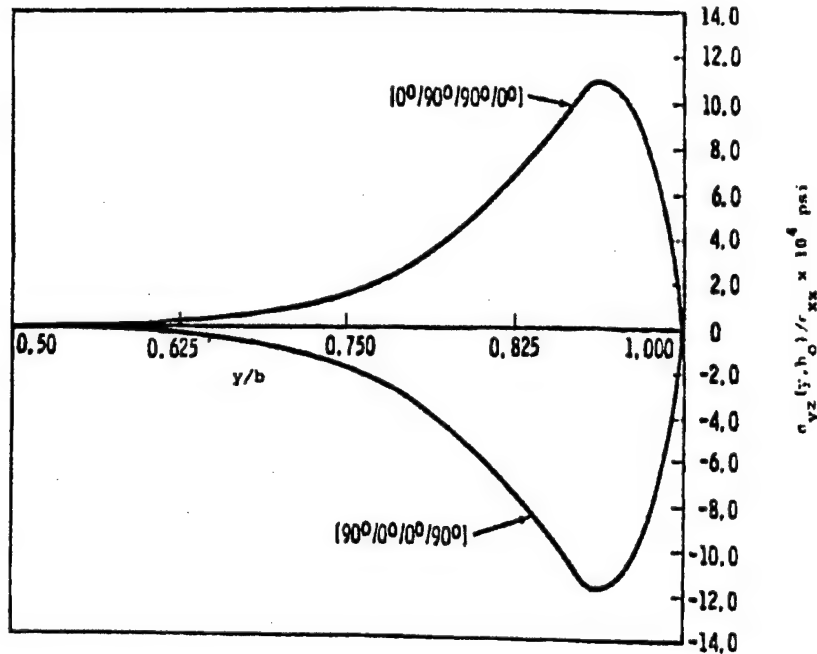


FIGURE 4.24. INTERLAMINAR SHEAR STRESSES AND STACKING SEQUENCE NORMALIZED WITH RESPECT TO THE APPLIED STRAIN [4.6]

The free edge problem occurs wherever ply stresses must become zero to satisfy boundary conditions. Thus, any free edge, including holes, may introduce interlaminar stresses. The consequences of these stresses obviously need to be evaluated for structural applications, particularly where fatigue loadings are present. This topic will be discussed later in the section on fatigue. It can become extremely complex to provide quantitative analytical treatment of free edge stresses in all but the most simple geometric shapes. In most cases, the possibility of delaminations due to the effects of free edge stresses is tested experimentally.

#### 4.6.5 Nonlinear Stress Analysis.

All of the preceding material in this chapter has related to laminae which behave in a linear elastic fashion. Yet composites can behave in a nonlinear fashion because of such factors as the occurrence of internal damage or because of the nonlinear stress-strain behavior of the polymeric matrix. Matrix nonlinearity (or microcracking) can result in laminae which have nonlinear stress-strain curves for transverse stress or axial shear stress. When this situation exists, it becomes necessary to replace the elastic laminate stress analysis of section 4.6.1 by a nonlinear analysis. An approach for such analysis for monotonic quasi-static loading has been presented in reference 4.7.

A suitable representation of nonlinear one-dimensional stress-strain relations has been given by Ramberg and Osgood [4.8]. For uniaxial stress, for example:

$$\epsilon = \frac{\sigma}{E} \left[ 1 + k \left( \frac{\sigma}{\sigma'} \right)^{m-1} \right] \quad (4.106)$$

where  $E$  represents the elastic Young's modulus, and  $k$ ,  $\sigma'$ , and  $m$  are three parameters to be obtained by curve fitting. The parameter  $\sigma'$  is sometimes called nominal yield stress. Equation 4.106 represents a family of curves with initial slope  $E_1$  and monotonically decreasing slope with increasing  $\sigma$ . The curves flatten out with increasing  $m$  (figure 4.25). Similarly, a stress-strain curve in shear can be represented in

$$\gamma = \frac{\tau}{G} \left[ 1 + \left( \frac{\tau}{\tau'} \right)^{n-1} \right] \quad (4.107)$$

where  $G$  is the elastic shear modulus.

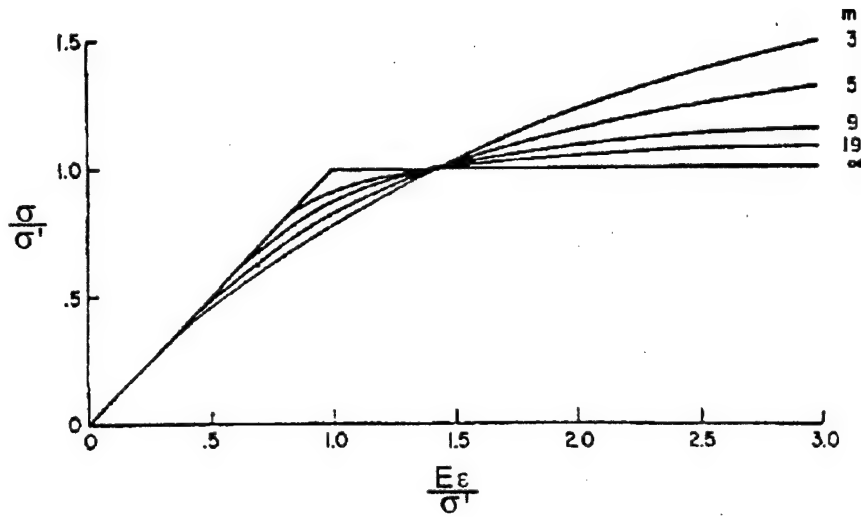


FIGURE 4.25. NONDIMENSIONAL RAMBERG-OSGOOD STRESS-STRAIN CURVES

It should be emphasized that (4.106) and (4.107) are valid only for one-dimensional cases. The question of their application to general states of stress and strain is discussed subsequently. For the case of a uniaxially reinforced material in which the matrix is nonlinear (with stress-strain relations in Ramberg-Osgood form) and the composite is subjected to uniaxial average stress  $\sigma_{22}$  in a direction transverse to the fibers

$$\epsilon_{22} = S_{22}(\sigma_{22}) \sigma_{22} \quad (4.108)$$

where the notation indicates that  $S_{22}$  is a function of  $\sigma_{22}$ . Similarly, if the only nonvanishing average stress is a  $\sigma_{12}$ , the shear stress-strain relation of the composite is given by (with  $S_{66}$  a function of  $\sigma_{12}$ )

$$2\epsilon_{12} = S_{66}(\sigma_{12}) \sigma_{12} \quad (4.109)$$

The inelastic effective compliances  $S_{22}$  and  $S_{66}$  are functions of the parameters of the inelastic Ramberg-Osgood stress-strain relations of the matrix, of the elastic properties of the fibers, and of the internal geometry of the composite. Actual prediction is a very difficult problem. However, just as matrix stress-strain relations are represented in Ramberg-Osgood form, the same type of curve fitting can also be applied for the effective stress-strain relations of the composite. Thus (4.108) and (4.109) are written in the form

$$\epsilon_{22} = \frac{\sigma_{22}}{E_T} \left[ 1 + \left( \frac{\sigma_{22}}{\sigma_y} \right)^{M-1} \right] \quad (4.110a)$$

$$2\epsilon_{12} = \frac{\sigma_{12}}{G_A} \left[ 1 + \left( \frac{\sigma_{12}}{\tau_y} \right)^{N-1} \right] \quad (4.110b)$$

where  $E_T$  is the effective transverse elastic Young's modulus;  $G_A$  the effective axial elastic shear modulus; and  $\sigma_y$ ,  $\tau_y$ ,  $M$ , and  $N$  are curve fitting parameters which may differ from the corresponding Ramberg-Osgood matrix parameters.

A question of fundamental and practical importance is the form of the stress-strain relations for the case of plane stress, taking into account interaction among the various stress components. It should be noted in this respect that (4.110) are special stress-strain relations which apply when  $\sigma_{22}$  or  $\sigma_{12}$  act only by themselves.

Since the total strain can be conveniently divided into linear strain  $\epsilon'_{ij}$  and nonlinear strain  $\epsilon''_{ij}$ , the total strain is given by adding both of these components:

$$\epsilon_{ij} = \epsilon'_{ij} + \epsilon''_{ij} \quad (4.111)$$

The linear strains  $\epsilon'_{ij}$  are given as before by equation 4.5. By assuming that the stress in the fiber direction  $\sigma_{11}$  is carried predominantly by the fiber alone with insignificant matrix contribution, while on the other hand the transverse stress  $\sigma_{22}$  and the shear stress  $\sigma_{12}$  are primarily carried by the matrix with little fiber contribution, the nonlinear strains are given by

$$\begin{aligned} \epsilon'_{11} &= 0 \\ \epsilon''_{22} &= S''_{22}(\sigma_{22}, \sigma_{12}) \sigma_{22} \\ 2\epsilon''_{12} &= S''_{66}(\sigma_{22}, \sigma_{12}) \sigma_{12} \end{aligned} \quad (4.112)$$

The final form of the Ramberg-Osgood equations for the inelastic strain components of such plane stress-strain relations were shown in reference 4.7 to be as follows

$$\begin{aligned}\epsilon''_{11} &= 0 \\ \epsilon''_{22} &= \frac{\sigma_{22}}{E_T} \left[ \left( \frac{\sigma_{22}}{\sigma_y} \right)^2 + \left( \frac{\sigma_{12}}{\tau_y} \right)^2 \right]^{\frac{M-1}{2}} \\ 2\epsilon''_{12} &= \frac{\sigma_{12}}{G_A} \left[ \left( \frac{\sigma_{22}}{\sigma_y} \right)^2 + \left( \frac{\sigma_{12}}{\tau_y} \right)^2 \right]^{\frac{N-1}{2}}\end{aligned}\tag{4.113}$$

The parameters  $E_T$ ,  $G_A$ ,  $\sigma_y$ ,  $\tau_y$ ,  $M$ , and  $N$  in (4.113) are those of the one-dimensional stress-strain relations (4.110) which may be regarded as experimentally (or perhaps theoretically) known.

The stress-strain relations defined by (4.111), (4.5), and (4.113) are used in the laminate analysis in place of (4.5). For an  $N$ -layered laminate, the stress resultants corresponding to (4.26) are given by

$$\sum_{k=1}^N \sigma_{ij}^{(k)} t_k = \begin{Bmatrix} N_{xx} \\ N_{yy} \\ N_{xy} \end{Bmatrix} \quad (ij = 1,1, 1,2 \text{ or } 2,2) \tag{4.114}$$

Also, a set of compatibility equations are defined in the form

$$\epsilon_{ij}^{(k)} = \epsilon_{ij}^{(k-1)} \quad k = 1, 2, \dots, N \tag{4.115}$$

The three equations given by (4.114) and the  $3N$  equations 4.115 define  $3N$  equations in the  $3N$  unknown stress components. It has been shown in reference 4.7 that these resulting equations can be reduced in a straightforward fashion to an efficient computer program for evaluation of laminate stress-strain behavior. The conclusions of that study were that practical composite laminates having fibers oriented in three or more directions showed little difference in their overall stress-strain curves for inelastic behavior as compared with the corresponding elastic results. Ply stresses will be different, however, and this may be of some importance. In particular, when thermal stresses are included [4.9], the nonlinear analysis does show important differences in laminate behavior. This subject area is of importance primarily for specialized applications such as dimensionally stable space structures. Hence, further treatment is considered to be beyond the scope of this text.

## 4.7 SUBCRITICAL DAMAGES, STRENGTH, AND FAILURE.

Methods of stress analysis of laminates subjected to mechanical loads, temperature changes, and moisture absorption were presented in section 4.6. The main reason for stress analysis is determination or assessment of the strength of a laminate. The problem is of primary practical significance, since design without knowledge of strength characteristics is clearly impossible. It is also quite clear that such information for laminates cannot be obtained on a purely experimental basis, because the number of candidate laminates is immense and each of them is an anisotropic structural element. Thus, in each case it would be necessary to determine a set of strengths and to incorporate them into a failure criterion for a laminate under combined load. The situation is much more complex than for a UDC; for that case, the one-dimensional strengths can be obtained experimentally and only one failure criterion under combined stress is needed. In the present case, however, the one-dimensional strengths of a laminate are by themselves of great variety, since they depend on stacking sequence and layer orientations. To make matters worse, it is necessary to consider both in-plane and bending loads.

This situation clearly requires analytical criteria for strengths of laminates. Unfortunately, however, we are as yet far removed from achieving this desirable goal. Consequently, approaches and methods to be discussed will be both quantitative and qualitative.

First, consider the case of a perfect laminate which does not contain defects of any kind. When such a laminate is loaded in its plane, a simple stress distribution results, consisting of plane stress in each layer and a complex three-dimensional stress distribution at the edges which involves interlaminar normal and shear stress. Some of these stress components may become very large at the edges; theoretically, they may become infinite. This, at once, indicates several modes of initial failure. Away from the edges, a lamina in a laminate may fail either in what may be called a fiber mode, implying rupture or buckling of fibers, or in what may be called a matrix mode, implying longitudinal cracking parallel to the fibers. The criteria for these failure modes have been discussed earlier (chapter 3, equations 3.112 and 3.113) and, since the state of stress is plane, there are no other failure modes. The advantage of the criteria is that they predict not only failure but also the mode. At the edges, the interlaminar stresses may produce delamination as the initial failure mode. The major difficulties of analytical strength definition are to determine subsequent failures beyond the initial failure and to provide a criterion for when these will produce ultimate failure of the laminate.

### 4.7.1 Initial Failure and Subcritical Damages.

For a laminate which is loaded by in-plane forces and/or bending moments, the stresses in the layers at a sufficient distance from the edges can be obtained by the methods developed in section 4.6. If there is no external bending and the membrane forces are constant along the edges and if the laminate is balanced and symmetric, the stresses in the  $k^{\text{th}}$  layer are constant and plane. With reference to the material axes of the laminae, fiber direction  $x_1$  and transverse direction  $x_2$ , they are written  $\sigma_{11}^k$ ,  $\sigma_{22}^k$ ,  $\sigma_{12}^k$ . Failure will occur when either one of the failure criteria (chapter 3, equations 3.112 and 3.113) is satisfied. Thus

$$(\sigma_{11}^k/\sigma_L^u)^2 + (\sigma_{12}^k/\tau_L^u)^2 = 1$$

fiber modes

$$(\sigma_{11}^k/\sigma_L^{cu})^2 + (\sigma_{12}^k/\tau_L^u)^2 = 1$$

(4.116)

$$(\sigma_{22}^k/\sigma_T^u)^2 + (\sigma_{12}^k/\tau_L^u)^2 = 1$$

matrix modes

$$(\sigma_{22}^k/2\tau_T^u)^2 + [(\sigma_T^{cu}/2\tau_T^u)^2 - 1] (\sigma_{22}^k/\sigma_T^{cu}) + (\sigma_{12}^k/\tau_L^u)^2 = 1$$

Sometimes the simplistic maximum stress criterion (or any other failure criterion, such as the Tsai-Wu criteria, equation 3.110) is used to assess the initiation of failure. For the  $k^{\text{th}}$  lamina, the maximum stress criterion assumes the form

$$-\sigma_L^{cu} \leq \sigma_{11}^k \leq \sigma_L^{tu} \quad (4.117)$$

$$-\sigma_T^{cu} \leq \sigma_{22}^k \leq \sigma_T^{tu} \quad (4.118)$$

$$|\sigma_{12}^k| \leq \tau_L^u \quad (4.119)$$

It should be noted that the maximum stress criterion usually overestimates the strength of a lamina since the interaction of stress components is neglected. Some stress interaction is obtained when the maximum strain criterion is used. This involves replacing the stresses by  $\epsilon_{11}$ ,  $\epsilon_{22}$ , and  $\epsilon_{12}$  and replacing the ultimate stresses by the corresponding ultimate strains.

Laminate failure criteria such as those of equations 4.116 or 4.117-4.119 must be applied to each layer. The layer for which the criteria are satisfied by the lowest external load will define the load which produces the initial laminate failure while identifying the layer which fails and the nature of the failure (i.e., fiber failure or cracking along fibers). This is called first-ply failure.

Bending occurs when there are external bending and/or twisting moments or when the laminate is not symmetric. In these cases, the stresses  $\sigma_{11}^k$ ,  $\sigma_{22}^k$ , and  $\sigma_{12}^k$  predicted by laminate analysis are linear in  $x_3$  (see figure 4.7). As a result, the calculated stresses in a given layer will be maximum at one of its boundaries, and the selected failure criterion is usually evaluated in terms of the stresses at such locations rather than at a midplane.



Although the prediction of initial failure in a ply based on an assumed failure criterion (or criteria) described above appears to be quite straightforward and is often used in the industry, the problem of matrix mode failure (which commonly occurs first in some of the laminae) appears to be a little more complicated. Many experimental studies on crossply laminates such as  $(0_m/90_n)_{ps}$  indicate that the tensile stress or strain to cause appearance of  $90^\circ$  ply cracks (parallel to fibers) in dilute concentration vary with the total thickness of the lumped  $90^\circ$  ply group and the laminate lay-up. The results show a trend which indicates that the tensile stress required for the development of ply cracks (in dilute concentration, which may be considered to be initiation of damages) is inversely proportional to the square root of the total thickness of the  $90^\circ$  ply group. Such a relationship suggests that a criterion based on the average energy release rate for the creation of ply cracks may be more appropriate [4.10 and 4.11]. However, if lumping is avoided and the thickness of each ply is the same (or does not vary significantly), then a stress based criterion may be acceptable for prediction of initial failure.

The situation is much more complicated for the edge stresses. Here the state of stress is three-dimensional and must be obtained by numerical analysis in each case. The major problem is that there are edge stress singularities; i.e., some interlaminar stresses become theoretically infinite. Numerical methods cannot uncover the nature of a singularity, but there exist analytical treatments [4.5] which do this. The major problem is how to assess the implication for failure of such edge stress singularities. This is a problem which is not resolved at the present time. The situation is reminiscent of fracture mechanics in the sense that stresses at a crack tip are theoretically infinite, thus singular. Fracture mechanics copes with this difficulty in terms of a criterion for crack propagation which is based either on the amount of energy required to open a crack or, equivalently, on the value of the stress intensity factor. It seems that similar considerations apply for edge singularities, but the situation is much more complicated, since a crack initiating at the edge will propagate between anisotropic layers. Further, the problem under consideration is different from the self-similar propagation of a crack since no initial crack or delamination is present and the nature of the stress singularity changes as soon as a delamination is created. In practice, some damage zone usually develops at very small load levels surrounding the point where the stresses are singular and a delamination tends to grow from it. Use of a critical value of the strain energy release rate (or an interaction criteria involving the three components of such rates,  $G_I$ ,  $G_{II}$ , and  $G_{III}$ ) has been attempted by some investigators [4.12] to predict catastrophic or slow growth of an assumed delamination of very small length. However, such approaches are still not widely used in the industry, possibly for the reason that edge delaminations are often found to appear after other kinds of damages, such as ply cracks and delaminations which originate from such cracks. Growth of free edge delaminations, however, appear to be more critical under cyclic loading especially near holes, which will be discussed in later sections.

#### 4.7.2 Subsequent Failures.

In many cases laminates have considerable load carrying capacity remaining after first-ply failure and there arises the difficult and important problem of analytically determining subsequent failures. As has been said above, this problem is far from resolved and is today one of the active research subjects in composite materials. The following discussion outlines a simplistic, well known approach to the problem. When initial failure of a layer takes place, the failure may occur in the fiber mode or in the matrix mode. In the first case, the ply stiffness in the fiber

direction  $E_1$  is reduced, and in the second case the ply elastic properties  $E_2$  and  $G_{12}$  are reduced. These elastic properties are not reduced to zero, for the initial failure produces cracks in the layer and the uncracked regions remain bonded to adjacent layers. It is possible to obtain precise estimates of these stiffness reductions as will be discussed later but their evaluation is a little complicated. The simplest (but quite drastic) assumption is that  $E_1$  reduces to zero in the fiber mode and that  $E_2$  and  $G_{12}$  reduce to zero in the matrix mode. Since a laminate, in most cases, will not survive a fiber mode failure, the progressive failure cases of interest are initial and subsequent failures in the matrix mode. If it is assumed that, for failure of a lamina group in the matrix mode,  $E_T$  and  $G_L$  of that group can be set equal to zero, eventually the basic assumptions of netting analysis will be approached (see section 4.6.3). For netting analysis, the ultimate load is defined by the state when  $E_2$  and  $G_{12}$  vanish in all laminae.

In order to demonstrate the effects of changes in ply stiffness, some specific examples will be helpful. In these examples, only membrane loadings will be considered. The unidirectional lamina properties used in the examples are listed in table 4.1.

The predicted load-strain response of a  $(0/\pm 45)_s$  laminate subjected to three different membrane loading environments is depicted in figures 4.26 through 4.28. Failure analyses for these examples have been performed utilizing the failure criteria of (4.116).

The laminate loading in figure 4.26 consists of uniaxial tension in the direction of the  $0^\circ$  fibers, the laminate x direction. The laminate response here is seen to be linear up to the load where the  $0^\circ$  fibers fail in axial tension. Since the failure mode is fiber breakage, it is assumed that no additional load carrying capability exists.

In figure 4.27, the laminate loading consists of uniaxial tension perpendicular to the  $0^\circ$  fiber direction, the laminate y direction. The laminate response here is not linear up to first fiber failure. Two distinct knees exist in the load-strain response. The first slope discontinuity corresponds to a matrix tensile mode failure in the  $0^\circ$  fibers. At this point, the lamina properties for the  $0^\circ$  plies, the moduli  $E_2$  and  $G_{12}$ , are set equal to zero and the laminate properties are reformulated.

Subjecting this damaged laminate to additional loading then yields matrix tensile mode failure in both the  $45^\circ$  and  $-45^\circ$  plies, resulting in the second knee in the load-strain curve. A new laminate was again formulated with all plies having moduli  $E_2$  and  $G_{12}$  set to zero. Additional loading then produced fiber compressive mode failure in the  $0^\circ$  plies (followed immediately by fiber tensile mode failure in the  $45^\circ$  and  $-45^\circ$  plies), which corresponds to the ultimate strength under  $N_{yy}$  loading.

The final membrane loading state considered was an applied  $N_{xy}$  (figure 4.28). The response under this shear loading produces a single matrix mode failure prior to ultimate, or fiber mode, failure.

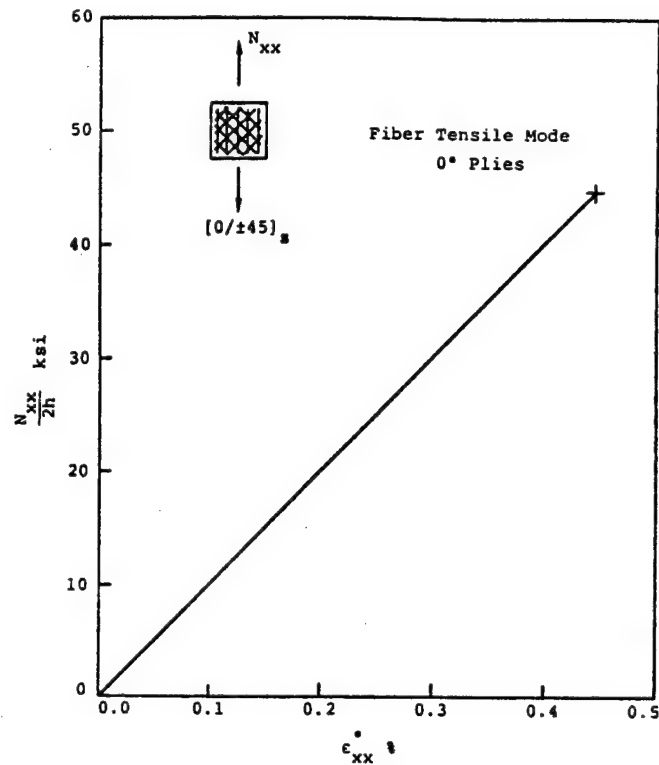


FIGURE 4.26. STRESS-STRAIN RESPONSE, TENSILE  $N_{xx}$  LOADING

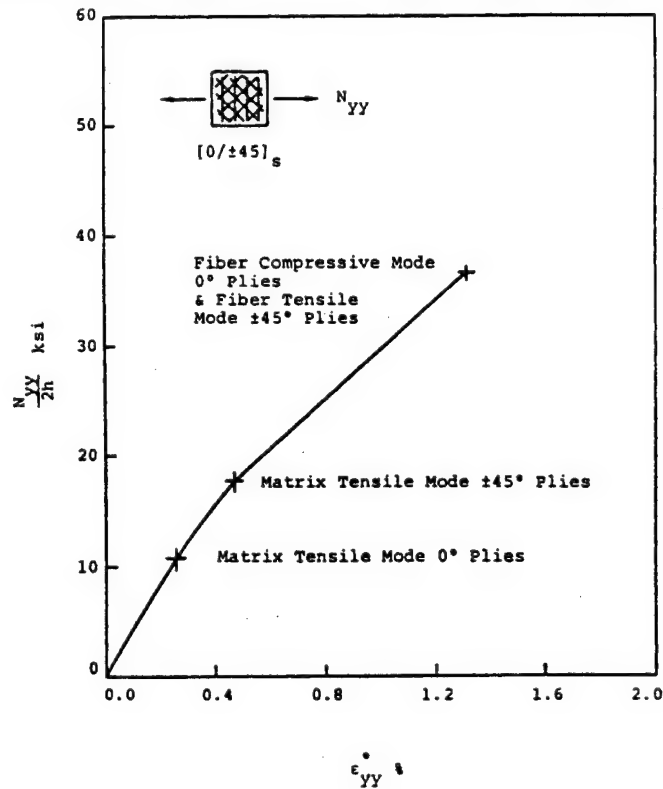


FIGURE 4.27. STRESS-STRAIN RESPONSE, TENSILE  $N_{yy}$  LOADING

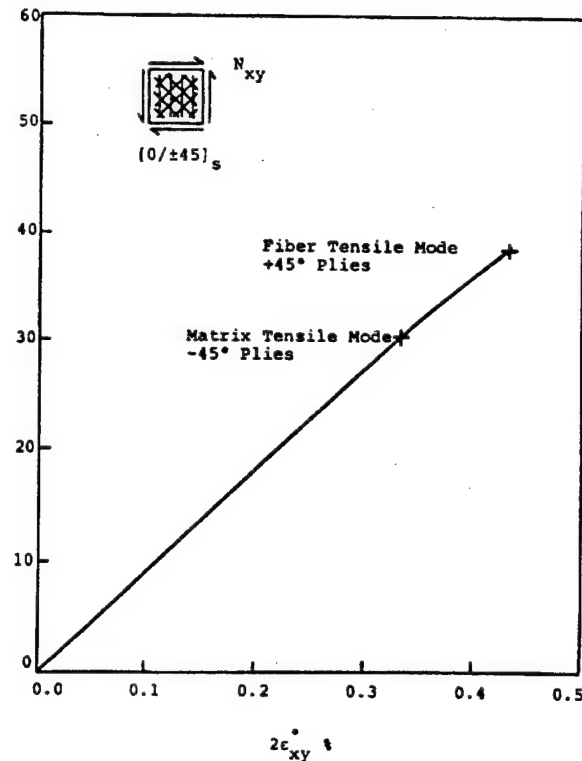


FIGURE 4.28. STRESS-STRAIN RESPONSE, TENSILE  $N_{xy}$  LOADING

Examination of these three figures reveals major differences in laminate response under different loading states. The reason for these differences is simply that the ply stress states are very different from each other. This can be seen easily by referring to table 4.7 in which the states of stress in each ply of the laminate are listed at first-ply failure under the three membrane loadings applied. The stresses listed in table 4.7 demonstrate that at the three different first-ply failure loads, different stress components in different plies are critical. When subjected to  $N_{xx}$  loading, the fiber direction stress in the  $0^\circ$  plies reaches the lamina strength value first, hence promoting failure. The other ply stresses are not critical at this load. Under  $N_{yy}$  loading, the first stress component to reach the lamina strength is the transverse stress in the  $0^\circ$  plies. Shear loading produces a critical stress in the  $-45^\circ$  plies in transverse tension. Thus, the critical stresses are dependent on loading direction.

The difference between first-ply failure and ultimate failure are depicted graphically in figure 4.29, in which the laminate failure surface for combined in-plane extensional stresses is shown for the laminate treated above. The dashed curve defines the combination of applied laminate stresses for which the first ply failure occurs in the matrix mode. The solid curve defines the combined laminate stress states which results in failure of a ply in the fiber mode. Note that for most positive values of  $N_{yy}$ , a matrix mode failure precedes the first fiber mode failure. Conversely, for negative values of  $N_{yy}$ , the first-ply failure is always a fiber mode failure. The large region between these two surfaces indicates the potentially limiting effect of low transverse and shear strengths of the individual plies, hence, the limiting effect of the matrix properties.

TABLE 4.7. PLY STRESSES (ksi) AT FIRST PLY FAILURE, (0/±45)<sub>s</sub> LAMINATE

Loading, 10 <sup>3</sup> lb/in <sup>2</sup>	0° Plies			45° Plies			-45° Plies		
	$\sigma_1$	$\sigma_2$	$\sigma_{12}$	$\sigma_1$	$\sigma_2$	$\sigma_{12}$	$\sigma_1$	$\sigma_2$	$\sigma_{12}$
$\frac{N_{xx}}{2h} = 44.7$	110.0*	-3.6	0.0	12.8	1.10	-5.14	12.8	1.10	5.14
$\frac{N_{yy}}{2h} = 10.9$	-19.9	4.0*	0.0	22.4	1.95	2.23	22.4	1.95	-2.23
$\frac{N_{xy}}{2h} = 30.2$	0.0	0.0	4.35	82.2	-4.0	0.0	-82.3	4.0*	0.0

\* Critical Stress Value

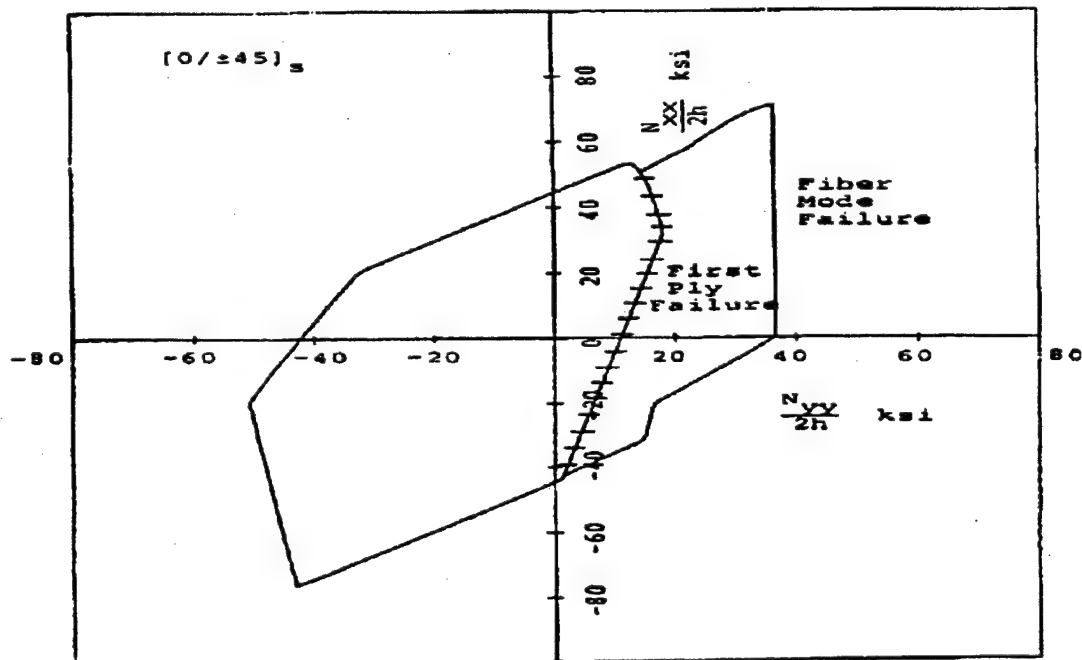


FIGURE 4.29. LAMINATE FAILURE SURFACE FOR COMBINED IN-PLANE EXTENSIONAL STRESS STATES

The related failure surfaces for combined laminate membrane extensional and shear stress are presented in figure 4.30. Here, for large membrane shear stresses, the first-ply failure is in the matrix mode. Again the potential for performance improvement through changes in matrix properties appears to be worthy of consideration.

The failure surfaces of figures 4.29 and 4.30 illustrate the importance of knowing the difference between the loads causing first-ply failure and ultimate failure. The first need is the determination of whether there is additional load capacity in the laminate beyond the point of first-ply failure. A necessary condition for this is that the laminate be stable (i.e., able to carry loads) after the loss of laminae stiffnesses associated with matrix mode failure. For example, an angle-ply laminate ( $\pm\theta$ ) experiencing matrix mode failure when subjected to an axial load will be unable to carry that load. However, any laminate having fibers oriented in three or more directions can generally carry load after matrix mode failure. An estimate of load carrying capability can be obtained by using netting analysis.

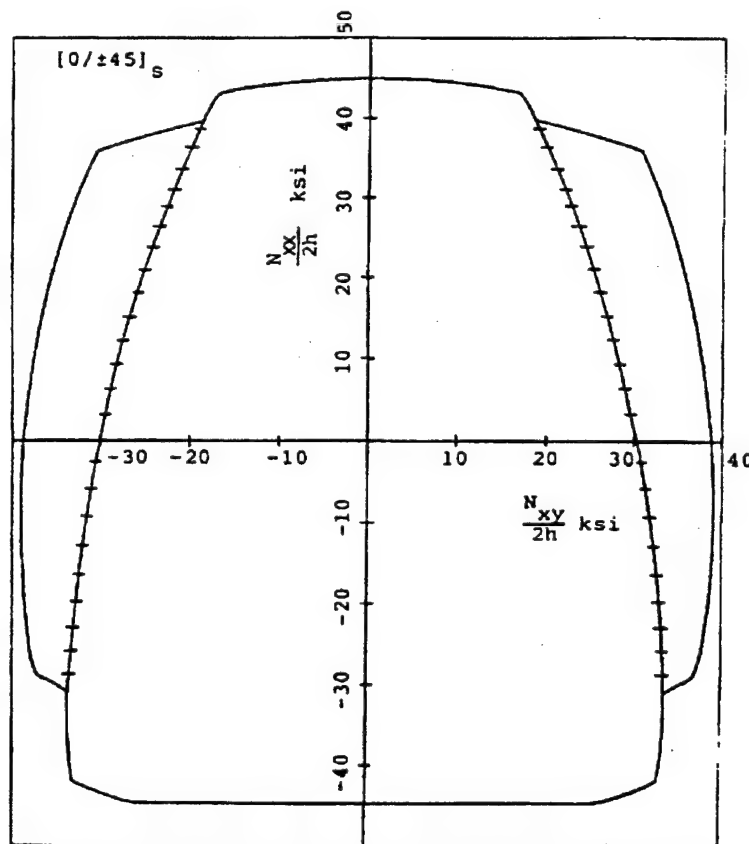


FIGURE 4.30. LAMINATE FAILURE SURFACE FOR COMBINED IN-PLANE EXTENSIONAL AND SHEAR STRESS STATES

In table 4.8, comparisons between laminate analysis predictions for first-ply failure strength and ultimate failure strength and netting analysis predictions for ultimate failure strength are shown.

In both the  $N_{yy}$  and  $N_{xy}$  loadings, the nettings analysis strength predictions are considerably larger than the first-ply failure laminate analysis predictions. This indicates that considerable strength remains beyond first-ply failure. The netting analysis, however, predicts a lower strength than lamination theory for  $N_{xx}$  loadings. The indication here is that first-ply failure corresponds to ultimate failure. Because of the trends of the type indicated in this table, netting analysis can be a useful tool in composite strength predictions.

TABLE 4.8. FAILURE LOADS AND MODES [0/±45], LAMINATE

Loading Type	Laminate Analysis				Netting Analysis	
	First-Ply Failure Load (10 <sup>3</sup> lb/in <sup>2</sup> )	Failure Mode	Ultimate Failure Load (10 <sup>3</sup> lb/in <sup>2</sup> )	Failure Mode	Ultimate Load (10 <sup>3</sup> lb/in <sup>2</sup> )	Failure Mode
$N_{xx}$ — 2h	44.7	Axial Tension 0° Plies	44.7	Axial Tension 0° Plies	36.5	Axial Tension 0° Plies
$N_{yy}$ — 2h	10.9	Transverse Tension 0° Plies	36.6	Axial Tension ±45° Plies Axial Compression 0° Plies	36.5	Axial Tension ±45° Plies Axial Compression 0° Plies
$N_{xy}$ — 2h	30.2	Transverse Tension -45° Plies	38.7	Axial Tension 45° Plies	36.5	Axial Tension 45° Plies Axial Compression -45° Plies

Recently many attempts have been made to quantify stiffness loss due to the development and growth of 90° ply cracks in crossply laminates [4.10 and 4.13] subjected to tension in the 0° direction. Significant load redistribution from cracked to uncracked plies also occurs and can be estimated. Stiffness loss in off-axis plies due to transverse tensile and shear stresses has also been modeled [4.11]. The results show that the cracked plies can carry quite a bit of load when the cracks are in dilute concentration. Their stiffnesses, however, gradually reduce as the density of such cracks increases. Use of such models is not yet widely accepted in the industry, since the results are slightly complicated and the nonlinearity in the laminate response due to the development of ply cracks is often masked in carbon epoxy composites because of the large stiffness of the 0° layers. These models are, however, more realistic than the ply discount scheme described earlier.

### 4.7.3 Strength.

A conventional definition of material strength is the maximum static stress or combination of stresses that can be carried by the material. For example, in a simple uniaxial tensile test, strength is the highest stress achieved before the material breaks. In a metal, it has been found that other points on the material stress-strain curve are also of significance in considering the maximum stress to be applied to a material. For example, the proportional limit stress and the material 0.2% offset yield stress are valuable measures of material strength. Similarly, in composites there are several characteristic stress levels which should be considered in the evaluation of strength. The primary stress levels of interest are the stress at which first ply failure or damage initiation occurs and the maximum static stress (stress resultant divided by laminate thickness) which the laminate can carry.

In the calculation of first-ply failure, consideration must be given to residual thermal stresses. Residual stresses are the ply stresses induced in a laminate as a result of fabrication processes. Typical resin matrix composites are formed under a combination of elevated temperature and pressure which promotes matrix curing. When the laminate is subsequently cooled to room temperature, significant residual processing stresses develop. A question exists as to how to include these stresses in the failure analysis. The rationale for including them is obvious: the stresses exist after processing, and therefore, they can be expected to influence the occurrence of first-ply failure. However, since all resin matrix materials exhibit viscoelastic, or time dependent effects, it may be assumed that some portion of the residual processing stresses will dissipate further through a process of stress relaxation. Additionally, the processing stresses may be reduced through the introduction of transverse matrix microcracking. A limited amount of cracking may occur without significantly affecting the laminate elastic properties. This problem is complicated by the difficulty of measuring the residual stresses in a laminate and of observing first-ply failure during a laminate test. For these reasons, the stress-free temperature is usually assumed to be lower than that at curing.

From an analytical point of view, when laminae properties are known, it is possible to calculate a laminate stress-strain curve (including or excluding residual thermal stress effect) and determine first-ply failure, subsequent ply failures, and maximum stress at failure. From an experimental point of view, it is possible to measure a laminate stress-strain curve and determine proportional limit stress and maximum stress. It is necessary to recognize that there are these different characteristic stress levels in laminated composite materials, just as in both a yield stress and an ultimate stress which characterize metallic materials. These stress levels for composites, as for metals, may be used with different factors of safety. A reasonable approach seems to be utilization of analytical strength predictions (both first-ply failure and ultimate failure) in the preliminary design phase and experimental strength values after laminate level material tests.

When experimental strength data are used for laminates, the problem of combined loading conditions arises again. The difficulties of combined load testing preclude the purely experimental approach; the uncertainties of failure mechanism cloud the choice of analytical interaction criteria. A reasonable approach is represented by the following sequence: analytical calculation of ultimate strength via netting analysis or any other straightforward method, use of the analytical result to define the shape of the interaction curve, use of the experimental data for



single stress components to define the amplitudes of the interaction curve, and confirmation via limited combined stress testing for a condition of practical interest.

It is common practice, in the aerospace industry, to neglect the residual thermal stresses in the calculation of ply failure. Data to support this approach do not appear to be available. However, at the present time, damage tolerance requirements limit allowable strain levels in laminates to 3000 to 4000  $\mu$  in/in for many material systems. This becomes the dominant design restriction, as will be discussed subsequently, and obviates the need to resolve the effects of residual thermal stresses. As materials of improved impact resistance are developed, first-ply failure calculations may become more significant. It appears that thermal stresses should be included in first-ply failure calculations unless their omission creates an improved degree of conservatism. Careful stress-strain testing of laminate coupons should be used to define design allowables.

An alternative to the use of sequential ply failure analysis is to treat failure at the laminate level as discussed in the appendix to chapter 4.

Whichever stress values are used, design charts in the form of so-called "carpet plots" are of great value for selection of the appropriate laminate. Figure 4.31 presents a representative plot of this type for the axial tensile strength of laminates having various proportions of plies oriented at  $0^\circ$ ,  $\pm 45^\circ$ , and  $90^\circ$ . Appropriate strength data suitable for preliminary design can be found for various materials in references 4.1 and 4.14.

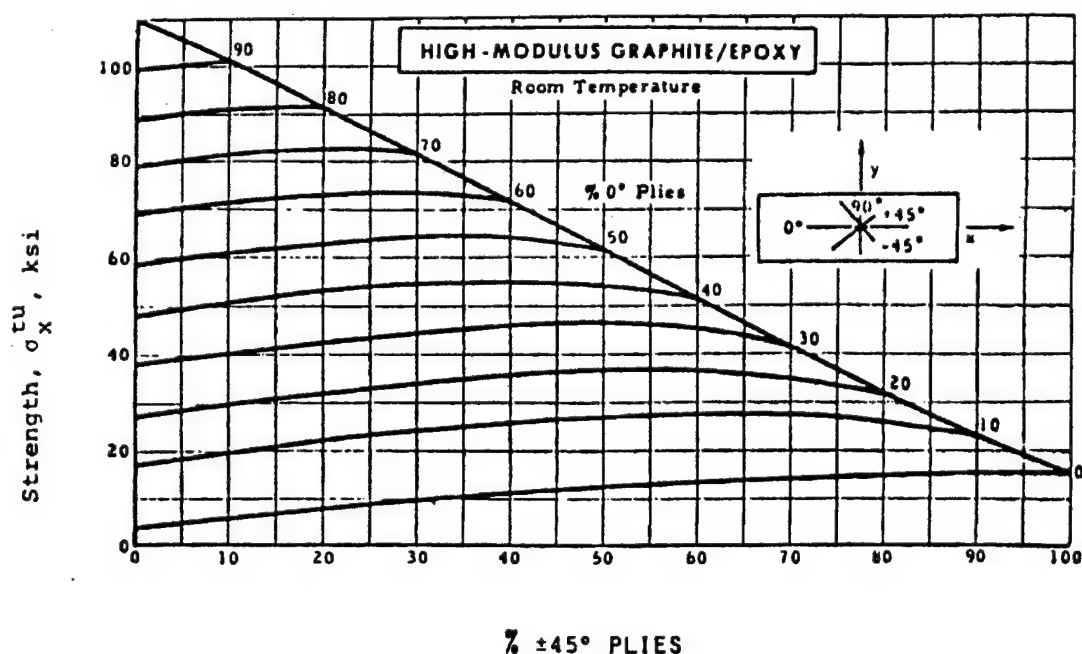


FIGURE 4.31. TENSILE STRENGTH OF  $(0/\pm 45/90)_s$  FAMILY OF HM-GRAPHITE/EPOXY LAMINATES

#### 4.7.4 Fracture Near Holes, Notches, or Cutouts.

The presence of a hole or other discontinuity in a structure introduces local stress concentrations. These high local stresses can result in initial localized failure. In ductile metals, yielding occurs in these regions and as the load is increased the size of the yield zone increases. However, growth of cracks can also occur when the notch is sharp. In brittle or semibrittle materials, a common consequence is the formation of a small crack at the region of stress concentration. When there is a combination of high stress intensity and low resistance of the material to crack propagation, the result is failure due to cracking. This failure mechanism is generally denoted as fracture. The mathematical technology which has been built up to treat this problem utilizes fracture mechanics methods and is called structural integrity technology [4.1].

For composite laminates, the problem is complicated by the heterogeneity of the material, both at the microscale and on a layer-to-layer basis. The complexity of this problem is illustrated by the laminate analysis of a plate with a hole. Consider a symmetric, balanced laminate having a circular hole subjected to in-plane axial tension. The plate may be regarded as an orthotropic plate whose properties are the effective laminate moduli defined in section 4.4. Solutions for stress concentrations in such a plate are available [4.15]. The stresses obtained from such a solution define local values of the stress resultants, which can be treated as the stress resultants applied to the actual laminate. In general, at any point in the plate, this will define a combined loading with all three stress resultants being nonzero. Following the methods of section 4.6, the stress state in each ply can then be found. This defines the variation of ply stresses throughout the plate.

Sample results, obtained by the above procedure, are presented in figure 4.32. The tangential stress around the periphery of the hole is plotted. The solid lines represent the stress from the orthotropic plate analysis, which is equivalent to the average value of the in-plane ply stresses. At the edge of the hole, these average tangential stresses are the only nonzero components of the stress resultants; elsewhere in the plate all three stress resultants generally will be nonzero. The dotted lines are the tangential stresses in the individual plies computed from laminate theory. In general, all the stress components in each ply will be nonzero, even at the edge of the hole. This is the same effect as was treated in the discussion of interlaminar stress in section 4.6.4; namely, that the boundary conditions are satisfied in laminate analysis only by the average stresses.

At the edge of the hole, the lamina stresses in figure 4.32 will not be correct and interlaminar stresses will exist. These interlaminar shear stresses are shown in figure 4.33 at the various ply interfaces, and the interlaminar normal stresses are shown in figure 4.34 at the middle surface interface. These interlaminar stresses are normalized with respect to the average applied stress. The magnitudes of these stresses are substantial.

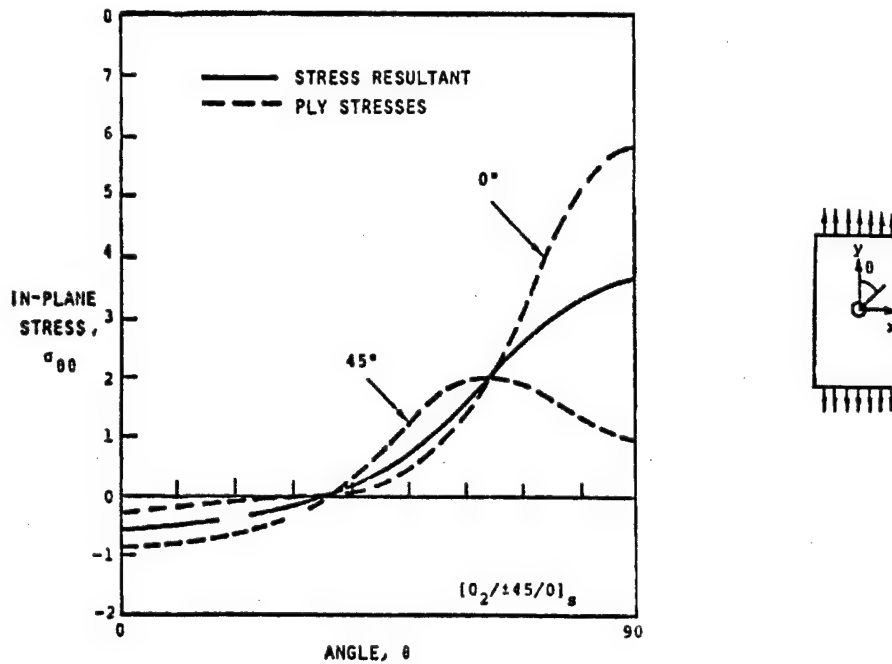


FIGURE 4.32. LAMINATE THEORY CALCULATIONS FOR STRESSES AROUND A HOLE

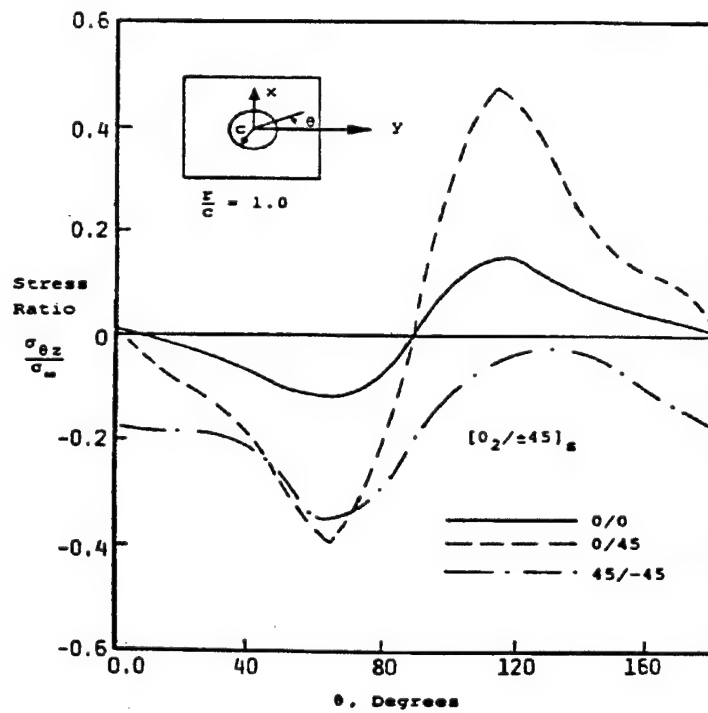


FIGURE 4.33. INTERLAMINAR SHEAR STRESS AT A HOLE

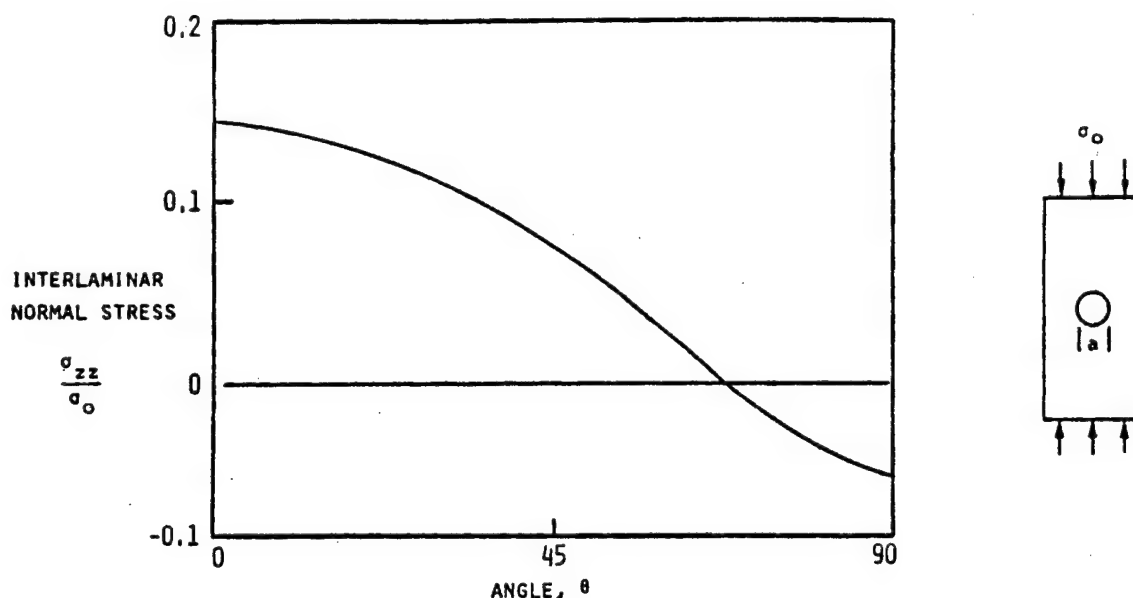


FIGURE 4.34. INTERLAMINAR NORMAL STRESS AT A HOLE

Associated with the interlaminar stresses described above is a modification of the in-plane stress state in each ply. Thus, as described for the free edge problem in section 4.6.4, the only non-zero in-plane stress component in each ply at the edge of the hole is the tangential stress,  $\sigma_{\theta\theta}$ . This combination of in-plane and interlaminar stresses varies strongly with coordinate. The variation takes place in the proximity of the hole, where the average in-plane stress components are also varying. This complex state of stress can cause various failure mechanisms. Clearly, interlaminar disbonding is a possibility at various locations at or near the edge of the hole. Intra-ply matrix mode failure in any ply is another possibility. At elevated stress levels, it is reasonable to expect diverse local matrix failures. A method for treating this complex problem is described below.

Using the methods presented in section 4.4, the effective in-plane laminate stiffnesses,  $E_x$ ,  $E_y$ , and  $G_{xy}$  may be calculated for any laminate. With these properties specified, a balanced symmetric laminate may be regarded, for purposes of structural stress analysis, as a homogeneous orthotropic plate. Failure of such a plate may be analyzed within the framework of a fracture mechanics problem or as a local overstress problem. Both approaches are in current use.

For the fracture mechanics approach, the concept of an intense energy region was introduced by Waddoups et al. [4.15]. It was assumed that this region has a characteristic length based upon an  $r^{1/2}$  type of singularity. Arguing that the energy balance in the region is more important than the details of the stress field for a fracture mechanics problem, a related problem was treated. Thus, the stresses associated with a small crack emanating from the edge of a hole in an isotropic material were considered. These can be obtained from the well known solution, due to Bowie [4.16]. For this solution, the ratio of the strength of an unnotched specimen to that of a similar specimen with a circular hole can be shown to be a function only of the ratio of the length of the small crack at the edge of the hole to the hole radius. Thus, correlation of experimental data

for strength as a function of hole size can be used to define a best-fit value for the characteristic length of the intense energy region.

Thus, the general procedure is to test specimens both unnotched and with a specific notch geometry inducing a stress concentration in order to define the material parameters. Then these values are used to predict strengths for other stress concentrations of similar geometry. One particular area of application for this method has been with bolted joints.

The other major approach to a notched plate is based upon the assumption that failure occurs when local stresses exceed the ultimate strength of similar unnotched laminates. Orthotropic elasticity theory may be used for evaluation of stresses around a hole in such a plate [4.17]. Examples of the resulting stress concentrations are shown in figure 4.35 for various carbon/epoxy laminates. The laminae orientation combinations influence both the magnitude and the shape of the stress variation in the vicinity of the hole. The high stresses at the edge of the hole may initiate fracture.

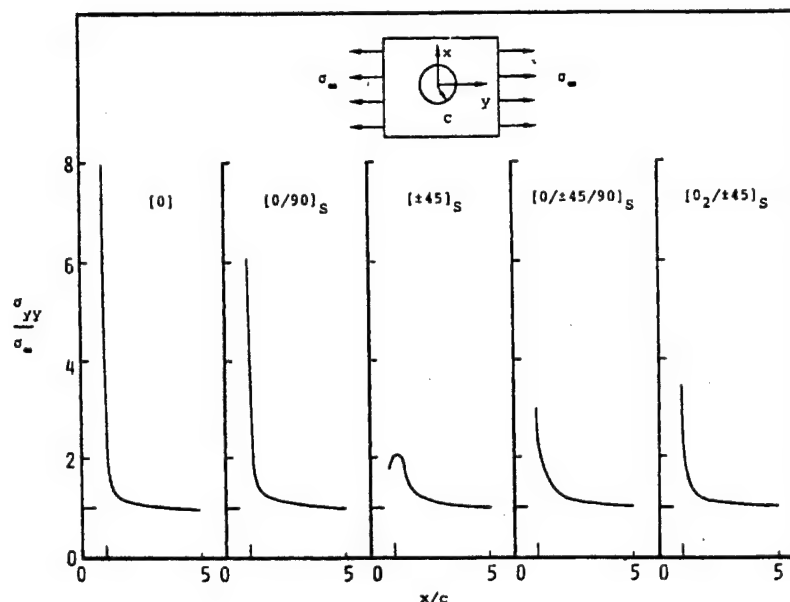


FIGURE 4.35. DISTRIBUTION OF STRESS  $\sigma_{yy}(x,0)$  NEAR A CIRCULAR HOLE IN A HOMOGENEOUS ORTHOTROPIC INFINITE PLATE

If the laminate fails as a brittle material, fracture will be initiated when the maximum tensile stress at the edge of the hole equals the strength of the unnotched material. In a tensile coupon with a hole, as in figure 4.35, the failure will occur at the minimum cross section and will initiate at the edge of the hole, where the stress concentration is a maximum. The stress concentration factor of interest is one which includes the finite width effect. This is illustrated in figure 4.36 for an isotropic plate with a central circular hole. Stress distributions are shown for various ratios of hole diameter,  $a$ , to plate width,  $W$ .

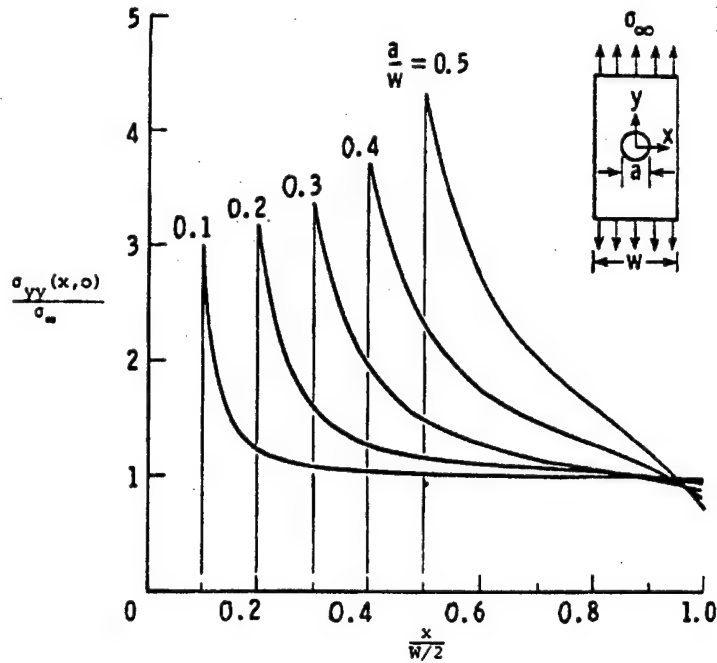


FIGURE 4.36. STRESS DISTRIBUTION AROUND A HOLE IN A FINITE WIDTH PLATE

The basic stress concentration factor for this problem is the ratio of the axial stress at the edge of the hole ( $x = a/2$ ;  $y = 0$ ) to the applied axial stress,  $\sigma_{\infty}$ . For small holes in an isotropic plate, this factor is equal to 3. For large hole sizes, the average stress at the minimum section,  $\sigma_n$ , is higher than the applied stress,  $\sigma_{\infty}$ , and is given by the following relation:

$$\sigma_n = \frac{\sigma_{\infty}}{\left(1 - \frac{a}{W}\right)} \quad (4.120)$$

The net section stress concentration factor,  $k_n$ , is the ratio of the maximum stress to this average stress. Thus

$$k_n = \frac{\sigma\left(\frac{a}{2}, 0\right)}{\sigma_{\infty} / \left(1 - \frac{a}{W}\right)} \quad (4.121)$$

Laminate fracture for the elastic-brittle case will occur at stress  $\sigma_{fr}$ :

$$\sigma_{fr} = \sigma^u / k_n \quad (4.122)$$

A material which fails in this fashion is denoted as a notch-sensitive material. In contrast, a ductile material will yield locally to alleviate the stress concentration effect. In the extreme, this will result in a uniform stress distribution at the net section, as shown in figure 4.37b. For this case, failure will occur when the average net section stress equals the material strength, i.e.,

$$\sigma_{fr} = \sigma^u \left(1 - \frac{a}{w}\right) \quad (4.123)$$

A material which fails in this fashion is denoted as a notch-insensitive material. Practical laminates may be expected to fail in a fashion which is neither of these two extreme cases.

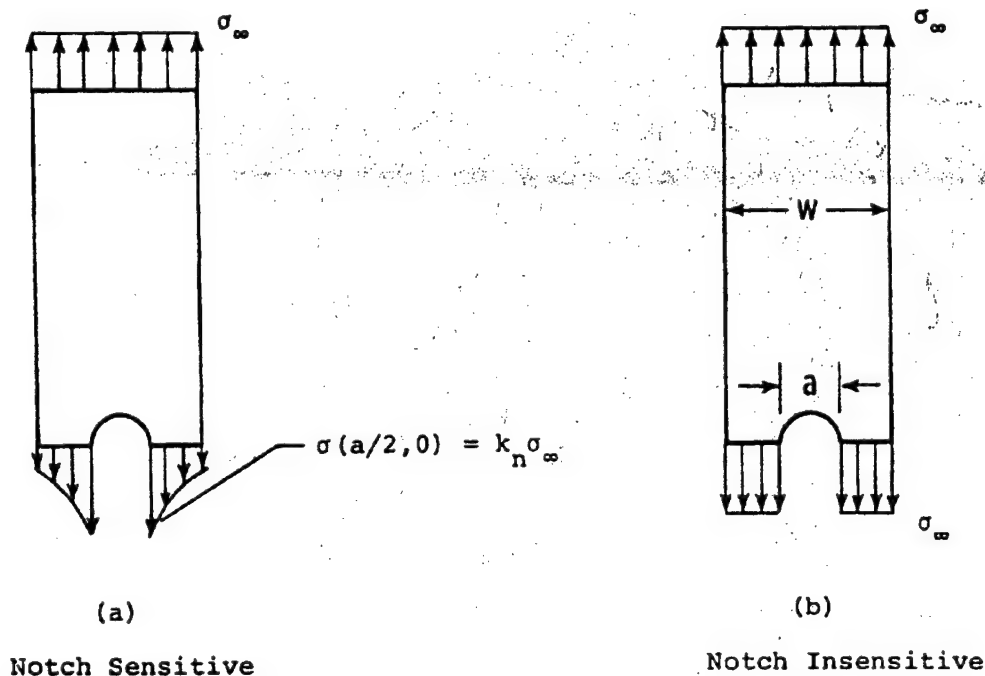


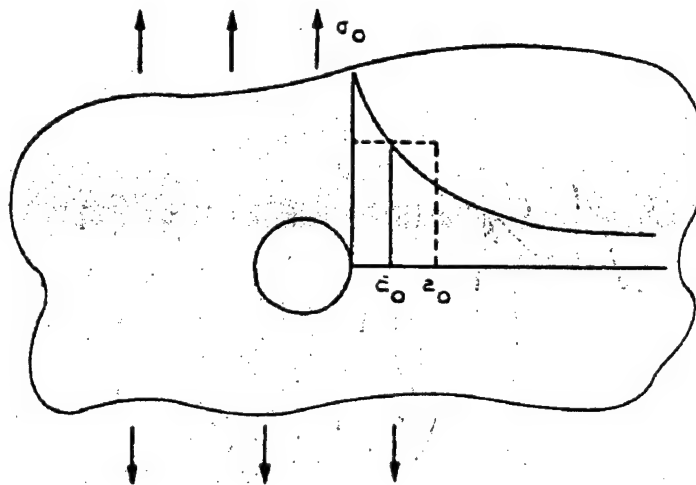
FIGURE 4.37. IDEALIZED LIMIT CASES FOR FAILURE

As discussed earlier, various matrix damage effects are expected to occur at the maximum stress locations. These localized damages reduce the material stiffness and diminish and spread the stress concentration effects. As a result, it is anticipated that although fracture will occur due to stress concentration, it will occur due to lesser stress concentration factors than those calculated from orthotropic elastic stress analysis of the notched laminate. Semiempirical methods for evaluating this reduction in stress concentration have been proposed.

The point stress theory [4.18] proposes that the elastic stress distribution curve, e.g., those of figure 4.35, be used but that the stress concentration be selected at a distance  $d_0$  from the edge of the hole. Thus, the numerator of equation 4.121 should be evaluated at the point  $x = a/2 + d_0$ . The characteristic length,  $d_0$ , must be evaluated experimentally. The average stress theory [4.18] takes a similar approach by proposing that the elastic stress distribution be averaged over a distance  $a_0$  to obtain the stress concentration. Thus

$$k_n = \frac{\int_{a/2}^{a/2+a_o} \sigma_y dx}{\int_{a/2}^{W/2} \sigma_y dx} \quad (4.124)$$

Again, the characteristic dimension,  $a_o$ , must be found experimentally. The two approaches are illustrated in figure 4.38. For both methods, the resulting stress concentration is used in equation 4.122 to define the fracture stress.



$a_o$  - PARAMETER FOR AVERAGE STRESS THEORY

$e_o$  - PARAMETER FOR POINT STRESS THEORY

FIGURE 4.38. REPRESENTATION OF CHARACTERISTIC DIMENSIONS FOR SEMIEMPIRICAL FRACTURE THEORIES

Representative results are plotted in figure 4.39 to illustrate the differences associated with the different types of material behavior. The ratio of strength of the plate with a hole,  $\sigma_{fr}$ , to that of an unnotched laminate,  $\sigma^u$ , is plotted as a function of hole size. For the notch insensitive material, the plot clearly shows a linear decrease in failure stress with hole size due to the reduction in net cross-sectional area. The lower curve, for a notch-sensitive material, shows an immediate drop in strength with the introduction of even a small hole due to the local stress concentration effect. The semiempirical theories (both have similar effects) show a rapid but more modest drop due to stress concentration. Experimental data for laminates support the use of either of the semiempirical theories for fracture of a laminate with a hole.



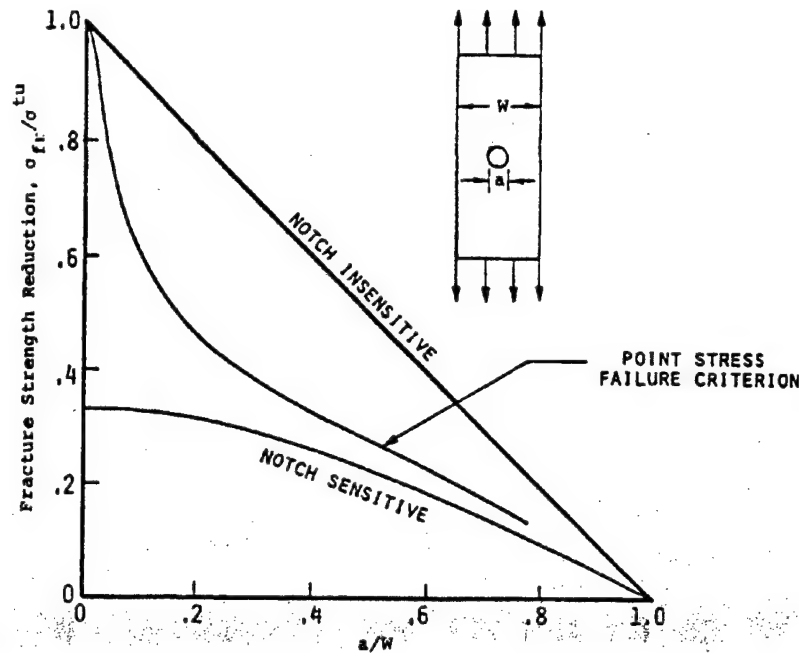


FIGURE 4.39. APPROXIMATE FAILURE THEORIES

#### 4.8 FATIGUE.

*I have steadily endeavored to keep my mind free so as to give up any hypothesis, however much beloved (and I cannot resist forming one on every subject) as soon as facts are shown to be opposed to it. . . . I cannot remember a single first-formed hypothesis which had not, after a time, have to be given up or be greatly modified.*

Charles Darwin

A critical design condition for aeronautical structures is the repeated application of loads of various amplitudes. This cyclic or fatigue loading at amplitudes below the static strength of the material can cause failure. It was shown earlier (see section 3.2.6) that for fatigue of unidirectional materials, there are different failure mechanisms depending upon the direction and type of load, just as there are for static loading. Hence, it is reasonable to expect that evaluation of fatigue induced failure of laminates will involve at least the complexity of static laminate failure. Actually the process of damage development in laminates is much more complex, as discussed in the next few subsections.

In a fashion, which is somewhat similar to the separate treatments of strength and fracture, the fatigue problem may be separated into treatment of continuous laminates and treatment of laminates containing discontinuities. A continuous laminate is a geometrically regular one which is representative of its fabrication process and which satisfies its acceptance criteria. However,

a continuous laminate may contain inherent, or "birth," defects of many types, including twisted or broken yarns or portions thereof, matrix-rich areas or matrix microcracks, interply disbonds, inclusions, etc. Under cyclic loading, these local defects may grow in size and number and may contribute to laminate fatigue failure. Continuous laminates are treated first in section 4.8.1.

A discontinuous laminate has in it a major discontinuity, such as a hole or a notch, which can cause a high local stress concentration and which may be regarded as a likely source of damage which can propagate under cyclic loading conditions, causing failure. Laminates of this type are discussed in section 4.8.2.

Continuous laminates may be subjected to damage in service which results in local failure. This can create a significant discontinuity which will dominate the subsequent response to cyclic load. This is discussed in section 4.8.3.

#### 4.8.1 Continuous Laminates.

Numerous experimental studies have been conducted to investigate the fatigue behavior of laminate coupons under unidirectional tensile and compression loading. Under tension-tension or tension-compression fatigue, ply cracks (which may involve fiber/matrix debonding) parallel to fibers develop in the off-axis plies (those with fibers perpendicular to or making a large angle to the loading direction). These cracks usually extend through the entire width of the coupon. The number of the cracks increases with increasing numbers of cycles, and delaminations begin to appear between the plies, blunting the ply cracks; the rate of ply crack growth also decreases drastically. The state of ply cracking at this stage is called the characteristic damage state (CDS), which is considered as a saturation crack pattern [4.19]. In addition to internal delaminations, edge delaminations often appear when the CDS is reached, and since the load is transferred from the cracked plies to load bearing plies (with fibers in the loading direction), fiber/matrix debonding and fiber breaks begin to occur at this stage [4.20]. Final failure occurs when the load bearing plies are sufficiently weakened. In many ways, the growth of damage with increasing numbers of cycles is similar to what is observed under increasing quasi-static loading of laminates, and the damage mechanisms are obviously quite different from those in unidirectional composites loaded in the fiber direction. However, Talreja [4.21] attempted to construct fatigue-life diagrams (similar to those for unidirectional materials discussed in section 3.2.6.2 and shown in figure 3.51) for crossply carbon/epoxy composites (figure 4.40). The upper horizontal scatter band in this case is taken as the static laminate failure strain, and the strain limit below which no drop in strength is expected is chosen as the so-called limiting strain for delamination. It appears that this limit is the strain below which transverse ply cracks do not develop (proportional limit for longitudinal stress—transverse strain plot), and it is usually lower than that for matrix cracking in the unidirectional composite. In this connection, it may be noted that the strain at which transverse ply cracks appear under static loading also depends on the ply thickness (as discussed in section 4.7.1). The sloping band in the strain-life diagram of laminates corresponds to growth of ply cracks and delaminations. Strictly speaking, the horizontal scatter band centered around the static composite failure strain is not horizontal but has a small initial slope due to growth of ply cracks and delamination, and the slope becomes larger for large numbers of cycles. The slopes of these bands are usually higher for higher-stiffnesses off-axis plies, as in glass/epoxy laminates, or for higher percentages of off-axis plies.

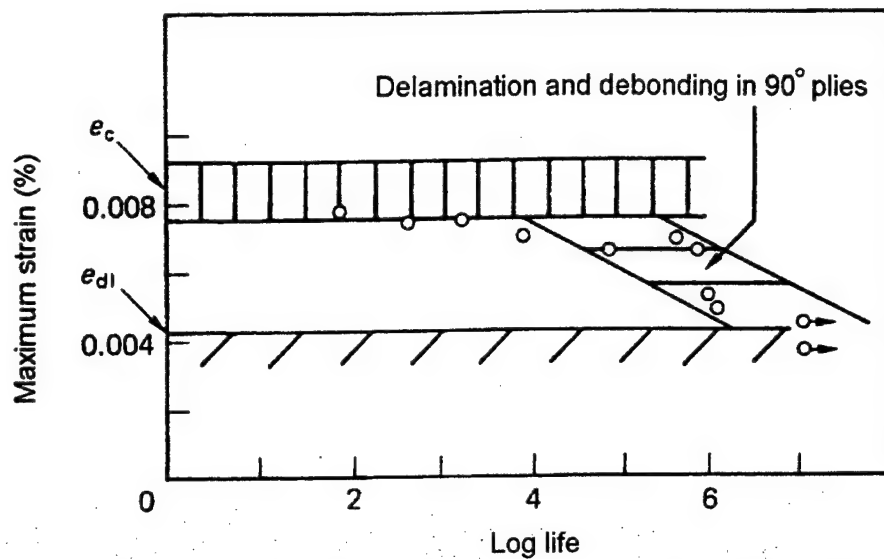


FIGURE 4.40. FATIGUE-LIFE DIAGRAM FOR A CROSSPLY GRAPHITE/EPOXY COMPOSITE [4.21]

It is clear that laminate fatigue failure is a result of a sequence of failures of individual plies. This is analogous to the treatment of static failure, wherein first-ply failure starts the laminate failure process.

One method of analysis of laminate fatigue consistent with the building block approach (estimating laminate properties from those of the laminae) of this text utilizes some fatigue data for unidirectional materials as the basis for determining fatigue characteristics of laminates. This approach is described below in section 4.8.1.1. As in the case of static laminate strength, it is found that this method of analysis is helpful for understanding laminate fatigue behavior for comparisons among various laminates and for generating preliminary data. It may not always provide the final design properties for fatigue.

The second method of analysis is based upon the concept that failure is the result of the continued accumulation and growth of dispersed local damage regions. This approach assumes that there is a quantitative relationship (which may or may not be known) between the inherent state of damage and the instantaneous strength (denoted the residual strength) of the composite. Utilizing an approach similar to that for metals, the growth of each of the existing damage regions under cyclic load can be modelled. However, the number and diversity of local damages precludes such an approach. Instead, the method of analysis is to hypothesize a law quantitatively relating increasing damage to decreasing strength and a law relating damage growth to existing damage and loading. As a consequence, there will be a degradation of strength with time (cycles of load) leading to fatigue failure. This approach appears to be a closer representation of the physics of failure but is less adaptable to precise mathematical formulation than the sequential laminae failure model. It is discussed in section 4.8.1.2.

The third class of analysis methods for fatigue failure of continuous laminates is motivated by the difficulty encountered in formulating the detailed mathematical model for the accumulation of damage approach. Since a semiempirical method appears necessary, the macromechanical approach de-emphasizes the details of the physical process and postulates mathematical expressions directly which are to be fitted to the experimental data. This approach is treated in subsection 4.8.1.3.

Each of these analysis methods may be viewed as a deterministic procedure for lifetime prediction. Since fatigue data exhibit significant scatter, however, a statistical approach to the problem is necessary. It is feasible to utilize each of the above three analysis methods in a statistical approach, and this is discussed in subsection 4.8.1.4. That discussion is preceded by treatment of the formulation of design criteria including the practicalities of variable loads and variability of material response.

#### 4.8.1.1 Failure Models Based Upon Lamina Properties.

##### 4.8.1.1.1 Initial Failure.

When a laminate is subjected to cyclic loads, the stresses in each ply are also cyclic. As long as the laminate remains elastic and no significant internal damage occurs (i.e., that which would reduce lamina stiffnesses), all of the procedures to determine internal stresses in the static case (section 4.6) remain valid for cyclic loads. If the membrane forces and bending moments are sinusoidal with the same R ratio (minimum/maximum amplitude) and the same frequency, as is usually the case, then all internal stresses will also be sinusoidal with the same R ratio and the same frequency. As discussed earlier, fatigue damage occurs in different ways. Cracks along fibers develop inside laminae, delaminations develop due to interlaminar stresses, and these two kinds of cracks can coalesce to form complicated crack patterns.

There is a fundamental difference between metal and laminate fatigue damage. In the former case, microscopic damage accumulates until a dominant crack emerges. This is called the initiation period. During continued cycling, the crack slowly propagates until it causes failure. This is called the propagation period. For metals this can be the dominant effect. By contrast, fiber composite laminates do not exhibit the phenomenon of propagation of a single dominant crack. Crack patterns in a laminate can be extremely complicated. From a macroscopic point of view, a laminate may be considered to spend its entire fatigue life in the damage initiation period.

The tremendous complexity of the evaluation of fatigue damage in laminates poses a practical dilemma. On the one hand, the fatigue failure process is too complex to be handled analytically, while on the other, the variety of candidate laminates is such that the testing of one is totally inadequate in terms of obtaining sufficient fatigue failure information for all. It will be recalled that a similar problem is presented by static failure of laminates (section 4.6). It is even more serious in the case of fatigue.

One approach which may be followed is, in spirit, similar to the one adopted for static strength. Some quantitative methods can be utilized for prediction of initial fatigue failures. Such methods

can provide insight into the relative merits of different laminate configurations. Design data for the laminate of choice are to be obtained from experimental data supplemented by analysis.

The procedure for the first-ply failure calculation in fatigue is as follows: given the S-N curves of the unidirectional fiber composite for cyclic stress in the fiber direction, transverse to the fibers and in axial shear, S-N curves for plane stress simultaneously involving these stress components can be constructed by the methods discussed in chapter 3, section 3.2.6.2 based on reference 4.22. A stress analysis of the laminate is performed and thus the cyclic stresses in all the laminae are known. Failure of each lamina is examined in terms of the lamina stresses and the failure criteria discussed in chapter 3, section 3.2.6.2. Initial failure occurs in the lamina which has the smallest lifetime and in the failure mode (fiber or matrix) determined according to this procedure.

To utilize this procedure, it is convenient to construct a curve of lifetime vs. maximum stress (for a fixed R value) for each failure mode in each ply of the laminate. For example, in a  $(0/90/\pm 45/90/0)$  laminate, as shown in figure 4.41, there is a fiber-dominated mode to be considered in the  $0^\circ$  ply and a matrix-dominated mode to be considered in the  $90^\circ$  ply, along with both modes in the  $45^\circ$  plies. In the static case ( $N = 1$  or  $\log N = 0$ ), the first ply to fail is the  $90^\circ$  ply (i.e., the transverse ply) in the matrix mode. The same failure mode will also occur at longer times for lower values of the applied stress. Each individual mode has an S-N curve, and each of these curves has a different shape. It is possible that, after a certain lifetime, an interchange in the order in which these failure mechanisms occur could take place. In the example of figure 4.41, the calculations indicate that transverse failure in the  $90^\circ$  case is always the first-ply failure. For other laminates, it is possible for this curve to cross others, such as those shown in figure 4.41 for the  $\pm 45$  plies; therefore, a change in the mode of failure would occur for longer lifetimes. Data that show this effect in the critical first-ply failure mode are, however, difficult to obtain because of the uncertainty of determining the occurrence of ply matrix mode failure.

The first analytical investigation of initial fatigue failure of laminates appears to be reference 4.22, which was concerned with angle plies and experimental verification for glass/epoxy laminates, and utilized failure criteria given in reference 4.23, which is essentially the one discussed earlier (chapter 3, section 3.2.6.2). The special characteristic of symmetric angle plies is that, for uniaxial stress in the principal material directions, the stress states in all plies are the same, and therefore, initial failure will occur simultaneously throughout the laminate. However, that does not necessarily imply failure of the laminate. Lamina failure in the matrix mode consists of propagation of cracks along the fibers. Since these cracks are in different directions in adjacent layers, the layers remain partially bonded and the fibers still carry load. Experimental work has shown, in reference 4.22, that angle plies fail more or less at initial laminae failure load for reinforcement angles of  $45^\circ$ - $90^\circ$ , while for smaller angles the ultimate failure load is larger than the initial failure load.

It should be noted that the angle ply laminate is not, in general, a practical laminate which will generally have fiber layers oriented in three or more directions and ultimate failure associated with the fiber failure mode. Other investigations of laminate fatigue failure using various lamina failure criteria have been reported in reference 4.24. The analysis method described on the

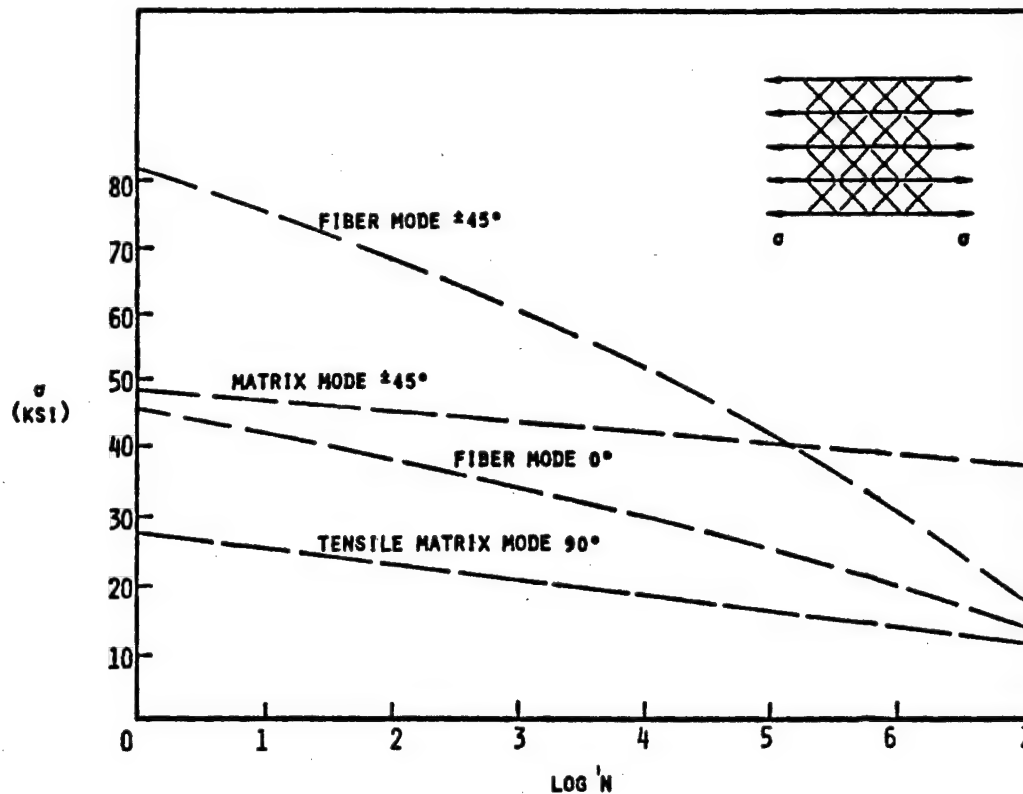


FIGURE 4.41. INITIAL FATIGUE FAILURE ( $0^\circ/90^\circ/\pm 45^\circ/90^\circ/0^\circ$ ).

previous page does not account for failure between plies. Particularly after the onset of some damage, interlaminar disbonds become a realistic possibility during fatigue loading as discussed earlier. Results for initial failures, however, provide the strain limits below which damage growth can be avoided. It also provides the starting point for estimation of subsequent failures addressed later in this subsection.

#### 4.8.1.1.2 Residual Properties.

The above discussion has focussed on the fact that fatigue failure is the result of the accumulation of dispersed damage. It is reasonable to expect that such dispersed damage will result in a decrease in the residual properties of the laminate, eventually to the level where failure occurs. Therefore, the loss in residual properties must be taken into account in the design of a laminate, and the continuing loss of residual properties can serve as the basis for lifetime prediction, just as the crack growth laws in fatigue can lead to the definition of lifetime and suitable inspection periods for metals. This is suggested schematically in figure 4.42.

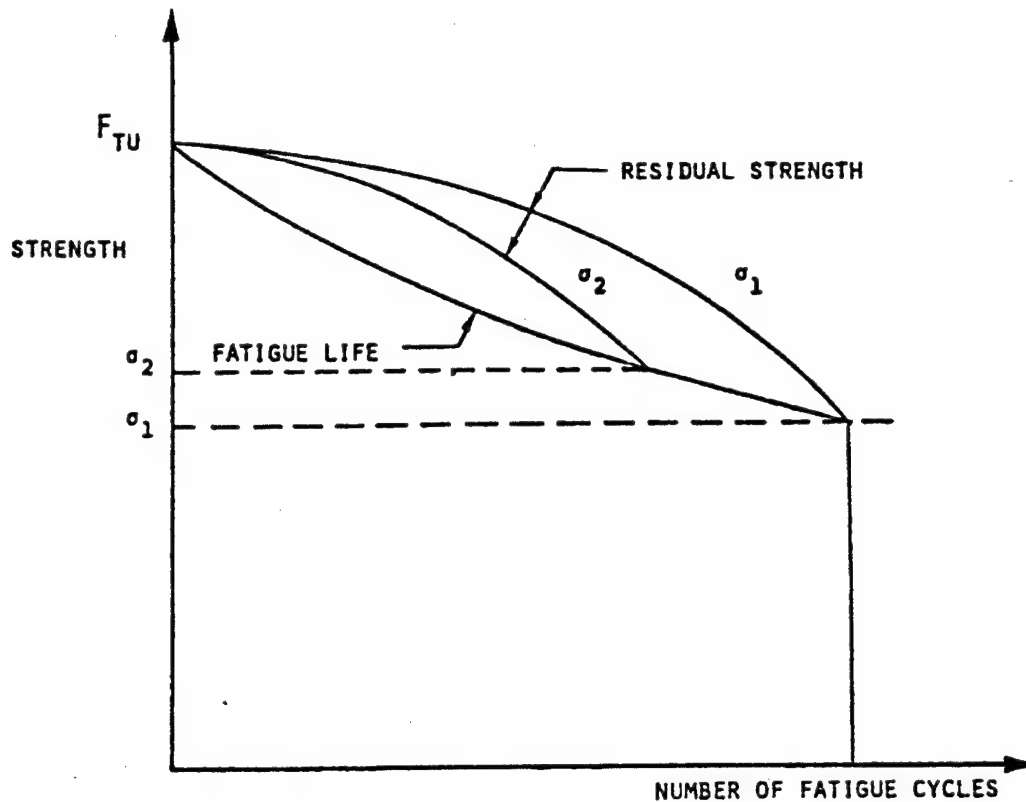
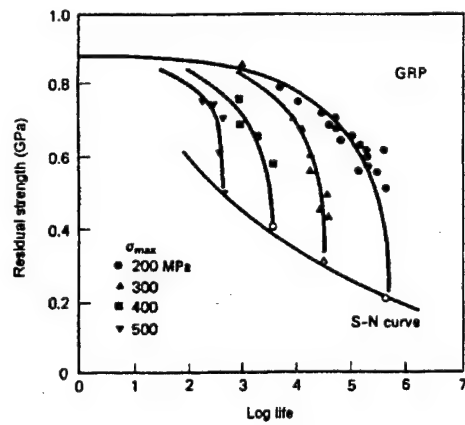


FIGURE 4.42. RESIDUAL STRENGTH AND FATIGUE LIFE

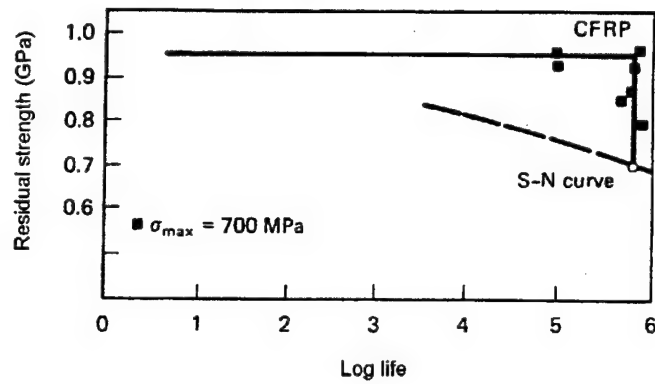
After cyclic load at some particular stress level for some number of cycles, the residual strength, as shown by the upper curves in figure 4.42, would be lower than the initial ultimate static strength of the material. Eventually, the residual strength will decay to where it is equal to the maximum applied stress, and that is exactly what defines a fatigue failure. A residual strength curve for a particular cyclic stress level terminates when it intersects the S-N curve. In other words, there is a family of residual strength curves which is dependent upon the amplitude of the loading, and the locus of the ends of those residual strength curves is the S-N curve for the material. Thus, there is a definite interaction between residual strength and fatigue life.

Some attempts have been made to compare fatigue damage and residual strengths of glass, carbon, and Kevlar reinforced crossply laminates [4.25] which show that residual strength degradation occurs in glass and Kevlar systems (figure 4.43) while carbon fiber composites do not show much reduction in strength till the point of failure, which is catastrophic (sudden death).

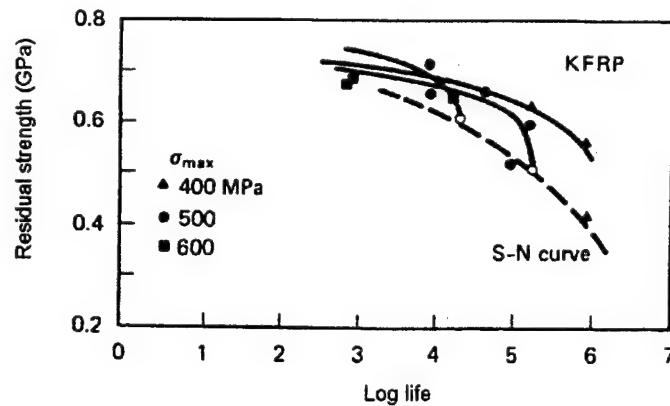
It has also been observed [4.26] that statically stronger materials usually have a longer life (discussed in the previous chapter for unidirectional composites) as suggested by various investigators [4.27 through 4.29].



(a)



(b)



(c)

FIGURE 4.43. RESIDUAL STRENGTH-LIFE CURVES FOR (a) GLASS, (b) CARBON, AND (c) KEVLAR FIBER-REINFORCED CROSSPLY LAMINATES [4.25]



For composites, the dispersed damage accumulation may result in reductions in residual stiffnesses as well as strengths. This is particularly pronounced in glass-reinforced plastics in which the loss in stiffness can easily become the dominant design condition, even though initially the strength may be the governing design condition. Figure 4.44 shows an example of fiberglass data wherein an S-N curve is given by the dashed line. The maximum cyclic stress (for  $R = 0$ ) is normalized with respect to static strength. The solid curve shows the conditions for a stiffness loss of 15%. It is seen that this occurs for a given stress level much earlier than failure. A 15% loss in stiffness of the material may well mean that the material is no longer suitable for a particular application. This is an example in which lifetime would be terminated due to stiffness loss before it is terminated due to strength loss. Similar results for carbon/epoxy have been reported in reference 4.30. However, stiffness loss in fiber dominated layups of carbon/epoxy systems is usually small because the stiffness is dominated by the fibers [4.31]. For crossply glass/epoxy laminates, the ply crack density increases with number of cycles and the stiffness reduction is proportional to the density of such cracks [4.31].

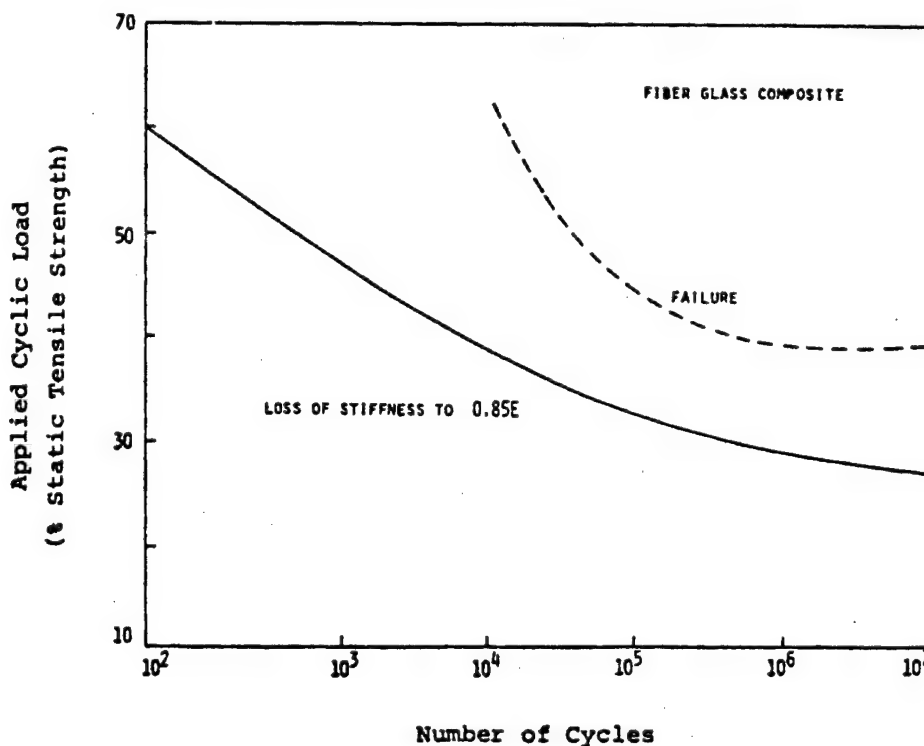


FIGURE 4.44. STIFFNESS LOSS IN SOME GLASS-REINFORCED COMPOSITES

#### 4.8.1.1.3 Subsequent Failures.

When first-ply failure is in the matrix mode, the failed laminae will have undergone a reduction in their strength and stiffness, at least locally. Thus, the subsequent response of the laminate to external loads will have been altered. Increasing the load will cause more widespread damage and redistribution of stresses among the plies. Estimates of this response can be obtained by utilizing reduced ply properties after initial failure.

Typical failures of three nominally identical specimens of a  $(\pm 45^\circ)_s$  boron/epoxy laminate subjected to longitudinal tension-tension loading are shown in figure 4.45. The loading has generated ply matrix mode failure involving a significant amount of material in the failure. The  $\pm 45^\circ$  plies are clearly visible and there is a considerable amount of separation along interlaminar planes, which permits specimen failure. Significant fiber pull-out is noticeable across the break, which is evidence of the substantial matrix damage that had occurred prior to final fracture.

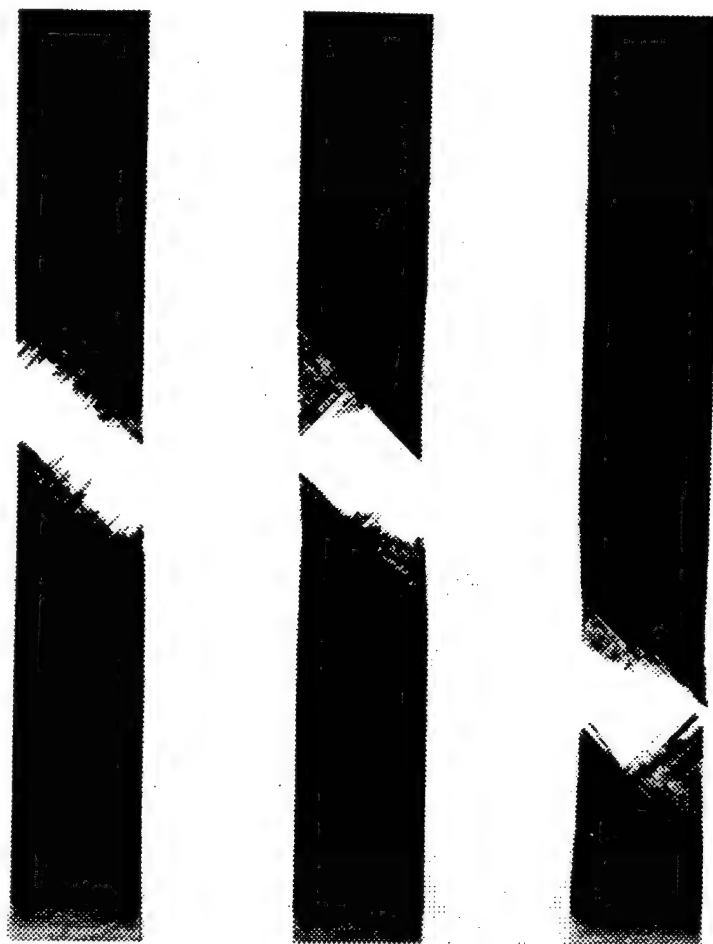


FIGURE 4.45. TYPICAL FAILURES OF  $[\pm 45]_s$  BORON/EPOXY LAMINATES SUBJECTED TO LONGITUDINAL TENSION-TENSION FATIGUE LOADING

In contrast to the  $(\pm 45^\circ)_s$  laminates in figure 4.45, a laminate having both  $0^\circ$  and  $\pm 45^\circ$  laminae (see figure 4.46) shows an irregular failure pattern reflecting dispersed damages accumulating and linking together to form a failure surface, as is normally observed in static failure for this material. This suggests that the use of a method similar to the static, ply-by-ply failure calculation can lead to useful results. Characterization of the individual plies in fatigue, in terms of S-N curves for individual stress components applied to a unidirectional fiber composite, is the first step in a building block approach to failure analysis starting from a first-ply failure criterion.



FIGURE 4.46. TYPICAL FAILURES OF  $[0_2/\pm 45]_s$  BORON/EPOXY LAMINATES  
SUBJECTED TO LONGITUDINAL TENSION LOADING

The procedure to be followed is similar to the static failure calculations in which first-ply failure is determined initially. Ply stiffnesses may then be modified to determine the progression of failure from first-ply failure to ultimate failure. It seems imperative to consider changes in ply properties in the fatigue case because it is expected that, at some relatively short lifetimes, ply cracks will be introduced in the material. It would appear to be undesirable to limit the useful lifetime of the structure to the number of cycles at which these ply cracks are initiated or to limit the load to an extremely low level to prevent such ply cracks. Thus, it is necessary to have the capability of proceeding beyond initial cracking for lifetime prediction. The procedure for predicting fatigue failure in continuous composite laminates subjected to specified cyclic loading can be described as follows:

1. Determine the lamina plane stress cyclic failure criteria on the basis of S-N curves for single stress components.
2. Find the cyclic stresses in all laminae and determine which lamina may fail first and in which mode.
3. Adjust failed lamina stiffness and recalculate stresses.

4. Determine which lamina fails next and in which mode and at what number of cycles.
5. Continue until the expected mode of failure for a lamina is the fiber mode. This defines laminate lifetime for the given cyclic loading.

When the mode of the predicted first ply failure is matrix failure (which is often the case), it is expected that degradation of transverse extensional stiffness and axial shear stiffness would commence and continue with cycling until these stiffnesses totally vanish. For convenience, this continuous stiffness degradation may generally be taken as a stepwise variation.

No application of this approach to laminates is reported in the literature. It is expected, however, that a conservative, first-cut approximation can be obtained if progressive ply failures are included by adjusting appropriate lamina stiffnesses. Such predictions may be too conservative, however, since the predicted failure of each ply does not actually result in complete loss in stiffness. Rather, it means that intralaminar cracking parallel to the fibers will occur at loads at which first-ply failure (which usually takes place in the matrix) is expected. Growth of such cracks is usually constrained because of the presence of adjacent layers; under these constraints the cracks tend to grow into interlaminar disbands which dissipate more energy per unit of fracture surface than other failure modes. This mechanism of damage growth is more noticeable in laminates with discontinuities, which are discussed in section 4.8.2.

Application of this approach to crossply carbon/epoxy laminates without such discontinuities appears to be quite straightforward since the stiffness losses due to ply cracks and delaminations are negligible and almost all of the load is carried by the  $0^\circ$  plies over the entire lifetime of the laminate. Figure 4.47 shows a plot of slopes of stress-life curves (stress normalized by static strength) of various unidirectional and crossply composites plotted against the fiber modulus [4.32] which has been discussed in chapter 3. It may be observed that the slopes for unidirectional and crossply HT-S carbon systems are identical. It appears, therefore, that in systems where stiffness loss is minimal, (the stiffness being dominated by the  $0^\circ$  plies) S-N curves for crossply materials can be estimated from those of the unidirectional material over a large portion of life. Some reduction in life is, however, expected; i.e., sudden death may occur earlier in crossply systems because of other damages whose effect on laminate response remains masked over the entire period of load cycling. A model for unidirectional material discussed in the last chapter (based on the concept discussed in reference 3.96 of a fatal crack consisting of fiber fractures linked by debonds), with due consideration for stress concentrations caused by fiber fractures, may be employed to explain such reductions.

On the other hand, it appears that S-N curves for crossply glass/epoxy have a slope which is higher than that in the unidirectional form of this material. The reason for this difference is the fact that as ply cracks and delaminations develop and grow in the  $90^\circ$  layers (which have a significant contribution in the initial stiffness of the laminate); the load carried by these layers is transferred to the  $0^\circ$  plies. Thus, the  $0^\circ$  plies are subjected to loads with increasing amplitude, and therefore, the life of the crossply laminate reduces at a greater rate than that of a unidirectional material. The reduction can be estimated if one utilizes more accurate estimates of ply crack and delamination growth as well as stiffness loss of the  $90^\circ$  plies to calculate the load transfer with increasing number of cycles and makes use of realistic cumulative damage models (use of Miner's rule may also yield reasonable results) for the  $0^\circ$  layers subjected to

variable amplitude loading. The main obstacle in such a procedure appears to be the modeling of ply crack and delamination growth. Power law type growth laws relating rate of increase of ply cracks and delamination densities to corresponding energy release rates are needed for such modeling. Some investigators have suggested [4.33] that critical energy release rates for delamination initiation may be lowered significantly because of load cycling and have proposed a model for life prediction based on this concept.

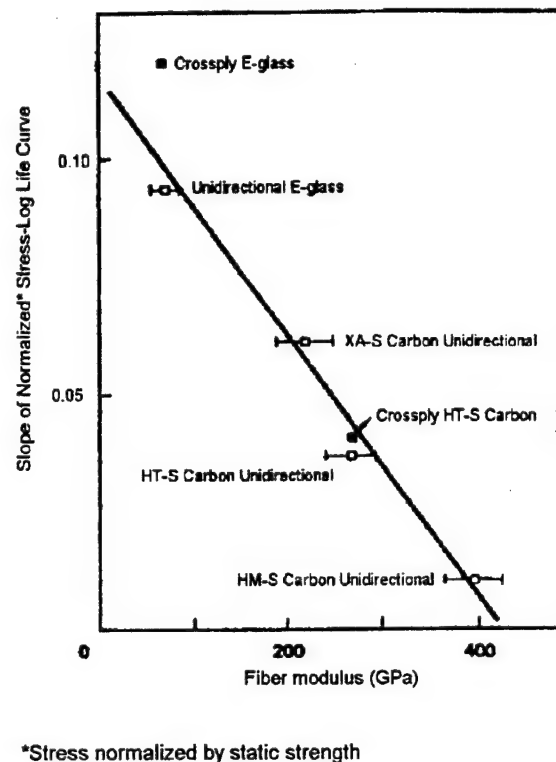


FIGURE 4.47. SLOPE OF CURVES OF STRESS (NORMALIZED BY STATIC STRENGTH) VERSUS LOG LIFE AS A FUNCTION OF FIBER MODULUS IN UNIDIRECTIONAL AND CROSSPLY LAMINATES [4.32]

It appears, therefore, that in materials showing significant stiffness loss, the complexity of tracing the progress of fatigue failure from initiation of first-ply failure to ultimate failure, including intra- and interlaminar failures, precludes exact analysis. One approach is the counterpart to netting analysis for estimating maximum strength. For this approach, the axial shear and the transverse stiffnesses of all plies are set to zero and the approach to first-ply failure described above is utilized. Here the first-ply failure becomes a fiber mode failure and may be taken as a first estimate of the ultimate fatigue lifetime associated with failure. Such an approach may be of value for preliminary design purposes.

When the laminate loading is compressive, additional failure mechanisms exist due to possible local instabilities. Thus, extensive cracking or interply disbonding may result in local buckling which could cause further damage propagation.

For actual design values, test data will be required. Fatigue lifetime data for some basic materials are shown in figure 4.48. Shown here are typical S-N curves for graphite/epoxy components (AS-3501 carbon/epoxy composites) for tension-tension fatigue ( $R = 0.1$ ). A very flat curve exists for tension in the fiber direction. For unidirectional materials, the compression loading curve has a much greater slope than the tension loading curve.

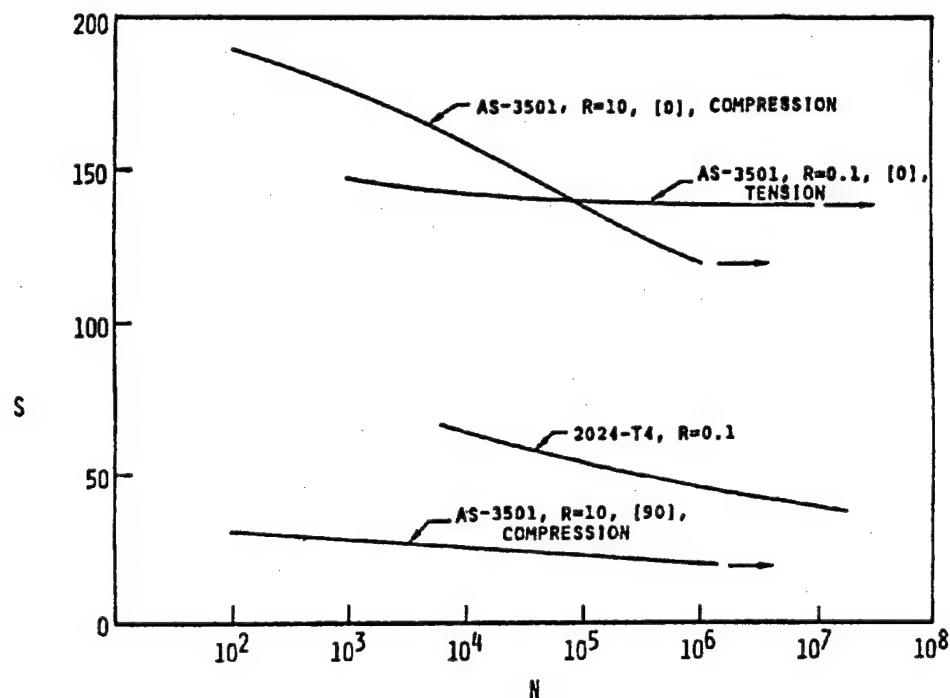


FIGURE 4.48. TYPICAL S-N CURVES

(Although not presented here, data for some materials show a steeper slope to the S-N curve for the case of negative  $R$  value or combined tension and compression cyclic loading.) For comparison, a 2024-aluminum alloy fatigue curve at the same  $R = 0.1$  is also shown in the figure. The slope of this curve is comparable to that of the composite in the fiber direction. The transverse compression curve for this composite is also very flat but at a much lower level than the  $0^\circ$  curve. Use of experimental fatigue data to generate design data is discussed in subsequent sections.

#### 4.8.1.1.4 Concluding Remarks.

The above portions of this subsection have dealt with the physical phenomena occurring during cyclic loading of fiber composite laminates. Understanding of these effects is important in the design of such materials.

The fatigue failure methodology discussed in this subsection is based upon consideration of the state of stress in individual plies and appears to be adequate for fatigue of angle-ply laminates and of lay-ups which do not show much stiffness loss before failure. Fatigue properties (S-N diagrams) of a unidirectional material in the axial and transverse directions as well as in longitudinal shear are assumed to be known. These should be known for the appropriate

environment of temperature, moisture, and frequency. For other kinds of laminates, these methods should yield a good estimate of first-ply fatigue failure. The approach can also be useful for evaluating the performance of other lay-ups if suitable models are used for quantifying the growth of ply cracks and delaminations. For practical applications, however, fatigue behavior of laminates with cutouts, holes, or other discontinuities often govern the design process. Damage growth near such discontinuities is more complex in nature and is addressed in a later subsection.

#### 4.8.1.2 Failure Models Based Upon Dispersed Defects.

When a general laminate is defined for use in a structure for which fatigue lifetime is important, a combination of test and analysis methods must generally be utilized for design. An analytical strength degradation model is desirable for this purpose.

An approach which has been utilized with success for studying fatigue of metals is based upon the concept that cyclic loading produces internal microcracking which progresses to cause failure. There is some appeal to utilizing the mathematical tools of the metals approach in the study of fatigue of composites. A discussion of this approach is presented below.

##### 4.8.1.2.1 A Wearout Model.

For a given structure or component or coupon, growth of damage implies that there is a probability of failure that varies with time. This information is the basis for failure calculations using the fracture mechanics methodology applied to metals. A related approach has also been utilized for composites as well as for bonded or bolted joints. This approach is called the wearout model [4.34 and 4.35], which is based on the following assumptions:

1. Initially, there exist some inherent flaws in the material.
2. These flaws grow in a deterministic pattern which depends on material properties, stress states near the flaws, and history of loading and environmental conditions.
3. Increased flaw size causes decreased material strength.

Because of the diversity of flaws in composite laminates, there will be many different damage growth patterns. Attempts to model these are beyond the reach of a practical engineering analysis method. Hence, the approach is to assume representative functional forms for effects of damage and for damage growth and to quantify the associated parameters by the use of experimental data. The functional relationships usually assumed in the wearout model are those used in metal fracture mechanics, as described in the following. The flaw growth relationship is of the power law type. Thus

$$\frac{da}{dn} = A (\Delta K)^m \quad (4.125)$$

where

A	=	a material property
a	=	the crack size
n	=	the number of load cycles
$\Delta K$	=	the range of the stress intensity factor
m	=	an empirical constant

The stress intensity factor,  $K$ , is defined by the geometry and loading conditions. For a sharp line crack normal to the applied tension in an isotropic infinite plate, the result is

$$K = \sigma \sqrt{\pi a} \quad (4.126)$$

where  $\sigma$  = the far field stress.

Equation 4.126 is valid for a sharp crack in an infinite plate. For other boundary conditions the right-hand side of the equation is multiplied by a function of those boundary conditions. For composites, use of this equation is a hypotheses which may be helpful as a curve-fitting approach to experimental data.

At any point in time, the failure stress for a notched material,  $\sigma_f$ , is considered to be the stress at which the crack propagation will become unstable. Thus

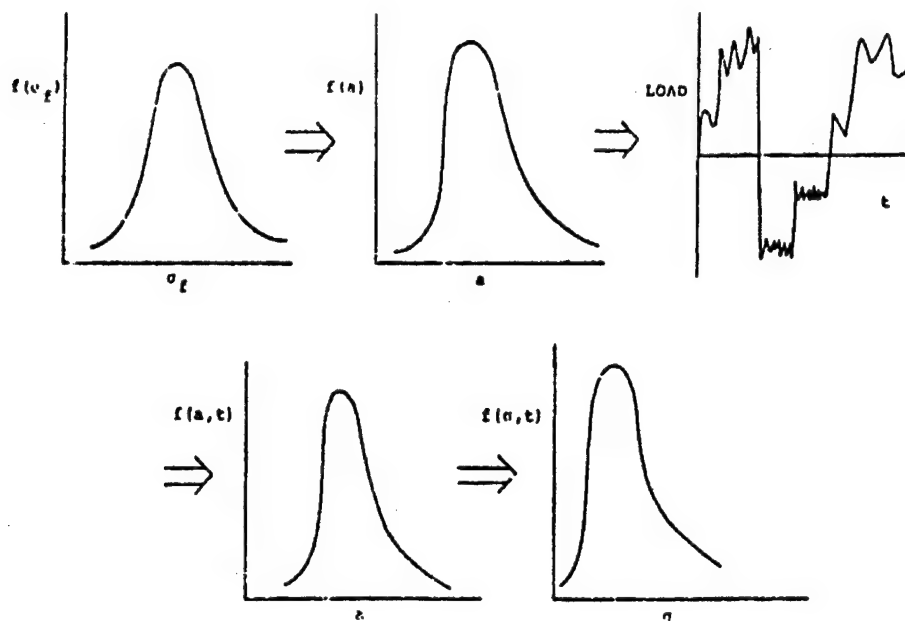
$$\sigma_f = \frac{K_c}{\sqrt{\pi a}} \quad (4.127)$$

where  $K_c$  is the critical stress intensity factor.

The wearout methodology is depicted schematically in figure 4.49. The initial statistical distribution,  $f(\sigma_f)$ , of material strength,  $\sigma_f$ , can be related to an initial distribution,  $f(a)$ , of material cracks of size ( $a$ ) by use of equation 4.127. When these cracks are subjected to cyclic load, they will grow in accordance with a crack growth law such as that of equation 4.125, such that at time  $t$  there will be a new distribution,  $f(a,t)$ , of material cracks. This new distribution of larger cracks defines, via equation 4.127, a new distribution of (lower) strengths,  $f(\sigma, t)$ .

An important effect of wearout is illustrated in figure 4.50. This representation of time dependent strength shows the initial static strength distribution function at time zero and the changes in this function with lifetime. The changes result from the effects of repeated loads and environmental exposure. At any particular point in time, there will be a strength distribution function. This deterioration of residual strength, with time, may eventually bring the material strength down within the applied load envelope, thus causing what is commonly described as a fatigue failure. Fatigue, in this terminology, is the reduction of the residual strength capability down to the applied stress levels.





TRANSLATION FROM STATIC DOMAIN TO FATIGUE DOMAIN

FIGURE 4.49. METAL WEAROUT

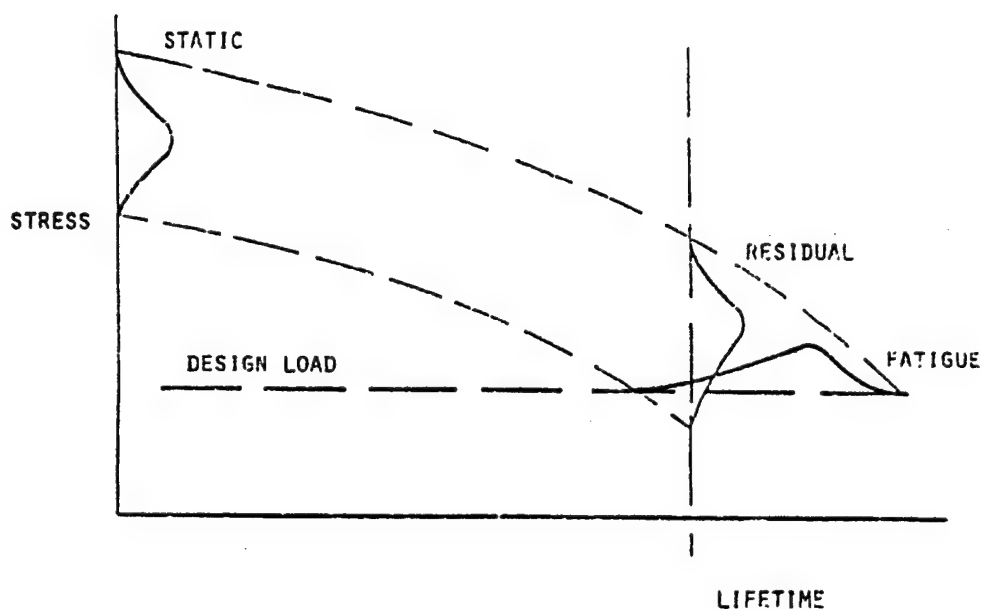


FIGURE 4.50. TIME-DEPENDENT STRENGTH

It is important to emphasize here that residual property characterization need not necessarily be limited to strength. In situations where stiffness critical design occurs, it may well be a deterioration of material stiffness, it may be a change in material damping characteristics, or it may be a change in the susceptibility of the material to any of the various aspects of its environment that becomes the critical design factor.

#### 4.8.1.2.2 Application to Composites.

The critical question here is how this methodology can be applied to composites. The main problem is that there are multiple failure modes so that initial defects do not necessarily propagate in a self-similar way. This is suggested in figure 4.51. A composite laminate is composed of layers of material which are highly anisotropic in their strength characteristics. Thus, there are possibilities for defects to grow perpendicular or parallel to any of the different fiber directions in the composite. The same defect may propagate in different modes depending upon the load history and the environmental effects. Thus, unlike metals, for which the most important damage growth mechanism is a self-similar propagation of an initial defect, in the case of flawed composites, it is necessary to deal with a multiplicity of failure modes.

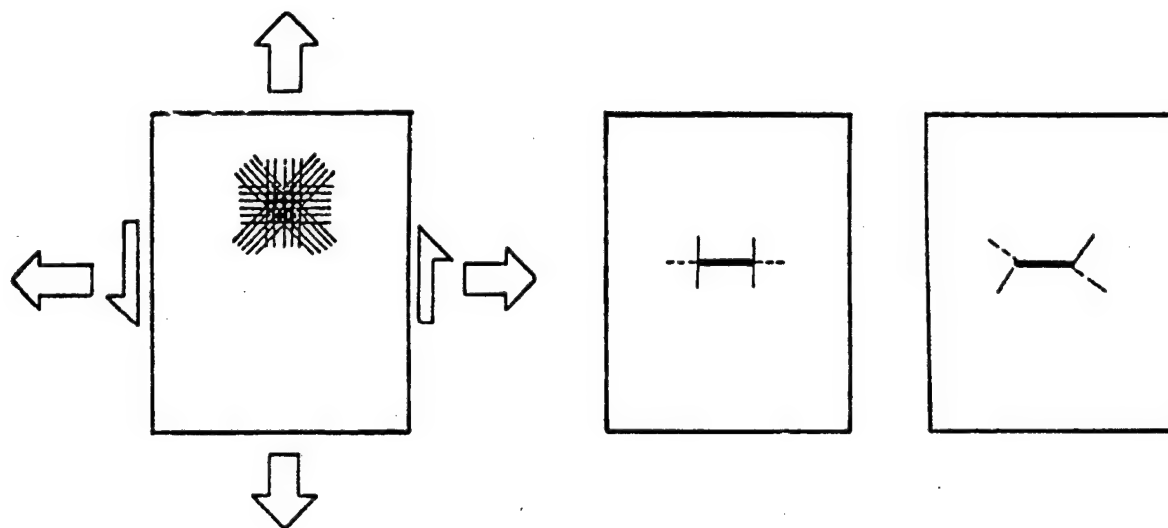


FIGURE 4.51. DAMAGE GROWTH

Initial defects may include fibers which are broken and intra- or inter-laminar defects in the matrix. This initial flaw geometry could change by propagation in the form of adjacent fiber breaks, which is similar to a metal defect. The initial damage could change due to matrix damage, resulting in a crack parallel to the fibers. This will be dependent upon load history and environment (e.g., moisture). Furthermore, there are damage mechanisms which will result from the interactions between layers which may cause local delamination. Thus, even for fiber-dominated laminates, the changes in the matrix stress-strain characteristics can influence the nature of the propagation and hence the design lifetime.

The importance of matrix effects is suggested in figure 4.52 by the fact that even in simple notched laminate tests of boron/epoxy laminates there is a change in failure mode as one switches from static to fatigue loads. Thus, for the two laminates,  $(0_2/\pm 45)$  and  $(\pm 45)$ , with a sharp central slit notch, static loading results in a collinear propagation to two-part failure of the specimen. Similar specimens subjected to fatigue loading experience failure mechanisms in which the plane of failure is parallel to a fiber direction. This change in failure mechanism can have serious consequences in the changes occurring in the flaw distribution functions of figure 4.49.

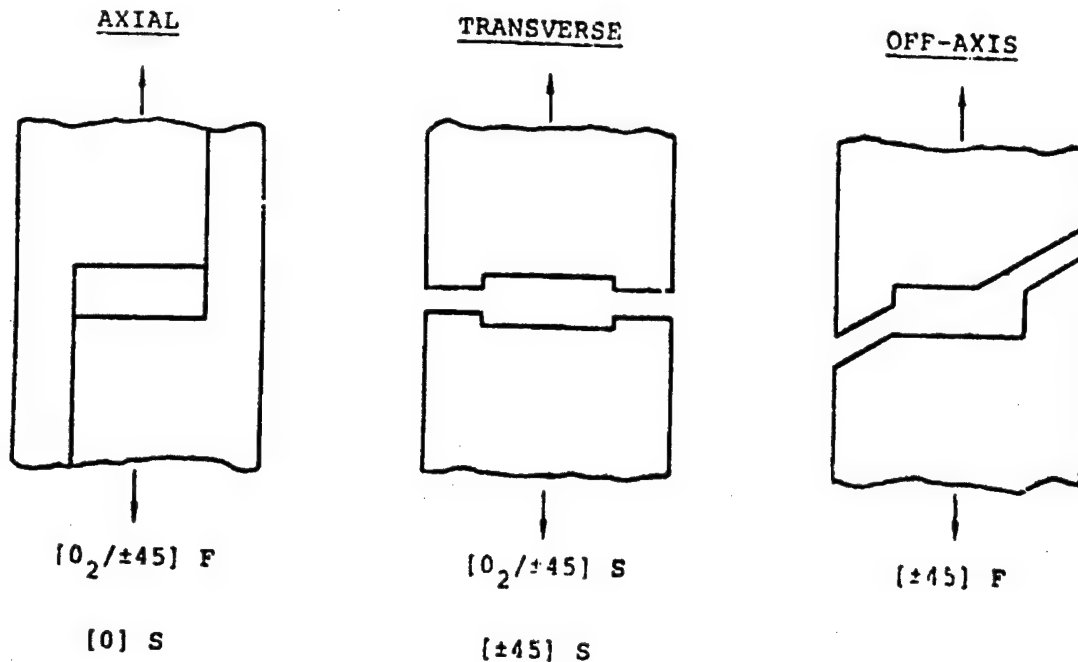


FIGURE 4.52. OBSERVED STATIC AND FATIGUE FAILURE MODES IN TENSION

One example of the problems associated with lifetime prediction for composites is presented in figure 4.53. The curve  $t = 0$  is the probability distribution function for the initial defect sizes. Two alternate damage growth paths are suggested on the right with the growth of the damage in either a collinear or self-similar fashion or in a mode which reflects some additional local failure mechanism in the material. The existence or nonexistence of either of those modes of failure can change the character of the distribution function for the flaws. For a self-similar propagation,  $db = 0$ , the results are the classical effects of the largest cracks growing fastest, the mean size of the flaw growing, and the dispersion in the flaw growing because the rate of growth is proportional to some power of the initial size. In the case of damage growth in the presence of secondary failure mechanisms  $db \neq 0$ , there can be a local blunting of some of the stress irregularities and this can serve to narrow the dispersion associated with the flaw distribution. Thus, although there is an increase in the mean flaw size, there will be a decrease in dispersion.

The primary consequence of these multiple failure modes upon lifetime is that the desired translation from static strength to lifetime may no longer be valid. Figure 4.54 is a simple schematic representation of this problem. The initial static strength distribution function has been broken down into two separate distribution functions which sum to give the measured strength function. If these two failure mechanisms are of the two types shown in figure 4.53, it is entirely conceivable that the change in dispersion of one failure mode can result in a situation in which lifetime prediction will be governed by a mechanism of failure that differs from the one that governs the initial static strength distribution. Thus, the critical life-limiting defects may not be identified by initial proof testing. The possibility exists that it will be necessary to make additional nondestructive inspections or, perhaps, even additional proof tests after a portion of the lifetime environment has been experienced by the structure.

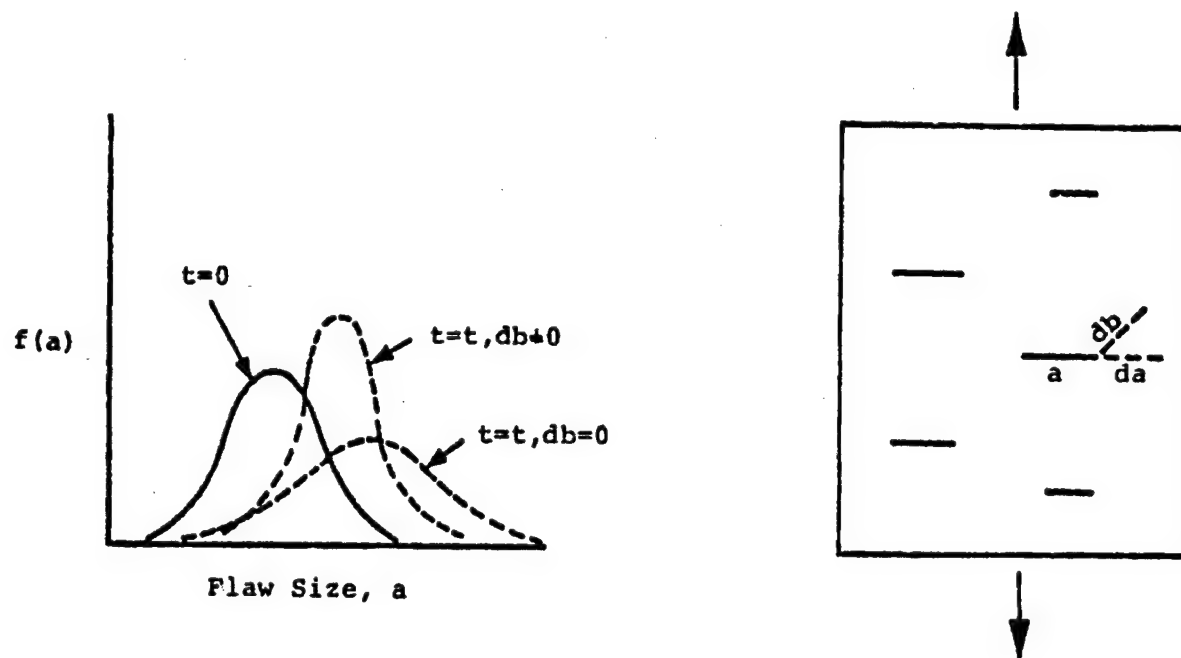


FIGURE 4.53. CHANGES IN FLAW DISTRIBUTION FUNCTION

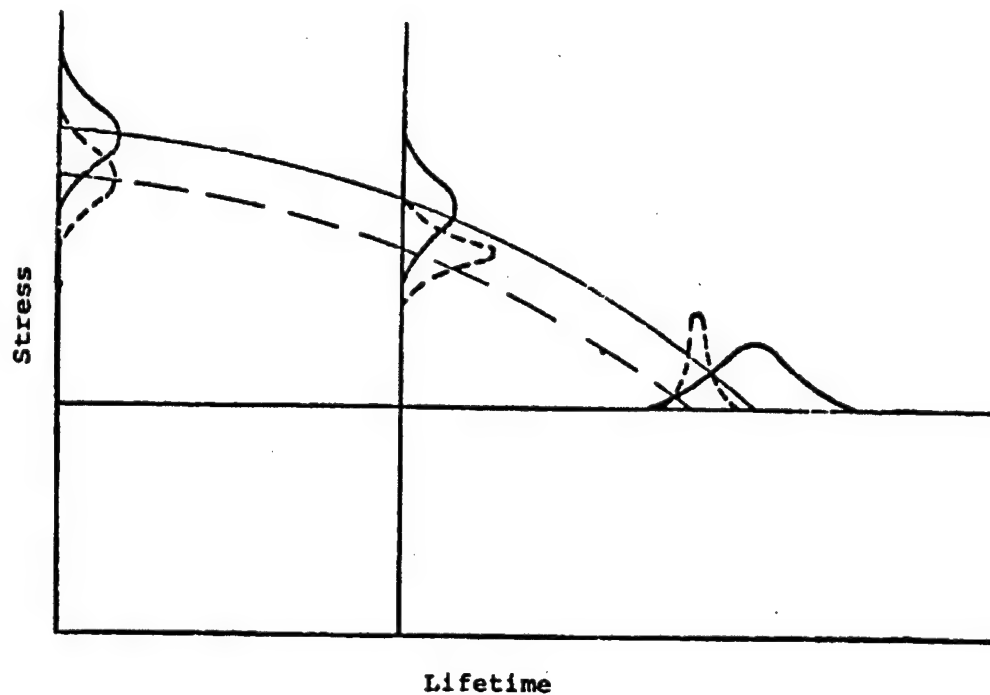


FIGURE 4.54. TRANSLATION FROM STATIC STRENGTH TO LIFETIME

#### 4.8.1.2.3 Concluding Remarks.

The multiplicity of failure modes in composite laminates contrasts with the self-similar propagation of microcracks in metals. As a result, the mathematical fracture mechanics models which have been used with success for metals may not be useful for unnotched composites. However, it should be recalled that a similar situation exists for static fracture of notched composites. In that case, it was found that semiempirical modification of the equations used for the metals provided reasonable correlation for composites data. There is a possibility that similar semiempirical modifications of the preceding approach may yield valid methods for fatigue of composites. This is discussed in section 4.8.1.3.

The merit of this approach is that it relates to the physical realism of damage growth from birth to failure. This suggests the possibility that, in the future, nondestructive evaluation may provide data which could be used to assess remaining life.

#### 4.8.1.3 Macromechanical (Curve Fitting) Models for Fatigue Lifetime.

The validity of analytical methodologies for fatigue of laminates has been demonstrated for only a limited number of cases. It is clear that a mechanistic approach to the problem of life prediction is very cumbersome because of the accumulation of a multiplicity of damage modes. In addition, the methodologies which are useful under one condition may not be applicable under other circumstances. Thus, both analysis and experiment are required. Even this may not resolve all uncertainties, however, so that large safety factors on predictions using the analytic approach are required.

The direct measurement of fatigue properties, a procedure which has been widely used in industry for metals, is difficult for composites. The reasons for this are numerous. A principal reason is that composites do not always show a fatigue, or endurance, limit. Thus, data in the range of  $10^6$  to  $10^7$  cycles of loading still indicate a negative slope for the S-N curve. Furthermore, there is interest in more than one single laminate configuration. If the additional complexities of combined stresses and spectrum loading are added to the need to run tests for large numbers of cycles for many types of laminates, the purely experimental approach becomes impractical.

Despite the above problems, a comprehensive test program is necessary to generate a data base for new components being developed. This data base has to be fairly large, in view of the considerable scatter usually observed in fatigue. Moreover, it is necessary to conduct tests with spectrum loading to simulate the service environment. Empirical methods are also often necessary to assess effects of fatigue in meeting various specifications associated with damage growth. For new design of aircraft components, a comprehensive test program on components or coupons is usually mandatory. For all of these reasons, an experimental data base is required for most composite components before the component is put into service. The data base requirement can be reduced, however, if use is made of analytical methodologies for prediction of life and of residual strength or stiffness.

#### 4.8.1.3.1 Representative Models.

The methods discussed in the previous section for measuring fatigue properties were based upon physical models of fatigue failure. Another approach is to postulate mathematical relationships which can be used to fit existing data and then extrapolated to predict stress levels for long lifetimes. A simple expression of this type which has been used to fit experimental data [4.36] is

$$S = b \ln N + c \quad (4.128)$$

where  $b$  and  $c$  are material constants.

Curves of the type described by equation 4.128 plot as straight lines on semilog graphs, such as figure 4.55. It has been shown that a straight line provides a reasonable fit to test data [4.36].

Another mathematical model used for characterization of S-N curves is the power law

$$S N^{1/m} = g \quad (4.129)$$

or

$$\ln S = \ln g - \frac{1}{m} \ln N \quad (4.130)$$

where  $m$  and  $g$  are material constants.

A comparison between equations 4.128 and 4.129 is shown in figure 4.55 for data representative of carbon/epoxy laminates.

It is of interest to note that the power law expression, equation 4.129, is related to the physical wearout model of the previous section. This is addressed in references 4.37 and 4.38 and a simplified explanation is presented here.

A crack growth law is assumed in the form of equation 4.125. For simplicity, the fatigue loading is assumed to be sinusoidal from  $\sigma = 0$  to  $\sigma = s$ . Thus, from equations 4.125 and 4.126

$$\frac{da}{dn} = A S^m (\pi a)^{m/2} \quad (4.131)$$

This may be written as

$$a^{-m/2} da = A_1 S^m dn \quad (4.132)$$

$$\text{where } A_1 = A\pi^{m/2}$$

Equation 4.132 may be integrated from  $n = 0$  to  $n$ , with crack size varying from initial value,  $a_0$ , to  $a$ .

Thus

$$a^{(1-m/2)} - a_o^{(1-m/2)} = \left(1 - \frac{m}{2}\right) A_1 S^m n \quad (4.133)$$

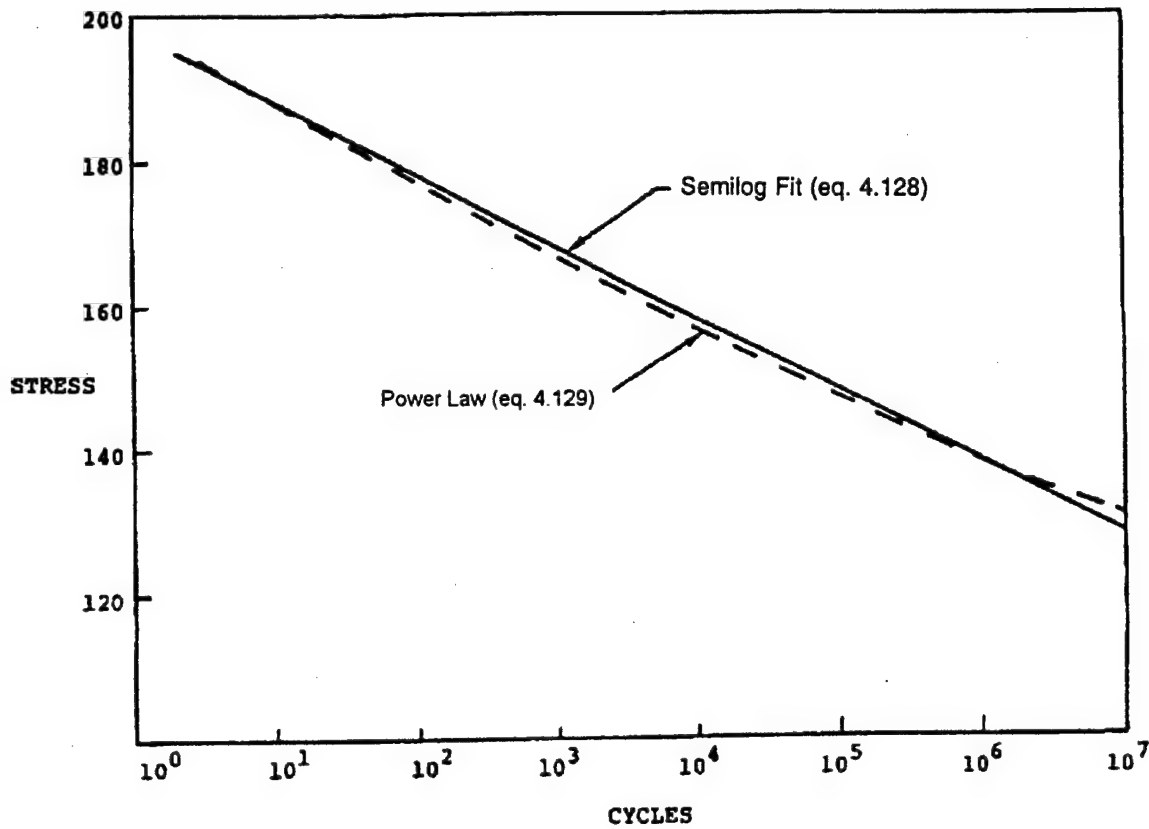


FIGURE 4.55. COMPARISON OF TWO DIFFERENT EXPRESSIONS USED TO FIT EXPERIMENTAL S-N DATA

The crack sizes can be related to strength utilizing equation 4.127. Thus

$$a_o^{(1-m/2)} = \left( \frac{\sigma_o \pi^{1/2}}{K_c} \right)^{m-2} \quad (4.134)$$

Fatigue failure will occur after  $N$  cycles when the crack size has grown to where it is the critical size,  $a_f$ , for failure at the maximum cyclic stress,  $S$ . Thus

$$S = K_c (\pi a_f)^{-1/2} \quad (4.135)$$

Substitution of equations 4.134 and 4.135 into 4.133 leads to

$$1 - \bar{S}^{m-2} = A_o \bar{S}^m N \quad (4.136)$$

where

$$\bar{S} = S/\sigma_s$$

$$A_o = a \text{ constant}$$

For cyclic stresses which are small fractions of static strength and for moderate values of  $m$ ,

$$\bar{S}^{m-2} \ll 1$$

and equation 4.136 is equivalent to the power law of equation 4.129.

The relative merits of the various laws postulated above can only be judged by comparison with experimental data. Such a comparison is made more difficult by the statistical variability of most fatigue behavior. This is discussed in section 4.8.1.4.

#### 4.8.1.3.2 Concluding Remarks.

The deterministic failure models discussed in sections 4.8.1.1 and 4.8.1.2 are attempts to predict failure based upon specific assumptions regarding failure mechanisms. The mathematical expressions presented in the first part of section 4.8.1.3 are attempts to characterize fatigue behavior without resort to a detailed understanding of the failure process. Any of these approaches must take into consideration that statistical variability of composite strength, which is of particular importance after cyclic loading. These methods must be utilized in conjunction with data from a well planned experimental program to provide the proper statistical characterization of the fatigue properties of fiber composite laminates subjected to uniform cyclic loading.

The use of a macromechanical failure model is desirable because it avoids certain complexities. The deficiency of the sequential lamina failure model is that it does not incorporate all the important failure mechanisms. The deficiency of the model for accumulation of dispersed damage is that it is too complex to cope with all practical defects. A mathematical model alone, however, is inadequate; without physical understanding, design with composites is hazardous. The combination of the merits of the different approaches of the section appears to be a desirable path to follow.

#### 4.8.1.4 Properties for Design.

##### 4.8.1.4.1 Allowable Stresses.

There are alternative means for formulating design criteria for composite materials. One approach is to specify deterministic static and fatigue properties. Thus, a static stress-strain curve



defines yield and/or ultimate stress for static loading and an S-N curve defines stress levels for fatigue. One or more safety factors can then be used; e.g., there could be one safety factor for yield stress, a different safety factor for the ultimate strength, and a lifetime factor for the S-N curve. The difficulty with doing this is associated primarily with the statistical variability, both in constituent material properties and in lifetime data. It is possible to account for this by characterizing material properties in a statistical sense. Material allowables can be used to obtain a desired confidence level for static strength properties (either yield stress or ultimate stress). For example, the A-basis value for a particular distribution is defined as a 95 percent lower confidence limit on the first percentile of the distribution and the B-basis is a 95 percent lower confidence bound on the tenth percentile of a specified population. Similarly, consideration of the distribution in fatigue lifetime data leads to the establishment of a scatter factor that is large enough to reduce failure probabilities to the desired level (see figure 4.56). The statistical approach to fatigue failure requires modifying the S-N curves so that they become P-S-N curves (probability-stress-number of cycles), figure 4.57. These are curves defining the maximum cyclic stress level which leads to different probabilities of failure at a specified lifetime. Considering the degree of lifetime scatter that is found in fatigue tests, it is reasonable to replace an S-N curve, which might represent the mean (or the mode) of the data, with a family of curves in which there are different probabilities of failure. This provides a direct counterpart between the statistical characterization of the fatigue data and the statistical characterization of the static material properties data.

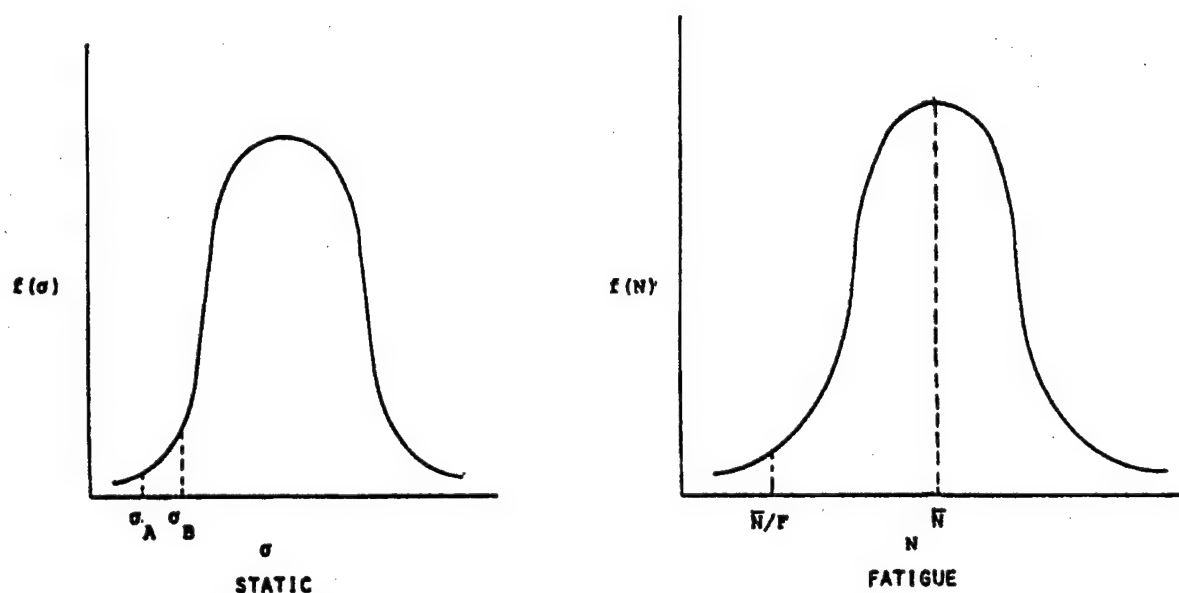


FIGURE 4.56. STATISTICAL MATERIAL PROPERTIES

In composite materials, a statistical approach to the definition of residual properties can also be taken. The residual strength distributions at different lifetimes can be used to generate curves of given probability for residual strength after specified numbers of cycles (see figure 4.58). This provides a mechanism for incorporating statistically based concepts into the definition of material allowables.

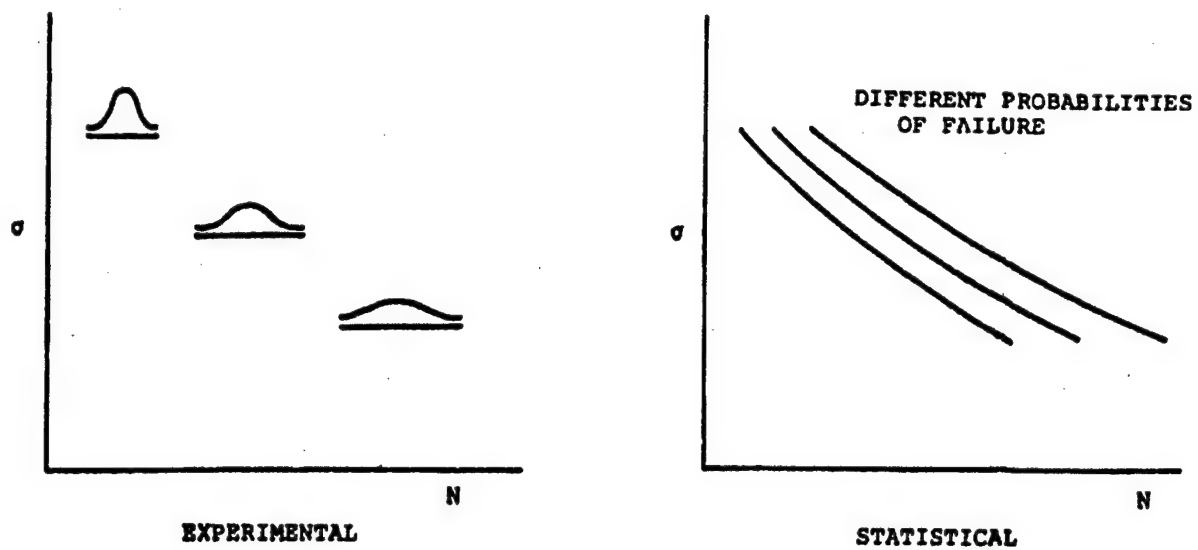


FIGURE 4.57. P-S-N CURVES

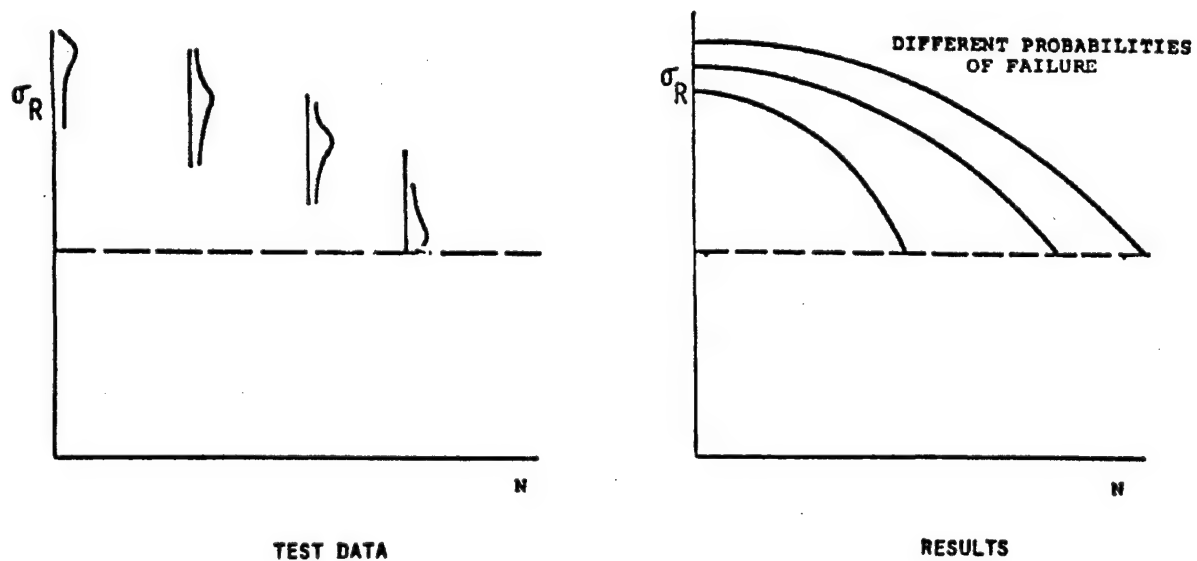


FIGURE 4.58. STATISTICAL RESIDUAL STRENGTH DATA

In addition to the fact that there is variability in the material properties, the load applied to aeronautical structures varies in time and should be described on a statistical basis. A loading spectrum for a particular component can be characterized in terms of a load exceedance curve, which specifies the frequency with which a load will be exceeded during a given time period as a function of the magnitude of the load. This will show a large number of loading cycles at low

loads with a continually decreasing number of cycles at large loads. Procedures exist to treat the effects of material variability as well as uncertain loading conditions. A load exceedance curve defines the probability of encountering a given load in a specified time period. This is combined with the strength distribution curve; namely, the probability of failure for a given load. The intersection of these two curves defines an expression for probability of failure. Thus, the probability that any part fails is really the probability of encountering a given load multiplied by the probability of failure when that load is encountered. This is obtained by evaluating the intersection of the load exceedance spectrum with a residual strength distribution function, as shown in figure 4.59.

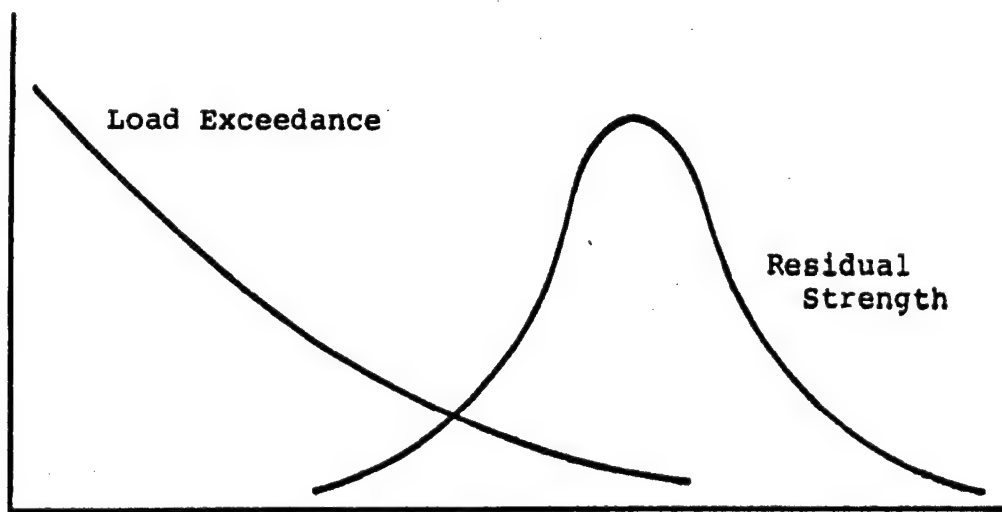


FIGURE 4.59. PROBABILITY OF STATIC FAILURE

If the probability density functions  $f(s)$  of exceedance of load  $s$ , and  $g(\sigma, t)$  of residual strength  $\sigma$  after time,  $t$ , are known, then the probability of failure  $p(t)$  for a maximum load level  $L$  of one number of a set can be calculated by the following:

$$p(t) = \int_0^L f(s) \left\{ \int_0^{\sigma(s)} g[\sigma(s), t] d\sigma \right\} ds \quad (4.137)$$

and the cumulative distribution function  $P(t)$  is given by

$$P(t) = \int_0^t p(\tau) d\tau \quad (4.138)$$

Hence, the reliability (i.e., probability of survival),  $R(t)$ , is defined by

$$R(t) = 1 - P(t) \quad (4.139)$$

Considering a set of  $n$  units (chosen in a random fashion), the probability of zero failures of  $n$  units at time  $t$ , denoted  $R_n(t)$ , is therefore

$$R_n(t) = [R(t)]^n \quad (4.140)$$

The probability of at least one failure of this group,  $P_n(t)$ , is

$$P_n(t) = 1 - R_n(t) \quad (4.141)$$

The distribution function for the time to first failure can, therefore, be obtained by differentiation using the following relationship

$$p_n(t) = \frac{d}{dt} \{1 - [R(t)]^n\} \quad (4.142)$$

From this, any desired characteristic of this distribution can be found. For example, the expected time to first failure,  $t_e$ , is

$$t_e = \int_0^{\infty} t p_n(t) dt \quad (4.143)$$

This time is a suitable measure of the lifetime of a class of structures. For any given member of this class, failure probabilities are defined by equation 4.137. The failure probability for the desired lifetime is used to calculate the reliability from equation 4.139. The desired reliability in a component is established by the process of breaking down system reliabilities into component reliabilities. It is then possible to assign a specific component reliability goal. For a certain reliability goal we also have a certain probability of failure at that lifetime.

#### 4.8.1.4.2 Cumulative Damage.

The development of models for the characterization of fatigue lifetime have addressed the condition of uniform cyclic loading. In practice, however, the structural loads are a complex combination of time varying loads, as discussed in chapter 3. Application of fatigue data for steady cyclic loads to the determination of fatigue lifetime under spectrum loading is known as the cumulative damage problem. The basic concept is that each load application causes a small, but definite, decrease in the remaining lifetime of the material.

In practice, a random loading spectrum is obtained for the aircraft structure. This can be represented by a sequence of uniform load cycles of various amplitudes and stress ratios. This sequence of blocks of cyclic loads defines a similar sequence of cyclic stresses at any laminate location. These stresses may be viewed at the laminate or lamina level for use in lifetime prediction.

Cumulative damage effects may be incorporated into any of the fatigue analysis methods discussed in this section. A desirable objective would be to compute the time to failure of a laminate under a cyclic loading program in terms of the fatigue characteristics and the

geometrical arrangement of the layers. This approach would have to consist of the following steps:

1. Construct a cumulative damage theory for unidirectional laminae in states of plane stress (see section 3.2.6.3).
2. Perform a stress analysis of the laminate and determine first failure.
3. Adjust lamina stiffnesses and repeat the procedure for subsequent failures until the load carrying capacity of the laminate is exhausted.

Unfortunately, such a fundamental approach is not feasible today because a reliable cumulative damage theory of unidirectional materials under combined cyclic stress is not available. A further complication arises since lamina stiffnesses may deteriorate with the number of elapsed cycles. This would have to be taken into account in the stress analysis of the laminate. It is possible to determine such stiffness reduction experimentally for constant amplitude cycling, but such an empirical approach for stiffness reduction for a sequence of cyclic loadings is completely impractical because of the infinite variety of possible loading programs. What would be required is a theory for stiffness reduction resulting from cyclic loading programs.

Failure analysis models based upon degradation resulting from growth of dispersed defects can also utilize cumulative damage models. Thus, if a damage growth law were known for a given inherent defect, it could be expressed as a function of applied stresses. Damage growth could then be determined by sequential application of the cyclic load program. In that case the residual strength law could be related to the resulting damage at any time. The methodology discussed in section 4.8.1.2 is then directly applicable.

The more common approach to incorporation of cumulative damage effects into the lifetime prediction methodology is via the use of macromechanical failure models. For a deterministic failure law for a laminate under uniaxial cyclic stress, cumulative damage effects are readily incorporated through the use of a damage hypothesis such as the Palmgren-Miner Rule (see section 3.2.6.3). Alternatively, rules for degradation of residual strength, or for damage curves using an equivalent cyclic loading postulate (as discussed earlier for unidirectional composites), could also be applied at the laminate level. All of these rules address only a single component of cyclic stress. Cumulative damage theories for laminates under combined stresses do not exist.

The literature on the subject of cumulative damage of laminates is sparse. One of the earliest investigations is reference 4.39, which gives experimental data for failure of glass/epoxy crossplies under two-stage loading and attempts to correlate the data in terms of a linear strength degradation model. More general treatments based upon more versatile strength degradation models have been given in reference 4.40. The experimental data are not in agreement with the simple Miner's rule, equations 3.127 and 3.128. There are cases in which the data are either conservative or unconservative with respect to Miner's Rule [4.41].

When statistics are incorporated into the failure model, as they must be, additional uncertainty arises. As pointed out in reference 4.42, the theories of cumulative damage are of deterministic type. Comparison procedures for experimental results, which show statistical scatter under

identical loading conditions, are not well established. It is not obvious that the mean of the statistical data is the appropriate parameter for comparison; perhaps some other statistical parameter should be used. A discussion of statistical characterization of fatigue lifetime follows.

#### 4.8.1.4.3 Statistical Characterization.

The design needs for fatigue data have been discussed and defined earlier. It has been shown that the conventional S-N curve is but the first step in material characterization for fatigue. The scatter in lifetime data makes P-S-N curves an imperative. Further, for composites, an endurance limit may not exist for all types of loading. Hence, long lifetime data are needed, and methods for accelerated lifetime testing are desired. Clearly, in order to avoid prohibitively large test programs, available data should be used to define the parameters in an appropriate mathematical model which can then be used to generate the required design data.

A common theme in the evaluation of composite fatigue data is the utilization of a two-parameter Weibull statistical distribution, which may be expressed in the form

$$F(x) = 1 - \exp [-(x/\beta)^\alpha] \quad (4.144)$$

where

$$\begin{aligned} F(x) &= \text{the cumulative distribution function} \\ \alpha &= \text{the shape parameter} \\ \beta &= \text{the scale parameter} \end{aligned}$$

The probability density function  $f(x)$  is found from equation 4.144 by differentiation:

$$f(x) = \frac{dF}{dx} \quad (4.145)$$

and this distribution can be characterized by its moments,  $M_i$ :

$$M_i = \int_0^\infty x^i f(x) dx \quad (4.146)$$

The mean value,  $\bar{x}$ , and the standard deviation,  $s$ , are defined by this moment function as

$$\begin{aligned} \bar{x} &= M_1 \\ s &= [M_2 - M_1^2]^{1/2} \end{aligned} \quad (4.147)$$

Substitution of equations 4.144 - 4.146 into equation 4.147 yields

$$\bar{x} = \beta \Gamma \left( 1 + \frac{1}{\beta} \right) \quad (4.148)$$

where  $\Gamma$  denotes the standard gamma function; the coefficient of variation is

$$\frac{s}{\bar{x}} = \frac{\left[ \Gamma \left( 1 + \frac{2}{\alpha} \right) - \Gamma^2 \left( 1 + \frac{1}{\alpha} \right) \right]^{1/2}}{\Gamma \left( 1 + \frac{1}{\alpha} \right)} \quad (4.149)$$

It is seen that the mean value depends only upon the parameter  $\beta$  and the coefficient of variation only upon the parameter  $\alpha$ , hence the use of the names "scale parameter" for  $\beta$  and "shape parameter" for  $\alpha$ .

A first approach to the data for a specific cyclic loading condition (i.e., a specified maximum stress and a stress ratio) is to fit distribution of time to failure using the functional form of equation 4.144. Thus, for example, the probability,  $P(N)$ , of survival after  $N$  cycles may be defined as

$$P(N) = 1 - \exp \left[ - \left( \frac{N}{N_o} \right)^\alpha \right] \quad (4.150)$$

where

$N_o$  = the scale parameter or characteristic time to failure  
 $\alpha$  = the shape parameter

The parameters in this distribution can be evaluated for each of the cyclic loading conditions for which experimental data are available. With this information, it is possible to construct P-S-N curves from the available data. Methods for establishing parameters in statistical distribution functions from limited data have received extensive treatment in the literature related to metal fatigue [4.43]. Treatment of statistical methods for data evaluation is not unique to composites and is beyond the scope of this text. (See MIL-HDBK-17-1D, reference 4.44, for a discussion of the subject.) The above treatment of P-S-N curves is primarily of value for interpolation over the region in which test data have been obtained. These data can be extended by the use of a mathematical fatigue hypothesis in conjunction with a distribution function. In reference 4.37, the distribution function (4.150) is utilized along with a fatigue power law, equation 4.129. In this approach, data for various load conditions are pooled to establish a single shape factor and the functional form of the relationship between stress and the scale parameter. This provides a format suitable for extrapolation of available data to longer lifetimes.

An alternate approach to this problem is to focus first upon residual strength characteristics. In place of equation 4.150, a distribution,  $F(\sigma_r)$ , of residual strength,  $\sigma_r$ , after a specified number of cycles,  $N$ , may be considered. Thus

$$F(\sigma_r) = 1 - \exp \left[ - \left( \frac{\sigma_r}{\beta} \right)^\alpha \right] \quad (4.151)$$

The parameters of this distribution can be evaluated from experimental residual strength tests. Then, in place of the fatigue power law, a residual strength decay law may be postulated [4.39, 4.45, and 4.46]. Yang and Liu [4.39] chose an expression of the form

$$\frac{d\sigma_r}{dN} = -f(S, r, \omega) / c \sigma_r^{c-1} \quad (4.152)$$

where

- $r$  = the stress ratio for cyclic loading
- $\omega$  = the frequency
- $c$  = a constant

Since fatigue failure occurs when the residual strength,  $\sigma_r$ , is reduced to the maximum applied cyclic stress,  $S$ , equations 4.151 and 4.152 can also provide a framework for fitting existing experimental data with expressions that can be used to predict longer lifetime behavior.

Still another approach is represented by the early work of Halpin, Jerina, and Johnson [4.35], who incorporated statistical variability into the wearout model. Other approaches exist as well. However, the key point is that when assumptions are made with regard to (a) the statistical form of lifetime data obtained for given cyclic loading conditions (or for residual strength data obtained after a given number of cycles) and (b) the functional form of the relationship between load and mean lifetime (or mean residual strength and lifetime) it is possible to establish a statistical representation of stress and lifetime which is useful for defining P-S-N curves over the full-time scale of interest. At the present time, this appears to be the most promising approach to fatigue evaluation of continuous laminates.

#### 4.8.2 Laminates with Discontinuities.

Understanding the fatigue failure of continuous laminates subjected to cyclic loading is but a first step in the fatigue design of aeronautical structures. Practical structures will have regions of stress concentrations which may be the origin of cracks or other forms of damage that can propagate to failure during cyclic loading. As a result, the design of composite aircraft structures for specified lifetime under a defined spectrum of loads is a complex task. An understanding of numerous failure mechanisms at various locations within the structure is required, including regions both with and without discontinuities.



For known external loading, the membrane stress state at any point in a structure is defined, and the lifetime can be determined by using the methods of section 4.8.1. This approach can be used, in particular, to find the structural location having the shortest predicted lifetime. The approach must be modified, however, when the critical region is in the vicinity of a free edge such as the periphery of a cutout. This approach is less useable when the location of interest contains high stress gradients corresponding to the presence of stress concentrations.

The problems resulting from stress concentrations and free edges are best illustrated by considering a laminate containing a circular hole. Static fracture for this case was considered in section 4.7.4. The stress distribution described therein (see figures 4.32-4.34) help explain the nature of the fatigue problem. The in-plane stress concentrations (figure 4.32) may give rise to in-plane cracks, and the interlaminar stresses (figures 4.33 and 4.34) may give rise to disbonding at the free edges. Each of these defects may grow as a result of cyclic loads, at different rates and in different directions, ultimately leading to failure. This problem is discussed in section 4.8.2.1.

Another difficulty associated with lifetime prediction for practical laminates stems from the fact that interlaminar disbonds can occur during manufacture or service. When a disbond exists in a region where the laminate is subjected to out-of-plane loads or to transverse shear, the disbond may propagate to critical dimensions under cyclic loading conditions. This problem is discussed in section 4.8.2.2.

Regions of discontinuity and stress concentration may also be introduced by abnormal conditions such as foreign object impact. Although this is discussed separately in section 4.8.3, service damage is a problem having much in common with the local failure due to stress concentrations or to imperfections resulting from the fabrication process. In all these cases, the concern is with the possible stable growth of local defects under cyclic load. Defect regions may reach a size at which the structure is weakened so that it may no longer be able to carry the design ultimate loads.

The subject of defect criticality is the focus of much current research. It is not intended that this text provide a detailed discussion of such contemporary research; rather, the material presented here is intended to describe the nature of the possible damage growth and to alert the reader to the necessity of a sound test program to validate defect tolerance of the structural design. Design procedures to address these issues will be discussed qualitatively.

#### 4.8.2.1 Damage Initiation and Growth at Unloaded Holes, Notches, or Cutouts.

The growth of a crack at a hole in a plate structure is the classic representation of a single isolated damage propagation mechanism which dominates structural failure. In fatigue of metals, a hole in a plate subjected to cyclic membrane loading gives rise to crack initiation at the edge of the hole, followed by stable crack propagation, and then by catastrophic failure. For composites, a number of experimental studies of fatigue behavior of laminates with circular holes have reported a similar sequence of damage initiation and propagation. Various damage growth mechanisms which are observed indicate that matrix mode failure corresponding to cracks parallel to the fibers is the first damage to initiate. As load cycling continues, these intralaminar cracks are followed by interlaminar disbonds. For the case of cyclic loading, the complexity of damage

growth mechanisms is increased because of local degradations in residual strength (and perhaps in residual stiffness). Depending upon the laminate construction, this damage progresses with increasing numbers of cycles, with either interlaminar or intralaminar cracking predominating. Depending upon the type and direction of damage growth, residual strength will change; ordinarily it will decrease monotonically. However, the residual strength of the laminate can sometimes increase because of a reduction in stress concentration due to local cracking at the hole. Consideration of changes in residual strength and simultaneously modelling growth of various kinds of damage poses a difficult problem. Combined modelling of intralaminar damage growth and strength degradation for correlation with experimental data has been attempted in reference 4.47. Growth of inherent interlaminar disbonds has been modelled in reference 4.48 by the use of semiempirical, self-similar crack growth laws, which are commonly used for metals. For compression, a wearout-type model to predict residual strength and/or lifetime based on buckling of the delaminated plies has also been attempted for data correlation purposes in reference 4.49. An attempt to model changes in residual strength as well as growth of intralaminar and interlaminar damage is reported in references 4.50 and 4.51. These studies clearly show two major problems with which one has to deal in modelling damage growth. The first problem is that a database does not exist for the changes in residual strength of the unidirectional lamina which includes tension and compression (in longitudinal and transverse directions) as well as in shear. The second problem is the complexity involved in stress analysis in the presence of both intralaminar and interlaminar damage.

The solution to the first problem can be obtained by a comprehensive test program. Alternatively, limited test data and reasonable estimation procedures (e.g., linear residual strength reduction) may be utilized.

An attempt to deal with the stress analysis problem just discussed by use of special finite element formulations is described in reference 4.52, where it is shown that fiber breakage, matrix crazing, crack bridging, matrix-fiber debonding, and axial splitting can occur near a built-in flaw in a unidirectional composite under quasi-static loading. However, use of this approach for studying damage growth during cyclic loading in laminated composites is likely to be too cumbersome as well as too expensive to be practical and has not been attempted to date. For compression loads, such micromechanical models should also include the effects of imperfections and the possibility of microbuckling of the fibers. For the study of laminated composites, use of 3D finite elements has been attempted in the past. Modelling each lamina as an assembly of plate-type elements may also be attempted. Modelling damage growth requires an iterative technique, in which case the use of 3D brick elements or plate elements becomes an expensive proposition. For many types of laminates subjected to tension loadings, the effects of normal displacements can often be neglected, and in such cases each lamina can be modelled using membrane elements to depict the in-plane response. Such an approach has been utilized in reference 4.53 where the nodes in adjacent laminae are assumed to be connected by shear springs which are assumed to be rigid under extension. The stiffnesses of the springs are calculated from the interlaminar shear moduli. To model damage growth under quasi-static loading of notched laminates, the model is loaded in steps, and after each step, appropriate stiffnesses of each element are reduced if failure is expected in a particular mode, following which the load is recalculated in an iterative fashion. To consider load cycling effects in tension fatigue, use is made of assumed degradation characteristics of each strength parameter. An iterative technique is again used. The methodology of reference 4.53 has been used for a compression fatigue study in reference 4.54.

The model of reference 4.53 will be described further to illustrate the phenomenon of damage growth. To study progressive damage growth the model considers the interactions of the individual plies and uses tensile or compressive matrix failure and ply disbonding as the failure mechanisms. Stress analysis in the presence of various damage modes is carried out in an iterative manner. The methodology consists of a finite element stress analysis together with a failure analysis. A detailed study of load cycling effects is not considered, but an attempt is made to determine effects of degradation of matrix material in each lamina and strength characteristics of the interfaces because of fatigue. However, use can be made of a fatigue analysis methodology similar to the ones utilized in references 4.49, 4.50, and 4.52 to consider the effects of load cycling on gradual strength degradation. This approach has the ability to predict the types of damage which may occur, in contrast with macromechanical life prediction methodologies based on empirically determined failure modes.

The laminate is modelled with membrane and beam elements. The membrane elements are used to represent the individual plies and are quadrilateral plane stress elements with orthotropic elastic properties. The beam elements are used as shear springs to represent the ply interfaces; they also have orthotropic elastic properties but do not allow relative displacements in the thickness direction. The moment of inertia of the cross section is adjusted to obtain the necessary shear displacement from the beam bending stiffness. This model appears suitable to demonstrate concepts; for a more detailed quantitative analysis, use of a more sophisticated finite element model may be necessary.

The objective of this analysis is the prediction of the load at which the different elements in the model will fail. Composite laminates can fail in various modes; hence, a number of different failure criteria are required to determine the likely mode of failure. The criteria used in the analysis of reference 4.53 are presented in table 4.9. These criteria deal with three types of failure: matrix and fiber failure within a lamina and interlaminar failure. In-plane and interlaminar failures are assumed to have no interaction; i.e., only the in-plane stresses are involved in in-plane failure mechanisms, and interlaminar failure results only from interlaminar shear and normal stresses.

The failure analysis methodology is outlined in figure 4.60. In every load step, static strength is considered first. Stresses are calculated with a finite element analysis for a unit load. For each element, assuming linear elastic behavior, failure load ratios are calculated by comparing the stress distribution with all the failure criteria. The lowest ratio is determined and both the failure load and the mode of failure for the element are predicted. The failure loads for all elements are compared with an applied load slightly higher than the lowest failure load, and all elements that have failed are identified. The possibility of gross laminate failure is then examined by comparing the applied load with the residual laminate strength. If failure is not predicted, loss of strength and stiffness of the failed elements is reflected in the next step by reducing their stiffnesses and load-carrying capacity. This analytical process can be repeated until the laminate fails.

Load-cycling effects can be considered readily if the methodology assumes that the principal effect of fatigue loading is the reduction in material strengths due to accumulation of localized damage. In practical fiber composites, the matrix is especially susceptible to fatigue damage, but the fibers remain largely unaffected. Due to matrix wearout, there is significant reduction in

TABLE 4.9. FAILURE CRITERIA [4.53]

Tensile Fiber Mode

$$\left( \frac{\sigma_{11}}{\sigma_L^u} \right)^2 + \left( \frac{\sigma_{12}}{\tau} \right)^2 = 1$$

Compressive Fiber Mode

$$\left( \frac{\sigma_{11}}{\sigma_L^{cu}} \right)^2 + \left( \frac{\sigma_{12}}{\tau} \right)^2 = 1$$

Tensile Matrix Mode

$$\frac{1}{(\sigma_T^u)^2} \sigma_{22}^2 + \frac{1}{\tau^2} \sigma_{12}^2 = 1$$

Compressive Matrix Mode

$$\frac{1}{\sigma_T^{cu}} \left[ \left( \frac{\sigma_T^{cu}}{2\tau} \right)^2 - 1 \right] \sigma_{22} + \frac{1}{4\tau^2} \sigma_{22}^2 + \frac{1}{\tau^2} \sigma_{12}^2 = 1$$

Tensile Interlaminar Mode

$$\frac{1}{(\sigma_T^u)^2} \sigma_{33}^2 + \frac{1}{\tau^2} (\sigma_{13}^2 + \sigma_{23}^2) = 1$$

Compressive Interlaminar Mode

$$\frac{1}{\sigma_T^{cu}} \left[ \left( \frac{\sigma_T^{cu}}{2\tau} \right)^2 - 1 \right] \sigma_{33} + \frac{1}{4\tau^2} \sigma_{33}^2 + \frac{1}{\tau^2} (\sigma_{13}^2 + \sigma_{23}^2) = 1$$

where

- $\sigma_L^u$  = axial tensile strength
- $\sigma_L^{cu}$  = axial compressive strength
- $\sigma_T^u$  = transverse tensile strength
- $\sigma_T^{cu}$  = transverse compressive strength
- $\tau$  = shear strength ( $\tau_L^u = \tau_T^u = \tau$ )

strength, but the composite stiffness remains essentially unaltered. Experimental results [4.53] confirm the validity of this observation. Fatigue failure loads are calculated for all elements on the basis of residual strength. This defines the failed elements at any load level after the specified number of cycles. Laminate residual strength can be determined by static analysis using the residual strengths of individual elements.

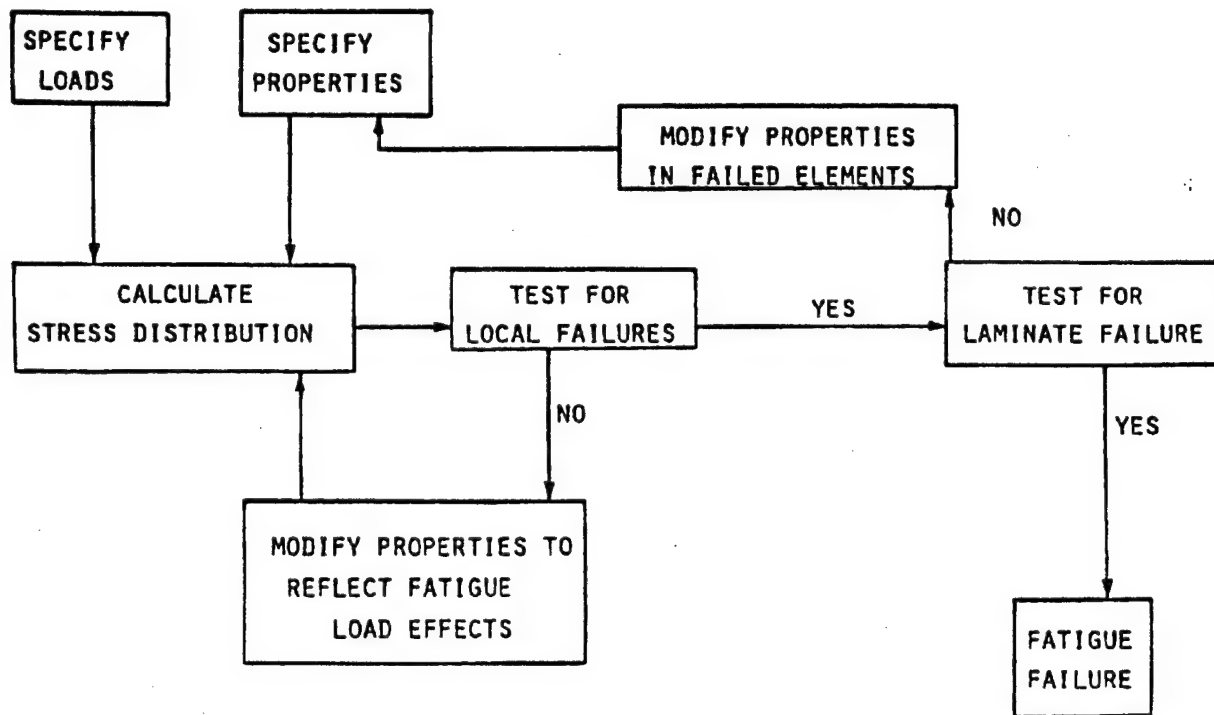


FIGURE 4.60. METHODOLOGY FOR FAILURE ANALYSIS WITH CONSIDERATION OF LOAD CYCLING EFFECTS [4.53]

Representative interlaminar disbond growth is illustrated in figure 4.61 [4.53] showing open hole test specimens with pin loaded end tabs for a typical carbon/epoxy laminate. Delamination initiates on both sides of the notch (at the 0/45 interface near the surface) at the axial tangent points and propagates towards the end tabs. The regions of delamination initially develop in all four quadrants around the notch in a uniform and symmetric manner. Growth of each region then progresses along the axial tangent line to the notch as well as along the circumference of the notch toward the center of the specimen. This circumferential progression eventually results in the bridging of the delamination in the upper two quadrants and, similarly, the lower two quadrants. If the delaminations at the tangent points progress to the point where they join up, the resulting combined delamination, which is contained within a region bounded by the axial tangent lines to the notch (figure 4.61), continues toward the specimen end tabs.

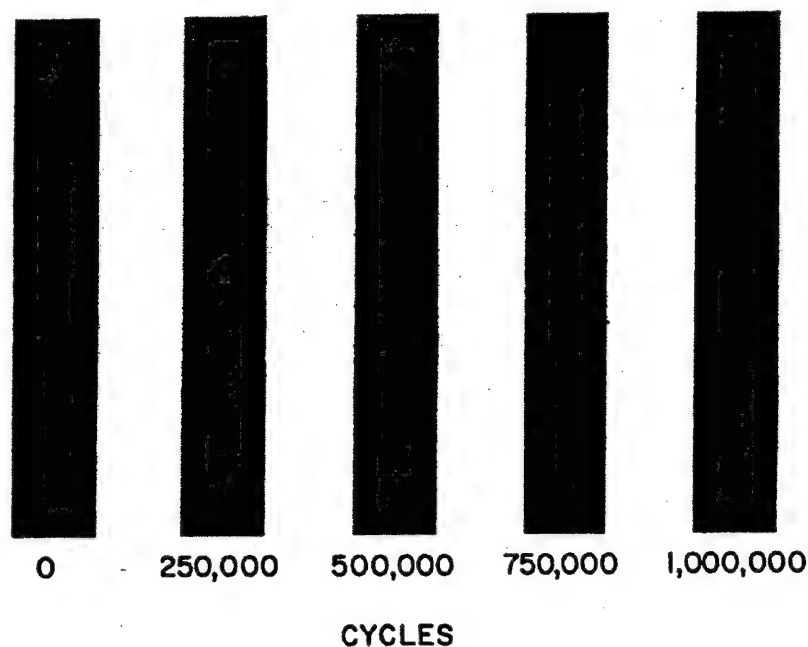


FIGURE 4.61. C-SCANS OF SPECIMEN OF  $[0_2/\pm 45]_s$  CARBON/EPOXY LAMINATE AT DIFFERENT LOAD CYCLE LEVELS

Photomicrographs of the axial and transverse sections of this specimen show typical intralaminar damage. Figure 4.62 shows an axial section tangent to the circular notch. Looking at the ultrasonic C-scans (figure 4.61), it becomes evident that this section contains a damage zone along the right side of the hole. Visual inspection of the photomicrograph reveals numerous intralaminar microcracks occurring in the  $+45^\circ$  and  $-45^\circ$  plies. Close examination shows that, in practically all cases, the cracks appear to have either initiated or terminated at the  $0^\circ$  ply interface. The distribution of cracks is relatively random, and in most cases, the crack distribution is directed perpendicular to the  $0^\circ$  fiber direction.

A section of this specimen which is a cut in a transverse direction tangent to the notch is shown in figure 4.63. Aside from a small number of randomly distributed cracks the majority of cracks are shown to be oriented collinearly and confined essentially to the  $0^\circ$  plies. The cracks extend completely through each group of two  $0^\circ$  plies and terminate at the angle ply interfaces. It should be noted that all of the cracks in the collinear orientation are aligned with the cracks in the  $0^\circ$  plies on the surfaces, which are observed to originate at the edge of the hole on the C-scan (figure 4.61). The only obvious delamination is found at the  $0/\pm 45$  interface nearest to the surface, as noted earlier. This indicates that while the delamination is limited mainly to the surface layers, as indicated on the C-scans, the axial crack propagation shown on the surface  $0^\circ$  plies also extends in a similar fashion through each set of  $0^\circ$  plies throughout the thickness.

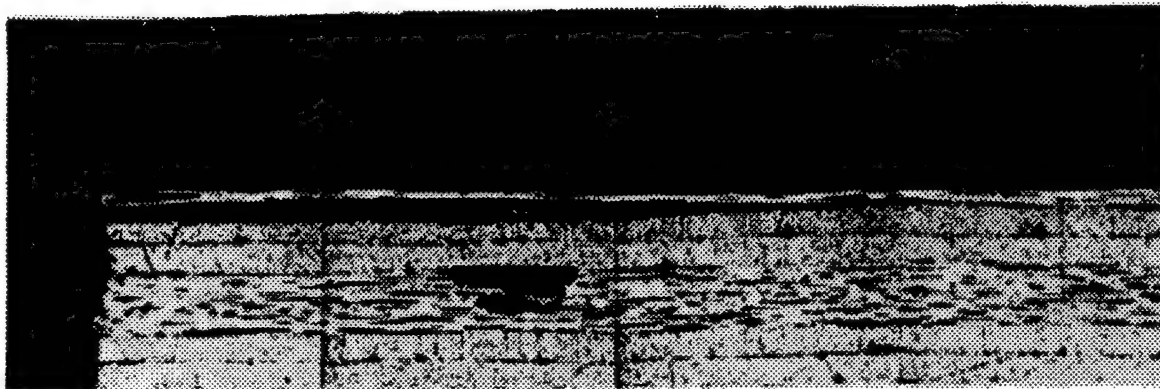


FIGURE 4.62. AXIAL SECTION OF SPECIMEN OF  $[0_2/\pm 45]_{5s}$  CARBON/EPOXY LAMINATE

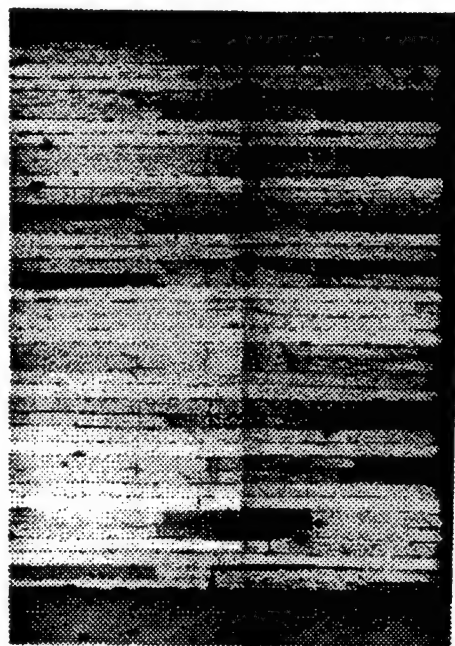


FIGURE 4.63. TRANSVERSE SECTION OF SPECIMEN OF  $[0_2/\pm 45]_{5s}$  CARBON/EPOXY LAMINATE

Although various analytical models and criteria have been developed for through-the-thickness defects like cracks or holes and the damage mechanisms which develop under static and cyclic loading are relatively clear, quantitative assessment of the criticality of such defects remains a complicated task. The reason for this complexity is the growth of delaminations between various laminae (see section 4.8.2.2) and disbonds in the matrix and/or fiber-matrix interfaces in the individual layers. For this reason, use of fracture mechanics methodologies to solve this problem has met with only partial success.



Under static loading, use of a stress criterion at a point a short distance away from the crack tip [4.55] is considered a viable method of strength prediction by many designers. Finite element modelling or progressive damage growth modelling may yield more realistic assessments of damage growth, although they have their own limitations, especially from the point of accuracy as well as cost. Modelling of damage growth under cyclic loading is still in the state of research and development. References 4.42, 4.56, and 4.57 present reviews of the status of this work. A considerable amount of work is still to be performed to put the analytical methodology for assessing two-dimensional growth of damage starting from the edge of a hole on a sound footing. In the interim, experimental treatment of structural elements containing holes is necessary.

There are indications that tension fatigue of laminates with holes may be less serious than compression fatigue. In the latter case, the disbonds can lead to localized compressive instabilities which are catastrophic [4.42 and 4.49]. Methods for assessing disbond growth are treated in the following section.

#### 4.8.2.2 Growth of Interlaminar Disbonds.

The disbond reflects the second major representative problem of fatigue in the presence of discontinuities. Growth of damage of this type can occur without breaking any fibers. Since the matrix is the weak constituent, this represents a potentially critical failure mechanism. Disbond growth can occur without any visible indication on the surface of the part. Hence, this failure mechanism is a serious hazard to flight safety and numerous investigations have been performed to study the disbond propagation phenomenon. This subsection attempts to review the state of the art. Important works are cited, but the list of works is by no means a comprehensive one.

Disbonds can propagate as a result of transverse shear, out-of-plane loading, or in-plane compression. For all of these loads, there will be interlaminar shear and normal stresses in the plane of the disbond with singularities at the periphery. Since the disbond propagates entirely within the matrix material, methods of classical fracture mechanics appear appropriate. There is a strong relationship between this type of damage growth and the failure of an adhesively bonded joint. Fracture propagation can occur in a crack opening mode, denoted Mode I; in forward shear mode, denoted Mode II; or in a lateral shear mode, denoted Mode III.

Growth of isolated disbonds in Mode I, Mode II, or combined modes under quasi-static or cyclic loading has been modelled by various investigators using fracture mechanics methodologies and fatigue crack growth laws. This subject has been reviewed in reference 4.56, in which it is reported that growth of disbonds from surface flaws or from edges has also been studied. In all such studies, strain energy release rates or stress intensity factors are calculated by analytical or numerical methods, and other semiempirical parameters are determined from correlation with experimental data. In most of these experimental studies, either the growth of implanted flaws is one-dimensional or correlation with a one-dimensional model is attempted.

Two-dimensional finite element methods [4.57-4.63] appear to be attractive for numerical calculations because of their versatility in considering various boundary conditions, such as free edges or surface flaws. These methods can be expensive, however, and their accuracy is dependent upon mesh size and element shape. One-dimensional theories [4.64-4.66] and elasticity solutions [4.67 and 4.68] are comparatively inexpensive, but they have been used for



isolated disbonds only. Extension of such methods to consideration of disbonds near free edges or surface flaws is complicated but has been attempted in some studies.

Techniques of modelling self-similar disbond growth are well advanced, but before they can be used as practical design tools, a significant amount of experimental/analytical correlation is needed to extend them to the more general case of disbond growth which is not self-similar. Use of 3D finite element analysis has been advanced as a method for calculation of strain energy release rates in reference 4.69. In this approach, three-dimensional brick elements are used for calculation of strain energy release rates for disbond propagation. When the change in strain energy exceeds the critical strain energy, the disbond is permitted to propagate. Power law type relations are often used for modeling delamination growth under cyclic loading.

Finite element methods are attractive tools for studying the stress field near disbonds with 2D planforms, but useful results for such problems have also been obtained by the use of modified laminated plate theories [4.70]. Use of 3D elasticity theories is reported in reference 4.71. A considerable amount of experimental work has also been performed to determine the various material constants which are used in modelling growth of disbonds.

Disbond defects represent a serious source of laminate failure but they lend themselves to detection by nondestructive inspection (NDI) techniques. The state of the art of NDI is quite advanced and many improved techniques are being investigated and used at the present time. Some of the common techniques are discussed later.

#### 4.8.3 Impact and Damage Tolerance.

The subject of impact and impact related phenomena in composite materials has been an area of vigorous investigation within the materials and structures communities. Some important works addressing various issues related to impact are discussed here, but the list of works is in no way a comprehensive one. The interest in this subject stems primarily from the various modes and locations of impact induced damage within composite structures. It is quite possible for an impact event to induce considerable damage within a composite structure without any visible indication of the damage on the exterior surfaces of the structure. Thus, a structure may be significantly degraded with respect to its performance requirements without any readily available indications of the performance loss.

Directly related to the subject of impact is the question of damage tolerance. If composite structure suffers a delamination, for example, how well will the structure respond to subsequent loading environments? Obviously, a centrally located delamination will have no effect on performance under tension loading but may be severely detrimental under compression, bending, and shear loading. Therefore, careful evaluations of the effect of such delaminations under different expected loading conditions are necessary.

Evaluations of impact in composites are fundamentally different from those in metals. In a metal, the evaluation of impact is typically performed using an Izod or Charpy impact test. These tests provide the amount of energy required to promote fracture at a dominant flaw in the specimen. In a composite, however, this approach yields little, if any, useful information for design since flaw networks rather than dominant flaws are present. A good measure of impact

resistance in a composite material is the energy required to initiate failure in one of several modes such as delamination, backface ply splitting, surface crushing, backface ply separation or spallation, or fiber breakage.

Typically, composite materials require a different type of test in order to determine these energy levels. One of the more common test methods is the drop test. Here a metallic impactor is dropped from sufficient height to attain a specific amount of kinetic energy prior to impact. If higher energies are required, some sort of accelerating mechanism such as an air gun may be used. The major idea here is that energy to promote total failure is not a particularly useful parameter, since a partially damaged structure may or may not be degraded beyond useful service.

An interesting feature in composites subjected to impact loadings is the variation in failure mode with impactor velocity. At low velocity, the response typically will take the form of vibration modes which involve primarily shear and bending deformations. According to some investigators, the problem of very low velocity impact may be considered equivalent to the quasi-static indentation problem. At very high velocities, the response will be ballistic: damage to the structure will be a function of the propagation and reflection of stress waves, and the damage produced will consist of backface spallation and shear failures not related to bending. Moderate velocity impact produces a combination of all of these responses and damage modes and is considerably more difficult to evaluate.

Investigations into the response of composite materials subjected to impact loadings can be classified into three groups: (1) experimental efforts, (2) analytic modeling, and (3) analysis of low-velocity impact.

Initial experimental efforts [4.72-4.74] closely followed the procedures used in metals by utilizing Charpy and Izod impact testing. This type of testing is probably more suited to quality assurance than material property evaluations. Later work included ball drop testing with damage threshold monitoring [4.75 and 4.76]. In addition to monitoring the damage threshold energy levels, damage modes and combined static and impact loadings were evaluated. There has been a recent trend toward standardization of the test methods for evaluating impact resistance [4.77].

The effects of compressive panel loadings during plate impact have been shown to be very significant [4.75], as seen in figure 4.64. The solid curve here represents the boundary between the range of applied compression strains for which no failure occurred at a given impact velocity (corresponding to the open symbols) and the strain level range (solid symbols) for which failure occurred. The data represented in figure 4.64 confirm that, as might be expected, as the applied static compressive strain is increased, the impact energy required to promote a catastrophic failure decreases.

Figure 4.65 presents residual compressive strength data for those specimens represented in figure 4.64 which did not fail during impact. (The failure threshold curve from figure 4.64 is retained here for reference.) These results show a significant reduction in postimpact compressive strength for specimens exposed to 75 m/s and greater impact velocities. In addition, it can be seen that the strains corresponding to residual strength of specimens which were below the threshold strains (and therefore not failed) during impact is typically greater than the failure

threshold strains above which failure occurred during impact. Rhodes [4.75] interprets this as an indication that the failure threshold level may be considered a lower bound for the residual strength.

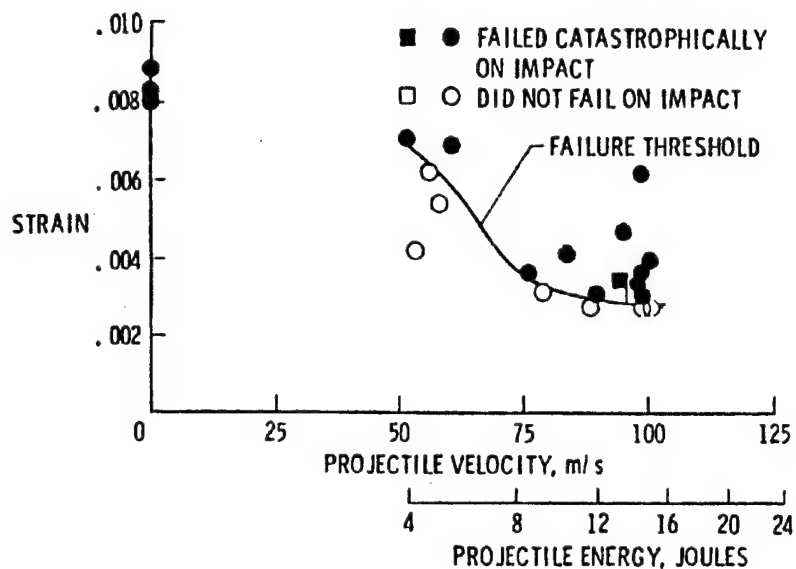


FIGURE 4.64. IMPACT OF COMPRESSION LOADED  $[(\pm 45/0_2)_2/\pm 45/0/90]_{2s}$  GRAPHITE/EPOXY LAMINATE [4.75]

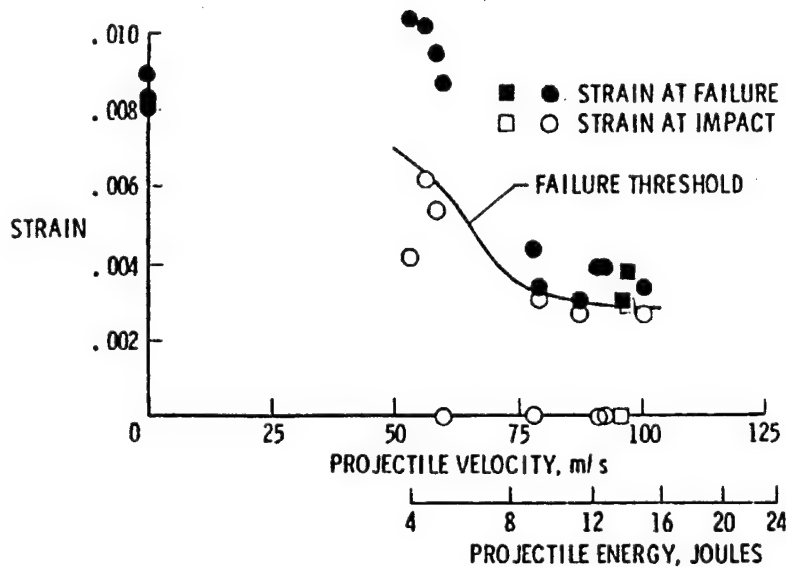


FIGURE 4.65. RESIDUAL COMPRESSIVE STRENGTH OF IMPACT/COMPRESSION LOADED  $[(\pm 45/0_2)_2/\pm 45/0/90]_{2s}$  GRAPHITE/EPOXY LAMINATE [4.75]

The data presented in figures 4.64 and 4.65 appear to suggest that the deleterious effects of impact can be ignored by simply limiting the allowable compressive strains in this laminate to 0.25%-0.30%. The data also appears to suggest that the impact/compression failure threshold level and the residual compressive allowable strains are asymptotically approaching 0.25%-0.30% strain. Careful review of these limited data, however, demonstrates that this is an erroneous conclusion. First and foremost, only static compressive residual strength is considered in figure 4.65. The state of affairs under subsequent fatigue loading, impact loading, bending loading, etc., will probably be very different. Additionally, the range of impact velocities studied is certainly not all inclusive. Very high-velocity impacts produce types of failure different from those produced by low- or moderate-velocity impacts. A final consideration is the mass of the impactor: larger masses at lower velocities can generate the same amounts of kinetic energy while producing different damage modes and amounts of damage.

All of these uncertainties lead to the realization that designing for impact of composites must include specific information as to the types of impact and subsequent loading environments that have to be sustained. Considerable testing to verify design must be performed in order to demonstrate the desired level of structural integrity.

Analytical endeavors in impact work were initially limited to wave propagation due to the application to ballistic response. Some of the earlier work in this area was performed by Moon [4.78]. Utilizing Mindlin plate theory, which incorporates shear deformations, and ignoring through-the-thickness stress waves, predictions of in-plane bending and extensional stress waves were made. Analyses were performed for a limited number of angle-ply laminates. The results were most interesting in that the orthotropy of the composite laminates produced distorted wave fronts. In many cases, cusps were found and the wave surfaces were not convex. This was reported as indicating that the stress waves were being focused by the large axial-to-transverse stiffness ratio in graphite/epoxy systems.

Later analytical work was involved in the response of composite materials subjected to lower velocity impact. Work by McQuillen [4.79] demonstrated good correlation between experimental results and a structural dynamics analysis for low-velocity impact. This work showed an increasing proportion of energy being contained in higher-frequency bending modes as the impactor velocity was increased. Even though this analysis was limited to beam structures, it did provide correlation with experimental work and validated the structural dynamics analysis approach for low-velocity impact. With this approach validated, other researchers [4.80] expanded the analysis to plate structures and included damage initiation and propagation effects.

Analytical procedures have been developed which couple the high-velocity wave propagation effects with the low-velocity structural dynamics response [4.81 and 4.82]. The approach taken utilized a three-dimensional finite element analysis with Eulerian coordinate definitions to model the local impact region coupled with a general purpose finite element code (NASTRAN) to model the structure away from the impact site. Within the Eulerian zone, material yielding and flow are permitted for isotropic materials and appropriate failure criteria are used for composite materials. The composite moduli are set to zero as failure occurs. This particular methodology is best suited to high-velocity impact, and solution times are reported to be large.

The analyses which have been described can be complex and costly to perform. The rationale for utilizing these analytical models is the requirement for the determination of failure modes and locations in composite structures. This quantitative description of damage is required in order to evaluate investigations of the effects of damage on subsequent performance.

Each of the analytical procedures described is useful in examining the phenomenon of low-velocity impact. Insight into damage modes and propagation has to be obtained utilizing these techniques. For design purposes, these analyses have only limited application, since each must be considered to be in the research and development stage.

Evaluating the effects of damage in composites is considerably more difficult than in conventional materials. The majority of the complications which arise in damage tolerance evaluations are related to the multiplicity of failure modes, locations, and strengths. Damage tolerance evaluations are performed under fatigue, as well as static ultimate, loading. The repetitive loadings have the effect of promoting damage growth due to material degradation and stress concentrations. In composites, such evaluations are difficult. Because of the anisotropy and heterogeneity of the material, failure modes for low loads and many cycles may be different from those for higher loads and few cycles. Typically, cyclic transverse loadings will produce more degradation than cyclic axial loads. Therefore, under combined stresses, the failure mode may change from axial to transverse as the number of cycles to failure increases.

A very interesting phenomenon can be seen in the fatigue of notched laminates. Some laminates show an increased notched strength after fatigue loading, as discussed earlier. The increase is produced through a decrease in the effective stress concentration factor due to fatigue induced damage around the notch. In effect, the shape and dimensions of the notch change with damage, which changes the stress concentration factor.

Experimental evaluations of damage tolerance are typically performed utilizing NDI. Ultrasonic C-scans, acoustic emission, and optical and visual inspection appear to be the most widely used tools for NDI at this point in time. X-ray radiography using opaque penetrants has a good potential in this direction. Other techniques such as thermography, dye penetrants, and attenuation measurements are still in the stage of research and development. Very few of the NDI techniques have been shown to yield accurate quantitative measurements of damage size and shape. Others are useful for detecting and locating flaws. Utilizing these techniques at various stages in a fatigue loading spectrum identifies growth or damage. Identification of the mode of the damage, however, is still very difficult.

Contemporary materials research is oriented towards development of resins of improved impact resistance [4.83]. Test methods for quantitative assessment of such improvements have recently been proposed in reference 4.77. Considering the fact that the potential for impact damage is currently the dominant limitation in allowable design strain levels for fiber composite laminates in aircraft structures, uses of stitched laminates, through-the-thickness reinforcements, thermoplastics, and other modifications are being investigated.

#### 4.8.4 Fatigue Design Philosophy.

This section first addresses the behavior of unnotched laminates under cyclic loading conditions. Such laminates may be regarded as having dispersed initial flaws which are inherent in the fabrication process. The lifetime of these materials may be defined as the durability problem. This influences the life cycle cost of ownership, and therefore, it is an economics issue [4.84].

The second major aspect of fatigue failure discussed here deals with the discontinuity from which a major damage growth leading to failure could occur. This may be defined as the damage tolerance problem. This is a safety issue [4.84] which defines the inspection periods necessary to ensure flight safety.

The design approach for durability requires the generation of experimental data on specimens representative of the actual fabrication process.

Ideally, these data could be treated by the analysis methods based upon the sequential ply failure model (see section 4.8.1.1) or upon the growth of dispersed damage model (see section 4.8.1.2). However, in practical applications, a macromechanical model (see section 4.8.1.3) is commonly utilized.

Mechanistic approaches to the analysis of fatigue may be defined in a deterministic fashion. The experimental data for lifetime under specified cyclic loads, however, will show scatter because the inherent defects in a laminate vary. Thus, for example, the classic S-N curves must be replaced by P-S-N curves (see section 4.8.1.4). Because the cyclic load program is generally not known in a deterministic fashion, it is necessary to have a cumulative damage approach to the fatigue design problem. This must be taken into account in the experimental as well as the analytical efforts. The objective of these efforts is the development of a reliable set of P-S-N curves which can be used to establish design stress levels appropriate for desired lifetime at the desired confidence level. For a discussion of such statistical issues see MIL-HDBK-17-1D [4.44].

The design approach for damage tolerance has two major elements: the use of a conservative analysis and a program of realistic testing. The major elements of a conservative design analysis are the use of low-strain allowables, special analysis of complicated design details, special treatment (e.g., reinforcement) for problem areas (such as cutouts), establishment of inherent defect acceptance criteria, and the use of representative defects for design analyses to increase reliability. Realistic testing involves coupon testing to develop a statistical data base which allows for environmental effects and subcomponent testing for verification of failure modes and levels. Both the analysis and the experiments will address the basic problems of laminates with holes and with disbonds. Design allowables will be generated for basic loading conditions. These results will be used to address actual design complexities by drawing upon treatment of combined stresses utilizing interaction curves, load spectrum effects utilizing cumulative damage hypotheses, environmental effects utilizing reduced allowables and revised stress analyses, and lifetime calculations utilizing residual strength distributions at moderately long times in conjunction with effective crack growth laws. All of these methodologies are in a continuing state of development. Hence, present day design approaches are usually conservative. It is common to use a factor of safety over the weakest strength obtained at the maximum lifetime



of interest. It must be recognized, however, that it may not always be possible to do that in a realistic, practical structure. Thus, this basic design procedure must be supplemented by structural testing.

The test program will generally involve a full-scale structure under fatigue. It should be recognized, however, that fatigue behavior can be profoundly influenced by environmental effects, and realistic full-scale environmental testing can be prohibitively expensive. Therefore, it is necessary to establish an estimate of mean lifetime with a full-scale fatigue test in an ambient environment. Coupon and element testing are then used to obtain a definition of material and structural variability effects. It is necessary to utilize a procedure whereby test coupons with holes establish the statistics of failure. Such coupons are also used to treat the environmental effects. At the element level, representative small components that contain realistic stress fields representing actual design features should be tested to rule out the influence of unanticipated mechanisms on failure.

All of these complexities and apparent difficulties in development of durable, damage tolerant composite structures are offset by the fact that the experience with composite structures has been very good. This is primarily a result of the fact that the fiber direction fatigue characteristics of carbon fiber composites are exemplary. The factors of safety for static design, and the reliability considerations for static design, generally reduce operating stress levels so that they are far below the static strength. As a result, for a multidirectional laminate with fibers controlling the behavior in all directions, it is feasible to avoid fatigue problems, particularly for designs governed by the strain limitations of 3000-5000 in/in, which are widely used at the present time in order to achieve impact resistance. It appears reasonable to expect that, in the future, enhanced understanding will lead to reliable, cost-effective designs operating at higher strain levels.

#### REFERENCES

- 4.1. Advanced Composites Design Guide, 3rd edition, January 1973.
- 4.2. Shen, C. and Springer, G.S., Moisture Absorption and Desorption of Composite Materials, J. Composite Mats., Vol. 10, p. 1 (1976).
- 4.3. Gillat, O. and Broutman, L.J., The Effect of an External Stress or Moisture Diffusion and Degradation in a Graphite Reinforced Epoxy Laminate, ASTM STP 658 (1977).
- 4.4. Pipes, R. B. and Pagano, N.J., Interlaminar Stresses in Composites Under Uniform Axial Extension, J. Composite Mats., Vol. 4, p. 538 (1970).
- 4.5. Wang, S.S. and Choi, I., Boundary Layer Thermal Stresses in Angle-Ply Composite Laminates, in Modern Developments in Composite Materials and Structures, Vinson J. R., Ed., pp. 315-342, ASME (1979).
- 4.6. Pipes, R.B., Boundary Layer Effects in Composite Laminates, from Research Workshop, Mechanics of Composite Materials, Duke University, October 1978.

- 4.7. Hashin, Z., Bagchi, D., and Rosen, B.W., Nonlinear Behavior of Fiber Composite Laminates, NASA CR-2313, April 1974.
- 4.8. Ramberg, W. and Osgood, W.B., Description of Stress Strain Curves by Three Parameters, NASA TN-902 (1943).
- 4.9. Hashin, Z., Rosen, B.W., and Pipes, R.B., Nonlinear Effects on Composite Laminate Thermal Expansion, NASA CR-3088, February 1979.
- 4.10. Nairn, J.A., "The Strain Energy Release Rate for Composite Microcracking: A Variational Approach," J. Composite Mats., Vol. 23, p. 1106 (1989).
- 4.11. Chatterjee, S.N., Wang, E.C.J., and Yen, C.F., "Modeling Ply Crack Growth in Laminates Under Combined Stress States," ASTM STP 1156, p. 195 (1993).
- 4.12. O'Brien, T.K., "Characterization of Delamination Onset and Growth in Composite Laminates," ASTM STP 775, p. 140 (1982).
- 4.13. Hashin, Z., "Analysis of Cracked Laminates: A Variational Approach," Mechanics of Materials, Vol. 4., p. 121 (1985).
- 4.14. Polymer Matrix Composites, Volume 3, Utilization of Data, MIL-HDBK-17-3D, Dept. of Defense, February 1994.
- 4.15. Waddoups, M.E. et al., Macroscopic Fracture Mechanics of Advanced Composite Materials, J. of Composite Mats., Vol. 5, pp. 446-455, October 1971.
- 4.16. Bowie, O.L., "Analysis of an Infinite Plate Containing Radial Cracks Originating from the Boundary of an Internal Circular Hole," J. Mathematics and Physics, Vol. 35, p. 60 (1956).
- 4.17. Savin, G.N., Stress Distribution Around Holes, NASA TT-F-607, November 1970.
- 4.18. Whitney, J.M. and Nuismer, R.J., Stress Fracture Criteria for Laminated Composites Containing Stress Concentrations, J. Composite Mats., Vol. 8, pp. 253-265 (1974).
- 4.19. Riefsnyder, K.L. and Highsmith, A.L., "The Relationship of Stiffness Changes in Composite Laminates to Fracture Related Damage Mechanisms," Proc. 2nd USA-USSR Symp., Bethlehem, PA, March 1981.
- 4.20. Stinchcomb, W.W., "NDE of Damage Accumulation Process in Composite Materials," Comp. Sci. Technol., Vol. 25, p. 103 (1986).
- 4.21. Talreja, R., "Fatigue of Composite Materials and Fatigue Life Diagrams," Proc. Royal Soc. London, Vol. A 37, p. 461 (1981).



- 4.22. Hashin, Z. and Rotem A., A Fatigue Failure Criterion for Fiber Reinforced Materials, J. Composite Mats., Vol. 5, p. 448 (1973).
- 4.23. Hashin, Z., Failure Criteria for Unidirectional Fiber Composites, J. Appl. Mech., Vol. 47, pp. 329-334 (1980).
- 4.24. Hahn, H.T., Fatigue Behavior and Life Prediction of Composite Laminates, ASTM STP 674, p. 383 (1979).
- 4.25. Adams, T., Dickson, R.F., Jones, C.J., Reiter, H., and Harris, B., "Power Law Damage Model for Fiber Reinforced Plastics," Proc. I Mech E. 200C3, p. 155 (1986).
- 4.26. Baron, C.H., Schulte, K., and Harrig, H., "Influence of Fiber and Matrix Failure Strain on Static and Fatigue Properties of CFRP," Comp. Sci. Technol., Vol. 29, p. 257 (1987).
- 4.27. Awerbuch, J. and Hahn, H.T., "Fatigue and Proof Testing of Unidirectional Graphite/Epoxy Composites," ASTM STP 636, pp. 248-266 (1977).
- 4.28. Chou, P.C. and Croman, R., "Residual Strength in Fatigue Based on the Strength-Life Equal Rank Assumption," J. Comp. Mats., V. 12, p. 177 (1978).
- 4.29. Bernard, P.M. and Young, J.B., "Cumulative Fatigue and Life Prediction of Fiber Composites," Final Report, RAE Cont. XR/Mat11494 2028-0134, Cranfield Institute of Technology, U.K. (1986).
- 4.30. Sims, D.F. and Brogen, V.H., Fatigue of Filamentary Composite Materials, ASTM STP 636, pp. 185-205 (1977).
- 4.31. Bader, M.G. and Boniface, L., "Damage Development During Quasi-Static and Cyclic Loading in GRP and CFRP Laminates Containing 90° Plies," ICCM5, San Diego, Proc. ASME, p. 221 (1985).
- 4.32. Jones, C.J., Dickson, R.F., Adam, T., Rieter, H., and Harris, B., "The Environmental Fatigue Behavior of Reinforced Plastics," Proc. Royal Soc. London, Vol. A 369, p. 315 (1984).
- 4.33. O'Brien, T.K., Rigamonth, M., and Zanoti, C., "Tension Fatigue Analysis and Life Prediction for Composite Laminates," Int. J. Fatigue, Vol. II, p. 379 (1989).
- 4.34. Tsai, S.W. and Hahn, H.T., Technical Report AFML-TR-77-33 (1977).
- 4.35. Halpin, J.C., Jerina, K.L., and Johnson, T.A., Characterization of Composites for the Purpose of Reliability Prediction, ASTM STP 521, pp. 5-64 (1973).
- 4.36. Halpin, J.C., Waddoups, M.E., and Johnson, T.A., Kinetic Fracture Models and Structural Reliability, Int. J. Fracture Mech., Vol. 8, pp. 465-468 (1972).

- 4.37. Hahn, H.T. and Kim, R.Y., Fatigue Behavior of Composite Laminate, J. Composite Mats., Vol. 10, pp. 156-180 (1976).
- 4.38. Whitney, J.M., Fatigue Characterization of Composite Materials, ASTM STP 723, pp. 133-151 (1981).
- 4.39. Yang, J.N. and Liu, M.D., Residual Strength Degradation Model and Theory of Periodic Proof Tests for Graphite/Epoxy Laminates, J. Composite Mats., Vol. 11, pp. 176-220 (1977).
- 4.40. Broutman, L.J. and Sahu, S., A New Theory to Predict Cumulative Fatigue Damage in Fiberglass Reinforced Plastics, ASTM STP 497, pp. 170-188 (1972).
- 4.41. Yang, J.N. and Jones, D.L., Load Sequence Effects on the Fatigue of Unnotched Composite Materials, ASTM STP 723, pp. 213-232 (1981).
- 4.42. Saff, C.R., Compression Fatigue Life Prediction Methodology for Composite Structures, NADC78203-60, June 1980.
- 4.43. Hashin, Z., A Reinterpretation of the Palmgren-Miner Rule for Fatigue Life Prediction, J. Appl. Mech., Vol. 47, pp. 324-328 (1980).
- 4.44. Military Handbook "Polymer Matrix Composites" MIL-HDBK-17-1D Volume 1, Chapter 8 (1994).
- 4.45. Mann, N.R., Schafer, R.E., and Singpurwalla, N.D., Methods for Statistical Analysis of Reliability and Life Data, Wiley (1974).
- 4.46. Hahn, H.T. and Kim, R.Y., Proof Testing of Composite Materials, J. Composite Mats., Vol. 9, p. 297 (1975).
- 4.47. Yang, J.N. and Lue, M.D., Residual Strength Degradation Model and Theory of Periodic Proof Tests for Graphite/Epoxy Laminates, AFML TR-76-225 (1976).
- 4.48. Badaliane, R. and Diu, H.D., Compression Fatigue Life Prediction Methodology for Composite Structures, McDonnell Aircraft Company, Report No. MDCA5723, February 1979.
- 4.49. Ratwani, N.J. and Kan, H.P., Compression Fatigue Analysis of Fiber Composites, NADC- 78049-60, September 1979.
- 4.50. McLaughlin, P.V., Jr., Kulkarni, S.V., Huang, S.N., and Rosen, B.W., Fatigue of Notched Fiber Composite Laminates I. Analytical Model, NASA CR-132747, March 1975.

- 4.51. Ramkumar, R.L., Kulkarni, S.V., and Pipes, R.B., Evaluation and Expansion of an Analytical Model for Fatigue of Notched Composite Laminates, NASA CR-145308, March 1978.
- 4.52. Kanninen, M.F., Rybicki, E.F., and Griffith, W.I., Preliminary Development of a Fundamental Analysis Model for Crack Growth in a Fiber Reinforced Composite Material, ASTM STP 617, pp. 53-69 (1977).
- 4.53. Humphreys, E.A. and Rosen, B.W., Development of a Realistic Stress Analysis for Fatigue Analysis of Notched Composite Laminates, NASA CR-159119, May 1979.
- 4.54. Rosen, B.W., Nagarkar, A.P., Pipes, R.B., and Walsh, R., Research Study to Define the Critical Failure Mechanisms in Notched Composites Under Compression Fatigue Loading, Final Report on NASC Contract N00019-79-C-0633, NSC TFR 1201/1801, March 1981.
- 4.55. Nuismer, R.J. and Whitney, J.M., Uniaxial Failure of Composite Laminates Containing Stress Concentrations, ASTM STP 593 (1975).
- 4.56. Chatterjee, S.N. and Pipes, R.B., Composite Defect Significance, NADC 80048-60, MSC TFR 1208/1107, August 1981.
- 4.57. Proceedings of the Symposium on Nondestructive and Analytical Evaluation of Criticality of Defects in Structural Composite Laminates, Chatterjee, S.N., Ed., Materials Sciences Corp., Philadelphia, November 1980.
- 4.58. Wang, A.S.D., On Free-Edge Delamination in Laminated Composites, Drexel University, Philadelphia (1978).
- 4.59. Wang, A.S.D. and Crossman, F.W., Initiation and Growth of Transverse Cracks and Edge Delamination in Composite Laminates I. An Energy Method, Drexel University, Philadelphia (1979).
- 4.60. Wang, S.S., An Analysis of Delamination in Angle-Ply Fiber-Reinforced Composites, J. Appl. Mech., Vol. 47, pp. 64-70 (1980).
- 4.61. Wang, S.S., Delamination Crack Growth in Unidirectional Fiber-Reinforced Composites Under Static and Cyclic Loading, ASTM STP 674, pp. 642-663 (1979).
- 4.62. Wang, S.S., Delamination Fracture from Surface Notch in [ (+45) / 0 / 90 ], Graphite/Epoxy Composites, Proceedings of the Second International Conference on Composite Materials (ICCM-II) TMS-AIME, pp. 277-291 (1978).
- 4.63. Wang, S.S. and Mandell, J.F., Analysis of Delamination in Unidirectional and Crossplied Fiber Reinforced Composites Containing Surface Cracks, NASA CR-135248 (1977).

- 4.64. Wang, S.S. and Wang, H.T., Interlaminar Crack Growth in Fiber-Reinforced Composites During Fatigue, J. Engng. Mats Tech., Vol. 101, pp. 34-41 (1979).
- 4.65. Devitt, D.F., Delamination Fracture Toughness of a Unidirectional Composite, M.S. thesis, Texas A&M University (1979).
- 4.66. Devitt, D.F., Schapery, R.A., and Bradley, W.L. A Method for Determining the Mode I Delamination Fracture Toughness of Elastic and Viscoelastic Composite Materials, J. Composite Mats., Vol. 14, pp. 270-285 (1980).
- 4.67. Ramkumar, R.L., Kulkarni, S.V., and Pipes R.B., Definition and Modeling of Critical Flaws in Graphite Fiber Reinforced-Epoxy Resin Matrix Composite Materials, NADC-76228-30, January 1978.
- 4.68. Chatterjee, S.N., Hashin, Z., and Pipes, R.B., Definition and Modeling of Critical Flaws in Graphite Fiber Reinforced Resin Matrix Composite Materials, NADC-77278-30, August 1979.
- 4.69. Wilkins, D.J., Eisenmann, J.R., Camin, R.A., Margolis, B.S., and Benson, R.A., Characterizing Delamination Growth in Graphite-Epoxy, ASTM STP 775, pp. 168-183 (1982).
- 4.70. Chatterjee, S.N. and Pipes, R.B., Study of Graphite/Epoxy Composites for Material Flaw Criticality, NADC 78241-60, November 1980.
- 4.71. Chatterjee, S.N., "Three- and Two-Dimensional Stress Fields Near Delamination in Laminated Composite Plates," Int. J. Solids & Structures, Vol. 23, p. 1535 (1987).
- 4.72. Chamis, C.C., Hanson, M.P., and Searafini, T.T., Designing for Impact Resistance With Unidirectional Fiber Composites, NASA TN-D-6468, August 1971.
- 4.73. Beaumont, P.W.R., Riewald, P.G., and Zweben, C., Methods for Improving the Impact Resistance of Composite Materials, ASTM STP 568, pp. 134-159 (1974).
- 4.74. Nova, R.C. and Decrescente, M.A., Impact Behavior of Unidirectional Resin Matrix Composites Tested in the Fiber Direction, ASTM STP 497, pp. 311-323 (1972).
- 4.75. Rhodes, M.D., Impact Tests on Fibrous Composite Sandwich Structures, NASA TM-7819, October 1978.
- 4.76. Rhodes, M.D., Williams, J.G., and Starnes, J.H., Jr., Low-Velocity Impact Damage in Graphite Fiber Reinforced Epoxy Laminates, 34th Annual Conference, Reinforced Plastics/Composites Institute, The Society of the Plastics Industry, Inc., January 1979.
- 4.77. Standard Tests for Toughened Resin Composites, NASA Ref. Pub. 1092, May 1982.

- 4.78. Moon, F.C., Wave Surface due to Impact on Anisotropic Fiber Composite Plates, NASA TN D-6357, September 1971.
- 4.79. McQuillen, E.J., Llorens, R.D., and Gause, L.W., Low-Velocity Transverse Normal Impact of Graphite Epoxy Composite Laminates, NADC-75119-30, December 1975.
- 4.80. Humphreys, E.A., Development of an Engineering Analysis of Progressive Damage in Composites During Low Velocity Impact, NASA CR-165778, July 1981.
- 4.81. Lee, C.H., CELFE: Coupled Eulerian-Lagrangian Finite Element Program for High-Velocity Impact I. Theory and Formulation, NASA CR-159395 (1978).
- 4.82. Lee, C.H., CELFE: Coupled Eulerian-Lagrangian Finite Element Program for High-Velocity Impact II Program User's Manual, NASA CR-159396 (1978).
- 4.83. Palmer, R.J., Investigation of the Effect of Resin Material on Impact Damage to Graphite/Epoxy Composites, NASA CR-165677, March 1981.
- 4.84. Wilkins, D.J., Eisenmann, J.R., Camin, R.A., Margolis, W.S., and Benson, R.A., Delamination in Graphite/Epoxy Composites, Proc. Symposium on Nondestructive and Analytical Evaluation of Criticality of Defects in Structural and Composite Laminates, Chatterjee, S.N., ed., pp. 13-42, Materials Sciences Corp., Philadelphia, November 1980.

## APPENDIX TO CHAPTER 4—LAMINATE LEVEL FAILURE ANALYSIS

In composites laminates, there are two characteristic stress or strain levels which can be considered in the evaluation of strength. One is the stress or strain state at which a noncatastrophic first-ply failure can occur and the other is the maximum static stress or strain state which the laminate can carry. In those cases where the material exhibits minimal microcracking or where the application is such that effects of microcracking need not be considered, a failure criterion based only upon fiber failure may be used. A common practice in the aerospace industry is to use a failure criterion based only upon fiber strain allowables, where fiber failure in any lamina is considered laminate ultimate failure. Hence, failure is a single event rather than the result of a process.

Perhaps the most common example of this laminate level failure criterion is a modification of the maximum-strain criterion. The same assumptions of no external bending, membrane forces constant along the edges, and a balanced and symmetric laminate are initially used. The basic lamina failure envelope is the same as the conventional maximum-strain envelope for tension- and compression-dominated loads but introduces truncations in the tension-compression (shear) quadrants as shown in figure A4.1. A critical assumption in this criterion is that the laminate behavior is fiber-dominated meaning that there are fibers in sufficient multiple directions such that strains are limited by the presence of the fibers to inhibit matrix cracking. In many practical applications, this typically translates into having fibers in (at least) each of four directions relative to the primary loads:  $0^\circ$ ,  $90^\circ$ , and  $\pm 45^\circ$ . Furthermore, plies are not clustered (that is, several plies of the same orientation are not laid together) in order to inhibit matrix macrocracking. With these assumptions, the first translation of the maximum strain criterion to the laminate level is a limiting of the strain in the transverse direction,  $\epsilon_{90}$ , to the fiber direction limiting strain to reflect the fact that such well-designed laminates with fibers in multiple directions restrict strains in any in-plane direction. Alternatively, if there is reason to believe that matrix cracking will be structurally significant, the  $90^\circ$  strain cutoff based on fiber direction strain could be replaced by an empirically established tensile limit reflecting a matrix-dominated mode. This limit was originally expressed as a constant strain limit. However, if such a limit is based upon the case of a constant  $90^\circ$  stress in a ply, this would result in a sloped line in the strain plane with the slope related to the Poisson's ratio of the unidirectional lamina:

$$\alpha = \tan^{-1} \left( \nu_{LT}^{lamina} \right) \quad (A4.1)$$

Such a cutoff is parallel to the uniaxial load line shown in figure A4.1. It should be further noted that possible limitations due to lamina level shear strains are inoperative due to the assumption that the fibers in multiple directions restrict such strains to values below their failure values.

Many users recognize a need to truncate the maximum strain predictions in the tension-compression quadrants. While the particular truncations vary, perhaps the most widely used version is that shown in figure A4.1. These truncations were originally based on data obtained for shear loading of such fiber-dominated laminates. These data lie in the second and fourth quadrants. The  $45^\circ$  cutoffs represent the locus of constant shear strain. These two symmetric

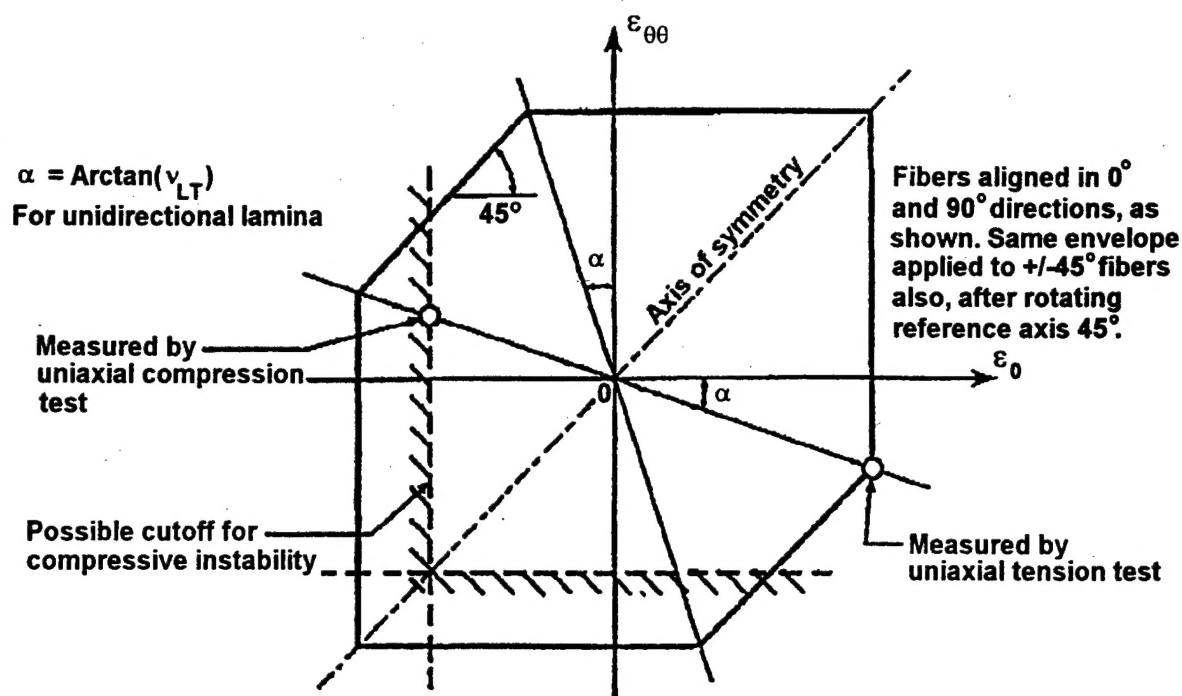


FIGURE A4.1. ILLUSTRATION OF LAMINATE LEVEL FAILURE APPROACH

truncations are located by finding the intersections of the limiting uniaxial strain lines with the lines representing pure uniaxial stress conditions in fiber directions in  $0^\circ$  and  $90^\circ$  unidirectional plies. At this point the axial strain becomes more critical than the shear. The endpoints of the truncations are therefore found by drawing lines through the origin with angles,  $\alpha$ , from the relative axes, which accounts for the unidirectional ply Poisson's ratio (see equation A4.1), thereby yielding the desired pure uniaxial state of stress in the fiber direction. The intersection of these two lines with the greater of the two pure uniaxial stress conditions in the unidirectional plies locates the endpoint of each cutoff. It is always necessary that the cutoff be located by the higher of the uniaxial strengths since, otherwise, the cutoff would undercut the measured uniaxial strain to failure at the other end. This procedure results in the same failure diagram for all fiber-dominated laminates. It should be emphasized that this procedure requires the use of the Poisson's ratio of the unidirectional ply even when the laminate contains fabric plies.

This failure model, as represented in figure A4.1, has been developed from experience with fiber-reinforced polymer matrix composites used on subsonic aircraft, particularly with carbon-epoxy materials, for which the lamina  $\nu_{LT}$  is approximately 0. It should not be applied to other composites, such as whisker-reinforced metal-matrix materials. Figure A4.1 addresses only fiber-dominated failures because, for the fiber polymer composites used on subsonic aircraft, the microcracking in the matrix has not been found to cause reductions in the static strength of laminates, particularly if the operating strain level has been restricted by the presence of bolt holes or provision for damage tolerance and repairs. However, with the advent of new composite



materials, cured at much higher temperature to withstand operation at supersonic speeds, this approach may no longer be appropriate. The residual stresses developed during cool down after cure will be far higher because of the greater difference between the cure temperature and the minimum operating temperature.

This set of truncations together at the laminate level with the original maximum strain criterion results in the following operative set of equations applied *at the laminate level* with respect to axes oriented along and normal to each fiber direction in the laminate

$$\begin{aligned} \epsilon_{11}^{cu} &\leq \epsilon_{11}^i \leq \epsilon_{11}^{tu} \\ \epsilon_{11}^{cu} &\leq \epsilon_{22}^i \leq \epsilon_{11}^{tu} \\ |\epsilon_{11}^i - \epsilon_{22}^i| &\leq (1 + \nu_{LT}^{lamina}) |\epsilon_{11}^{tu} \text{ or } \epsilon_{11}^{cu}|^* \end{aligned} \quad (A4.2)$$

\* whichever is greater

However, it is important to note that these equations can only be applied in the context of a fiber-dominated laminate as previously described. It should further be noted that the limits on the transverse strain in each ply,  $\epsilon_{22}^i$ , are set by the fibers in plies transverse to the ply under consideration and thus cannot characterize matrix cracking. This must be carefully taken into account if hybrid laminates are utilized. Furthermore, as previously discussed, if matrix cracking is considered to be structurally significant, a stress or strain cutoff must be added based on empirical observation. In this case, an assessment of the effects of the matrix cracks on subsequent properties of the laminate must be made.

As noted in section 4.7, bending occurs when there are external bending and/or twisting moments or when the laminate is not symmetric. In these cases, as with other failure criteria, it is necessary to take into account the fact that the laminate level strains vary through the thickness.